2015

Improved Understanding of Coal Pillar Behavior and Bump Potential through the Ground Response Curve

Kevin W. Harris
University of Kentucky, kevin.harris@uky.edu

STUDENT AGREEMENT:

I represent that my thesis or dissertation and abstract are my original work. Proper attribution has been given to all outside sources. I understand that I am solely responsible for obtaining any needed copyright permissions. I have obtained needed written permission statement(s) from the owner(s) of each third-party copyrighted matter to be included in my work, allowing electronic distribution (if such use is not permitted by the fair use doctrine) which will be submitted to UKnowledge as Additional File.

I hereby grant to The University of Kentucky and its agents the irrevocable, non-exclusive, and royalty-free license to archive and make accessible my work in whole or in part in all forms of media, now or hereafter known. I agree that the document mentioned above may be made available immediately for worldwide access unless an embargo applies.

I retain all other ownership rights to the copyright of my work. I also retain the right to use in future works (such as articles or books) all or part of my work. I understand that I am free to register the copyright to my work.

REVIEW, APPROVAL AND ACCEPTANCE

The document mentioned above has been reviewed and accepted by the student's advisor, on behalf of the advisory committee, and by the Director of Graduate Studies (DGS), on behalf of the program; we verify that this is the final, approved version of the student's thesis including all changes required by the advisory committee. The undersigned agree to abide by the statements above.

Kevin W. Harris, Student

Dr. Kyle A. Perry, Major Professor

Dr. Braden T. Lusk, Director of Graduate Studies

IMPROVED UNDERSTANDING OF COAL PILLAR BEHAVIOR AND BUMP POTENTIAL THROUGH THE GROUND RESPONSE CURVE

DISSERTATION

A dissertation submitted in partial fulfillment of the
requirements for the degree of Doctor of Philosophy in the
College of Engineering
at the University of Kentucky

By
Kevin Ward Harris
Lexington, Kentucky

Director: Dr. Kyle A Perry, Assistant Professor of Mining Engineering
Lexington, Kentucky

2015

ABSTRACT OF DISSERTATION

IMPROVED UNDERSTANDING OF COAL PILLAR BEHAVIOR AND BUMP POTENTIAL THROUGH THE GROUND RESPONSE CURVE

Continued depletion of easier coal reserves has necessitated development at deeper overburdens. At greater depth, operations often encounter more difficult ground conditions due to higher stresses and potential multiple seam interactions. Pillars which are left intact as the primary support mechanism experience an increase in loading. Mine design improvements are often incorporated to combat increased loads, principally by increasing pillar size. However, the potential for coal bumps, which are a rapid and violent failure of coal pillars, has increased due to these higher stresses and the use of larger width-to-height (W/H) ratio pillars.

Many efforts have been made to predict coal bumps; however, coal is a naturally occurring, inhomogeneous, and discontinuous geologic material. As a result, the best means for understanding coal pillar bursts are not efforts to predict the events themselves, but to advance knowledge of the associated environmental factors including geologic influences, stresses, and mining method. These factors have a tremendous impact on the loading distribution and resulting behavior of coal pillars. Of particular importance is the post-failure behavior of coal pillars which influences the mechanisms and functionality of pillar failure. Unfortunately, understanding of the post-failure behavior of squat coal pillars and the recognition of functional pillar strain has been limited.

The Ground Response Curve (GRC) has traditionally been used to evaluate the behavior of rock mass to the mining process by comparing the ground response/convergence curve to the support (e.g. pillars) response curve. The GRC has been employed in an effort to improve understanding of squat coal pillar behavior for numerous case studies with varying geologic and geometric conditions. The relationship between the GRC and individual pillar deformation has been examined using numerical modeling techniques. Using these widely accepted methods, a range of typical coal geologies and mining geometries was investigated, seeking to establish relationships between pillar performance, energy release, and the resulting mode of failure. The physical and dynamic properties of the rock and rock mass for coal and surrounding strata, geometric considerations, and pillar interface properties have been determined to be important

indicators of squat coal pillar behavior and ultimately bump potential. As a result, new understanding of post-failure ground response has been developed and improvements have been made towards enhanced classification of mine-specific bump criteria, or bump “red zones”.

KEYWORDS: Coal Mining, Underground Mining, Rock Mechanics, Ground Control, Coal Bumps

Kevin W. Harris
Student’s Signature

11-11-15
Date

IMPROVED UNDERSTANDING OF COAL PILLAR BEHAVIOR AND BUMP POTENTIAL THROUGH THE GROUND RESPONSE CURVE

By

Kevin Ward Harris

Dr. Kyle A. Perry
Director of Dissertation

Dr. Braden T. Lusk
Director of Graduate Studies

11-11-15

DEDICATION

This dissertation is dedicated to my wonderful wife Ashley, along with all my family and friends. I would also like to dedicate this dissertation to all the coal miners in our great nation, who have sacrificed life and health to support their families, communities, region, and our country. This has been a wonderful opportunity which I pray benefits the health and safety for all coal miners, particularly those who live and work in my home of Harlan County. Being raised and influenced by coal country and coal families is a unique blessing that too few know.

This journey started when I nearly lost my dad to a coal bump in 1996. Though I didn't fully understand at the time, the example you set prior to and following that event, even unto this day, provides the framework and inspiration for which I endeavor.

The Good Lord has blessed me beyond belief, and I thank you my Lord for all that you have and will continue to do.

Psalm 95:3-4

For the *Lord* is a great God, and a great King above all gods.
In his hand are the deep places of the earth: the strength of the hills is his also.

ACKNOWLEDGEMENTS

I would like to thank Dr. Kyle Perry for his knowledge, guidance, and support through this process. I would also like to thank him for the opportunity he provided in allowing me to return for graduate school. I would like to thank Dr. Braden Lusk, Dr. Thomas Novak, and Dr. Jonathan Wenk for being part of this research effort, committing time and effort to help me reach my goals. Finally, I would like to thank the Department of Mining Engineering at the University of Kentucky. The department will always have a special place in my heart and is “home”.

TABLE OF CONTENTS

LIST OF TABLES

LIST OF FIGURES

1 Introduction

1.1 Historical Background

The United States coal industry has made tremendous strides to improve the safety and health of underground coal miners. Improvements in technology and training have led to increased productivity and efficiency. Regulations have led to increased government oversight, improvements in the discipline of mine safety, and the development of operational best practices. The coal mining industry has also focused more intently on safety; in many cases requiring coal miners receive in-depth training on equipment, practices, conditions, and emergency situations which can greatly exceed minimum requirements. The combination of these technological advances and increased regulatory oversight has reduced miner exposure to dangerous conditions which have potential to result in injury and/or death. Figure 1-1 illustrates the decrease in the number and trend of fatalities in the mining industry in the hundred years spanning from the early 20th century to first decade of the 21st century. The number of coal mining fatalities has decreased from a high of several thousand annually to modern day lows which average below fifty per year.

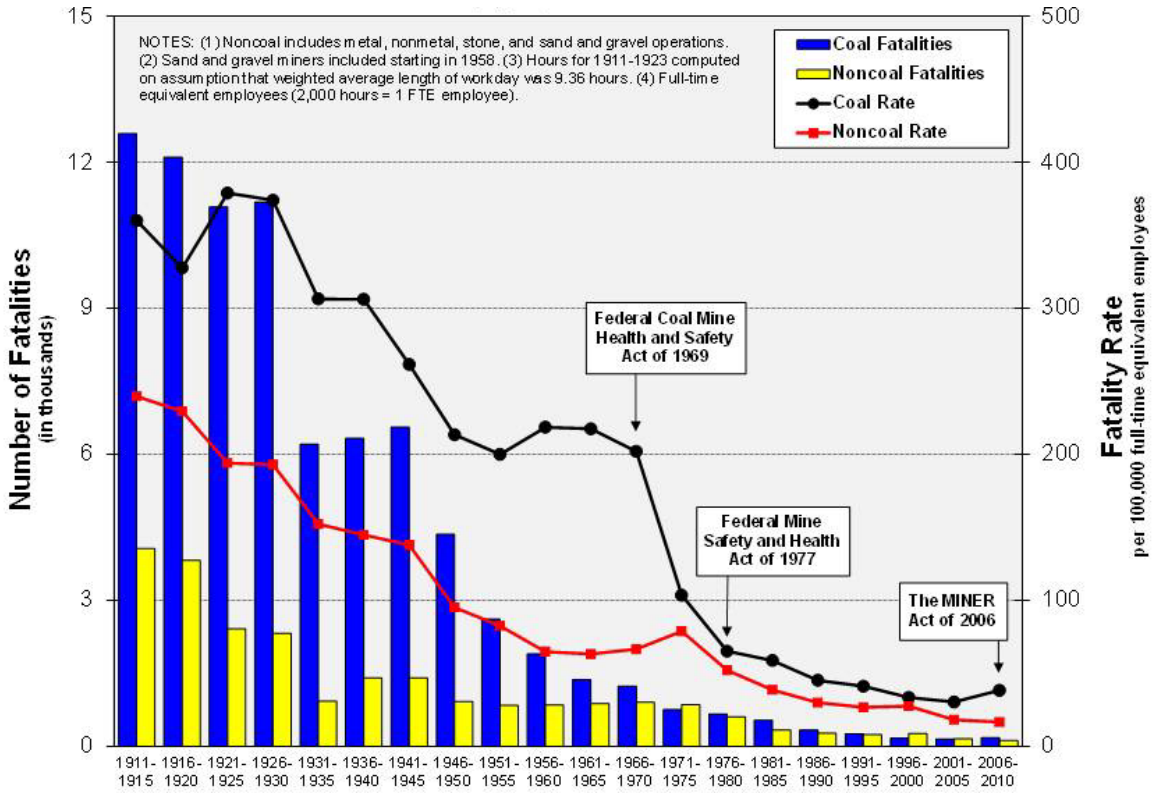

Figure 1-1 Number and rate of fatalities for mining industry, 1911-2010, (Office of Mine Safety and Health Research, 2012d)

However, when looking at the number and rate of fatalities for the first decade in modern underground coal mining, the trend is highly volatile (Figure 1-2). Caution should be exercised when exploring statistical measures for a low quantity of case studies, however it is important to understand and quantify the roots of this volatility.

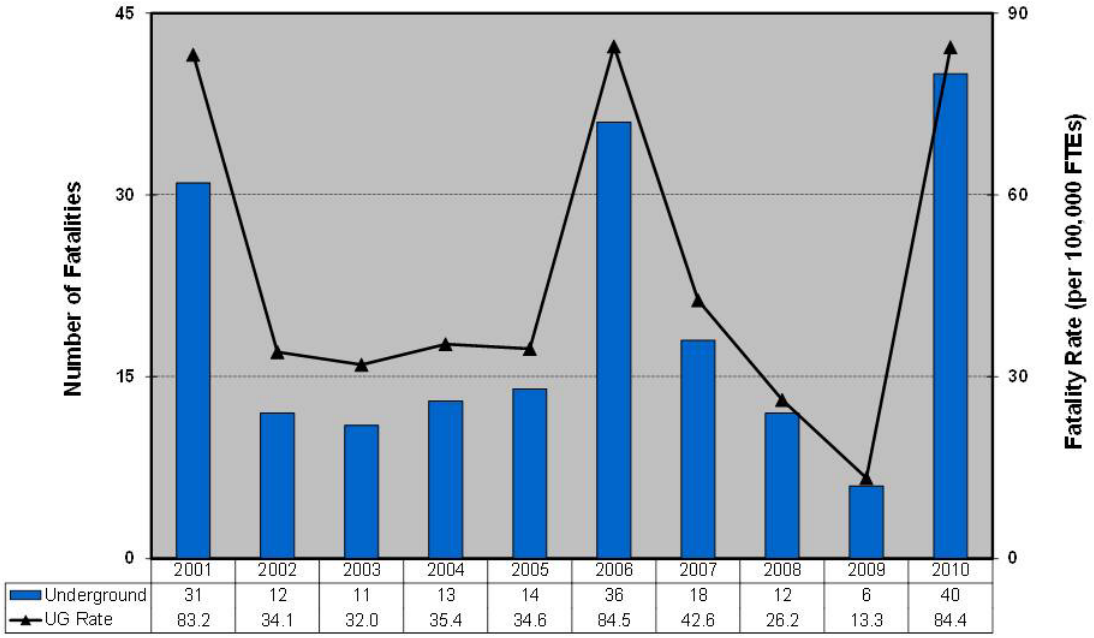

Figure 1-2 Number and rate of underground coal mining fatalities, 2001-2010 (Office of Mine Safety and Health Research, 2012a)

"Fall of ground" remained a significant source of fatalities for all underground mines between 2001 and 2010 (Figure 1-3). This category is second only to ignition/explosion of gas/dust, which has much higher potential to affect a greater population of miners in a hazardous manner. The Upper Big Branch accident in April 2010 resulted in the death of 29 coal miners as a result of a massive gas and coal dust explosion (MSHA, 2010). Furthermore, when examining nonfatal lost-time injuries in underground coal mines for the same period (Figure 1-4), fall of ground is again recognized as one of the leading causes of injury. Fall of ground is essentially a "catchall" phrase meant to indicate instabilities and failures involving rock mass. It is therefore unmistakable that ground control problems remain one of the most prevalent dangers in underground coal mining today, often resulting in injury and/or death to miners. Consequently, the advancement of knowledge in the rock mechanics discipline has the potential to greatly improve understanding of underground mining conditions and ultimately enhance the safety of coal miners.

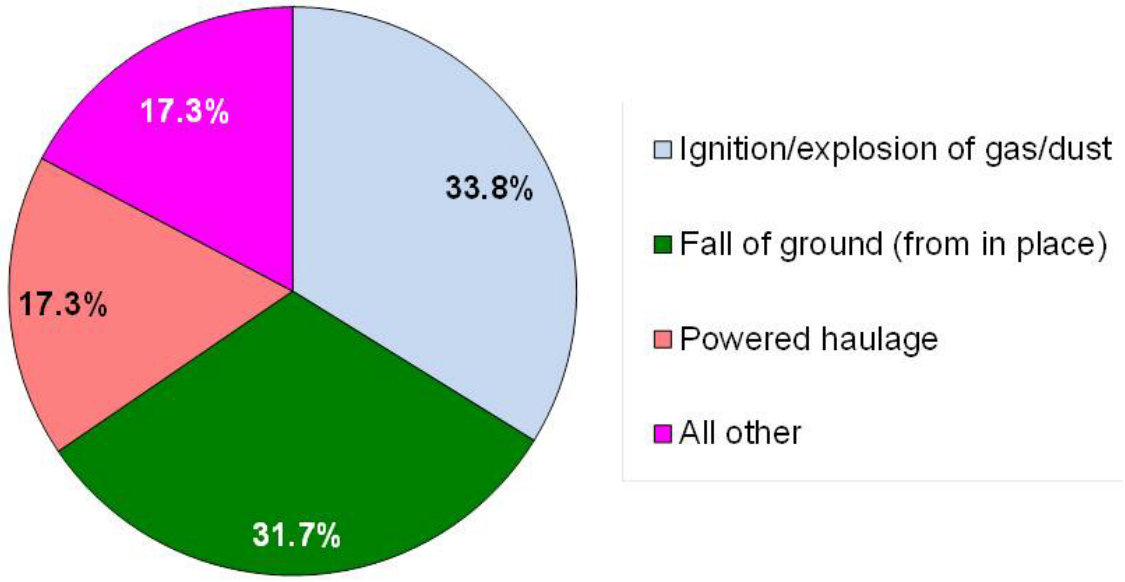

Figure 1-3: Fatalities by accident class, all underground mines, 2006-2010 (Office of Mine Safety and Health Research, 2012c)

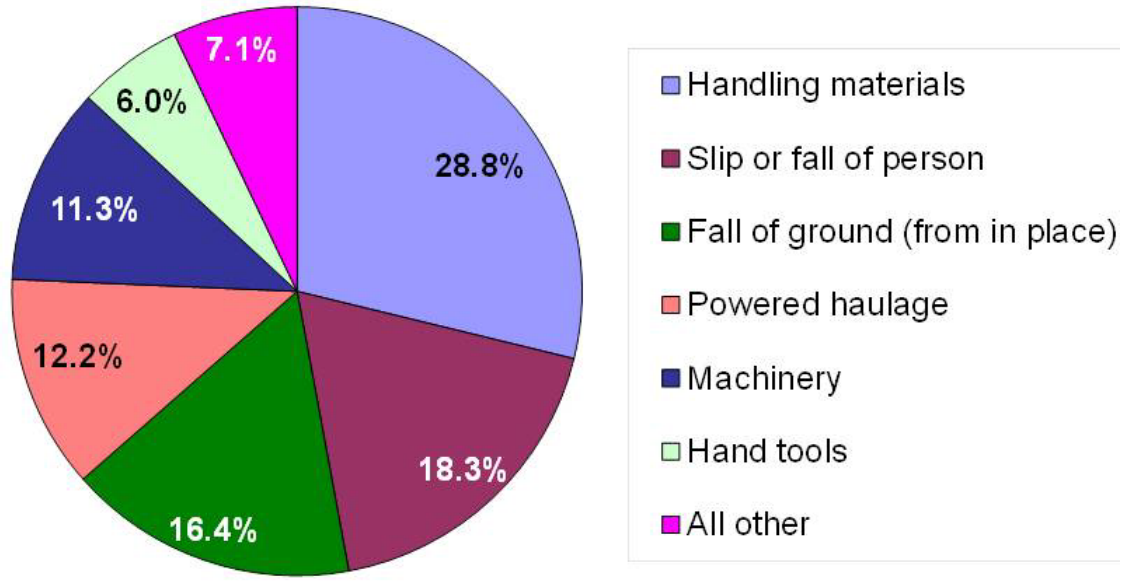

Figure 1-4 Nonfatal lost-time injuries by accident class, underground coal mines 2006-2010 (Office of Mine Safety and Health Research, 2012b)

1.2 Modern Context

One of more dangerous ground control problems in underground coal mining is a type of pillar failure known as a coal bump/burst. Coal bumps are a dynamic and catastrophic failure of a pillar(s) due to high stress, resulting in the violent ejection of coal into entries and crosscuts (Harris and Perry, 2014). Because coal bumps most often occur on active sections where exposure is highest, this type of failure is a significant risk to the safety of coal miners. Despite advances in technology and engineering knowledge of underground coal mining, coal bumps are still not well-understood and occur nearly every year in U.S underground coal mines. Bumps occur in both the Western U.S. and Appalachian coalfields and while the average number of occurrences has decreased, the quantity and pattern illuminates a persistent hazard to the safety of underground coal miners (Figure 1-5).

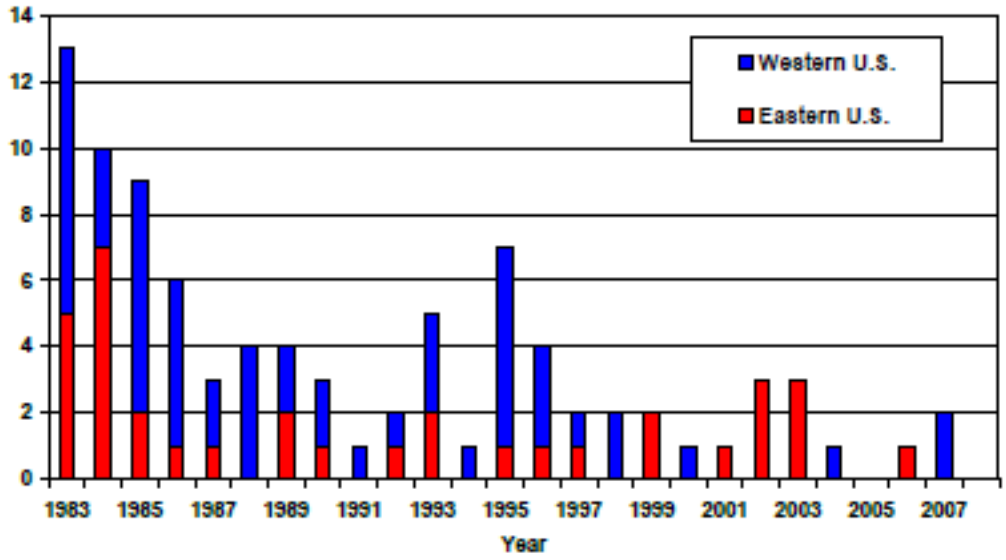

Figure 1-5 Frequency of annual coal burst incidents in U.S. coal mines, 1983-2007 (Office of Mine Safety and Health Research, 2010)

More recent coal bumps have illustrated the need for advanced research into the field of rock mechanics. The Crandall Canyon accident in August of 2007 resulted in the death of six workers and three rescue workers as a result of multiple coal bumps according to the report of investigation completed by MSHA (2007). This report attributed the bumps to high vertical stress and a "flawed mine design." Even as recent as 2014, two mine

workers were killed as the result of a coal burst at the Brody Mine No. 1 in southern West Virginia that occurred during retreat mining (Office of Mine Safety and Health Research, 2014). Consequently, improved understanding of coal pillar behavior and ground response is an endeavor necessary to further the understanding of coal bumps and further improve the health and safety of coal miners.

1.3 Research Goals

Research is necessary to develop improved understanding of coal pillar behavior, with particular focus on post-failure ground response and bump potential. This has been primarily accomplished through the use of numerical modeling techniques, which are becoming increasingly popular and useful tools for the coal mining industry. Numerical modeling allows for the prediction of stress, deformation, and stability for mine design purposes at both local and global scales. Many studies have presented the benefit of using this capability to evaluate a multitude of factors and conditions. Common research areas including examination of coal pillar behavior for varying roof/floor interface properties or the investigation of specific case studies. As such, numerical modeling provides a practical and efficient technique to evaluate the post-failure ground response of coal pillars for a variety of geological and geometrical environments with the ultimate goal of deriving/quantifying those factors or relationships which influence bump potential. The advent of modern numerical modeling efforts is an effort to circumvent many of the problems associated with geologic materials and the mining process, which unfortunately provide practical limitations to physical or analytical approaches. As a result of using a numerical approach, several stages including review, calibration, and validation are necessary to proceed with a new investigation. The project has been divided into five primary stages, Section 1.3.1 – 1.3.5, with brief descriptions of each.

1.3.1 Review

A comprehensive review of existing literature on the subject of geology, rock mechanics, pillar design, analysis techniques, and associated parameters has been completed. Particular focus was placed on those studies for which numerical modeling was used to model coal pillar behavior, post-failure ground response, or efforts were made to examine

bump potential or bump-related mechanisms. This review encompasses the following topics at a minimum:

- Coal Geology
- Ground Control Issues
- Coal Bumps
- Deep Cover Retreat Mining
- Multiple Seam Mining
- Roof/Floor Interface
- Strain Rate
- Analytical Methods
- Empirical Relationships
    - ARMPS 2010
- Numerical Techniques
    - Boundary Element Methods
    - Finite Element/Difference Methods
    - Discrete Element/Fracture Methods
- Constitutive Models
    - Mohr-Coulomb Model
    - Ubiquitous-Joint Model
    - Strain-Hardening/Softening Model
    - Hybrid Approaches
- Rock Fracture Models
    - Coulomb Sliding
    - Continuously Yielding
- Ground Response Curve
- Recent Findings

1.3.2 Calibration

Distinct element and finite difference modeling software were employed to reestablish foundational relationships precipitated from the studies referenced in the review stage. Critical parameters including the selection of constitutive model, joint/interface model

and properties, rock mass properties, zone density, model size, and boundary conditions were selected based on this initial review. Model calibration allowed for the selection of proper and consistent zone densities. Using the Ground Response Curve (GRC) and the defined numerical bump indicators, the models were numerically calibrated using reasonably accepted material properties and constitutive models. Since validation of this initial research approach is centered on the reestablishment of previous research studies as a primary mode of model calibration, modeling is not dependent on site-specific data but instead encompassed a range of rational material inputs using reliable constitutive relationships which are commonly employed in ground control applications.

1.3.3 Primary Tasks

Using these calibrated models, an array of expected site-specific geologic parameters and global geologic and geometric properties, including pillar interface, near-seam lithology, mining method, panel design, and other geometric considerations were examined, aimed at investigating the influence of variations in roof/floor composition, depth of cover, panel width, and mining methodology. The GRC was used to numerically and qualitatively identify those parameters which influenced pillar performance, ground response, and bump potential. Successful design is intrinsically identified as the appropriate pillar response in terms of plasticity state (yielding), pillar strain, low bump potential, and/or comparison to existing empirical and/or analytical standards. This is expected to include a numerical evaluation of the influence for the following parameters:

- Pillar Interface Properties
- Weak/Strong Roof/Floor
- Overburden Stress and Panel Width
- Side Abutment Loading
- Barrier Pillar Deformation

1.3.4 Projected Goals

Upon model validation and the investigation of said parameters, new relationships which have potential to provide indicators of ground response, pillar performance, post-peak pillar behavior, and the likelihood of success/stable failure versus unstable failure, were

investigated. Important findings which contribute to new understandings of squat coal pillar behavior in bump-prone ground were summarized. These findings were then employed to formulate new understanding of coal pillar performance and post-failure ground response which aids in the improvement of criteria for determining mine-specific bump potential, otherwise known as “red zones”. Red zones are those areas qualitatively designated as higher risk for bump potential and are often utilized by mining engineers in the mine design process.

1.3.5 Supplemental Study

Numerical modeling studies typically necessitate validation studies to approve of the use of specific material models, properties, assumptions, and ultimately results. Validation of geomechanical problems is especially important. However, this study relies on the calibration of the previously identified parameters not with specific data but within the confines of a range of traditionally accepted values and modes. Direct validation of this investigation will not be circumstance to the pragmatism of results. Nonetheless, a case study was conducted which briefly incorporated the new conclusions regarding localized influences on pillar behavior and global stress response using the Ground Response Curve to demonstrate the quantitative ability to assess bump potential.

1.4 Novel Contribution to Research

The objective of this dissertation was to elevate the field of rock mechanics and contribute to the industry’s understanding of coal pillar behavior by numerically evaluating several geologic and loading parameters which were believed to influence coal bump potential. Historically, empirical and analytical relationships have been used to advance the knowledge of coal pillar design in underground workings; however, these approaches lack the ability to apply appropriate site-specific geologic properties to efficiently investigate a variety of expected loading conditions and mechanisms. Recent numerical efforts have provided a solid foundation for better understanding of coal pillar behavior. Furthermore, these numerical techniques have demonstrated the ability to capture the important mechanisms which are typically associated with coal bump events. However, a comprehensive investigation of the mechanics, post-peak behavior, and bump potential for squat pillars has not been directly investigated. Following this study, it is

believed that those parameters which influence bump potential can be more precisely identified and quantified with the aim of improving the identification of bump potential, or "red zones". In summary, this dissertation sought to improve the fundamental knowledge in rock mechanics through the following five objectives:

1. Improving Understanding of Squat Coal Pillar Behavior
    - ✓ As coal operations develop deeper and more difficult reserves, the use of higher W/H ratio pillars has increased, necessitating further understanding of the behavior of these squat pillars. Squat pillars are more susceptible to hazardous instabilities such as bumping. Existing research into the behavior of squat coal pillar behavior is limited.
2. Developing Further Understanding of Post-Peak Coal Pillar Behavior
    - ✓ The use of more squat pillars is restricted by the need to minimize improve economics and recovery, demanding that more critically sized pillars be used. As a result, the need to successfully differentiate between a stable versus unstable failure becomes increasingly important to both safety and the bottom line. While existing research has somewhat examined this topic, the studies have been limited in scope or practicality.
3. Elevating the Importance of Coal Bump Potential Recognition
    - ✓ Coal bumps present a unique but severe threat to the safety of coal miners. Recent bump events at Crandall Canyon and others has renewed interest of and demonstrated the need to reinvest research efforts into the topic.
4. Quantifying the Impact of Individual Geologic/Geometric Components
    - ✓ Past empirical studies have successfully identified geologic and/or geometric considerations which seemingly increase bump potential. Geologic composition of the seam, roof, and floor, along with the overburden and mining methodology, obviously has a profound impact on coal pillar behavior. However, a comprehensive numerical study which isolates, examines, and quantifies many of these components has not been undertaken.
5. Refining Existing Guidelines for the Development of Coal Bump "Red Zones"

- ✓ Bump “red zones” are great tools for mining engineers to communicate the apparent increase bump potential for a specific location to operations and personnel. However, the use and applicability has mostly been limited to site specific locales. Consequently, the refinement of existing guidelines which have been used to develop these zones is necessary to provide uniformity to both industry and government.

2 Literature Review

2.1 Overview

Underground coal mining is primarily carried out using one of two mining methods: room-and-pillar and longwall mining. With the room-and-pillar mining technique, coal pillars are left intact to support the overburden as development recovers coal from entries and crosscuts, leaving behind a "checkerboard" like array (Figure 2-1). Many times operators also conduct what is known as "retreat mining" or "pillaring". This secondary process involves the extraction of the coal pillars which were initially left intact, leading to a systematic and controlled failure of the overburden that increases recovery of the reserve and may enhance productivity of the operation.

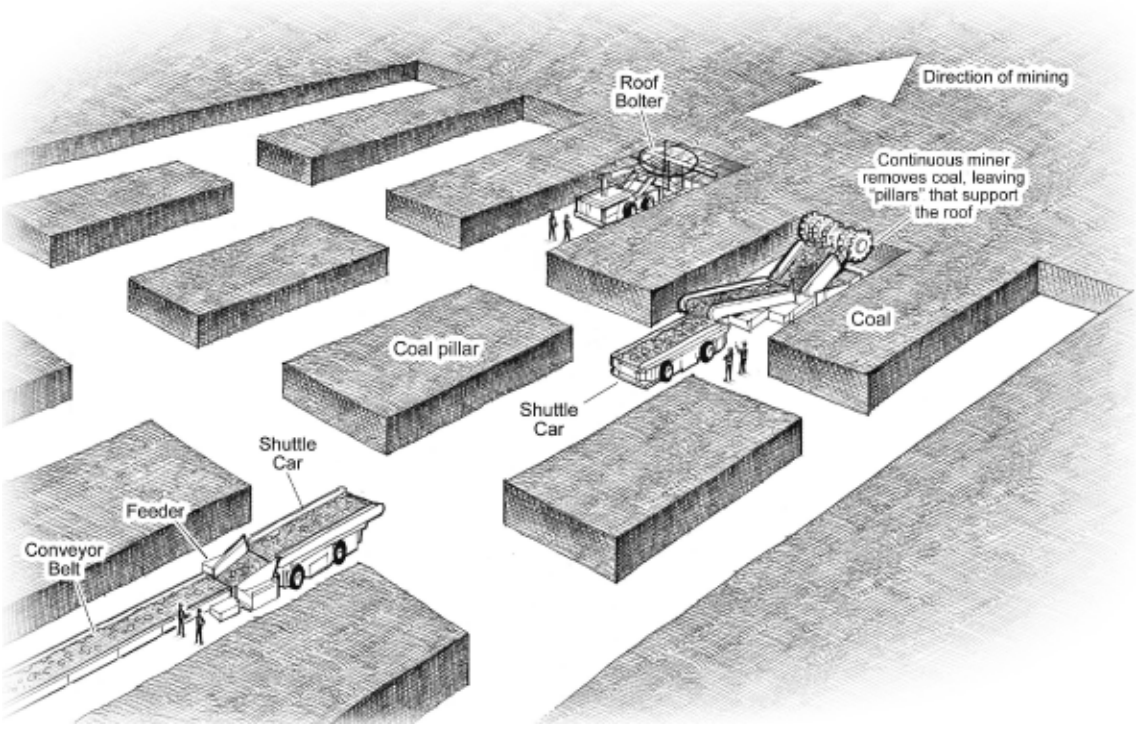

Figure 2-1 Typical schematic of room and pillar mining demonstrating coal pillars left intact to support overburden (Arch Coal, 2009)

Longwall mining involves the development of a large block of coal (typically hundreds of feet in width and thousands of feet in length) using traditional room and pillar methods, leaving developments which are known as gate roads. Once this large block has been developed, coal will be extracted from the face by the longwall shearer (Figure

2-2). The face is temporarily supported by hydraulic shields, which methodically advance with the face and allow the immediate overburden behind the shield to fail and cave. This method is inherently more capital intensive; however operating costs, recovery, and efficiency are typically improved when compared to the room-and-pillar mining method.

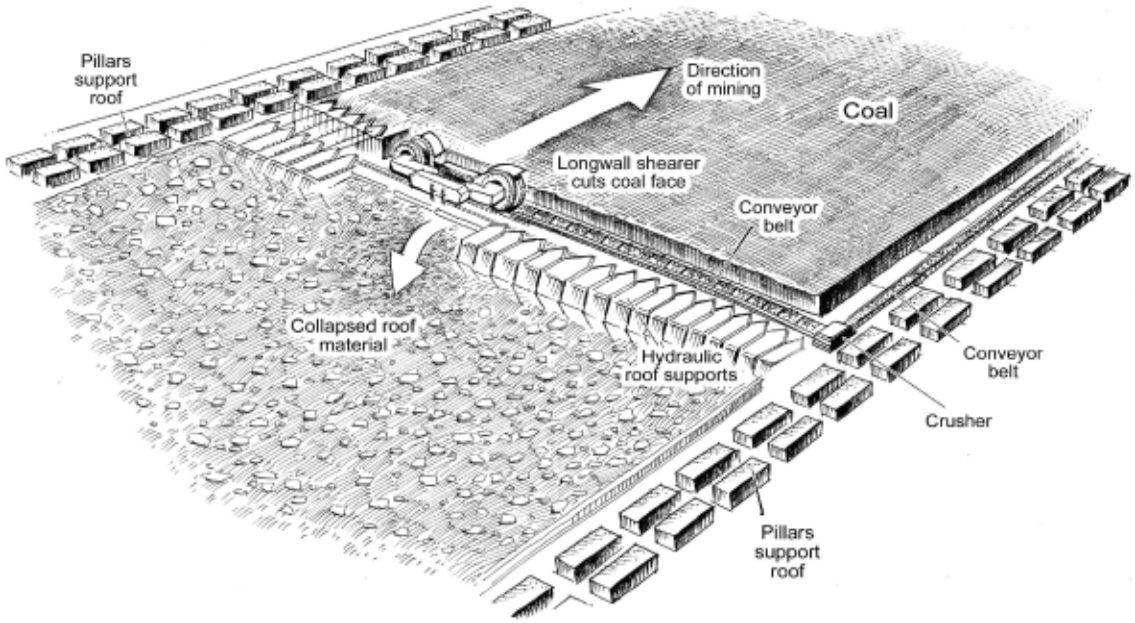

Figure 2-2 Typical schematic of longwall mining demonstrating gate entry pillars left intact to support overburden and facilitate mining process (Arch Coal, 2009)

While each of these underground coal mining methods is often considered unique, the need to solve complex ground control problems and ensure adequate stability is not. Peng (2008) defined ground control as "the science of studying and controlling the behavior of rock strata and coal in response to mining operations" or "the application of rock mechanics principles to mining operations." Jeremic (1985) described strata mechanics as "the theoretical and applied science of the mechanical behaviour of rock." Underground coal ground control studies must not only consider the properties/behavior of the coal seam itself, but also those of the nearby strata and overburden. Ground control issues are prominent with both of the aforementioned mining methods and are often considered within the context of two categories: local stability and global stability.

Local stability is characterized as the stability of smaller regions which are controlled by limited factors including roof bolting, standing support, and even pillar design. It is typically the result of localized geologic and stress influences. The consideration of roof falls or rib damage is often reflected within this context. Barczak (2011) defined local stability as the "control of the near-seam ground around the mine opening and pillar ribs typically through support intervention." Global stability is defined as the stability and behavior of a large system of underground workings and is predominantly controlled by pillar design. It is the result of broader geologic and stress conditions. According to Barczak (2011), global stability involves the control of the overburden primarily through pillar design and mine layout. While these two classifications are often considered as separate and distinct, it is important to recognize that they actually represent a continuum whereby both local and global stability are governed by similar factors. The understanding of this continuum is therefore imperative towards the understanding of any ground control problem.

2.2 Coal Geology

Coal bearing strata in the United States primarily consists of sequences of clays, coals, shale, siltstones, sandstones, and limestone among others, each with its own material properties and behavior dependent on deposition, location, and time. Unlike many engineering disciplines, mining engineering is uniquely challenging as geologic material must be handled in its natural state and the practice of rock mechanics involves the acknowledgement of complications due to variability in in-situ rock properties (Peng, 2008). These complications are inherently a result of deposition and stress. The depositional environment influences the thickness, extent, strength, and discontinuities for each lithology (Peng, 2008). More importantly, the depositional environment also affects the types of geologic discontinuities or anomalies, including pinch outs, horsebacks, kettle bottoms, slickensides, bedding planes, laminations, fractures, and faults (Peng, 2008). The author emphasized the importance of geology on the study of ground control, though it was recognized that the importance of geology to mining engineering has at many times not been fully considered in the study of ground control problems. This is at least partly due to the difficulty and/or impossibility in obtaining

accurate material properties for rock masses which are necessary to an engineering representation (Peng, 2008).

Jeremic (1985) indicated that it is important to note the influence that geological and structural factors have on mine design and stability. The author also recognized the importance of depositional environment, burial history, and orogenic history on the deformation and stability of coal bearing strata, detailing the following factors which should be considered in any analysis of coal bearing strata:

- The geological representation of coal bearing strata as an alternative to a purely engineering or mechanical representation
- The importance of sedimentology whereby stability is at least partially controlled by sedimentary features in the coal seam or nearby strata
- The recognition that the diagenesis of coal bearing strata is an important element in mine stability, deformation, and failure of mine roof and floor
- The role tectonics plays on the deformation history and subsequent failure mechanism of coal bearing strata

While many standard engineering tools (e.g. numerical methods) have been used to study ground control problems, the nature and properties of coal geology must be incorporated for any such method to have meaningful results. Therefore mining engineers have sought to bridge geological and engineering approaches by acknowledging the need to employ hybrid methodologies: those which rely on traditional engineering concepts but incorporate important geologic parameters such as large-scale discontinuities and the scaling of rock mass properties. These hybrid methods have traditionally relied on empirical evidences to derive key relationships; however, empirical methods do not fully account for localized properties or significant deviation from the case studies considered. As a result, empirical methods may be limited and the use of methods which incorporate site-specific data is becoming more popular and appropriate.

The prediction of rock mass behavior necessitates a model that must sufficiently represent rock reality; that is, “the model should contain the necessary physical variables mechanisms, and associated parameters – and be able to simulate the perturbations

introduced by engineering activities" while accommodating "the discontinuous, inhomogeneous, anisotropic, and non-elastic behavior of rock masses" (Jing and Stephansson, 2007). These facts have led to an accelerated use of numerical methods which have the capacity to accommodate these parameters and properties.

2.3 Ground Control Issues

Underground coal mining invokes the need to understand many scientific fields, including but not limited to electrical engineering, fluid dynamics, chemistry, and mechanics of materials. One of the most important mining engineering disciplines is rock mechanics, which involves the derivation of governing principles seeking to identify and understand the factors which influence rock and rock mass behavior. Because the mining process seeks to extract and control geologic material, which is natural, inhomogeneous, and discontinuous, difficulties often arise which can unfortunately result in injury and/or death. Underground coal mines are particularly susceptible to ground control problems because of the highly discontinuous nature of coal seams and nearby strata resulting in a relative weakness when compared to other types of rock mass (e.g. sandstone) or engineered material (e.g. steel).

Figure 2-3 Example of rib failure due to excessive stress (Office of Mine Safety and Health Research, 2011)

Ground Control problems in underground coal mining can take many forms, including rib rolls (Figure 2-3), roof falls (Figure 2-4), floor heave, and pillar failure (Figure 2-5).

Compared to other underground health and safety concerns, these types of ground control problems pose a significantly higher risk to underground coal miners as demonstrated by the high injury/fatality rates. Unfortunately, the potential for these ground control problems to occur appears to be increasing as a result of progressively more difficult reserves. The continual depletion of easier coal necessitates that operations exploit deeper reserves, which are often in more difficult geologic conditions and are more likely to encounter ground difficulties associated with higher stress and/or multiple seam mining.

Figure 2-4 Example of roof fall covering Mobile Roof Support during retreat mining (Office of Mine Safety and Health Research, 2012e)

2.4 Coal Bumps

Coal bumps are violent failures of coal pillars which provide a rare but dangerous threat to underground coal miners. They are the result of the energetic release of stored strain energy (Harris and Perry, 2014). As the outer pillar elements become overstressed and the onset of yielding begins, load is transferred internally towards the core of the pillar.

While the core of the pillar is much stronger, benefiting from the confinement generated as the pillar interfaces impose frictional restraint, excess stress may allow for instability within these inner core elements (Harris and Perry, 2014). If this failure occurs in an unstable manner, then the outer pillar elements may be released and ejected violently towards entries and crosscuts, a phenomenon known as a coal bump or burst.

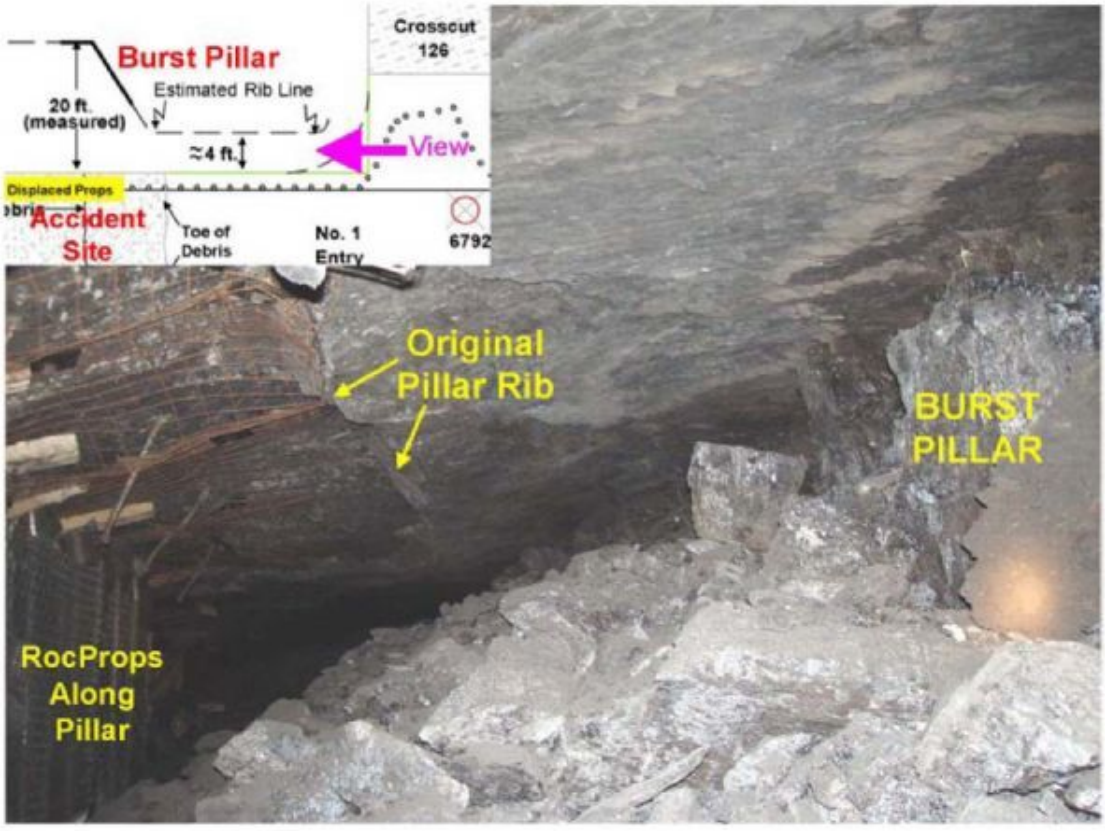

Figure 2-5 Bump damage outby Crandall Canyon Accident Site (MSHA, 2007)

While high vertical stress is unquestionably a factor in all bump events, Iannacchione and Zelanko (1995b) cited three primary environmental factors that impact the occurrence of coal bumps: geology, stress, and mining method. The authors also identified three principal mechanisms associated with the occurrence of bumps: high vertical stress, dynamic shock, and de-confinement. Pressure bumps are generally considered to be static events whereby the pillar core becomes overstressed and lacks sufficient pillar strength (Harris and Perry, 2014). However, dynamic stresses may also be a significant

mechanism that triggers both dynamic shock and de-confinement processes. Dynamic stresses may be imposed from seismic vibrations caused by failure of near-seam strata or pillar strength may be abruptly lost if de-confinement occurs, often resulting in the dynamic release of stored strain energy (Iannacchione and Zelanko, 1995b). Research efforts seeking to improve our understanding of these dangerous failures must adequately consider a range of these environmental factors and contemplate the processes associated with these three mechanisms.

Coal bumps have been the focal point of many previous research efforts; however, the methodologies employed have taken many different approaches. A fundamental approach to understanding these mechanisms has widely been employed (Iannacchione and Zelanko, 1995a; Iannacchione and Zelanko, 1995b; Maleki, 1995; Iannacchione and Tadolini, 2008; Whyatt, 2008) while statistical analysis has also been used (Mark, 2009). Site/mine specific bump case studies (Hoelle, 2008; Newman, 2008) have also provided valuable insight into the occurrence of bump events. The results of these efforts typically advocate for or devise bump potential awareness through the development of bump "red zones". These zones are areas where bump potential is elevated as the result of a coalescence of multiple bump factors/mechanisms.

While bump "red zones" have been in use in the mining industry in areas of bump prone ground and provide necessary awareness of elevated bump risk, the Office of Mine Safety and Health Research (2010) concluded that research should be conducted to improve understanding of coal bumps and develop enhanced bump risk guidelines. This study also advocated for further research into the understanding of pillar loading and deep cover coal mining in an effort to enhance modeling accuracy, particularly noting studies into pressure arch theory, squat coal pillar behavior, and the impact of roof/floor strata on bump potential.

The Office of Mine Safety and Health Research (2010) has advocated for the use of pre-mining burst risk assessments, synonymous with bump "red zones" (Figure 2-6). The study concluded that the risk for coal bumps becomes elevated when the following factors are present:

- Elevated overburden depth
- Rapid changes in depth of cover
- Mining that crosses remnant structures in previously mined seams
- Massive sandstone(s) in close proximity to the coal seam in either roof or floor
- Sandstone channels that may concentrate stress
- Faults
- Rapid changes in seam structure

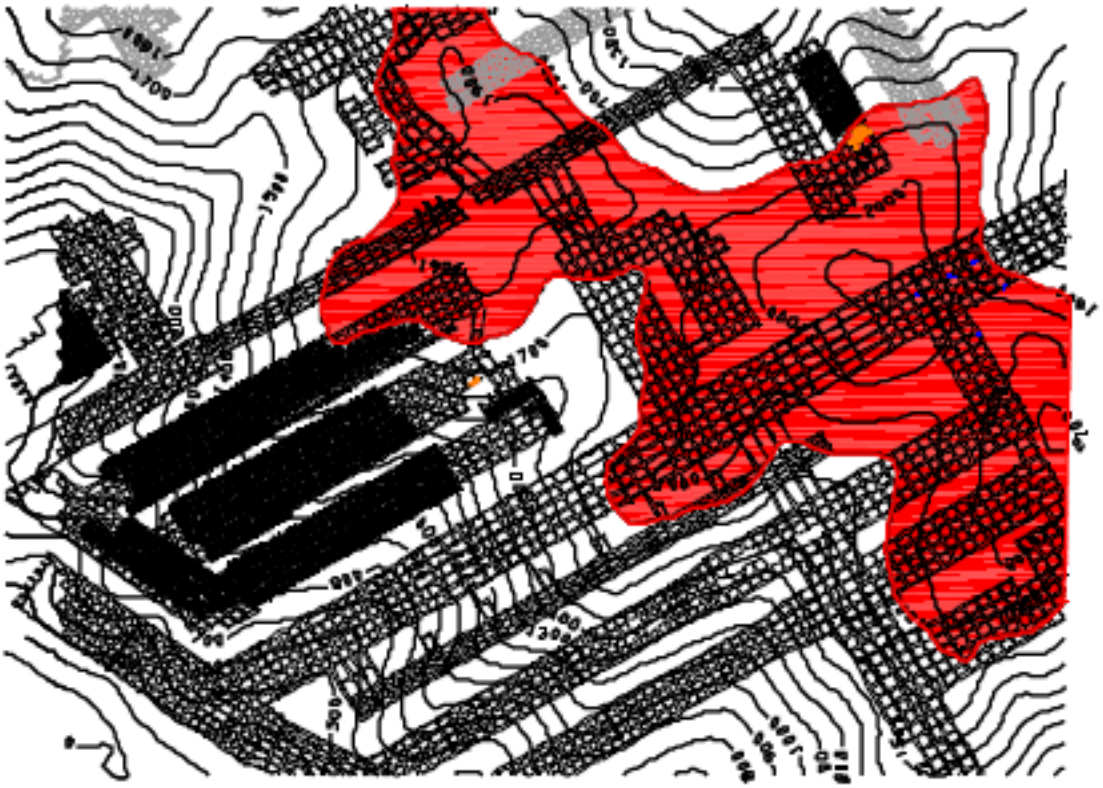

Figure 2-6 Example of bump red zone defined by overburden depth only (Office of Mine Safety and Health Research, 2010)

2.5 Deep Cover Retreat Mining

A prerequisite for many ground control problems, and particularly coal bumps, is high vertical stress. Given the focus on coal bumps and the need to include deeper overburden mines in the database, a study was conducted by Mark (2010) to update the ARMPS (Analysis of Retreat Mining Pillar Stability) empirical software. One of the biggest

updates was the development of the pressure arch model of pillar loading (Figure 2-7) that has been observed in deep cover coal mines as a replacement to the traditional tributary area loading concept.

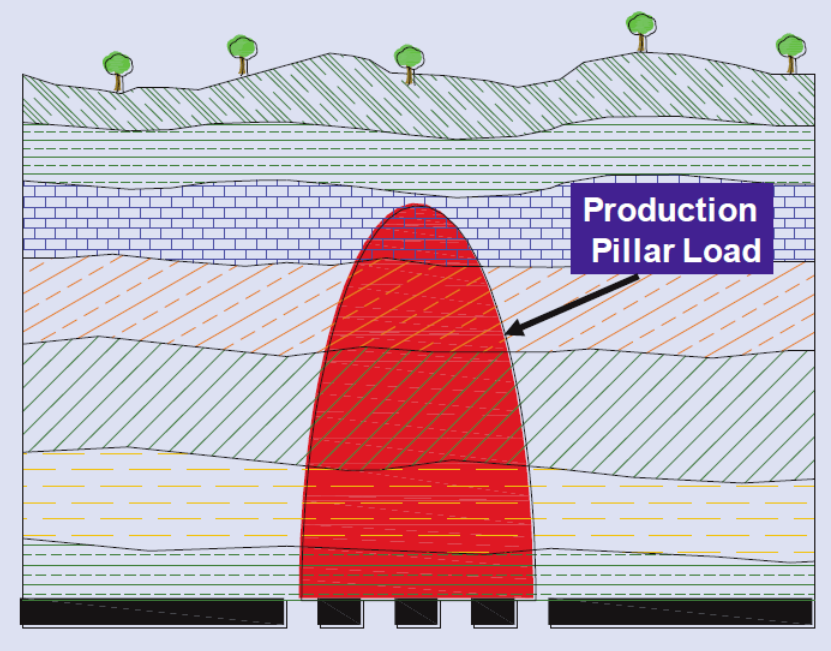

Figure 2-7 Conceptual pressure arch loading for underground coal mine (Mark, 2010)

Mark (2010) subsequently conducted a secondary numerical study using FLAC to evaluate the pressure arching mechanism and concluded the following two factors:

- Massive and strong overburden lithology enhances the development of a pressure arch, which is believed to be the result of the relative stiffness difference between it and the coal seam
- Narrower panels and deeper cover increases the formation of pressure arching

The study also correlated the pressure arch concept to the Ground Response Curve, a concept which quantitatively describes the ground convergence response to decreasing support pressure, and used the findings to develop an empirical pressure arch factor relationship which reduces the tributary area load as a function of panel width and overburden depth.

2.6 Multiple Seam Mining

Multiple seam mining interactions are the result of stress or displacement influence from overmining and/or undermining with respect to the active coal seam and are often associated with severe ground control problems. Zipf (2008) identified four factors which are the result of multiple seam interactions:

- Vertical Stress Concentration
- Horizontal Stress Concentration
- Stress Redirection
- Bedding Plane Slip

Ultimately, multiple seam mining has the potential to affect underground coal mines through both stress concentration and damage in the active seam from tensile stresses due to potential subsidence concerns (if mining exists below the active seam). Zipf (2008) identified many of the factors that govern the severity of multiple seam interactions:

- Overburden Depth
- Interburden Thickness
- Seam Thickness
- Immediate Roof Quality
- Interburden Geology
- Mine Layout

Pressure arching and particularly the practice of retreat mining redistributes load to surrounding strata, resulting in the potential for high stress concentration that may be observed in other seams with high overburden or insufficient interburden thickness. The Office of Mine Safety and Health Research (2010) stated that approximately 80% of deep cover retreat mines are located in a multiple seam environment with an interburden thickness less than 200 feet. While most of the coal bumps in the Central Appalachian coalfields have occurred during retreat mining, Newman (2007) documented multiple coal bumps that occurred on development in Southeastern Kentucky. The study cited high overburden and severe stress concentrations from underlying workings that contained large barrier pillars and/or gob-solid boundaries at relatively low interburden

thickness. Consequently, multiple seam mining has the potential to be a significant source of high vertical stress that is a widespread requirement for a coal bump to occur.

2.7 Roof/Floor Interface

The strength and behavior of near seam strata, and particularly the response of the roof/floor contact or interface, is one of the most important factors that influences pillar strength, behavior, and mode of failure. Empirical methods have traditionally been relied on to calculate pillar strength; however, these relationships do not consider the influence of the pillar interface. Mark (1999) emphasized that much more work remains to answer the longstanding questions for pillar designs, however the author principally noted that "much remains to be learned about the mechanics of squat pillars and roof-pillar-floor interactions", citing the lack of a unified approach "to determine frictional characteristics of these contacts".

Lu et al. (2008) advocated for the use of a bi-linear failure model (Figure 2-8) for the peak and residual strength of roof/floor interfaces when modeling coal pillars following the work from direct shear testing of Appalachian coals (Peng et al., 1983). This method yields two linear segments which delineate the shear strength envelope. The first segment is defined by the initial friction angle, $\emptyset$, up to a value of normal stress σ_T. At this point, a residual/basic friction angle, $\emptyset_b$, dictates the strength envelope, which if extended to zero normal stress would result in cohesion C_j. Using this model, Lu et al. (2008) was able to demonstrate the variations in minimum pillar stress (confinement) that may be generated for various interface cohesions and geometries (Figure 2-9). Using the assumption of a bi-linear interface model, Perry et al. (2013) numerically investigated various W/H ratio pillars, interface cohesions values, and near-seam lithology. The authors were able to demonstrate the dependence that peak pillar strength and post-peak behavior have on interface strength. Of particular importance was the fact that this dependency was more pronounced for squat pillars which have high W/H ratios.

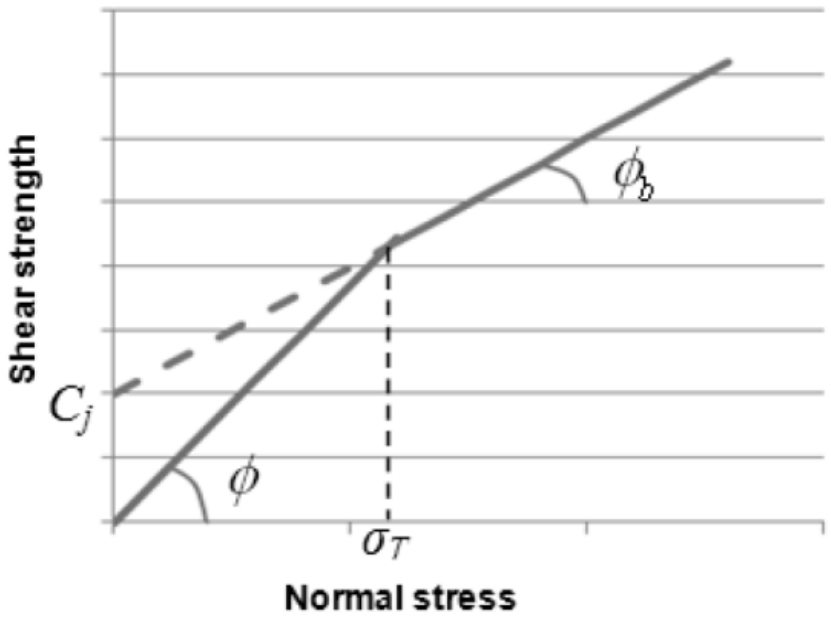

Figure 2-8 Idealized bi-linear model for coal pillar interface (Lu et al., 2008)

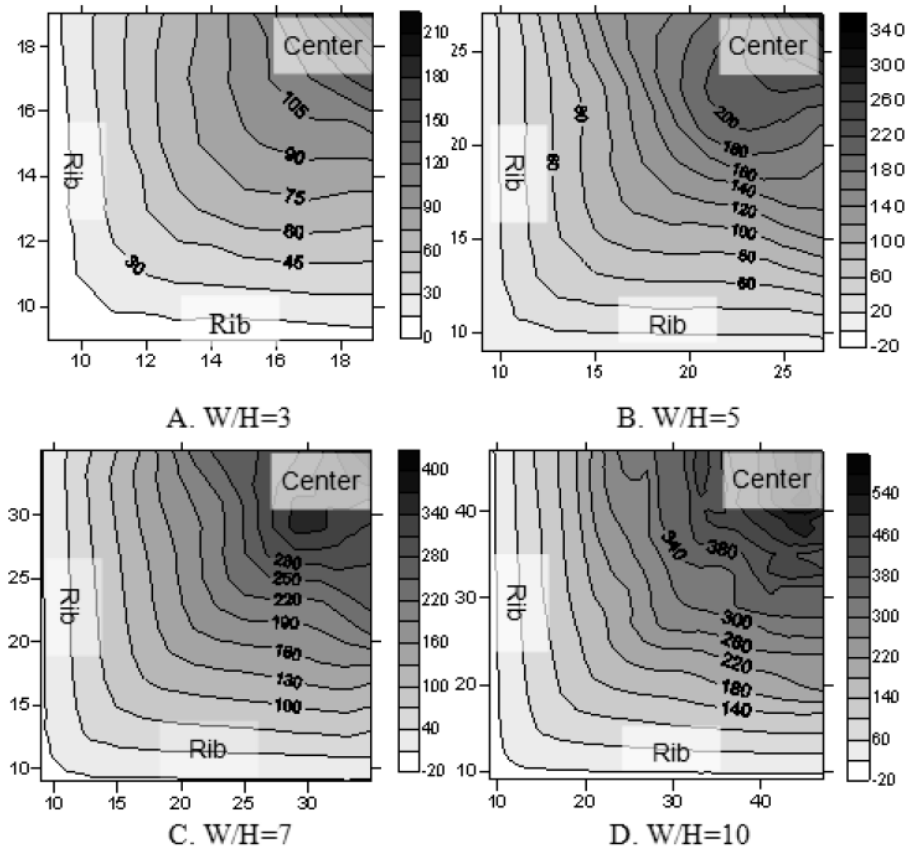

Figure 2-9 Pillar confinement contours for various pillar W/H ratios with constant interface cohesion (Lu et al., 2008)

2.8 Strain Rate

While Iannacchione and Zelanko (1995b) noted many of the environmental factors and mechanisms associated with coal bumps, one important factor not specifically discussed that is associated with the behavior of the rock materials under dynamic conditions is strain-rate dependency. Rocks are strain-rate sensitive and coal bumps generally occur at high-strain rate conditions. Testing of dynamic material parameters for rocks has been advanced according to the development of accurate dynamic loading techniques, which are those experimental techniques that can generate a consistent and reproducible dynamic load during testing of a specific material. Strain-rate sensitivity is observed when the stress-strain relationships or material properties for a specific material are dependent on the strain-rate which is applied. The relationship between strain-rate and material properties can be conceptualized according to the changes of the initial elastic modulus and the ratio between the dynamic and static strain at peak stress. Testing geologic material under high-strain rates has been done for a numbers of lithology types such as limestone, sandstone, marble, and granite (Ai and Ahren, 2006; Kimberley and Ramesh, 2011; Li et al., 2005; Singh et al., 1989).

Singh et al. (1989) examined the effect of strain rate on the mechanical behavior for a variety of rock types, such as the influence on peak strength, elastic modulus, failure strain, and failure behavior. The authors found that the failure strength increased as the strain rate increased, particularly noting a more pronounced effect for sandstone specimens. The difference in strain rate dependency was attributed to differentiation in rock composition, particularly citing the propagation along transgranular fractures. Furthermore, the study also cited an increase in elastic modulus with an increase in strain rate while ultimate strain was found to be independent of strain rate. Qian et al. (2009) concluded similar relationships and attempted to explain the sensitivity of rock strength to strain rate. The authors classified this result into two mechanisms, a thermo-activated mechanism and a macro-viscous mechanism, while advocating for a strain-rate dependent constitutive model.

Zhang and Zhao (2013) provided a comprehensive review of dynamic experimental techniques and mechanical behavior of rock masses, attempting to define and explain the

strain rate effect. The authors indicated that the physical mechanisms resulting in a strain rate dependency may be attributed to the following:

- Laboratory machine inertia
- Thermal activation effects due to temperature
- Viscous mechanisms associated with micro fractures
- Micromechanical-based effects from the quasi-brittle and inhomogeneous nature of rock materials:
    - Stress concentrations due to microscopic redistribution mechanisms
    - Change in failure mechanism due to fracture propagation

2.9 Analytical Methods

Analytical methods seek to apply the laws of physics to mathematically derive solutions to problems in a traditional engineering sense. One of the most popular analytical approaches to solving coal pillar design issues is the Wilson equation, which involves the derivation of coal pillar strength as a function of site-specific material properties using a customary solid mechanics approach (Figure 2-10). Scovazzo (2010) advocates pillar design based on the Wilson equation using the following procedure:

- Collection of rock/coal core samples
- Laboratory strength testing for roof, coal, and floor material
- Analysis of laboratory testing results including the development of proper failure envelopes/criterion
- Development of site-specific pillar strength equation based on Wilson approach
- Determination of pillar stress and resulting stability

Scovazzo (2008) detailed the advantages of the Wilson equation, citing an ability to predict the stress distribution from rib to pillar core based on the premise that vertical stress will result in compression and a horizontal Poisson response, which is resisted by the shear resistance of the pillar interfaces. Furthermore, the author noted the flexibility of the formulation to handle site specific data and failure criteria. Starting with the basic formulation following the free body diagram (Figure 2-10), the Wilson equation starts with the following form (Equation 2.1) presented by Wilson and Ashwin (1972):

$$(\sigma_H + d\sigma_H)ml - (\sigma_H)ml = (d\sigma_H)ml \quad 2.1$$

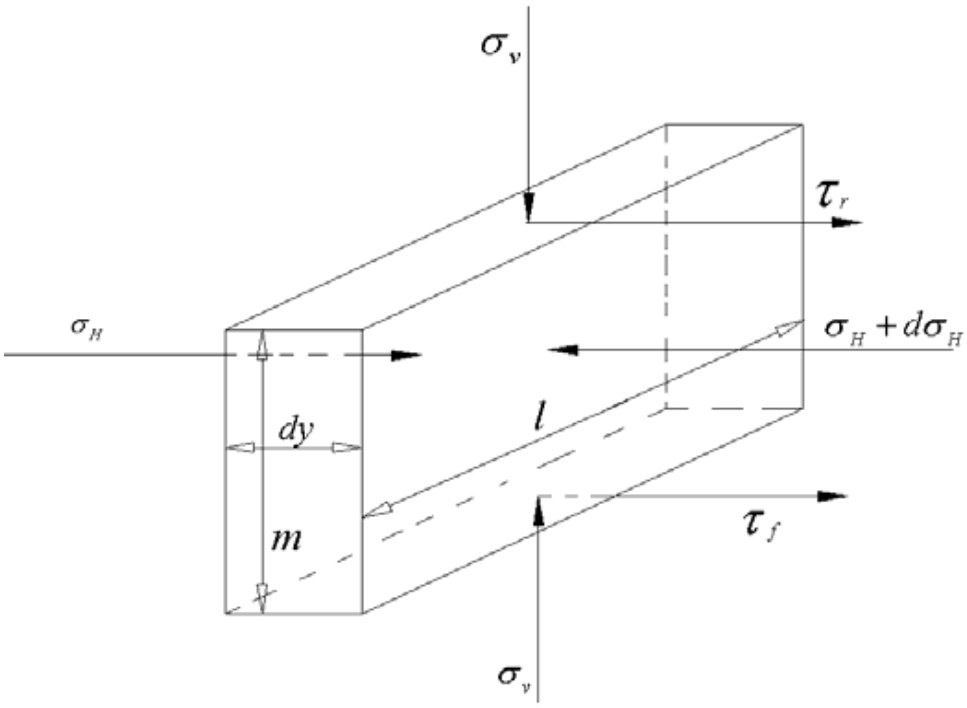

Figure 2-10 Free body diagram following Wilson Equation (Scovazzo, 2010)

Scovazzo (2010) then defined the horizontal stress over the element width as follows (Equation 2.2):

$$dy = (d\sigma_H)ml \quad 2.2$$

Horizontal stress is resisted by the available sum of the shear strength of the pillar roof and floor interfaces, τ_R and τ_F (Equation 2.3) (Scovazzo, 2010):

$$(\tau_R + \tau_F)dy = (d\sigma_H)m \quad 2.3$$

If y is the perpendicular distance into the pillar from the rib, then simplification and setting the limits of integration results in the following integral form (Equation 2.4) (Scovazzo, 2010):

$$y = m \int_{\sigma_C}^{\sigma_{max}} \frac{d\sigma_H}{(\tau_R + \tau_F)} d\sigma_V \quad 2.4$$

Coal is often assumed to behave following the Carter failure equation, which has derivative as shown on Equation 2.5 (Scovazzo, 2010):

$$d\sigma_H = -\frac{\sigma_T}{R\sigma_C}\left(\frac{\sigma_V}{\sigma_C}\right)^{\left(\frac{1}{R}-R\right)} d\sigma_V \qquad 2.5$$

Finally, if the roof and floor rock is assumed to follow the Hoek-Brown empirical formula, then the final form of the Wilson equation may be set as Equation 2.6 (Scovazzo, 2010):

$$y = m \int_{\sigma_C}^{\sigma_{max}} \frac{-\frac{\sigma_T}{R\sigma_C}\left(\frac{\sigma_V}{\sigma_C}\right)^{\left(\frac{1}{R}-R\right)}}{A_R\sigma_R\left(\frac{\sigma_V}{\sigma_R}-T_R\right)^{B_R} + A_F\sigma_F\left(\frac{\sigma_V}{\sigma_F}-T_F\right)^{B_F}} d\sigma_V \qquad 2.6$$

Where m, R, A, T, and B = Curve Fitting Parameters

R, F = Subscripts representing property for Roof or Floor

σ_{max} = Maximum Vertical Stress at Pillar Core

σ_T = Tensile Strength, Coal

σ_C = Compressive Strength, Coal

σ_R = Compressive Strength, Roof

σ_F = Compressive Strength, Floor

σ_V = Vertical Stress at y

y = Distance into the pillar

The benefit of this approach is that the failure criterion for roof, floor, and coal elements may be modified to reflect any form following site specific data, and additional roof or floor components may be added (Scovazzo, 2010). Nonetheless, such an analytical approach relies on laboratory testing of materials which must be revised ad-hoc to mirror changes in conditions, must be properly scaled, and fundamentally does not consider the large-scale fractures or discontinuities which may control pillar behavior. This flaw may constitute a part of the reason that Scovazzo (2010) typically suggests a safety factor

ranging from 2 to 3 when using the Wilson analytical procedure, suggesting unrealistically high pillar strength when calculated. Furthermore, pillar loading must still be estimated for comparison with pillar strength and the calculation of pillar stability.

Using the analytical Wilson pillar strength equation, Scovazzo (2010) did summarize many important observations:

- Most seam specific results indicated higher pillar strength when compared to the widely accepted Mark-Bieniawski stress relationship
- There is significant statistical deviation in the calculate pillar strength
- The highest pillar strengths involved strong, massive roof and floor lithology, however these are also typically associated with high bump potential
- There is an observed independence between coal strength and the calculated stress profile, a finding supported by Mark and Barton (1997)
- The constants in the Mark-Bieniawski pillar strength formula may be back-calculated to mirror the Wilson stress profile, making it easier to implement site-specific analytical results into empirical techniques (e.g. ARMPS)

2.10 Empirical Relationships

While analytical methods take a fundamental mechanics approach to solving for the strength and stability of coal pillars, many complexities associated with geologic materials remain which simply cannot be handled by such approaches. The difficulties associated with geologic material have conventionally led to a reliance on empirical studies which seek to use experimental or case study results to formulate relationships which may be used for additional applications. While seeking to provide a determination of coal pillar strength, Bieniawski (1996) noted that experimental results from tests on rock and coal samples demonstrated a significant scale effect – that is, there exists a strength-reduction with increasing size. The author highlighted one of the most common scaling laws for determining the in-situ strength of cubical pillars, σ_1, which exceed 36 inches in height, *h*, is as follows (Equation 2.7):

$$\sigma_1 = \frac{k}{\sqrt{h}} \qquad 2.7$$

Equation 2.8 illustrates that the constant k is determined from laboratory scale uniaxial compressive tests of the coal material (Gaddy, 1956):

$$k = \sigma_C \sqrt{D} \qquad 2.8$$

If the cubical pillar does not exceed 36 inches in height then the relationship simplifies to Equation 2.9:

$$\sigma_1 = \frac{k}{6} \qquad 2.9$$

Using this in-situ pillar strength, many empirical based pillar strength formulas have been proposed based on testing of coal pillars located in specific regions. Bieniawski (1996) conducted large-scale in-situ strength testing on coal pillars in South African coal mines, which were generalized to the following form, Equation 2.10, for use in the United States coalfields:

$$\sigma_P = \sigma_1 (0.64 + 0.36 \frac{w}{h}) \qquad 2.10$$

Where σ_P = Coal Pillar Strength

σ_1 = In-Situ Coal Strength

w = Pillar Width

h = Pillar Height

While admitting that empirical relationships do not consider internal pillar mechanics or have the capacity to consider site-specific geological parameters, Mark (1999) demonstrated the result of deriving the implied stress gradient, σ_V, from the Bieniawski relationship (Equation 2.11) for any point located at distance x into the pillar:

$$\sigma_V = \sigma_1 (0.64 + 2.16 \frac{x}{h}) \qquad 2.11$$

Extending this pillar stress gradient to consider the effect of pillar length, l, Mark (1999) modified the Bieniawski pillar strength formula, which is known as the Mark-Bieniawski pillar strength formula, to reflect the change in strength when using rectangular pillars (Equation 2.12):

$$\sigma_P = \sigma_1(0.64 + 0.54\frac{w}{h} - 0.18\frac{w^2}{lh}) \quad 2.12$$

The Mark-Bieniawski pillar strength formula is the most widely used and recognized pillar strength relationship in the United States today. Its success is predicated on three central elements (Mark, 1999):

- A hypothesis which simplifies the practical environment but maintains the incorporation of the most important details
- A significant quantify of case studies which have been developed with a consistent and detailed methodology
- An appropriate and precise statistical analysis using relevant numerical techniques

In addition to these important relationships, Mark (1999) made numerous observations on the use and future of empirical approaches. The author particularly noted the great potential for synergistic hybrid approaches which use numerical methods based on empirical evidences/relationships to solve ground control problems. This also led to the conclusion of several findings:

- The apparent insignificance of lab testing of coal samples towards the prediction of coal pillar strength
- The difficulty in predicting the strength of coal pillars as the W/H ratio increases (pillars become more squat)
- The relationship between W/H ratio and mode of pillar failure
- The relevance of entry stability to coal pillar behavior

2.10.1 ARMPS 2010

Mark (2010) developed the ARMPS software as an empirically derived mine design tool for underground room and pillar coal mines. Similar empirical software, Analysis of Longwall Pillar Stability (ALPS), has been developed for longwall gate roads. The original database considered around 150 case histories throughout the United States for a variety of conditions and basins. Pillar strength was assumed to be governed by the Mark-Bieniawski pillar strength formula and loading following tributary area loading and the abutment angle concept. Using these mechanics, the ARMPS stability factor for each

case study was determined and plotted as a function of overburden (Figure 2-11). Mark (2010) made two conclusions:

- Success occurred at many ARMPS stability factors and many case studies were successful at a stability factor below a value of 1.50
- No one single value for the ARMPS stability factor adequately differentiated between success and failure

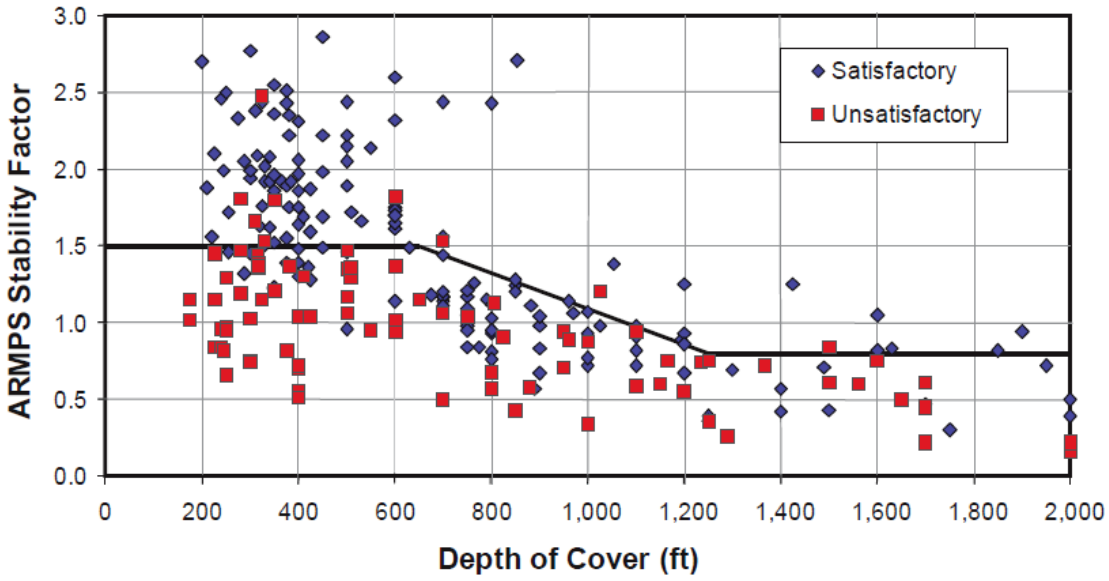

Figure 2-11 Recommended ARMPS SF from original 2002 database (Mark, 2010)

As a result, Mark (2010) developed a piecewise linear function (Figure 2-11) whereby the recommended stability factor is a function of the overburden depth and allowed for differentiation between weak and strong roof. However, many additional case studies with particularly focus on deeper overburdens were subsequently added (Figure 2-12). Seeking to reconcile ARMPS with numerical modeling results, Mark (2010) implemented the pressure arch concept which helped explain the success of narrow panels under deeper cover.

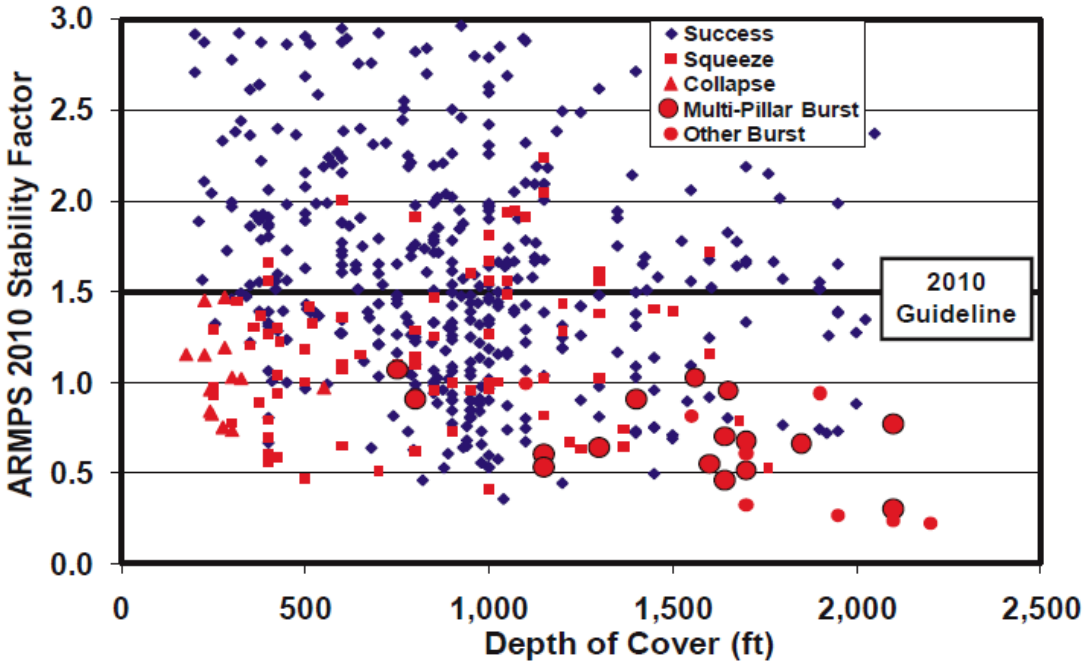

Figure 2-12 Revised ARMPS SF from ARMPS 2010 database (Mark, 2010)

With the pressure arch concept in place, Mark (2010) recommended a minimum ARMPS stability factor value of 1.50. However, there were many cases under deeper overburden which were still quite successful. Mark (2010) concluded that most of these case studies had narrow panels, and subsequently developed alternative guidelines for the ARMPS stability factor for narrow panels under deep cover as shown on Table 2-1.

Table 2-1 Alternative guidelines for narrow panel under deep cover (Mark, 2010)

Depth of Cover (ft)	Panel Width (ft)	ARMPS SF	Barrier Pillar SF
650 - 1,000	< 425	1.5-[0.2 x ((Depth-650)/350)]	2.0
> 1,000	< 425	1.30	2.0

One particular advantage of this approach is the simplicity and ease of use for quickly assessing the stability of proposed/existing underground room and pillar workings. However, site-specific data is not incorporated and the premise is based on the statistical strength of the database. Furthermore, while general trends may be observed, the prediction of the mode of pillar failure which may occur is limited and the incorporation of complex geometry or loading condition limits the software's applicability.

2.11 Numerical Techniques

Empirical methods have been traditionally relied upon because of ease-of-use and the link to some practical case studies; however there are many difficulties encountered which cannot be adequately modeled with empirical approaches and thus exceed the scope of the original empirical investigation (Heasley and Chekan, 1999). Examples of such difficulties may be as simple as deeper overburden or as complex as multiple-seam mining. As a result, Heasley and Chekan (1999) promoted numerical techniques such as finite-element, boundary-element, discrete-element, or finite-difference as methods to more accurately model complicated stress conditions.

Barczak (2011) highlighted the potential that numerical modeling has to evaluate ground control issues from an engineering viewpoint while overcoming the inability to conduct controlled experimentation in a mine setting. The author believed that numerical modeling will move rock mechanics research beyond the traditional empirical approaches, citing the need to properly simulate rock mass failure and bridge the gap between existing limitations and the constraints imposed with the rock mass continuum.

Hakala noted that numerical methods employed to solve rock mechanics problems depend on the physical approach, model, and solution method. Common numerical methods include:

- Boundary Element
- Displacement Discontinuity
- Finite Element
- Finite Difference
- Discrete Element
- Discrete Fracture Network

According to Hakala, the selection of numerical method is highly dependent upon many parameters including the following:

- Continuum vs. Discontinuum Approaches
- In-situ Stresses

- Model Geometry/Dimensions
- Available Input Data

2.11.1 Boundary Element Methods

The boundary element method is a boundary integral equation formulation which applies surface elements on a three-dimensional domain and line elements on a two-dimensional domain, making the technique good for problems with complicated geometries, stress concentration, infinite domains, and many others (Liu, 2013). Because of the reduction of dimensions compared to other numerical methods, the boundary element method is very accurate and computationally efficient.

One of the more widespread numerical tools for modeling underground coal mines today is LaModel. LaModel was developed as a displacement-discontinuity variation of the boundary element method, mainly reserved to model stresses and displacements in thin, tabular deposits such as coal (Heasley, 2009). As with any other numerical technique, the results are dependent upon material properties. Heasley and Chekan (1999) noted that one of the key disadvantages of numerical techniques such as LaModel is the difficulty in acquiring precise material properties, which may be misunderstood or difficult to obtain. As a result, a standardized calibration technique for LaModel has been offered by Heasley (2009) which incorporates the large empirical database used by the ARMPS software, a synergistic approach that Mark (1999) emphasized thereby taking advantage of the knowledge of empirical studies but utilizing the greater flexibility of numerical techniques. This specific calibration methodology for LaModel involves three critical parameters:

- Rock Mass Stiffness
- Gob Stiffness
- Coal Strength

Calibration of rock mass stiffness follows the concept of the abutment zone distance and is governed by the fundamental laminated overburden model, presented as Equation 2.13 (Heasley, 2009):

$$t = \frac{2E_s\sqrt{12(1-v^2)}}{Eh}\left(\frac{D_n - d}{\ln(1-n)}\right)^2 \qquad 2.13$$

Where E = Elastic Modulus of Overburden

$\not\square$ = Poisson's Ratio of Overburden

E_s = Elastic Modulus of the Coal Seam

h = Coal Seam Thickness

d = Extent of the Coal Yielding Abutment Zone

n = Percentage of the Abutment Load

Consequently, the rock mass stiffness is primarily governed by the elastic modulus of the coal seam and overburden, seam height, and the extent of the abutment zone, which is normally assumed to be the yield distance that contains 90% of the abutment load. One advantage of this mathematical representation is the ability to calibrate the rock mass stiffness to site-specific conditions based on empirical observation or in-mine stress testing.

Coal and pillar strength are equally as important to determining the stress environment and predicted stability. Heasley (2009) recommends that the in-situ coal strength in LaModel remain at 900 psi and prescribe to the Mark Bieniawski pillar strength formula as follows (Equation 2.14):

$$S_p = S_i\left(0.64 + 0.54\frac{w}{h} - 0.18\frac{w^2}{hl}\right) \qquad 2.14$$

Where S_p = Pillar Strength

S_i = In-situ Coal Strength

w = Pillar Width

h = Extraction Height

l = Pillar Length

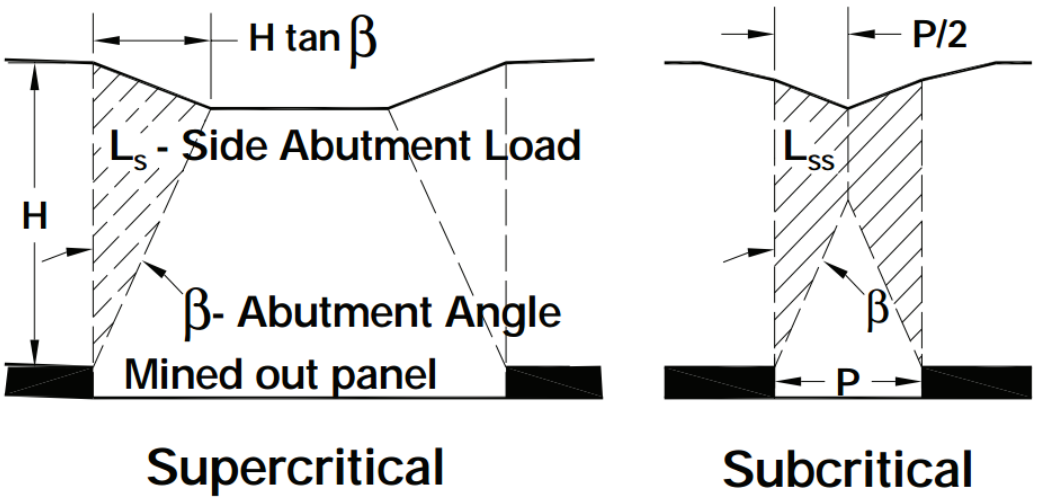

Figure 2-13 Illustration of abutment angle concept for gob calibration (Heasley, 2009)

One of the most important factors which influence the underground stress environment is gob behavior. However, because of the inability to directly measure gob stress, only indirect or empirical evidences have been previously utilized. Heasley (2009) recommends that the calibration of gob material, otherwise known as gob stiffness or final gob modulus, follows the same abutment angle concept as used by the empirical software ARMPS and ALPS (Figure 2-13). For a supercritical panel the average gob stress is determined from Equation 2.15:

$$\sigma_{Avg} = \left(\frac{H * \delta}{144}\right)\left(\frac{P - (H * \tan\beta)}{P}\right) \qquad 2.15$$

For a subcritical panel the average gob stress is determined from Equation 2.16:

$$\sigma_{Avg} = \frac{P}{4}\left(\frac{1}{\tan\beta}\right)\left(\frac{\delta}{144}\right) \qquad 2.16$$

Where σ_{avg} = Average Gob Stress

H = Overburden Depth

$\not\square$ Overburden Density

P = Panel Width

⏥ Abutment Angle (21 Degrees)

LaModel is widely used in the mining industry because of computational efficiency in modeling large tabular deposits such as coal and has a significant history of successful application at coal mines (Office of Mine Safety and Health Research, 2010). Like other numerical methods, LaModel offers the primary advantage of flexibility and efficiency to simulate many geometric and geologic parameters (Heasley and Chekan, 1999). The development and success of numerical approaches such as LaModel has certainly offered a medium to explore new avenues of bump related research, such as the Crandall Canyon bump event which occurred in 2007 (Figure 2-14).

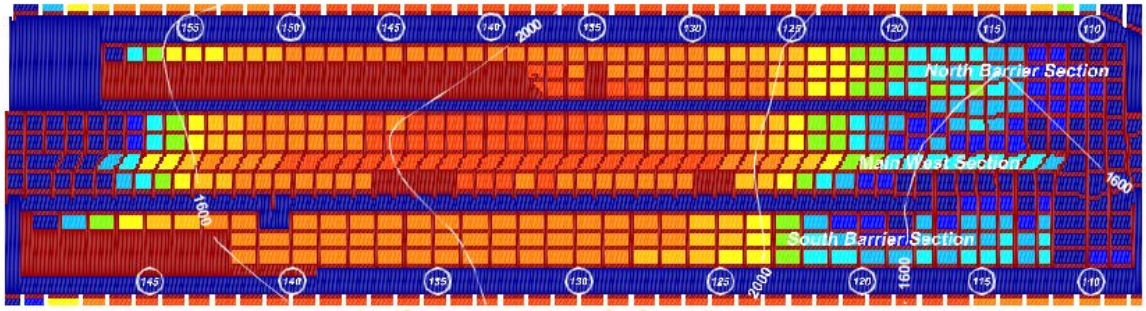

Figure 2-14 Pillar stress SF for final bump configuration at Crandall Canyon mine (Heasley, 2008)

Sears and Heasley (2009) incorporated an Energy Release Rate (ERR) calculation into the LaModel program as a method to correlate risk of violent failure in coal pillars, citing increased interest in coal bump research as the result of more recent bump events like Crandall Canyon. The result of this development allows for the calculated stress and strain for any element to then be classified into stored elastic strain energy, input kinetic energy, and released kinetic energy as a method to compare mining methods, changes in material model, cut sequences, etc. (Figure 2-15).

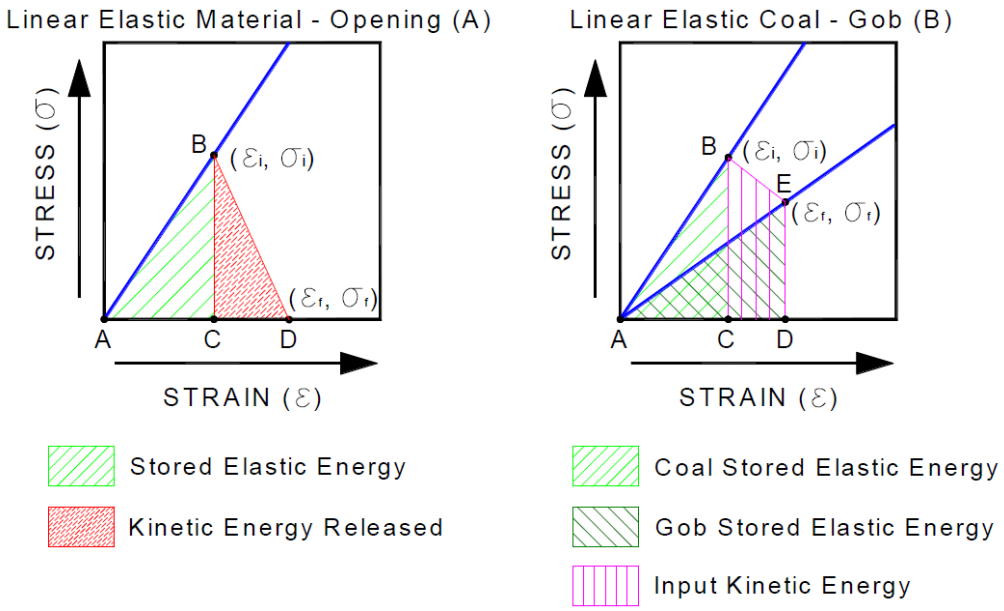

Figure 2-15 Examples of kinetic energy released for coal element due to a) mining and b) change in material code (Sears and Heasley, 2009)

2.11.2 Finite Element/Difference Methods

The finite element/difference method is a differential equation formulation used to approximate partial differential equations which arise in engineering problems such as rock mechanics (Liu, 2013). Pariseau (2011) argues that LaModel, like many boundary element methods, is insufficiently equipped to provide adequate stress analysis because the pillar is not in the solution domain and thus excavation induced stress distribution is not considered. As a result, numerical approaches seeking to improve understanding of coal bumps must incorporate the geological factors associated with the mechanisms that can cause coal bumps, such as de-confinement. Pariseau (2011) concluded that the finite-element or finite-difference codes which are currently in use within industry meet all requirements for mine pillar design analysis. However, the author also cited the need for improved understanding of software capability used for geomechanical analysis, particularly referencing the need for education on approach and calibration.

Esterhuizen et al. (2010a) provided insight into numerical calibration of finite-difference models used to simulate underground coal mining, including coal properties, gob

behavior, and overburden response. Effectively modeling underground coal mining problems requires an efficient methodology to handle the computational difficulties encountered with large geometries and arrays of elements/zones. Esterhuizen and Mark (2009) have provided insight into equivalent element techniques aimed at reducing solution run time while adequately capturing the stress-strain behavior of coal pillars and nearby strata (Figure 2-16).

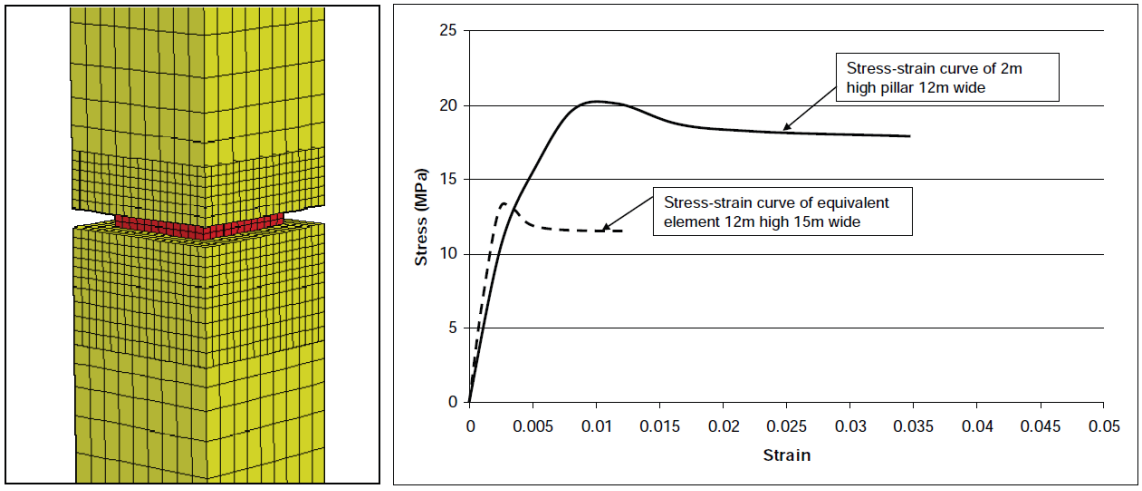

Figure 2-16 Example of finite difference model showing stress-strain comparison for single pillar and equivalent element (Esterhuizen and Mark, 2009)

2.11.3 Discrete Element/Fracture Methods

The discrete element method is a numerical technique which approximates the volume/domain as set of small particles. With the advent of more advanced and efficient computational resources, the discrete element method has become one of the most widely used tools to solve geotechnical problems due to its ability to more precisely model discontinuous media.

Scholtés et al. (2001) examined scale effects on the strength of coal with a distinct element model, seeking to distinguish between the effects due to sample size and those due to the mechanical response of the fracture network. By numerically simulating a triaxial test and comparing with laboratory results for a variety of samples, the authors were able to integrate structural effects (Figure 2-17) induced by seam discontinuities

which result in behavioral dependencies such as scale effects. The study successfully demonstrated a relationship between the strength and the existing discontinuity set (Figure 2-18), concluded as a strength dependency on the density of the discrete fracture network.

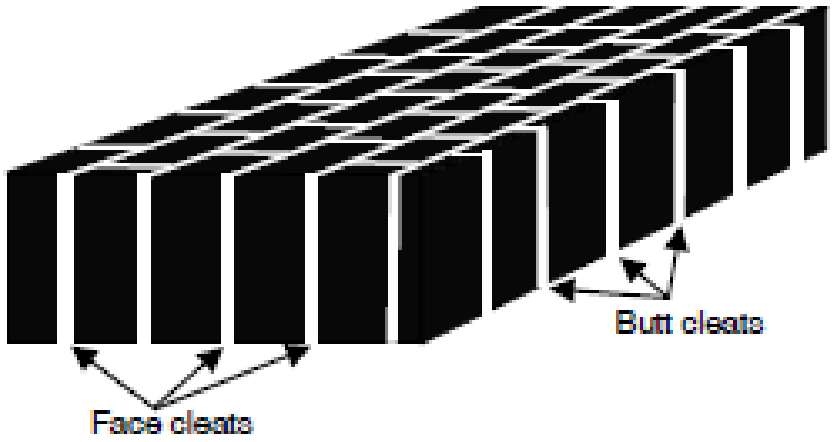

Figure 2-17 Illustration of coal specimen with structural discontinuities including face and butt cleat (Scholtés et al., 2001)

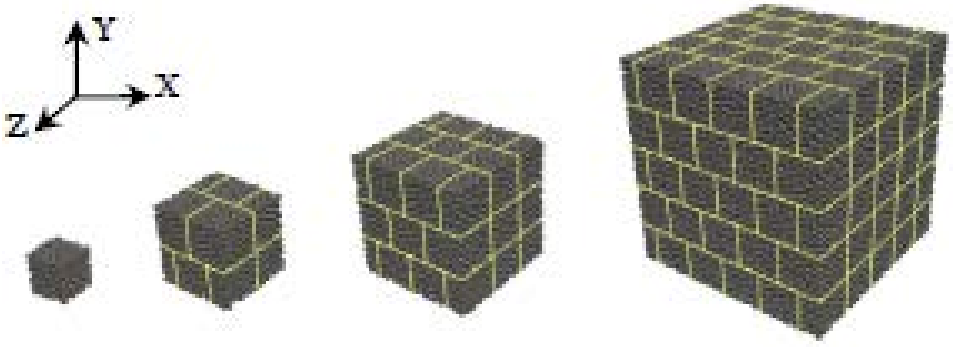

Figure 2-18 Example of the four numerical sample size with constant element size and DFN (Scholtés et al., 2001)

Similarly, Pine et al. (2006) sought to more precisely model fractured rock mass by maximizing the representation of the existing rock jointing geometry and using this result within a loading model to analyze mine pillars. The discrete fracture model was based on mapping of underground pillars and rock faces with data synthesized using numerical fracture network software. Pillar failure was modeled for progressively higher loads for a variety of typical pillar geometries and compared with traditional empirical relationships. The authors noted an accelerated increase in pillar strength as the W/H ratio increased, and a decreasing dependence on the fracture network.

Bidgoli & Jing (2014) sought to highlight the importance of the anisotropy of strength and deformation of geologic material as a critical issue which must be considered in the study of any rock mechanics problem. Due to the inability to practically conduct laboratory testing with large samples, the authors used two-dimensional discrete element modeling techniques to demonstrate the anisotropic nature of strength envelopes (Figure 2-19) and elastic deformation parameters such as Young's Modulus or Poisson's Ratio. Using numerical results, the authors presented a comparison to traditional equivalent strength criterion such as Mohr-Coulomb or Hoek-Brown.

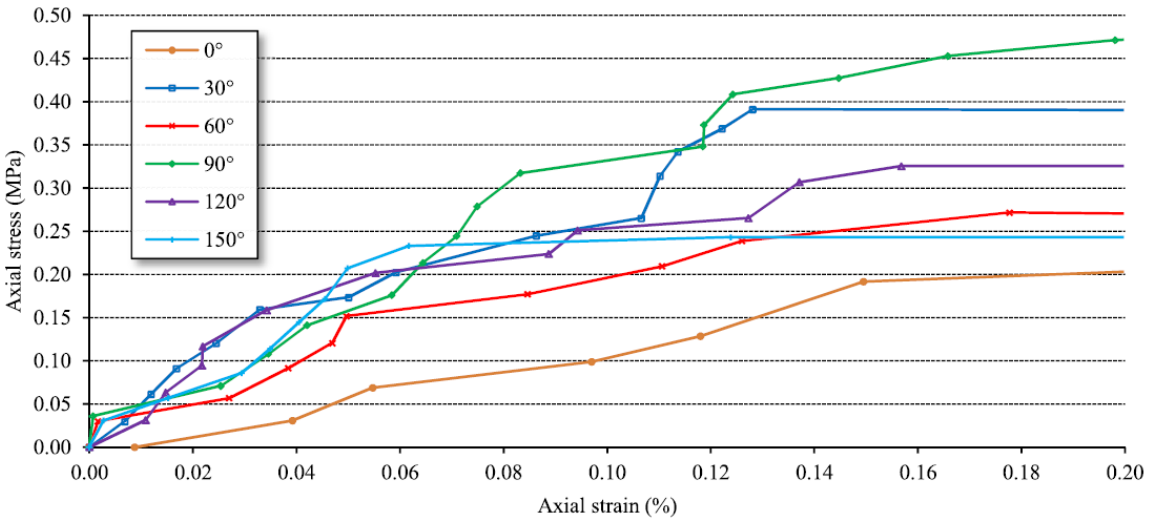

Figure 2-19 Axial stress-strain results for rotated DEM models of rock samples (Bidgoli and Jing, 2014)

2.12 Constitutive Models

Like all numerical analysis of engineering materials, constitutive models for rock mass are developed seeking to maintain consistency with the conservation laws and observed behavior of the material. According to Jing and Stephansson (2007), proper constitutive models of rock mass and discontinuities are essential to numerical modeling efforts of rock behavior, whereby the models must achieve two primary goals:

- Constitutive models must have the ability to capture conceptual rock mass behavior as observed in laboratory studies or in the field within an acceptable tolerance
- Constitutive models must adequately simulate both rock and fracture behavior for basic loading conditions and the associated stress-strain paths without violating the second law of thermodynamics

However, geologic material provides inherent difficulties. While these two primary goals are intuitive to the study of the mechanics of any material, Jing and Stephansson (2007) also identified three difficulties associated with the development of constitutive relationships for fractured rocks:

- The scale effect representing the variation in mechanical properties with the size of the rock mass
- The inherent path dependency of stress, meaning that deformation depends on the magnitude and path of stresses
- Transitions in material behavior, such as the transition from small-scale ductile response due to strain localization to a broader scale of rock mass behavior

These difficulties have been well recognized throughout industry during modern times. As a result, engineers and scientists have traditionally relied on empirical approaches to understand and predict rock mass behavior and stability for a given state of stress because of the simplified approach; however, recent developments in numerical techniques and the advent of more appropriate constitutive models has allowed for better research in the field of rock mechanics.

2.12.1 Mohr-Coulomb Model

The Mohr-Coulomb model is a conventional constitutive model widely used to represent the shear failure in geologic medium such as rock or soils (Itasca, 2009). Failure occurs when the shear stress, τ, exceeds the available shear resistance provided by the material cohesion, C, and the frictional restraint determined by the product of the normal stress, σ_n, and the tangent of the angle of internal friction, ϕ (Equation 2.17). The result is a linear failure envelope which has been widely used within numerical techniques for rock and soil.

$$\tau = C + (\tan \emptyset)\sigma_n \qquad 2.17$$

2.12.2 Ubiquitous-Joint Model

The ubiquitous-joint model is an anisotropic plasticity model that implements a plane of weakness for a Mohr-Coulomb material (Itasca, 2009). For a given plane orientation, a composite Mohr-Coulomb failure envelope with a tension limit is determined and once failure is initially calculated, plastic corrections are applied (Itasca, 2009). The ubiquitous-joint model has been more prevalent in recent numerical modeling efforts due to its inherent correlation to natural rock mass behavior, particularly in sedimentary measures such as coal, as the model allows for failure to occur either in the intact rock matrix or along the plane of weakness.

2.12.3 Strain-Hardening/Softening Model

The strain-hardening/softening model allows for the representation of non-linear hardening or softening in a Mohr-Coulomb solid as a function of the plastic strain (Itasca, 2009). Itasca (2009) defines this modification as the possibility to allow for hardening or softening of the material cohesion, friction angle, dilation angle, and tensile strength once plastic yield begins, a result that has been confirmed for many geologic materials.

2.12.4 Hybrid Approaches

Hybrid approaches have been developed which seek to resolve important rock properties with currently available constitutive models. Lavoie (2011) examined the development of an analytical geomechanical upscaling approach for modeling jointed rock mass behavior based on the results of laboratory testing and discrete fracture network

modeling. The result of this study was a ubiquitous joint rock mass constitutive model that successfully captured the softening effect observed in rock masses along with the perceived dependence on directionality that is the result of rock mass discontinuities, representative of kinematic weakening within the rock mass fabric. The resulting approach successfully reproduced the strength scale effect. Nevertheless, the accurate representation of rock mass behavior using numerical methods requires the development of constitutive relationships which also govern rock fracture behavior.

2.13 Rock Fracture Models

Rock fractures are often submitted to complex loading conditions; however modern numerical methods which seek to more precisely capture rock mass behavior must incorporate numerical mechanisms that emulate rock mass discontinuities. Approaches such as the finite element/difference method often allow for a more simplified approach since discretization is not heavily influenced by these discontinuities. However, the distinct element method is heavily reliant upon these interfaces, effectively treating them as boundary conditions and allowing for the usage of more complex joint models. Traditionally, there are two approaches to numerically simulate major rock discontinuities: empirically based formulations such as the Coulomb Sliding model or more progressive numerical approaches, such as the Continuously Yielding model, which seek to capture the more realistic non-linear joint behavior.

2.13.1 Coulomb Sliding

The Coulomb Sliding model is an empirically derived formulation that is nearly equivalent to the Mohr-Coulomb constitutive model, and is similarly based on laboratory testing that relies on simple loading conditions (Itasca, 2013b). Like the Mohr-Coulomb constitutive relationship, failure along the interface is initiated as shear failure that is resisted by the available shear strength for a given normal stress. The failure envelope is linear, and is influenced by the normal and shear stiffness, tensile and shear bond strength, and dilation along the interface which may increase normal stress from volumetric changes (Itasca, 2009).

2.13.2 Continuously Yielding

The continuously yielding joint model is a more practical discontinuity model in that it replicates non-linearity which is typically observed in physical tests (Itasca, 2013a). Failure is governed by a non-linear shear stress envelope that has a peak strength and displacement value, followed by a specified level of residual strength. The behavior of a particular discontinuity is influenced by the defined joint shear stiffness, normal stiffness, roughness, friction angle, dilation, bounded strength, shear stress, and normal stress (Itasca, 2013b).

2.14 Ground Response Curve

One such concept for numerically evaluating coal pillar performance and ground response is the Ground Response Curve (GRC), which mathematically defines the ground convergence response to decreasing support stress. According to Barczak (2011), the idea of using the ground response curve was originally developed in the civil engineering discipline to investigate tunnel ground problems whereby the ground support measure was selected by monitoring the support pressure against the excavation deformation. The author presented similar uses for underground coal mining. Such an example is the work of Dolinar et al. (2009), who used the ground reaction curve concept to investigate the use of different support design considerations for tailgate support in an Illinois Basin longwall mine. Both efforts highlighted several important parameters including the non-linear shape and slope of the ground response curve (Figure 2-20).

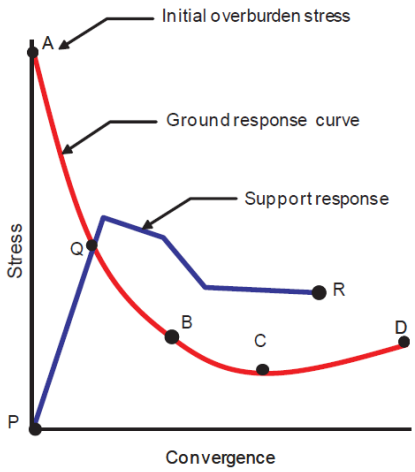

Figure 2-20 Conceptual GRC and support curve (Esterhuizen et al., 2010b)

Barczak (2011) also mentioned the research of Esterhuizen et al. (2010b), demonstrating that the ground response curve concept is not limited to support design only, but may be applied to pillar design requirements. More specifically, Esterhuizen et al. (2010b) explored the use of the GRC to evaluate coal pillar behavior, particularly examining the impact of overburden depth and panel span for both development and retreat mining (Figure 2-21). The influence of the GRC on pillar stress and strain was confirmed for various overburden properties, and the slope of the GRC also indicated a connection to pillar yielding (Figure 2-22). Furthermore, the study demonstrated the successful application of the GRC while attempting to capture the transition of a pillar from stability to post-peak and the success/functionality of this transition. However, the study only considered potential failure within the coal pillar and not the near-seam strata.

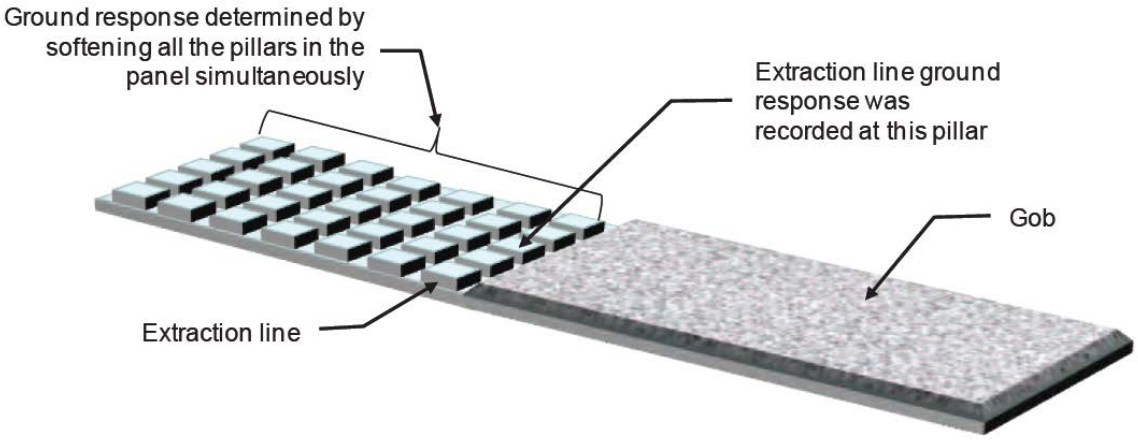

Figure 2-21 Schematic of single retreat mine panel used by Esterhuizen et al. (2010b) to determine GRC at pillar line

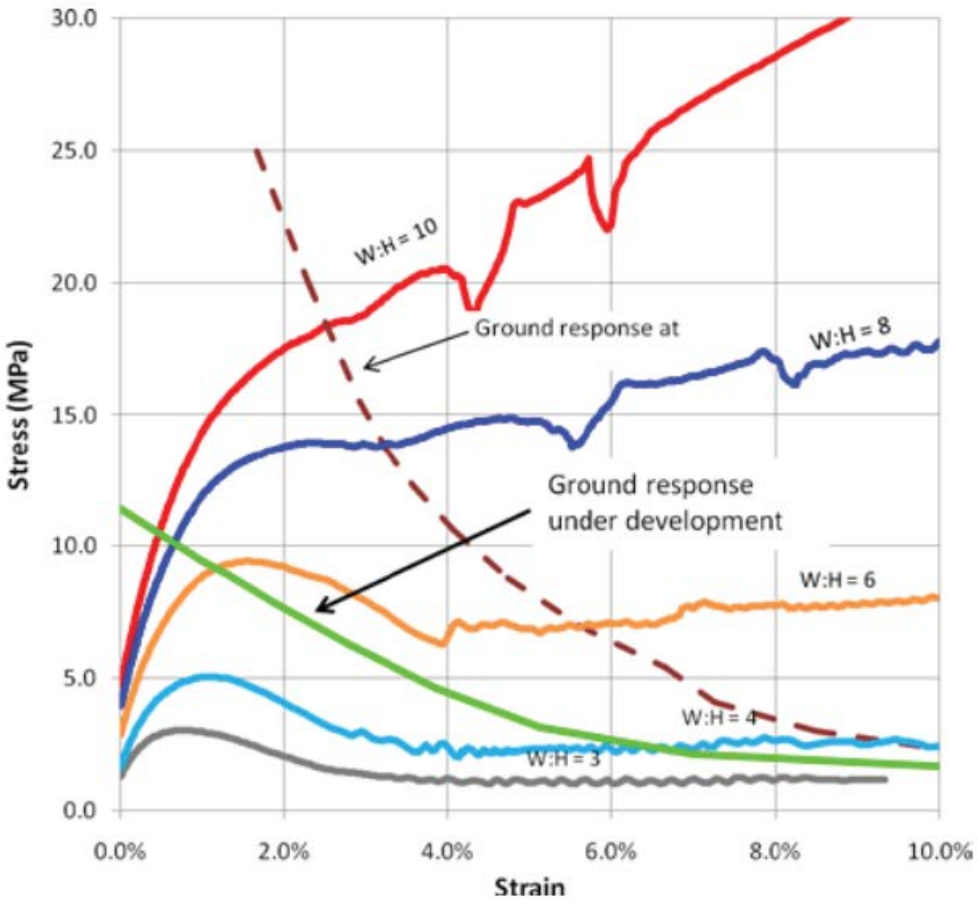

Figure 2-22 Example of pillar stress-strain and GRC for various pillar geometries at both development and retreat (Esterhuizen et al., 2010b)

2.15 Recent Findings

While the studies of Esterhuizen et al. (2010b) provided meaningful result in demonstrating the capacity to use the GRC to explore pillar behavior, the authors advocated for further research into relationships between pillar strain and the likelihood of success for a range of typical geologies and panel layouts, along with the impact of failure in near-seam strata. Specifically the authors advocated for investigation into a myriad of relationships including:

- Potential impact of weak roof and floor strata on pillar response
- Impact of side abutment loading from adjacent mining
- Barrier pillar deformation

Mark (1999) recognized some of these facts early, citing the need to learn more about the behavior and mechanics of squat pillars and the influence of roof-pillar-floor interactions in the pursuit of answering these pillar design questions. The Office of Mine Safety and Health Research (2010) has provided recommendations to enhance the safety of underground coal mines and reduce the risk of coal bumps, primarily emphasizing burst hazard assessments and adequate pillar design. This led to numerous research recommendations including:

- Determination of criteria for high bump risk or "red zones" to improve the science of developing enhanced guidelines
- Determination of classification and reporting criteria for coal bumps
- Further understanding of pillar loading and behavior for deep cover mining, including pressure arch behavior, the mechanics of squat coal pillars, and the effects of roof/floor/partings.

Numerical studies have since been undertaken to improve understanding of coal bump mechanisms. Gu (2013) utilized a two-dimensional distinct element technique to evaluate de-confinement mechanisms associated with near-seam strata in an effort to assess the potential for unstable failure of coal pillars and determine an appropriate interface model. The author advanced knowledge of de-confinement mechanisms based on the properties of the coal-rock interface properties and mining geometry by examining both normal and shear stress/displacement rates along these interfaces. While the study demonstrated potential for capturing de-confinement of near-seam strata by assessing shear displacement of pillar interfaces, the need for three-dimensional modeling that adequately captures more realistic conditions, properties, and geometries to improve in unstable failure analysis was admitted.

2.16 Summary

Underground coal mining is inherently a dangerous profession; however, technological improvements, the promulgation of necessary regulation, and industry awareness have greatly improved the safety of the occupation. However, easier coal reserves are being depleted and ground control problems are continually encountered while becoming progressively more difficult. Coal bumps are one of these potential problems and

represent a unique but significant threat to the safety of underground coal miners. The traditional reliance on analytical and/or empirical techniques has provided significant progress in the field of ground control; however these methods are limited in the ability consider site-specific geologic complexities which are important to the identification of bump potential. Consequently, there is a need to evaluate the influence that these localized parameters, including geologic properties and features, have on the probability for a coal bump to occur.

The use of numerical techniques has demonstrated a capacity to advance the fundamental knowledge of coal bump potential. Recent studies have provided a solid foundation towards the understanding of the use of numerical methods to investigate ground control problems, including material properties, constitutive and joint models, and a concept known as the Ground Response Curve. However, there is an obvious deficiency with respect to the understanding of squat coal pillar and post-peak coal pillar behavior. Squat coal pillars are increasingly common in more difficult ground conditions and typically exhibit strain-hardening behavior. Contemporary research has concluded that the strength and behavior of these squat coal pillars is highly complex and depends on a multitude of geologic and geometric parameters and properties, and not simply the size of the pillar. Consequently, there is an recognizable need to more thoroughly examine the correlation between these geologic influences, such as interface friction and near-seam lithology, and the resulting strength, behavior, and bump potential of squat coal pillars. Furthermore, it is important to fully realize the impact of global stress response to mine design principles. While literature points towards the importance of geometric properties (e.g. cover and panel width) to global stress behavior, a comprehensive examination which also includes geologic considerations and more complex mining configurations is a recognized deficiency. The advancement of this knowledge would greatly aid in the refinement of existing bump “red zone” guidelines, which provide an effective engineering tool to increase bump awareness and potentially reduce the likelihood of these dangerous failures.

3 Numerical Determination of Bump Potential

Unfortunately, the behavior of squat coal pillars (those pillars with a relatively high ratio of width to height, hereby defined as a ratio exceeding eight) is relatively unknown. While it is commonly accepted that squat coal pillars begin to demonstrate strain-hardening behavior, it then becomes difficult to delineate the definitive pillar strength, leaving mining engineers with uncertainty in the mine design process. While the strength of low W/H ratio coal pillars is most closely dependent on the pillar geometry, the strength and behavior of squat coal pillars undoubtedly becomes increasingly dependent on numerous parameters which can vary substantially. A comprehensive numerical study was therefore conducted, seeking to correlate the impact that numerous geologic and geometric parameters have on squat coal pillar behavior and bump potential. The results are expected to significantly improve the definition and identification of bump "red zone" guidelines, which increase bump awareness and provide a meaningful tool for mining engineers to communicate with coal operations. The research objectives of this numerical study are as follows:

- Enhance understanding of pillar loading and behavior for deep cover coal mining, focusing on the mechanics of squat coal pillars and the effects of localized geologic influences with respect to bump potential
- Increase knowledge of the global stress environment for deep cover coal mining with focus on the impact that varying mining, geologic, and geometric considerations have on local stiffness and the resulting ground response
- Focus on the union of knowledge concerning localized factors impacting squat coal pillar behavior and the influence of global contributing factors in order to improve the determination of criteria for high bump potential or "red zones"

3.1 Existing Guidelines

Iannachione and Zelanko (1995b) referred to three key factors which influence and can result in elevated bump potential: high stress, dynamic shock, and deconfinement. Pressure bumps are considered to be quasi-static events related to an overstressed pillar core which exceeds the critical threshold of pillar strength. The presence of high stress may be the result of deep cover, multiple seam interactions, or dynamic shock. Bumps

which occur as the result of deconfinement are the result of slip along near-seam discontinuities which causes a loss of strength and a dynamic transition from a state of stability to instability. The concept of bump potential recognition generally considers the coalescence of multiple factors which can increase the probability of a burst event.

Bump potential recognition has often come in the form of bump "red zones" which increase awareness of these factors; however the Office of Mine Safety and Health Research (2010) has advocated for improved understanding of bump risk guidelines. This study promoted for greater understanding of squat coal pillar behavior and the impact of near-seam roof/floor strata on bump potential as a fundamental basis for the formation of bump "red zones" which have historically included the following factors:

- Deep Cover
- Mining Configuration
- Multiple Seam Interaction
- Massive Sandstone
- Linear Features/Faults
- Rapid Changes in Seam Structure

This wide-ranging study is focused on investigating the influence many of these factors have on coal pillar bump potential through the use of discrete element modeling of single pillar models using a collection of accepted numerical indicators. A later chapter will discuss the results of global geologic and geometric parameters which influence the equilibrium of pillar loading and local mine stiffness.

3.2 Numerical Indicators

The development of practical indicators implemented within numerical modeling methods is important for the identification of unstable failure of coal pillars and a comprehensive study on bump potential. Gu (2013) used two-dimensional discrete element modeling to conclude that unstable shear failures at interfaces can cause unstable compressive failures such as coal bursts after considering indicators such as pillar stress-strain, shear displacement, unbalanced force, and damped energy. Garvey (2013) conducted discrete element and finite difference models of UCS tests, triaxial

compressive strength tests, and coal pillar models to research unstable rock failures of low ratio pillars while examining the use of such indicators as velocity, acceleration, strain increment, shear strain rate, and energy considerations. All of the said numerical identifiers have been shown to be employable and reliable indicators of unstable failures for explicit quasi-static numerical analysis for numerous reasons. First, these numerical identifiers are predicated on the concept that instability begins at a point and results in a velocity/acceleration, followed by the initiation of an unstable equilibrium (Garvey, 2013). Secondly, these numerical identifiers have a foundation in the basic laws of physics and analytical engineering analysis (e.g. conservation of mass, momentum, energy). Historically, coal bursts are classified as one of two types – a strain type burst due to high stress and high excess energy and those due to the unstable shearing resulting in rapid loss of strength due to deconfinement (Gu, 2013). Consequently, the following six numerical identifiers have been selected as the primary tools to assess the behavior of squat coal pillar behavior and bump potential:

- Pillar Stress-Strain
- Pillar Confinement
- Peak Shear Strain Rate
- Total Energy Release
- Kinetic Energy
- Joint Friction Work

3.2.1 Pillar Stress-Strain

The pillar stress-strain relationship is the most fundamental indicator of pillar response to loading. A FISH function was written in 3DEC to loop through all elements of the coal pillar and record the average pillar stress and convergence/strain for each timestep to investigate squat coal pillar behavior for numerous geologic and geometric conditions, particularly focusing on apparent post-failure response.

3.2.2 Pillar Confinement

Pillar confinement is an important indicator of not only the degree to which strain energy is stored as a result of loading, but influences pillar strength and behavior, particularly for

squat coal pillars. For a given geologic environment, high ratio pillars have increased strength due to the higher levels of minimum principal stress which confine rock mass and discontinuities alike. Numerous research efforts (Lu et al., 2008; Perry et al., 2013) have reported on the correlation between geologic environment, confinement, and pillar performance, with particular focus on the effect that pillar interface properties have on confinement. Since deconfinement is a primary cause of unstable failures such as bursts, pillar confinement should be considered an important gauge of bump potential. A FISH function was written in 3DEC to loop through all coal pillar elements and record the average minimum principal stress for each timestep, which will be reported for all model results.

3.2.3 Peak Shear Strain Rate

High stresses result in elevated levels of stored strain energy which are continually dissipated, mostly in the form of plastic deformation. However, as shear fracturing increases, rock failures may transition from a quasi-static failure process to a dynamic release of strain energy as the shear fracture zone propagates in an accelerated fashion (Whyatt and Board, 1991). Multistate triaxial testing of coal-measure rocks has indicated that strain rate dependency of stiffness and strength is particularly significant in fractured rock masses and is more pronounced at high levels of confinement, a state which is typically expected of squat coal pillars (Hamza et al., 2005). Singh et al. (1989) also noted that the failure strength of sandstone specimens increased as the strain rate was elevated, which was attributed to transgranular fractures and other compositional features. As a result, the shear strain rate should be a significant indicator of an unstable release of excess energy in the presence of high stress. A FISH function was written in 3DEC to loop through all elements of the coal pillar and record the peak shear strain rate for each timestep, and this data will be reported for all model results.

3.2.4 Total Energy Release

Energy considerations are of utmost importance because the field of rock mechanics concerns the continual transition from one equilibrium state to another whereby energy calculations allow for engineers to quantitatively assess and describe this process (Salamon, 1984). As the state of the coal pillar and the surrounding strata changes from

stability to instability (regardless of whether this instability is yielding or a coal burst), the theory of energy release can been used to quantify this transformation. In simplified terms, the concept of excess energy may be thought of as the difference between the energy imparted onto any system and the net differential between energy stored and dissipated. That is, the greater the energy imparted onto the system or the greater quantity of strain energy currently stored, the more energy that is available for release. Conversely, energy which has already been dissipated, for example the energy dissipated during plastic deformation or frictional processes, is no longer available for further release. In numerical terms, total energy released can be thought of as the difference between the boundary work (W) and the net total strain energy stored [strain energy (U_c) and potential energy (U_b)] and work dissipated [joint shear work (W_j) and plastic strain work (W_p)] as documented in Equation 3.1 (Itasca, 2015).

$$W_r = W - (U_c + U_b + W_j + W_p) \qquad 3.1$$

Boundary work is the energy imparted into the system as a result of force and displacement from the application of in-situ horizontal stresses at the model boundaries and a vertical velocity at the top of the model to mirror increasing overburden stress. Equation 3.2 details that the total boundary work can be represented as the product of the gridpoint force and displacement summed for all gridpoints along the model boundary for all time steps (Itasca, 2015):

$$W = \sum_{m=1}^{t} \sum_{n=1}^{gp} F_i u_i \qquad 3.2$$

U_c represents the change in total strain energy over the volume. Total strain energy for a given frame of reference, U, is total strain energy stored when an elastic body is strained, and may be represented as the integral of the strain energy density function, ϕ, over the boundary volume as shown in Equation 3.3 (Salamon,1984).

$$U = \int_V \phi \, dV \qquad 3.3$$

The strain energy density function (Equation 3.4) is a scalar valued function involving the product of the stress tensor and the strain tensor with components represented as Equation 3.5 (Salamon, 1984).

$$\phi = \frac{1}{2}\tau_{ij}\varepsilon_{ij} \tag{3.4}$$

$$\varepsilon_{ij} = \frac{1}{2}\left(\frac{\partial u_i}{\partial x_j} + \frac{\partial u_j}{\partial x_i}\right) \tag{3.5}$$

Itasca (2015) further rearranges the strain energy density function in terms of components of the stress tensor, elastic modulus, and Poisson's ratio relative to the standard coordinate system (Equation 3.6).

$$\varphi = \frac{1}{2E}\left[\sigma_x^2 + \sigma_y^2 + \sigma_z^2 - 2v\left(\sigma_x\sigma_y + \sigma_y\sigma_z + \sigma_x\sigma_z\right) + 2(1+v)(\tau_{xy}^2 + \tau_{yz}^2 + \tau_{xz}^2)\right] \tag{3.6}$$

The gravitational potential energy is then determined from the product of the gridpoint mass, gravitational acceleration, and the gridpoint displacement, which is then summed for all gridpoints within the model for all time steps (Equation 3.7) (Itasca, 2015).

$$U_b = \sum_{m=1}^{t}\sum_{n=1}^{ngp} m_i g u_i \tag{3.7}$$

The frictional energy dissipated through heating of joints is the irrecoverable exchange of elastic strain energy and is considered separately from the actual elastic stored strain energy of the joints (Itasca, 2015). Equation 3.8 expresses that the total frictional energy dissipated is the total joint friction work for all contacts summed for all time steps.

$$W_j = \sum_{m=1}^{t} U_{jf} \tag{3.8}$$

The total plastic work dissipated is then taken as the difference in the total energy from the complete state of stress/strain and the elastic strain energy as shown in Equation 3.9 (Itasca, 2015).

$$W_p = W_t - W_e \tag{3.9}$$

An equivalent numerical expression for the total energy released (Equation 3.10) can be obtained by summing the kinetic energy released (U_k), mass damping work (W_k), work done by viscous boundaries (W_v), and the previously excavated strain energy (U_m) (Itasca, 2015). If a quasi-static analysis is conducted and viscous boundaries are not considered, then this form of the energy balance essentially comes down to two terms: kinetic energy, which will be discussed in the next section, and damping energy, which counteracts and is proportional to the kinetic energy. This makes Equation 3.10 a very expedient form of the expression for quasi-static applications because the most important parameter, kinetic energy released, is conceptually recognized, directly appropriate to coal bumps, and is easily calculated. 3DEC calculates both forms of excess energy and this term will be reported for all modeling results as an important indicator of bump potential.

$$W_r = U_k + W_k + W_v + U_m \tag{3.10}$$

3.2.5 Kinetic Energy

Kinetic energy is a customary energy concept used by nearly all engineering disciplines. It is commonly employed in analytical problem solving and can therefore be straightforwardly implemented in numerical techniques. Within 3DEC, kinetic energy is incrementally calculated and summed for all gridpoints in the domain for a given timestep and therefore approaches zero for a state of stable equilibrium due to the work performed by mass damping (Itasca, 2015). Consequently, instability may be predicted when peaks in kinetic energy release are observed, which is conceptually comparable to the dynamic and violent release of excess energy when a burst occurs. Equation 3.11 is the formulation used within 3DEC to calculate the total kinetic energy release (Itasca, 2015). This term will be reported for all modeling results as an important measure of bump potential.

$$U_k = \sum_{i=1}^{ngp} \frac{1}{2} m_i (u_i)^2 \tag{3.11}$$

3.2.6 Joint Friction Work

Many coal bumps are believed to occur as result of unstable shearing of joints resulting in deconfinement of the coal pillar and an instantaneous loss of strength, particularly at the pillar contact. In many bump occurrences a reddish-brown dust has been observed at the roof/floor interface during and immediately prior to the pillar burst, which is evidence of frictional heating. Joint friction work is a measure of the total energy dissipated through the frictional heating of all joints within the model domain. This work is an irrecoverable exchange of elastic energy from the surrounding strata and is direct evidence of unstable joint shearing (Itasca, 2015). The coal pillar and surrounding strata were modeled as a continuum whereby the only explicit joints modeled were the roof/floor interface. Consequently, joint friction work should be a sign of unstable slip and frictional energy dissipation at the pillar interface. For a given timestep, joint friction work is calculated using Equation 3.12.

$$U_{jf} = \sum_{i=1}^{nc} \frac{1}{2}(f_s + f_s')u_s \qquad 3.12$$

4 Discrete Element Modeling of Coal Pillars

The discrete element method is a numerical scheme which approximates a medium as a subset of smaller particles with defined boundary conditions between subsets, enabling complex and discontinuous domains to be modeled in a relatively accurate and efficient manner. Geologic materials such as soils and rocks are naturally occurring and inherently inhomogeneous and discontinuous, thereby requiring the implementation of more complex numerical techniques if behavioral dependencies are to be truly captured. While geologic material is often approximated as a continuum, these behavioral dependencies such as scale effects, path dependence, and the influence of discontinuities make rock mechanics an ideal suitor for the discrete element method.

The discrete element method is theoretically capable of modeling the complex geomechanical response and failure of discrete coal elements, even at the microscopic level. For example, a coal pillar model may be represented as a continuum of coal dissected and made discontinuous by joint sets including cleats and bedding planes, which act to reduce the mechanical strength of the coal. The degree to which these discontinuities impact behavior depends on the frequency, spacing, orientation, and other physical parameters (Jeremic, 1985). While this could easily be modeled as an accumulation of discrete coal “cubes” with complex joint models representing these boundaries for each discrete element, several difficulties arise with this approach. First, the selection of an appropriate and representative element size which correctly represents the effective continuum material. This representative size must be appropriate to adequately capture strength and behavior dependencies such as scale effect or strength anisotropy of the medium but must also allow for efficient computational implementation.

Secondly, understanding of and the numerical capacity to accurately represent the behavior of these prescribed boundary conditions which represent the major discontinuities. While discrete element methods incorporated into software such as 3DEC (Itasca, 2013b) seemingly have the requisite joint models to represent these boundary conditions with necessary precision, the delineation and scaling of these discontinuities in coal measure rocks becomes a real issue. Numerous methods have

been utilized in an attempt to overcome this problem, including photogrammetry (Pate & Haneberg, 2011), LiDAR (Levy & Visca, 2009), and laser scanning (Slob et al., 2007); however the most representative characterization of these discontinuities remains statistically based since it remains unfeasible to practically identify all discontinuities and procure precise joint properties.

In the face of this challenge it is often better to simplify such approaches, and seek to include only the most important facets such as to minimize numerical and practical constraints. This is the recommendation of Hammah and Curran (2009), who advocate for the use of simplified numerical methods for mining geomechanics in "the face of large uncertainties, ill-posed questions, and limited resources." Coal bumps demonstrate the application of the discrete element method, as these instabilities result in the failure and subsequent transformation of strain energy into a dynamic release of discrete fragments of coal from the pillar. The size, scope, and characteristics of this release are a function of the both the global stress environment and the localized stress response. Therefore it is imperative that the investigation of coal bursts consider the union of two related factors: understanding of site-specific pillar behavior and the influence of global geologic and geometric considerations which influence this site-specific response.

Initial modeling efforts are focused on furthering understanding of the localized pillar behavioral influences through an investigation of single pillar models using the discrete element software 3DEC. The roof, pillar, and floor have been simplified into a single continuous "block", discretized into finite elements while the roof/floor interface is represented by the Coulomb Slip joint model. As with any numerical investigation, calibration against site-specific or empirical data is necessary to ensure validity of modeling results.

4.1 Coulomb Slip Joint Model

The contact between coal pillar and roof/floor, otherwise known as the pillar interface, is one of the most important parameters which must be considered in the study of coal bumps, as these events have often occurred as a result of instability at this interface. As stress accumulates in the joint and surrounding strata, strain energy builds in a quasi-steady state manner. Strain energy is then manifested as plastic work, which is evidenced

by roof/floor convergence, rib spalling, the propagation of fractures, and shear displacement of the pillar interface (Wang et al., 2014). In the case for which critical loading of the pillar interface is achieved, frictional heating often occurs, and may be visible as a reddish-brown dust present at the pillar interface. At the onset of instability, the pillar interface can instantaneously lose strength, leading to a loss of confinement and pillar strength. Numerous studies, including those of Lu et al. (2008) and Perry et al. (2013) concluded that interface properties have a profound impact on confinement and pillar strength.

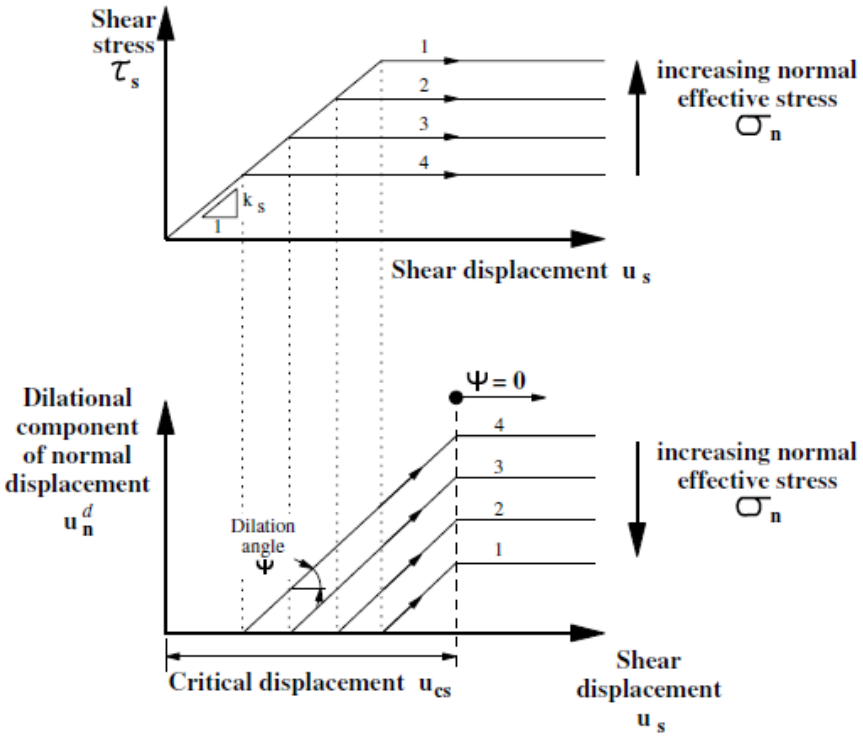

Figure 4-1 Coulomb Slip Joint Model (Itasca, 2013b)

Numerically, the behavior of the pillar interface cannot be ignored, and must capture typical behavior exhibited by rock joints. The Coulomb Slip model was selected because it is an empirically based relationship formulated in the context of customary strength parameters, including friction angle, cohesion, and tensile strength, and can also adequately capture the typical peak/residual strength behavior exhibited by rock joints. Failure along the joint is resisted by the available shear strength for a given normal stress state, until such point peak strength is lost and only residual strength remains (Figure

4-1). Physically, the relationship between peak and residual shear strength is governed by the state of stress and the physical characteristics of the discontinuity, including friction, compressive strength, surface geometry, and the presence of any infill material (Indraratna and Haque, 2000). Numerically, an intact joint is susceptible to either tensile failure (Equation 4.1) or shear failure (Equation4.2).

$$T_{max} = -TA_c \tag{4.1}$$

$$F^s_{max} = cA_c + F^n \tan \emptyset \tag{4.2}$$

4.2 Joint Model Calibration

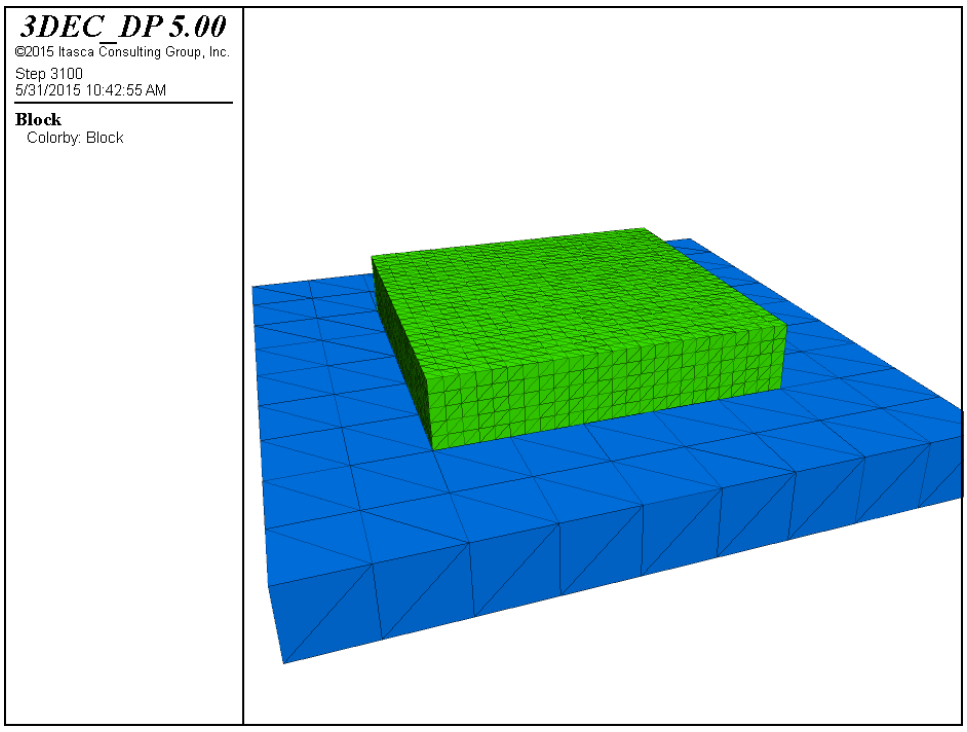

Figure 4-2 W/H=10 Direct shear test for various joint models

Joint calibration was undertaken with a numerical model of a direct shear test using 3DEC, seeking to determine the shear stress and displacement relationship with respect to important joint properties for varying levels of normal stress. Joint properties have been historically determined from laboratory direct shear testing; however it is important to

verify that numerical results produce a close match to published data. Because the ultimate focus of this investigation is on squat coal pillar behavior, the direct shear test focused on the interface shear strength envelope of a high W/H ratio pillar (Figure 4-2).

Most of the necessary joint strength parameters, including joint friction angle, cohesion, and tensile strength, were concluded from previous research efforts including Lu et al. (2008), Esterhuizen et al. (2010a), Perry et al. (2013), and Wang et al. (2014) as documented in Table 4-1. For the calibration study, the peak and residual friction angle were simplified and assumed to be equal, a result leading to zero dilation along the interface. The residual cohesion was assumed to be ten percent of the peak value while the residual tensile strength was assumed to be zero, both following the work of Zipf Jr. (2007). Joint stiffness controls the joint displacement as a result of normal and shear stresses. Since these values are not widely published, the joint normal stiffness was limited to the maximum reasonable value in relation to the equivalent stiffness of surrounding zones following Equation 4.3 and the joint shear stiffness was assumed be half of the joint normal stiffness (Itasca, 2013c). The shear strength envelopes are shown on Figure 4-3 while the resulting shear stress/displacement relationships for various normal stress levels are shown on Figure 4-4.

$$jkn \leq 10.0 \left[max \frac{K + {}^{4}/_{3}\, G}{\Delta z_{min}} \right] \qquad 4.3$$

Table 4-1 Initial Coulomb Slip Joint Model Parameters

Parameter	Description	Value	Units
jkn	Joint Normal Stiffness	3,600,000	psi/ft
jks	Joint Shear Stiffness	1,800,000	psi/ft
∅	Joint Initial Friction Angle	25	degrees
C	Joint Initial Cohesion	150	psi
σ_t	Joint Initial Tensile Strength	45	psi
$\emptyset_r$	Joint Residual Friction Angle	25	degrees
C_r	Joint Residual Cohesion	15	psi
$\sigma_{t,r}$	Joint Residual Tensile Strength	0	psi

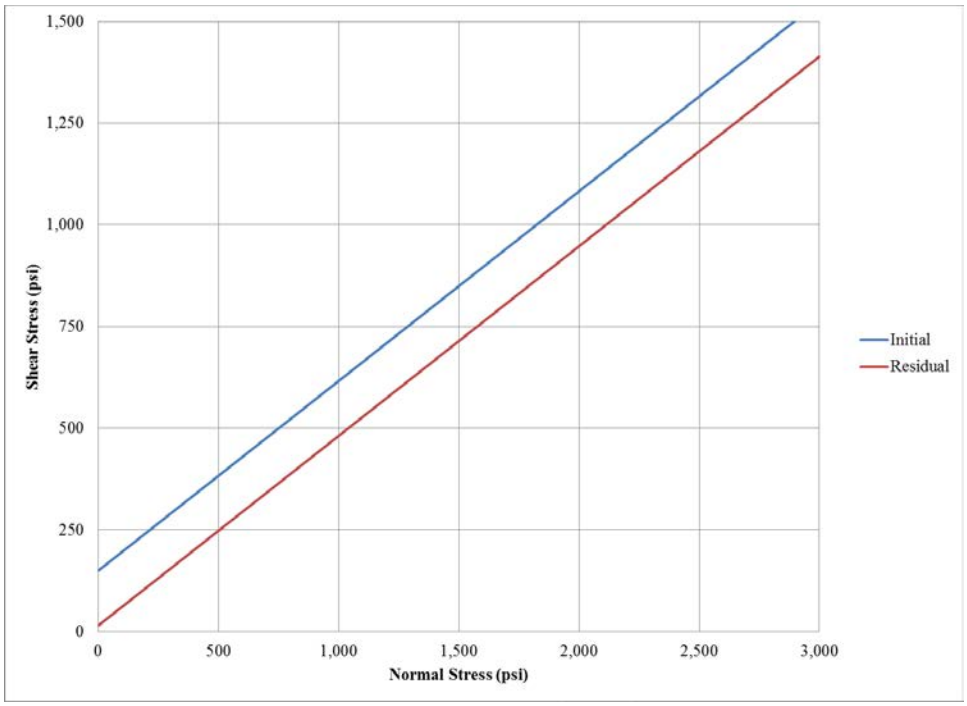

Figure 4-3 Shear Stress vs Normal Stress for initial and residual joint parameters

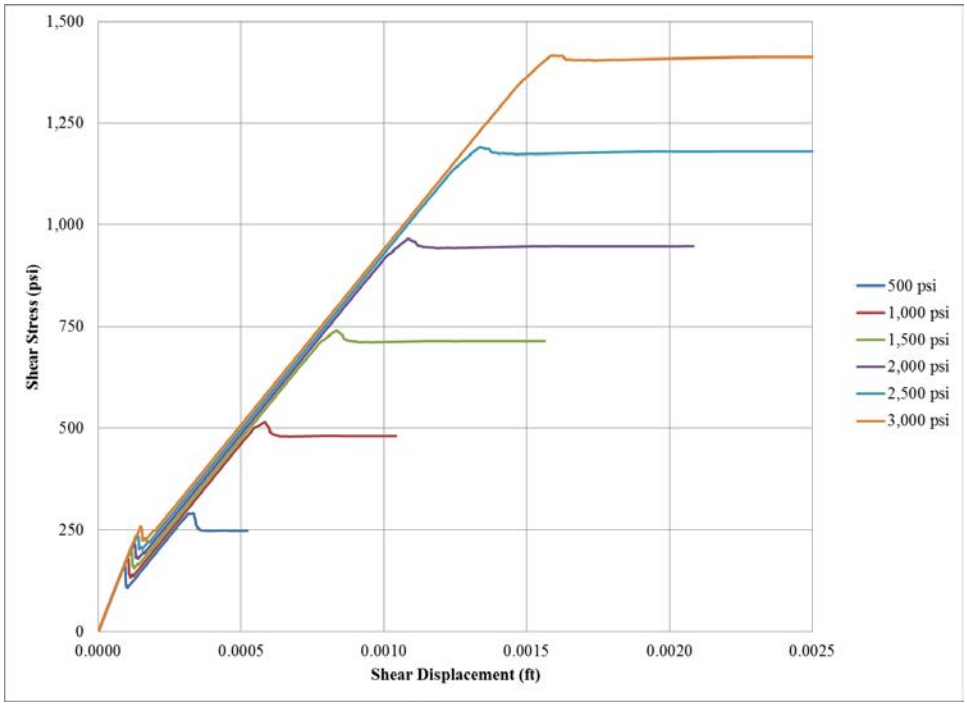

Figure 4-4 Shear Stress versus Shear Displacement for Mohr-Coulomb Joint Model

4.3 Material Model Calibration

With the joint model in place as the coal pillar interface model as the result of numerical direct shear tests, calibration of the coal model for the single pillar distinct element model began. For the initial calibration phase, all overburden was assumed to behave within a purely elastic material model (Table 4-2). The strain-softening material model was selected to represent the coal pillar, as this model is based on the Mohr Coulomb material model with non-associated shear flow and associated tensile flow rules (Itasca, 2013a). The strain-softening model has widely been used to simulate the behavior of brittle materials such as coal measure rocks. This selection allows for the specification of hardening/softening of numerous parameters, including cohesion, friction angle, dilation angle, and tensile strength, all as a function of accumulated plastic strain. This flexibility allows for adaptive calibration and more precise modeling of post-failure behavior, as many research efforts have demonstrated that proper calibration of the strain-softening model has led to realistic modeling of failure mechanics, calculations of stress and strain which are consistent with field measurements, and reasonable forecasts of rock support methodologies (Zipf Jr., 2007). A quarter pillar model (Figure 4-5) was simulated, taking advantage of two planes of symmetry to increase zone density of the coal pillar.

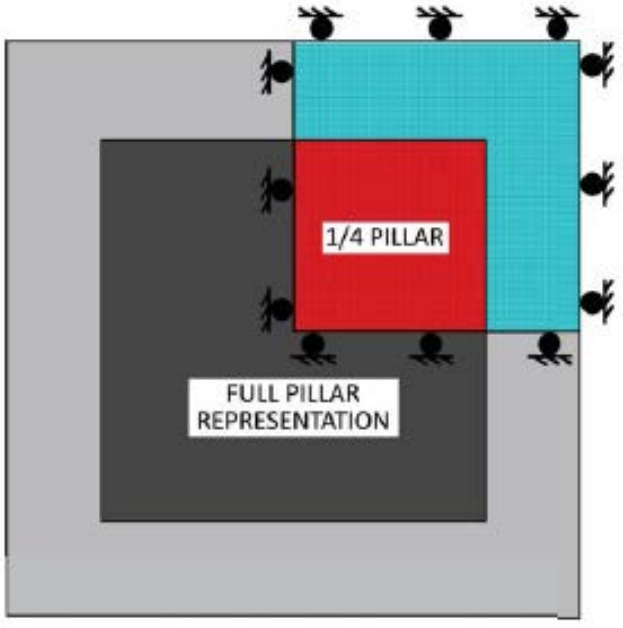

Figure 4-5 Quarter pillar model with roller boundary conditions (Garvey, 2013)

Table 4-2 Elastic overburden material properties

Parameter	Description	Value	Units
E	Elastic Modulus	3,000,000.00	psi
ν	Poisson's Ratio	0.25	
ρ	Density	160	pcf

Equation 4.4 and Equation 4.5 illustrate the shear and tensile yield functions implemented within the Mohr Coulomb material model, whereby the accumulated plastic strain is incrementally calculated and used to adjust the above-mentioned hardening/softening parameters according to the user-defined model (Itasca, 2013a).

$$f^s = \sigma_1 - \frac{1+\sin\emptyset}{1-\sin\emptyset}\sigma_3 + 2c\sqrt{\frac{1+\sin\emptyset}{1-\sin\emptyset}} \qquad 4.4$$

$$f^t = \sigma^t - \sigma_3 \qquad 4.5$$

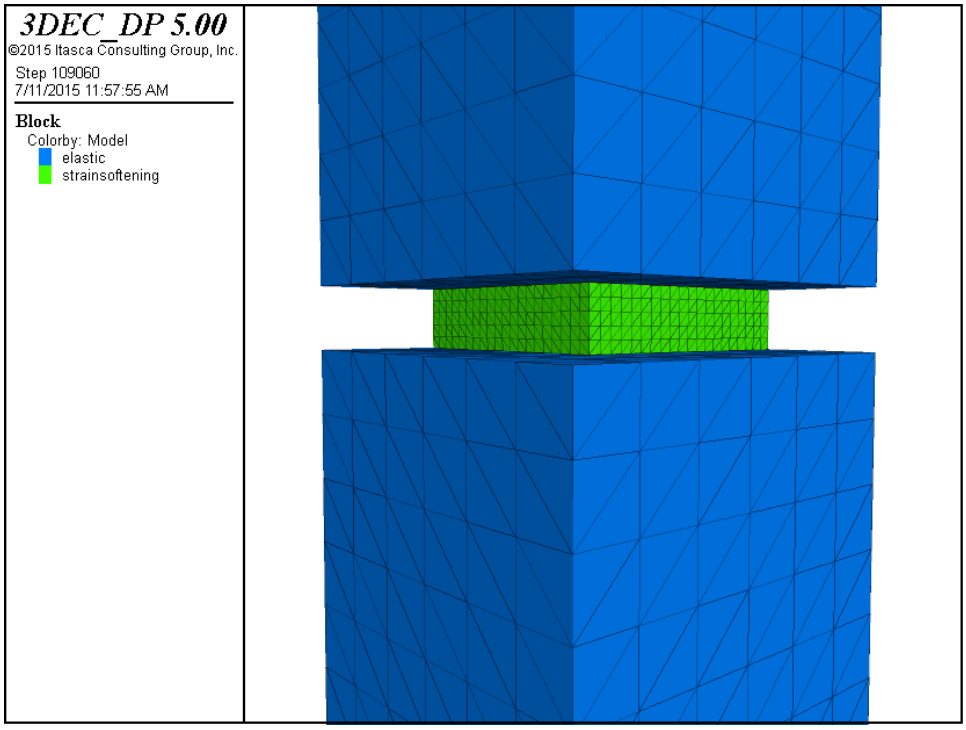

Figure 4-6 Quarter pillar model with elastic overburden and strain-softening coal model

4.3.1 Boundary and Initial Conditions

As previously referenced, the quarter coal pillar model took advantage of two planes of symmetry to facilitate a higher zone density with the use of roller boundary conditions on the sides in addition to a roller boundary condition along with the bottom model boundary. Initial stress conditions were designated to represent realistic in-situ horizontal stress represented by Equation 4.6 (minimum horizontal stress) and Equation 4.7 (maximum horizontal stress) based on the work of Mark and Gadde (2008). This study resulted in a comprehensive statistical comparison of global horizontal stress measurements for both coal and non-coal mining.

$$S_{H,min} = 1.2H + 0.00015E \quad (4.6)$$

$$S_{H,max} = 369 + 1.2H + 0.0003E \quad (4.7)$$

These equations were intended to yield practical levels of minimum and maximum horizontal stress for the pre-mining state of stress. Each includes a depth-dependent component and a tectonic component, which is also related to strata elastic modulus (Esterhuizen et al., 2010a). The horizontal stress was calculated using Equation 3.6 and assumed the equivalent elastic modulus used in the elastic overburden model. Though most of the vertical stress was applied as a velocity at the top of the model boundary to produce the pillar-stress curves, a small value of vertical stress was introduced to the pre-mining model state and the model was brought to an initial equilibrium prior to entry/crosscut excavation. The horizontal and initial vertical stresses applied to each W/H ratio model are summarized in Table 4-3, which are compared to the ARMPS software results to ensure high initial stability and a reasonable horizontal-to-vertical stress ratio as the velocity was applied (K Ratio). All ARMPS evaluations mirrored the modeled coal seam thickness of 5 feet and assumed a six-entry room and pillar system.

The final calibrated strain-softening coal model parameters are documented in Table 4-4 based on a summary of common values widely used by industry for each of the material parameters (Zipf Jr., 2007; Peng, 2008; Esterhuizen et al., 2010a; Mark, 2010). The friction angle was maintained at a constant value while the cohesion, dilation angle, and tensile strength were all softened to residual values as a function of accumulated plastic

strain. This effectively allowed for the coal to behave as a brittle material in a uniaxial or low confinement environment, but to demonstrate strain-hardening behavior as size and confinement increases. The softening of the cohesion, dilation angle, and friction angle with accumulated plastic strain is graphically illustrated on Figure 4-7.

Table 4-3 ARMPS Calibration Study Results

W/H Ratio	Centers ft	Cover ft	ARMPS SF	Vertical Stress psi	Horizontal Stress psi	K Ratio
2	30	50	2.42	55	510	9.28
4	40	125	3.33	139	600	4.32
6	50	250	3.23	278	750	2.70
8	60	500	2.91	556	1,050	1.89

Table 4-4 Strain-Softening Coal Material Properties

Parameter	Description	Value	Units
E	Elastic Modulus	300,000	psi
ν	Poisson's Ratio	0.25	
ρ	Density	80	pcf
$\emptyset$	Friction Angle	25	degrees
C	Initial Cohesion	250	psi
i	Initial Dilation Angle	10	degrees
σ_t	Initial Tensile Strength	75	psi
ε_p	Plastic Range	4.00	%
C_r	Residual Cohesion	25	psi
i_r	Residual Dilation Angle	0	degrees
$\sigma_{t,r}$	Residual Tensile Strength	0	psi

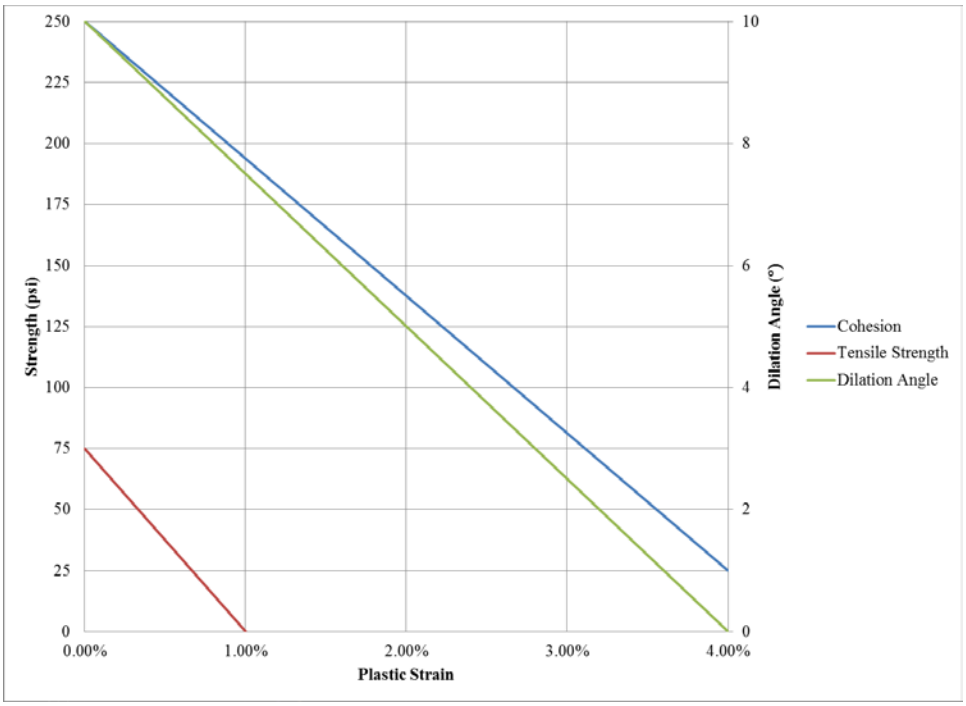

Figure 4-7 Cohesion, Tensile Strength, and Dilation Angle vs accumulated plastic strain

4.4 Calibration Results

The final calibration was examined to determine if the selected coal pillar model yielded comparable results to the Mark-Bieniawksi pillar strength equation (Equation 2.12) with respect to the resultant stress-strain relationship and post-failure behavior. The Mark-Bieniawski pillar strength equation is the most widely accepted pillar strength relationship used in modern coal mine design in the United States, and is the principal determination of pillar strength for both empirical software such as ARMPS (Mark, 2010) and numerical software such as LaModel (Heasley, 2009). The final calibrated coal model was applied to four widely researched pillar sizes (W/H 2-8) because they characteristically exhibit a definitive peak strength threshold. Furthermore, it is customary for the low ratio pillar sizes (W/H 2-6) to demonstrate a definitive strain-softening behavior with post-peak residual strength and the high ratio pillar sizes (W/H 6-8) to represent the transition from brittle, strain-softening behavior to a strain-hardening, elastic-plastic post-peak response.

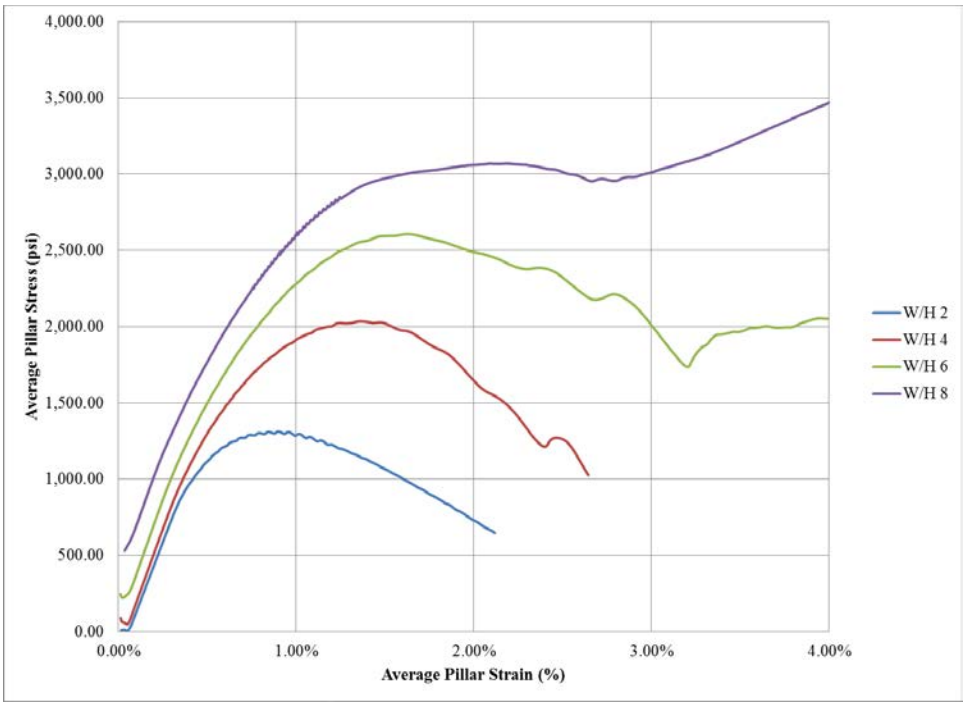

Figure 4-8 Average Pillar Stress versus Strain curves for calibration model, W/H 2-8

The resulting stress-strain curves for the final calibrated coal model are illustrated on Figure 4-8. As expected, strain-softening behavior was widely captured, with the high ratio pillar size (W/H=8) nearly exhibiting elastic perfectly-plastic post-failure behavior. The peak pillar strength values are noted on Table 4-5 and compared to the Mark-Bieniawski pillar strength formula. Good agreement was achieved with all models correlated within a ten percent difference while better agreement was realized for the higher ratio pillar sizes (W/H 6-8). The models also demonstrated non-linearity as the pillar size increased (Figure 4-9), which is common of most geologic materials.

Table 4-5 Comparison of calibration model and Mark-Bieniawski pillar strength equation

W/H Ratio	Peak Strength psi	Mark-Bieniawski psi	Difference psi	Difference %
2	1,311	1,224	87	7.10%
4	2,050	1,872	178	9.53%
6	2,627	2,520	107	4.26%
8	3,069	3,168	-99	3.14%

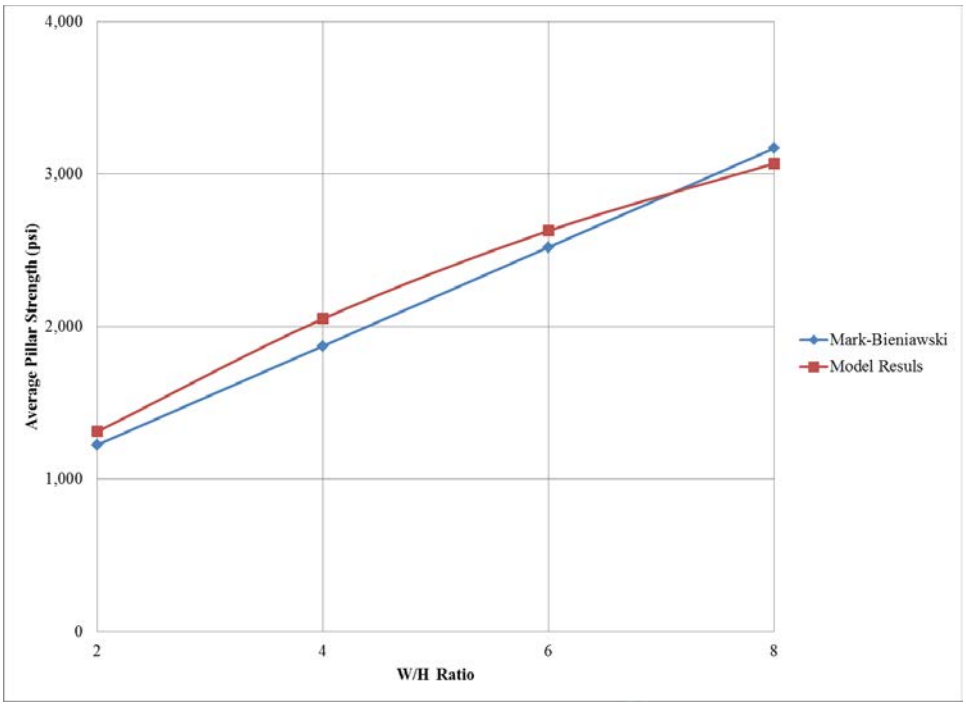

Figure 4-9 Calibrated model results versus the Mark-Bieniawski equation, W/H 2-8

Table 4-6 Boundary and Initial Conditions for Squat Pillar Studies

W/H Ratio	Centers ft	Cover ft	ARMPS SF	Vertical Stress psi	Horizontal Stress psi	K Ratio
8	60	500	2.91	556	1,050	1.89
10	70	750	2.92	833	1,350	1.62
12	80	1,000	3.02	1,111	1,650	1.49

Moving forward, this dissertation will be focused on examining squat coal pillar behavior, hereby defined as those with a W/H ratio greater than or equal to 8, which for an extraction height of five (5) feet results in pillar centers exceeding sixty (60) feet. The boundary horizontal stress and initial vertical stress conditions are shown in Table 4-6.

5 Influence of Coal Pillar Interface

The design of coal pillars has traditionally been predicated on a foundation of mechanical design. That is, the strength and behavior of the pillar is primarily defined by the pillar geometry based on a long history of empirical study. Mark (1999) concluded that much remains to be researched about the significant relationship between the mechanics of squat pillars and the pillar interface. This premise is grounded in the basis that the elastic core of the pillar is surrounded by a zone of yielding and plastic deformation which varies according to load and geologic environment. One consequence of this theory is the importance of an interface slip mechanism between the coal pillar and the surrounding strata which controls both the extent and distribution of stress and deformation in a coal pillar (Iannachione, 1990). Iannachionne (1990) also concluded numerous important characteristics of the coal pillar interface slip mechanism which include:

- The coal pillar interface has an array of properties based on a range from a sharp lithological break to a polished and slickensided surface
- The basic interface friction angle should range from 10 degrees to 20 degrees and cohesion should range between 0 and approximately 150 psi.
- Interface slip can control that rate at which the outer yielding zone develops in response to stress
- Interface frictional properties can greatly influence the ultimate strength of the coal pillar with low frictional properties significantly reducing pillar strength

Lu et al. (2008) examined the importance of various pillar interface models on pillar behavior and the level of confinement generated. Perry et al. (2013) numerically examined a wide range of pillar geometries and concluded the dependence of pillar strength and post-peak behavior on interface strength. As a consequence, to advance understanding of squat coal pillar behavior and study coal bump potential, it is necessary to further investigate the reliance of pillar strength and behavior on interface frictional characteristics. A wide range of interface properties will be examined with an elastic overburden followed by a more comprehensive numerical investigation which accommodates plastic deformation of the roof and floor strata.

5.1 Interface Model

The behavior of joints is critical to the understanding of stability analysis for jointed rock mass such as coal pillars. The shear behavior of non-planar joints, such as the coal pillar interface, is most significantly influenced by the joint surface roughness. That is, the rougher the joint the higher the shear strength. Consequently, the numerical representation of the roughness model is essential to the estimation of the shear strength, dilatancy, and stiffness of a rock joint (Indraratna and Haque, 2000). Obert et al. (1976) demonstrated that increases in normal stiffness reduce joint dilation and also increases the peak and delineation of the joint shear strength. The condition and shearing of the joint asperities which define joint roughness are important to the shear response. Patton (1966) conducted research on the behavior of regular saw-teeth artificial joints under a condition of constant normal load, which resulted in good agreement with a bilinear shear strength envelope. Barton (1973) introduced a non-linear strength envelope formulation (Equation 5.1) for non-planar rock joints under constant normal load which depends on the peak dilation angle, normal stress, uniaxial compressive strength, asperity angle, and a constant known as the Joint Roughness Coefficient (JRC).

$$\frac{\tau_p}{\sigma_n} = \tan\left(\phi_b + JRC \log_{10}\left(\frac{\sigma_c}{\sigma_n}\right)\right) \qquad 5.1$$

This result led Barton (1973) to empirically derive the Joint Roughness Coefficient (Equation 5.2) based on the fractal dimension, average height, and average base length of the joint asperities.

$$JRC = 85.27(D-1)^{0.57} \qquad 5.2$$

The strength envelopes observed in the studies of clean rock joints by Indraratna and Haque (2000) are primarily linear in nature, with an increase in shear strength at higher normal stress and a subsequent and sudden drop in shear stress to a residual level that is associated with the shearing of asperities. The Coulomb Slip joint model can adequately capture this observed behavior. Based on the initial calibrated Coulomb Slip joint model, a revised joint model with variations in initial and residual friction (Table 5-1) was conducted to simulate numerous coal pillar interface frictional models at increasing levels of normal stress. A total of six combinations of peak and residual friction angle were

investigated with the shear response for these combinations illustrated as Figure 5-1 through Figure 5-6.

Table 5-1 Coulomb Slip Joint Model Parameters for Elastic Interface Study

Parameter	Description	Value	Units
jkn	Joint Normal Stiffness	3,600,000	psi/ft
jks	Joint Shear Stiffness	1,800,000	psi/ft
∅	Joint Initial Friction Angle	25-35	degrees
C	Joint Initial Cohesion	150	psi
σ_t	Joint Initial Tensile Strength	45	psi
$\emptyset_r$	Joint Residual Friction Angle	20-25	degrees
C_r	Joint Residual Cohesion	15	psi
$\sigma_{t,r}$	Joint Residual Tensile Strength	0	psi

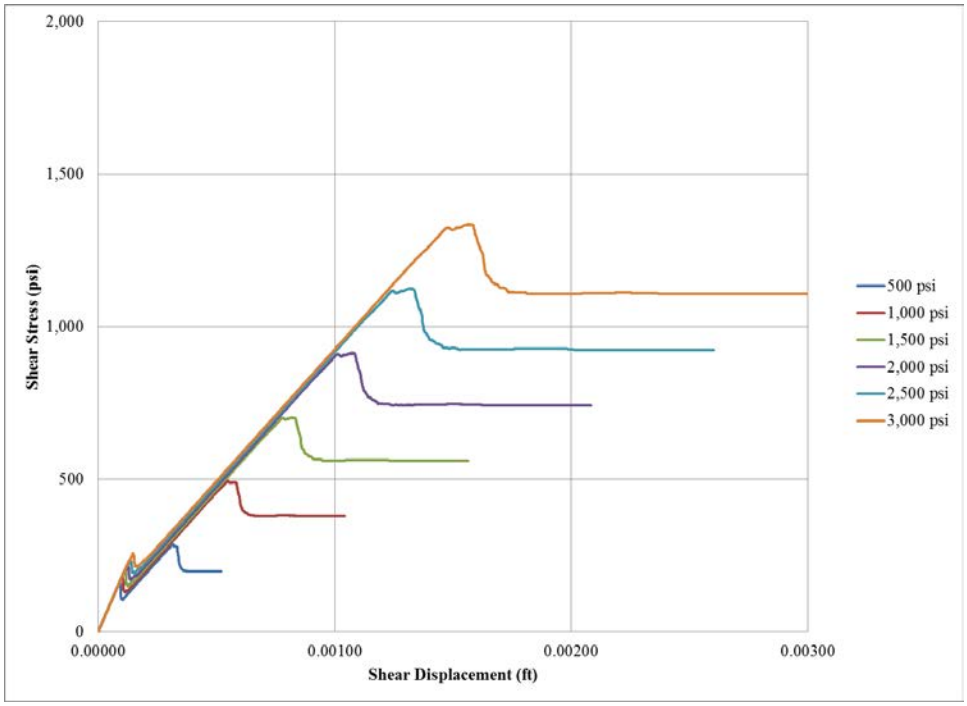

Figure 5-1 Shear Stress versus Shear Displacement for Peak (25) and Residual (20) Friction Angle

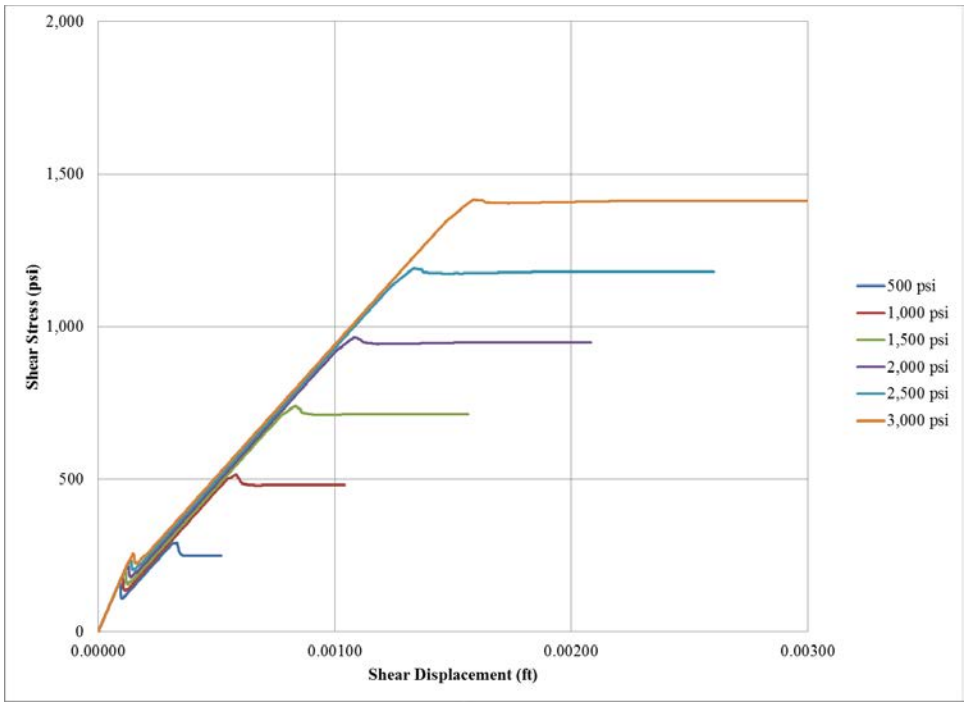

Figure 5-2 Shear Stress versus Shear Displacement for Peak (25) and Residual (25) Friction Angle

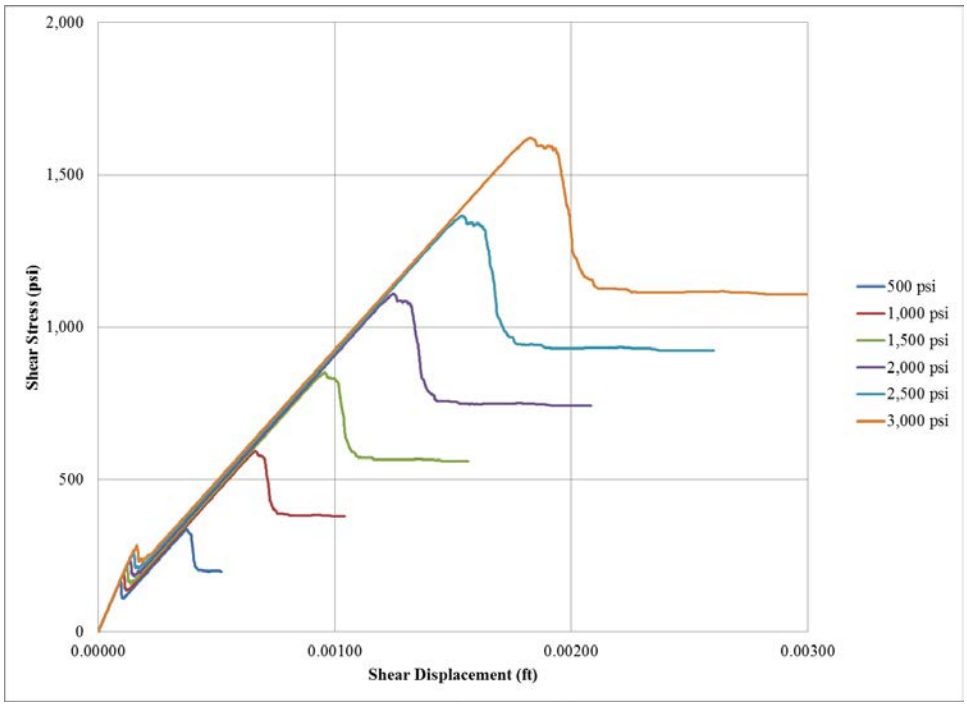

Figure 5-3 Shear Stress versus Shear Displacement for Peak (30) and Residual (20) Friction Angle

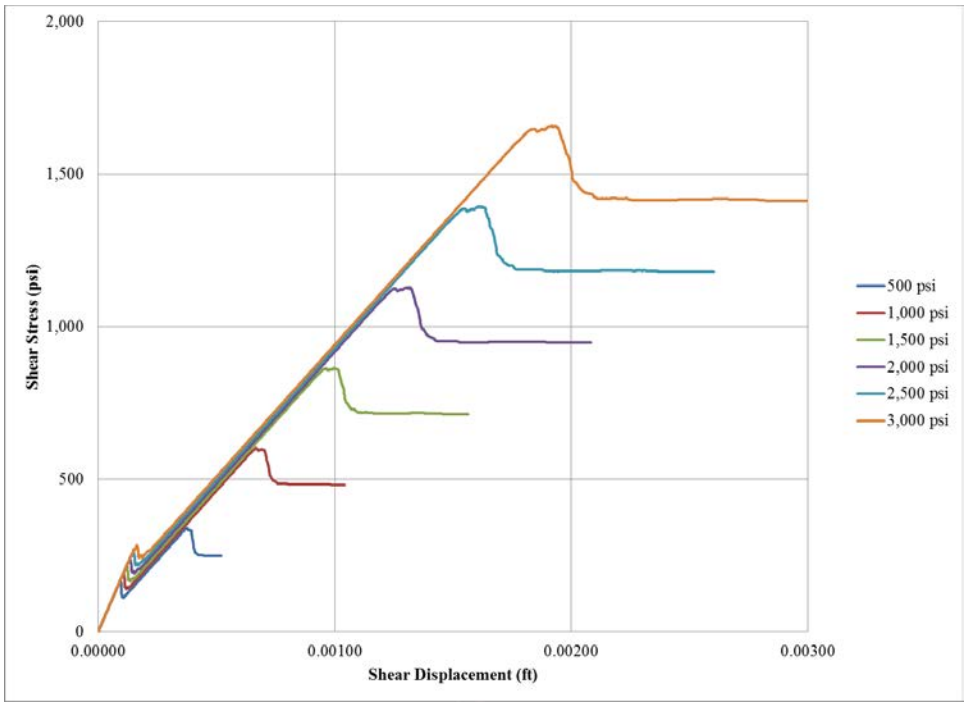

Figure 5-4 Shear Stress versus Shear Displacement for Peak (30) and Residual (25) Friction Angle

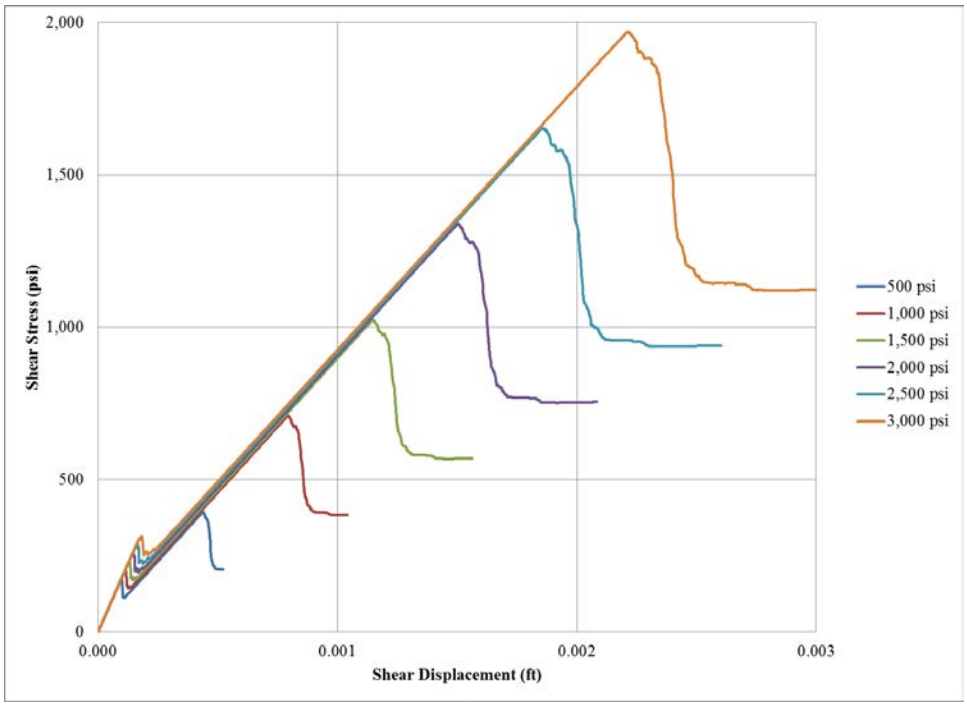

Figure 5-5 Shear Stress versus Shear Displacement for Peak (35) and Residual (20) Friction Angle

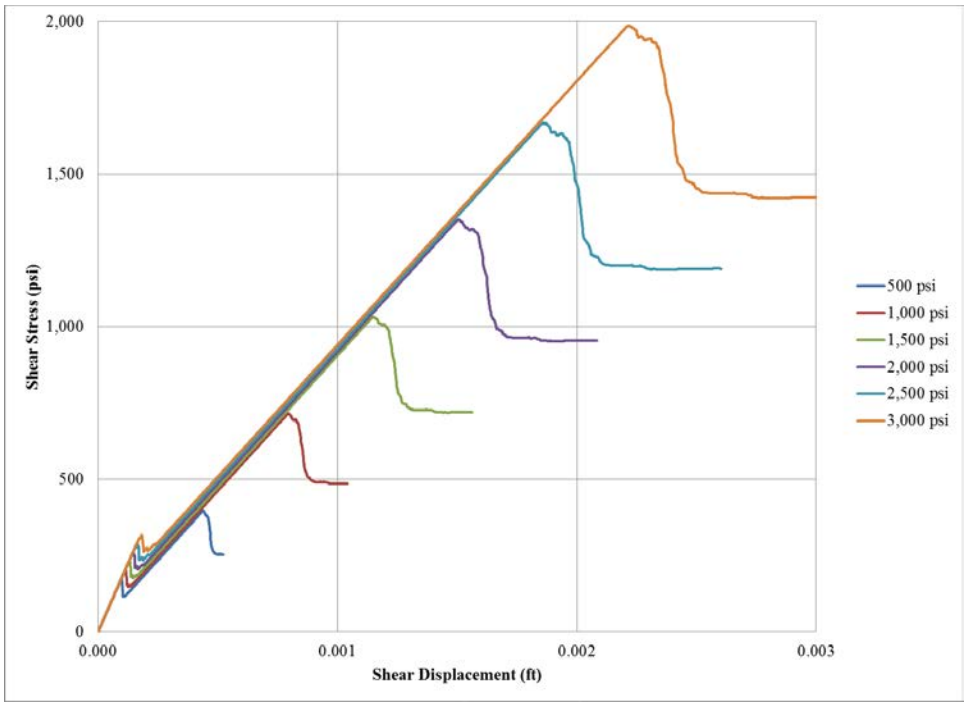

Figure 5-6 Shear Stress versus Shear Displacement for Peak (35) and Residual (25) Friction Angle

Each of the six combinations of peak and residual friction angle demonstrate predominantly linear increases in shear strength as the normal stress is increased for each of the numerical direct shear tests. The peak shear strength is primarily governed by the initial friction angle while the residual shear strength is dictated by the residual friction angle. Consequently, the severity of the sudden decrease in peak and residual shear strength appears to be largely a function of the apparent difference in peak and residual friction. Another consequence is the value of shear displacement at failure, which is proportional to the joint friction angle. Wang et al. (2014) determined that the initial stress state and the change in frictional characteristics as sliding occurs affects the peak shear strength of coal-rock interfaces, and that after unstable slip the shear displacement increased rapidly.

It is apparent that fine grained lithology, such as shale, have smaller granular features and asperity angles, resulting in lower joint roughness and a smaller apparent difference in peak and residual friction angle. On the contrary, coarse grained lithology, such as sandstone, have larger granular features and asperity angles, which result in a higher joint

roughness coefficient, increased shear strength, and a greater apparent differential in peak and residual friction angle. The disparity in peak and residual shear strength provides an important mechanism for joint "stick-slip", resulting in higher initial pillar confinement but also the capacity for unstable failure along the pillar interface. High normal stress and a condition in which the initial shear stress exceeds the shear strength create a potential transitional condition between stable sliding and stick-slip which result in violent energy release (Zou et al., 1989).

5.2 Elastic Overburden

5.2.1 Pillar Stress-Strain

Independent of pillar geometry, there appears to be only infinitesimal differences in the overall behavior of the stress-strain relationships for each of the six combinations of joint friction model, particularly during the elastic region of loading. However, as the pillar is strained further and plastic deformation leads to elastic-plastic (Figure 5-7) or strain-hardening behavior (Figure 5-8 and Figure 5-9), the interface frictional model begins to significantly influence the stress-strain behavior. For a given level of strain, the average pillar stress (defined as the average stress calculated through the quarter pillar block due to symmetry) is dependent on the initial friction angle, especially at high values of pillar strain. The residual friction angle appears to be a more vital indicator of general pillar behavior, as there is a clear delineation between groupings within every pillar size examined.

The disparity in initial and residual friction angle also shows to be an important indicator of post-failure pillar performance. The highest differentials existing between the initial and residual friction value consistently result in the ability for the pillar to suddenly lose strength at higher values of strain, indicative of a loss of confinement and interface "stick-slip". This consequence suggests unstable failure and should be reflected as high shear strain rates, peaks in kinetic energy release, and obviously high values of joint friction work. This result is obviously more prevalent in the W/H=8 ratio pillar than in the W/H=12 ratio pillar; however it is important to note that the strain level at which this result occurs continually decreases at the pillar size is increased.

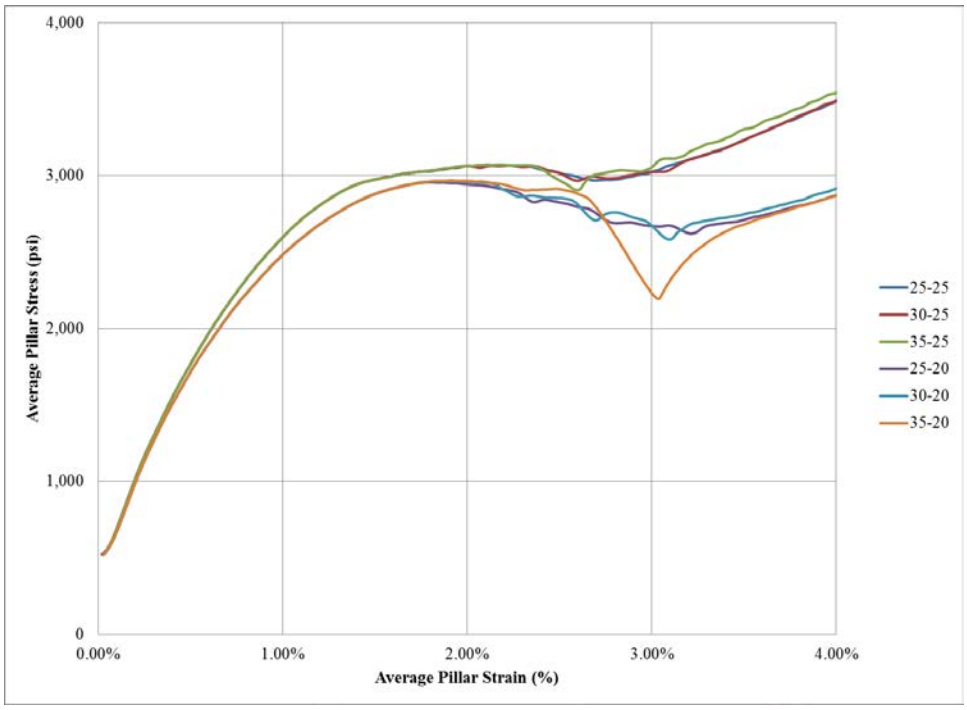

Figure 5-7 Average Pillar Stress versus Average Pillar Strain, W/H=8

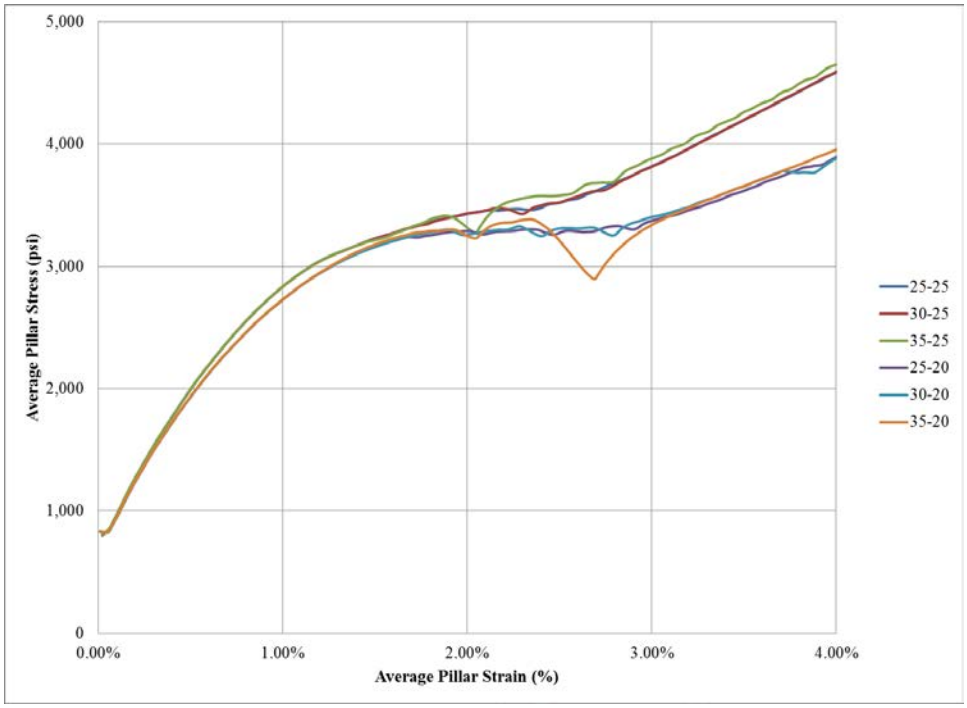

Figure 5-8 Average Pillar Stress versus Average Pillar Strain, W/H=10

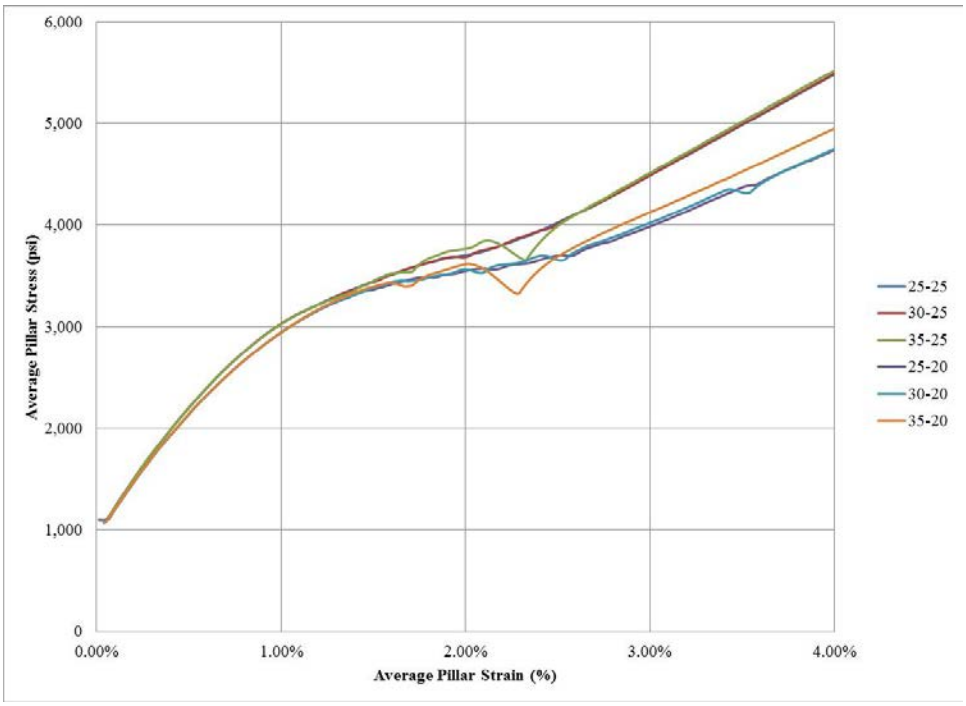

Figure 5-9 Average Pillar Stress versus Average Pillar Strain, W/H=12

5.2.2 Pillar Confinement

As both the initial interface friction angle and the differential in initial and residual friction angle increases, so does the volatility in the average level of pillar confinement. This consequence illustrates slip occurring along the pillar interface which can result in sharp decreases in confinement. While higher values of initial friction angle generally result in increased strength due to elevated levels of confinement, the residual friction angle appears to be a more conspicuous indicator of pillar strength at high values of strain, a result that was mirrored in the pillar stress-strain relationships. There appears to be a discernible relationship between the interface friction, the pillar geometry, and the level of confinement which may be lost at the onset of interface slip, as the degree of confinement lost at slip is more dramatic for the W/H=8 ratio pillar (Figure 5-10) when compared to the W/H=10 ratio pillar (Figure 5-11) or the W/H=12 ratio pillar (Figure 5-12).

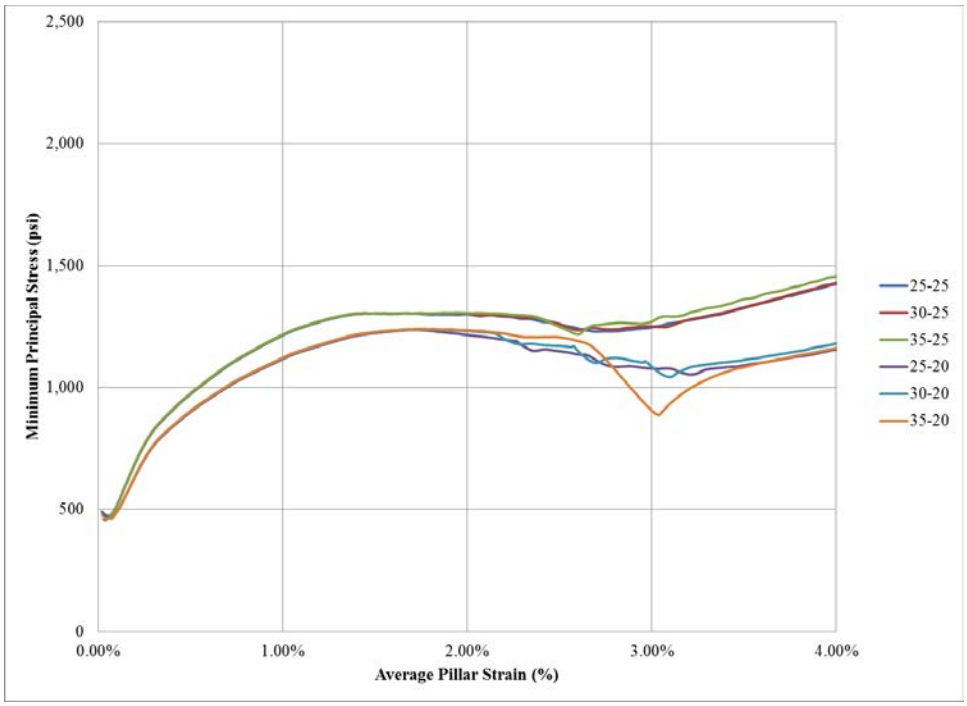

Figure 5-10 Average Confinement versus Average Pillar Strain, W/H=8

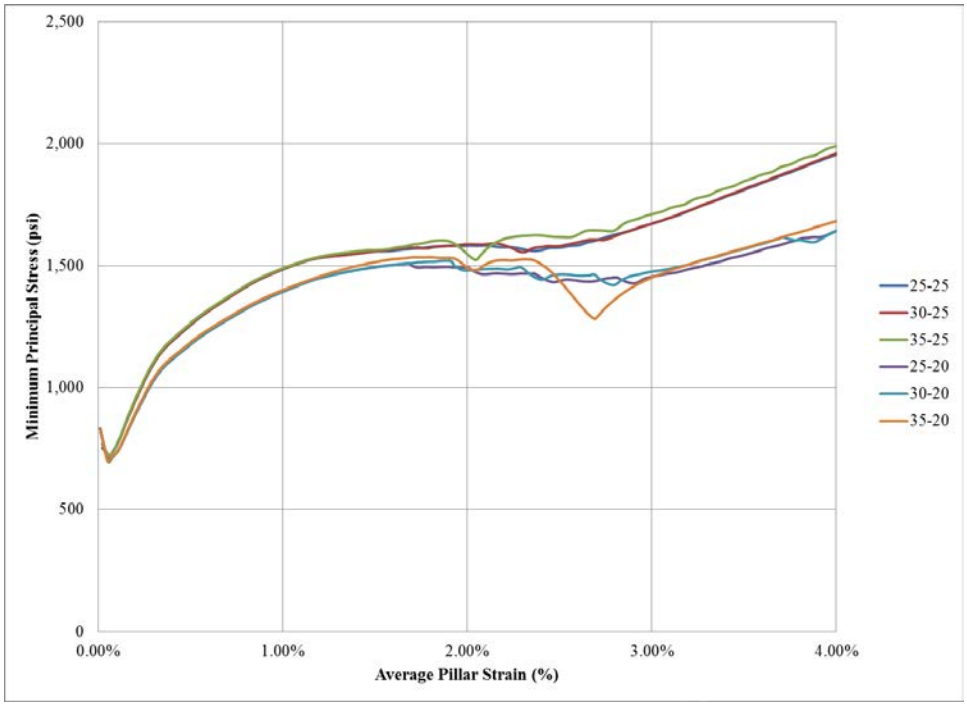

Figure 5-11 Average Confinement versus Average Pillar Strain, W/H=10

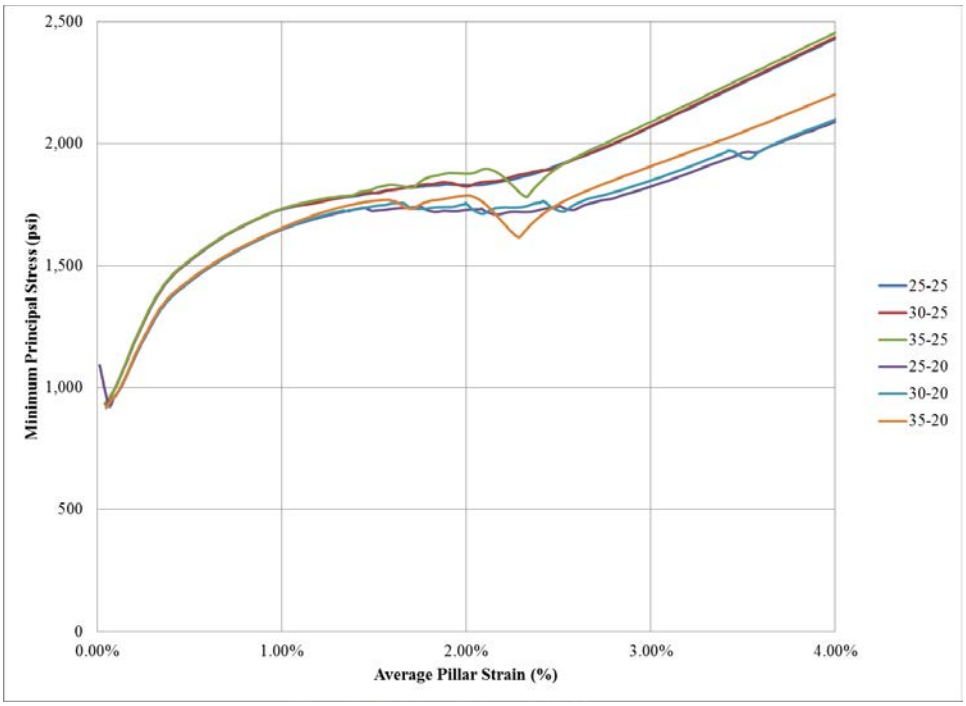

Figure 5-12 Average Confinement versus Average Pillar Strain, W/H=12

It is significant that the level of strain for which slip occurs actually decreases as the pillar size is increased, a finding consistent with the pillar stress-strain curves. Additionally, it is important to note that the results for pillar confinement are average values only for the entire pillar boundary, and that confinement lost near the pillar ribs is certainly more significant in value than that lost towards the pillar core. Therefore measureable losses in the reported average confinement are assuredly coupled with very severe decreases from the pillar rib extending in towards the pillar center.

Iannacchionne (1990) concluded from a numerical investigation of pillar interface slip that the delayed onset of plastic deformation in the low confinement zones could unstably hasten the commencement of plastic deformation in the high confinement zones located near the pillar core. This same mechanism would be explained by an interface frictional model which had high initial frictional strength and low residual strength, resulting in high initial confinement and the sudden failure of a significant portion of the pillar interface at the onset of failure. A similar correlation was resolved by Lu et al. (2008) who numerically observed the development of an elastic core as interface strength increased. This same investigation also studied the minimum principal stress distribution

in the pillar for various interface friction models and determined that the confinement effect is more pronounced at high interface strength and squat coal pillars.

5.2.3 Peak Shear Strain Rate

Higher W/H ratio coal pillars are capable of producing larger shear strain rates (Table 5-2) but the differences in magnitude are not nearly as great as first indicated. This makes intuitive sense, because while the total energy available for release is potentially larger for increased pillar sizes, coal pillar failure takes an outside-in approach. That is, stress concentrations and plastic deformation begin at the rib and the yield extent and transition zone may be very geometrically similar for a spectrum of pillar geometries, whereas the primary difference is unquestionably the size of the elastic core. Failure therefore, whether a stable yield or unstable burst, would undoubtedly follow this same mechanism.

Table 5-2 Maximum Peak Shear Strain Rate for each Joint Friction Model

W/H	Joint Friction	Peak SSR (s^-1)	Strain (%)	Avg. Strain (%)
8	25-25	0.29	2.18%	2.76%
	30-25	1.44	2.99%	
	35-25	1.65	2.51%	
	25-20	1.96	3.05%	
	30-20	2.99	2.96%	
	35-20	3.51	2.85%	
10	25-25	0.31	2.25%	2.41%
	30-25	1.51	2.16%	
	25-20	2.03	2.81%	
	35-25	2.32	1.97%	
	30-20	3.18	2.69%	
	35-20	3.87	2.59%	
12	25-25	0.33	1.99%	2.21%
	30-25	1.60	1.92%	
	25-20	2.23	2.50%	
	35-25	2.71	2.27%	
	30-20	3.47	2.42%	
	35-20	4.10	2.16%	

The average pillar strain at which peak shear strain rate occurred decreased as the pillar geometry increased, a result consistent with previous findings. Again, the most prominent result is the fact that the greatest potential shear strain rates occurred at the largest difference in peak/residual friction angle. For each pillar size examined the largest interface differential yielded the highest peak shear strain rate, and conversely when the friction angle was maintained at a constant value the models yielded the lowest peaks in shear strain rate. More importantly though is the magnitude and duration of this "spike" in peak shear strain rate, which logically is a more reliable indicator of burst potential. As the W/H ratio increases, the ability for this spike to be sustained appears to

increase as evidenced in the peak shear strain rate graphs for the W/H=8 pillar (Figure 5-13), W/H=10 pillar (Figure 5-14), and W/H=12 pillar (Figure 5-15). The largest differentials in peak/residual friction angle also resulted in the largest sustained shear strain rate interval, while the ability for a given interface friction to result in sustained peak shear strain rates increased with pillar size. It is also apparent that the net pattern of spikes in peak shear strain rate becomes more volatile as the pillar geometry increases, suggesting that unstable failures may actually occur over a broader range of pillar strain.

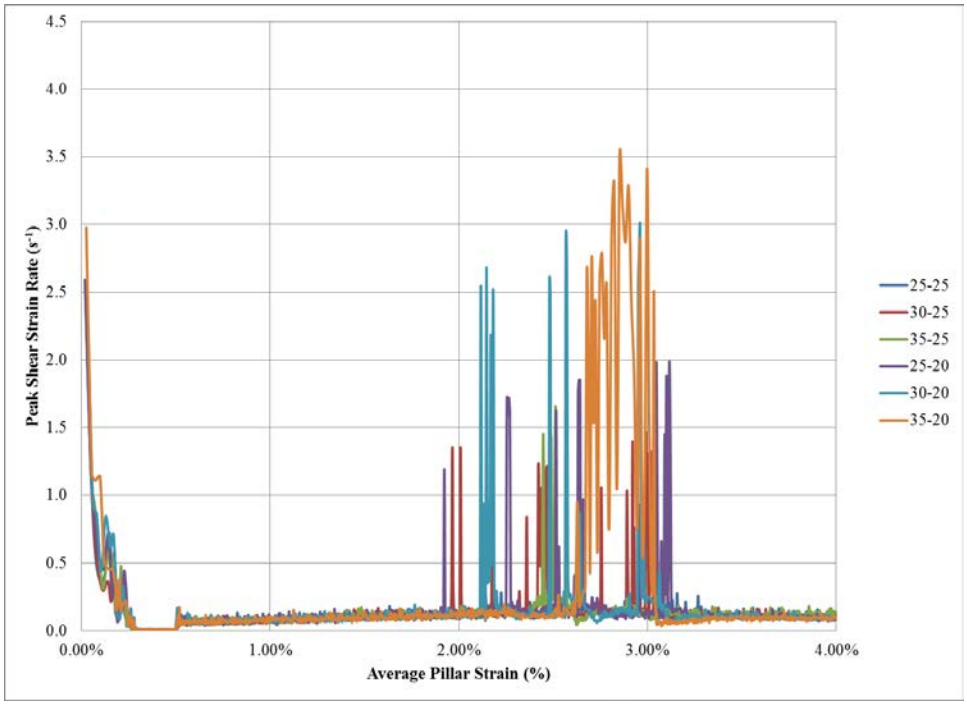

Figure 5-13 Peak Shear Strain Rate vs Average Pillar Strain, W/H=8

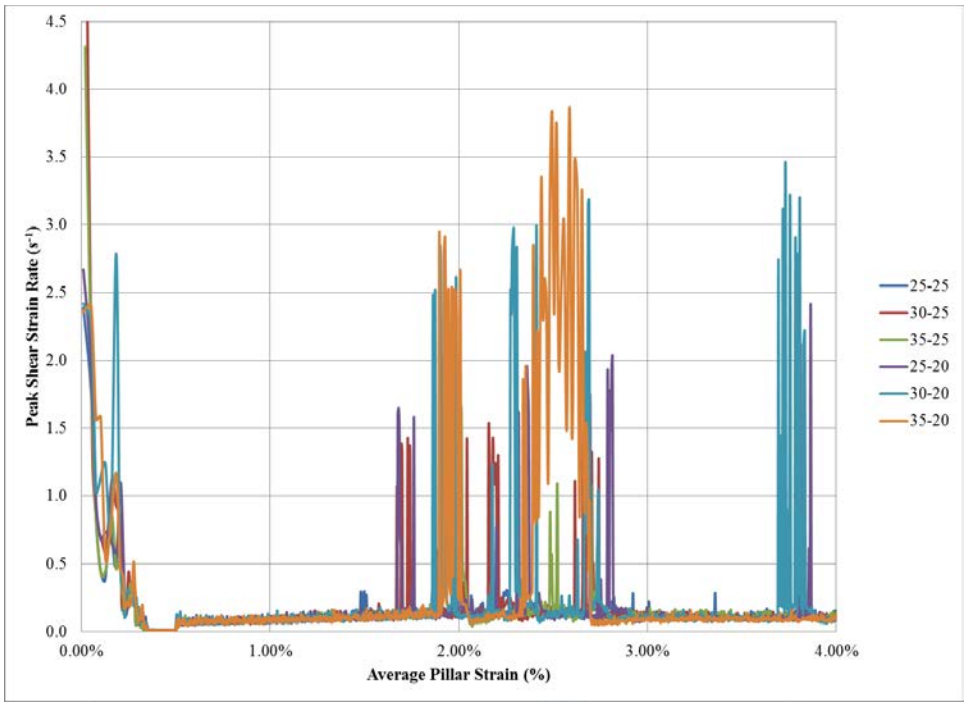

Figure 5-14 Peak Shear Strain Rate vs Average Pillar Strain, W/H=10

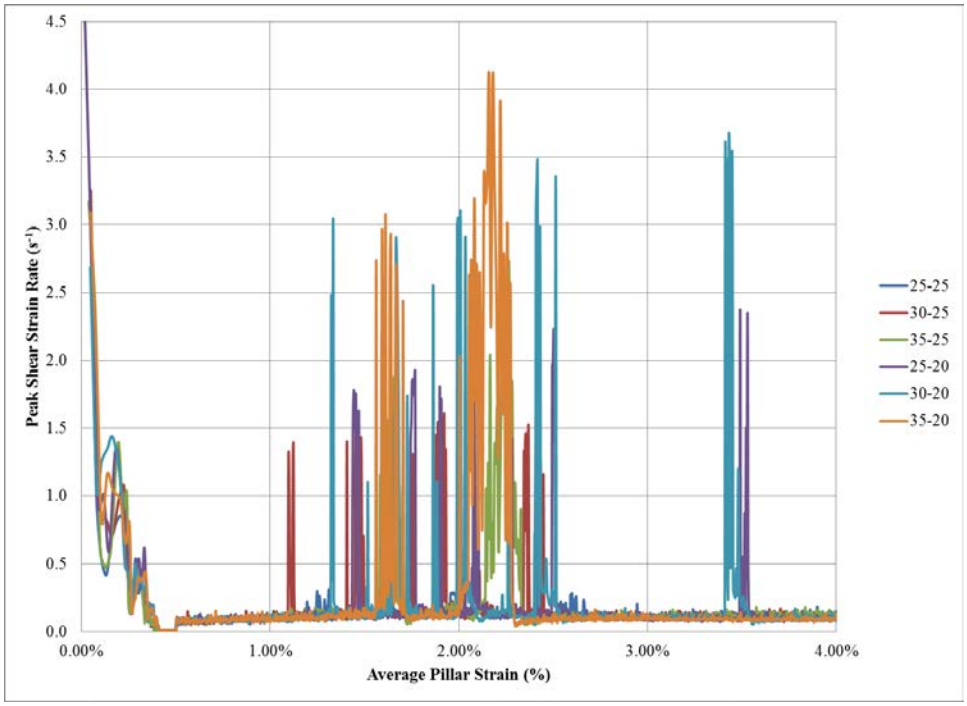

Figure 5-15 Peak Shear Strain Rate vs Average Pillar Strain, W/H=12

5.2.4 Total Energy Release

Total energy released is a central indicator of the excess energy that may be available for unstable failure. It is clear that as the pillar size increases, the total energy release curves are clearly transforming from a primarily linear basis for the W/H=8 (Figure 5-16) and W/H=10 (Figure 5-17) pillars to a higher order growth relationship for the W/H=12 pillar (Figure 5-18), indicative of greater releases of total energy. For example, the total energy release for at two percent strain for the W/H=8 pillar is approximately thirty percent of the excess energy released for the W/H=12 pillar at the same level of strain. Furthermore, as the pillar size is increased the interface friction model becomes a more projecting factor in the total energy released, especially for higher values of average pillar strain. It is also clear that while the total energy released is largely independent of initial friction angle over the range of strain examined, it seems to be more glaringly dependent on the residual friction angle. This dependence appears to be more prominent at higher levels of strain. Poeck et al. (2015) correlated energy release from a two-dimensional model of coal bump case studies and concluded that a potential failure mechanism of squat coal pillars is the unstable shear slip along the coal/rock interface.

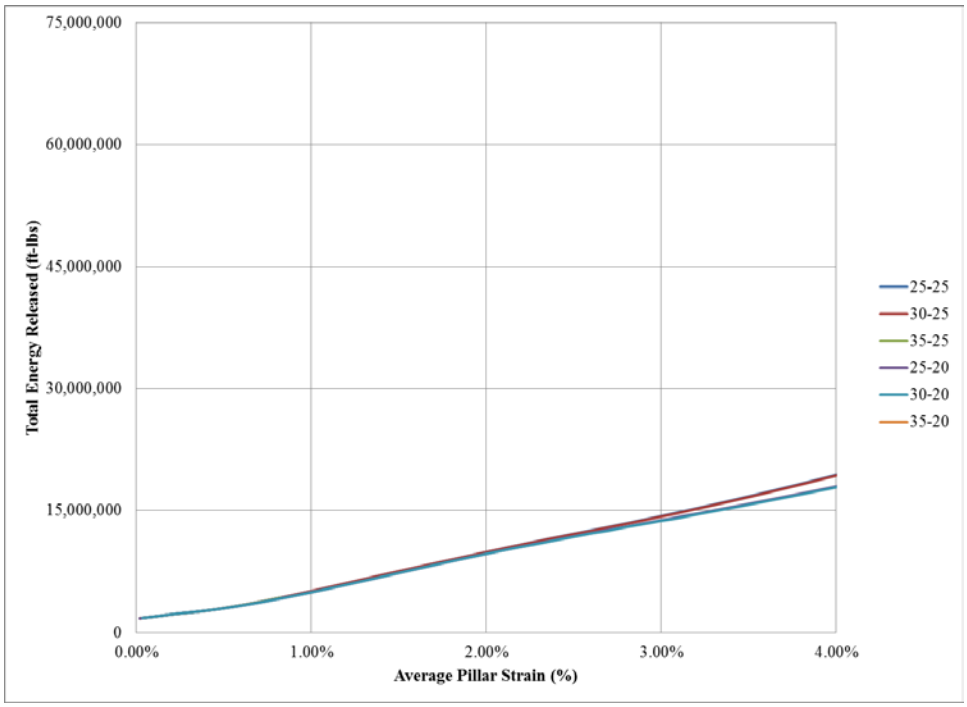

Figure 5-16 Total Energy Released vs Average Pillar Strain, W/H=8

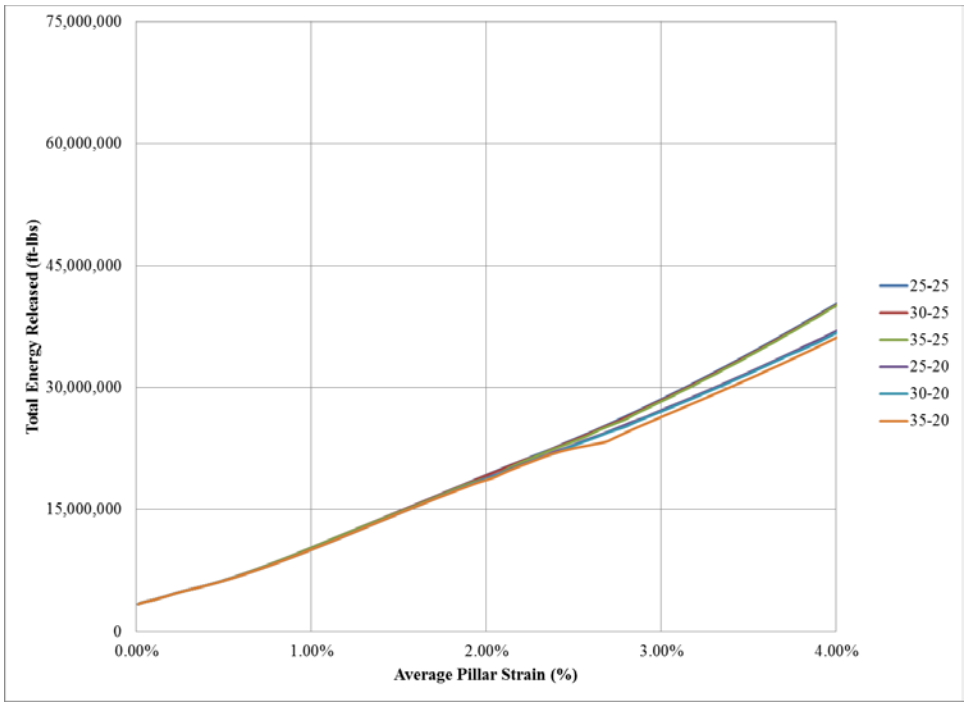

Figure 5-17 Total Energy Released vs Average Pillar Strain, W/H=10

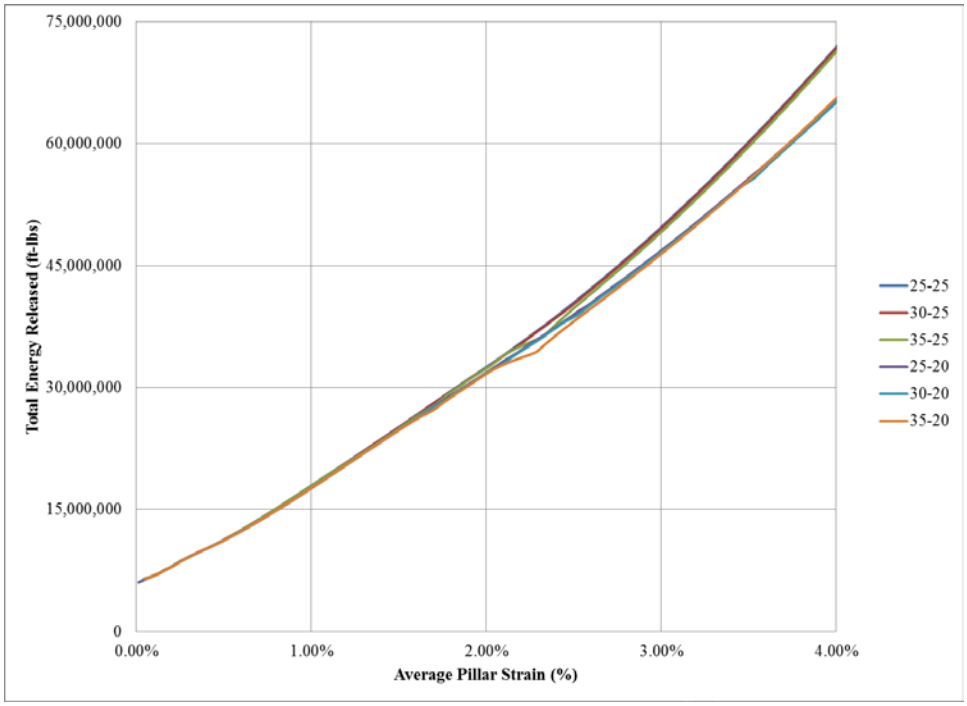

Figure 5-18 Total Energy Released vs Average Pillar Strain, W/H=12

5.2.5 Kinetic Energy

Each of the squat coal pillar models demonstrated the capacity to abruptly release kinetic energy in an unstable manner, but the quantity released was truly dependent on the frictional model (Table 5-3). High kinetic energy release was consistently present when the interface friction model had the largest difference in initial and residual friction angle. The maximum kinetic energy release for each pillar examined was an order of magnitude greater than that minimum kinetic energy release, which always occurred when the friction angle was maintained at a constant value.

Table 5-3 Maximum Kinetic Energy Release for each Joint Friction Model

W/H	Joint Friction	Kinetic Energy (ft-lbs)	Strain (%)	Avg. Strain (%)
8	25-25	214.16	2.50%	2.64%
	30-25	253.80	2.54%	
	35-25	305.45	2.57%	
	25-20	345.40	2.71%	
	30-20	567.17	2.63%	
	35-20	2728.59	2.90%	
10	25-25	275.87	2.31%	2.25%
	30-25	380.33	2.26%	
	25-20	414.59	2.42%	
	30-20	569.40	1.91%	
	35-25	921.29	2.00%	
	35-20	4305.38	2.59%	
12	25-25	299.78	1.92%	2.15%
	30-25	386.32	1.97%	
	25-20	443.98	2.08%	
	30-20	738.61	2.46%	
	35-25	1799.58	2.27%	
	35-20	3226.60	2.20%	

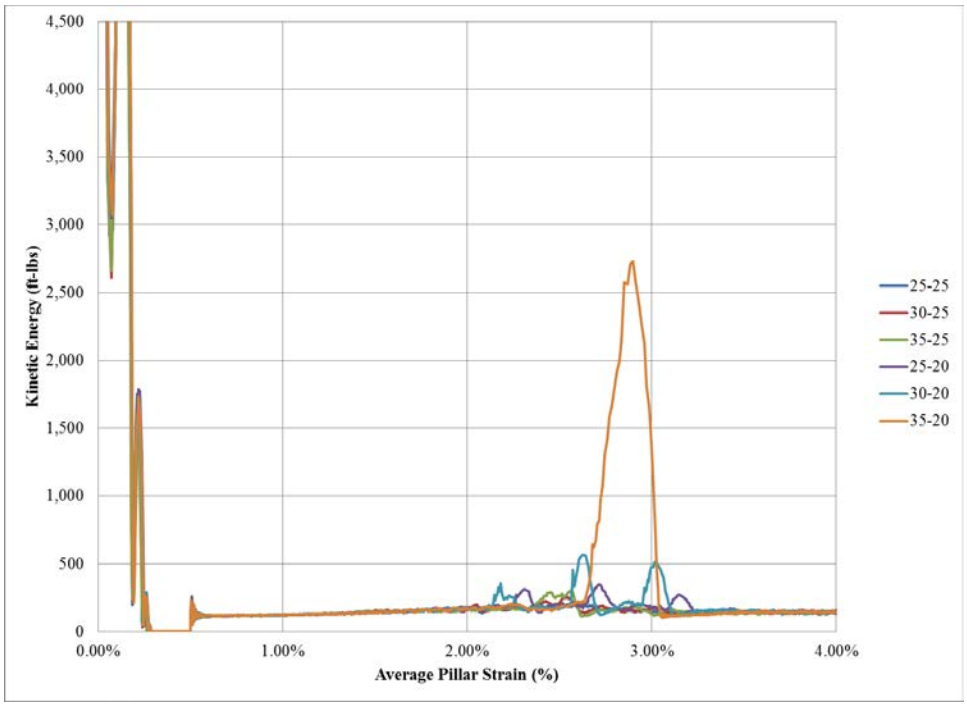

Figure 5-19 Kinetic Energy vs Average Pillar Strain, W/H=8

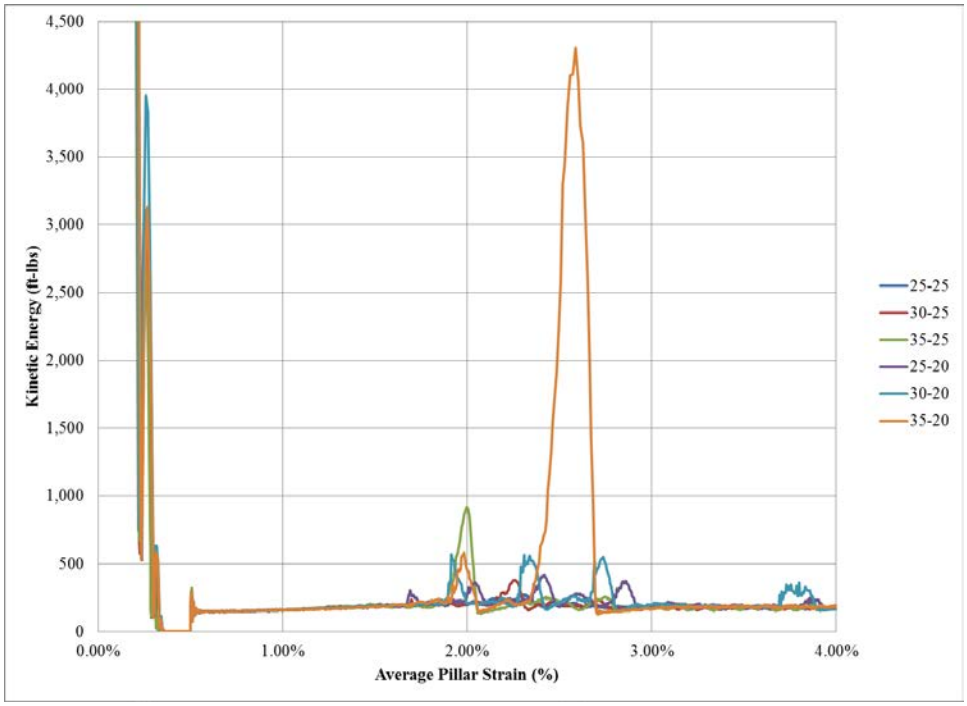

Figure 5-20 Kinetic Energy vs Average Pillar Strain, W/H=10

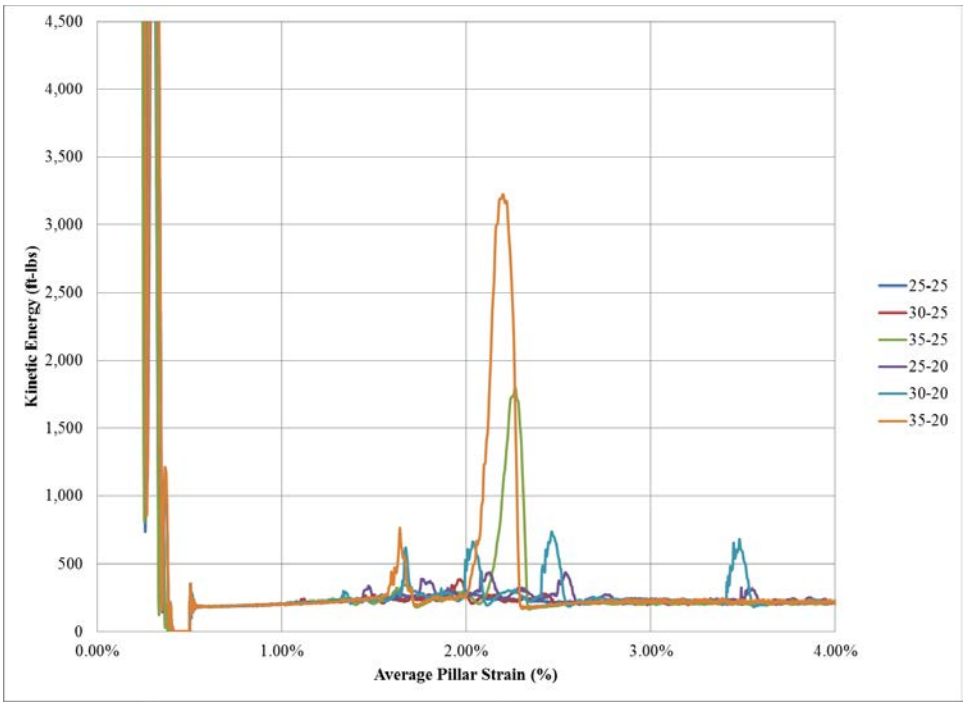

Figure 5-21 Kinetic Energy vs Average Pillar Strain, W/H=12

Contrary to the results indicated for the total energy release, the largest kinetic energy release occurred for the W/H=10 pillar (Figure 5-20), while the kinetic energy release for the W/H=8 pillar (Figure 5-19) and W/H=12 pillar (Figure 5-21) were very similar. This suggests that for a given geologic and loading environment, an optimum pillar configuration could therefore exist whereby the probability for unstable failure may be inherently greater. Consistent with previous findings, the average pillar strain at which the peak kinetic energy release occurred decreased as the pillar size increased. It is also interesting to note that less significant kinetic energy releases were observed for the higher ratio pillars; however these occurrences were arising across nearly all joint friction models examined and spread over a wide range of pillar strains. However the occurrence of these more common kinetic energy releases were more closely dependent on the initial friction angle than the residual friction angle. The use of kinetic energy release as an indicator of unstable coal pillar failure was an importance centerpiece of the work of Kias (2013).

5.2.6 Joint Friction Work

Joint friction work is the energy dissipated as heat at the pillar interface due to unstable shearing. Consequently, abrupt and rapid upturns in the joint friction work are undoubtedly a key confirmation of this instability which could result in a coal pillar burst. Figure 5-22, Figure 5-23, and Figure 5-24 illustrate the joint friction work against the average pillar strain for each of the W/H=8 pillar, W/H=10 pillar, and W/H=12 pillar modeled, respectively. It is immediately obvious that once again, a greater difference between the initial and residual friction angle is the principal driver of the sudden increases in joint friction work. The degree of this increase becomes more severe as the pillar size increases, and also begins to occur over a broader range of friction models and levels of strain.

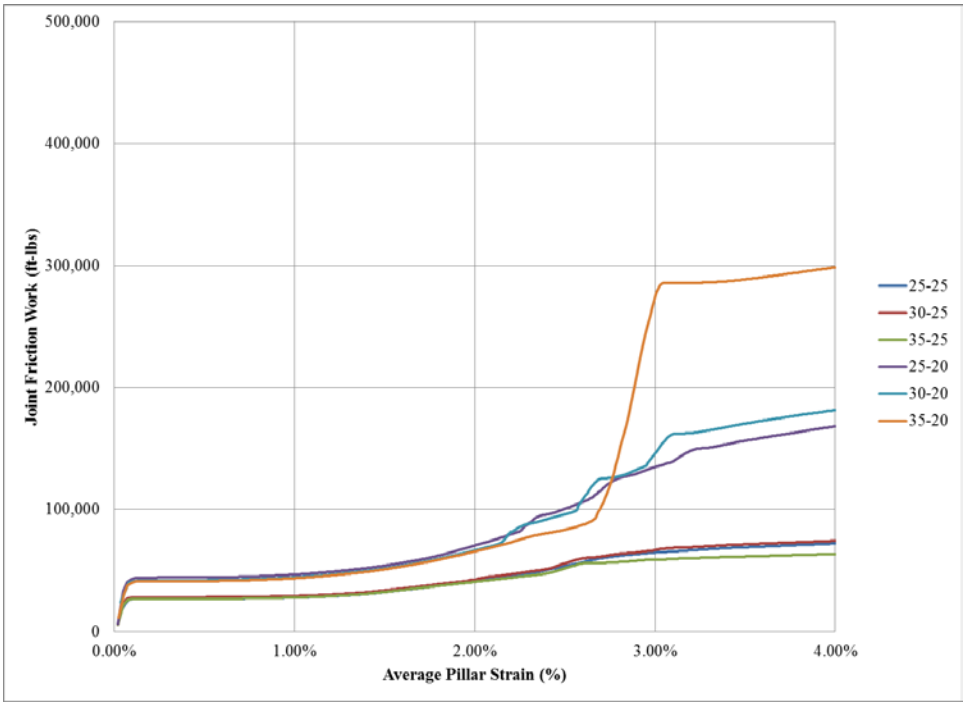

Figure 5-22 Joint Friction Work vs Average Pillar Strain, W/H=8

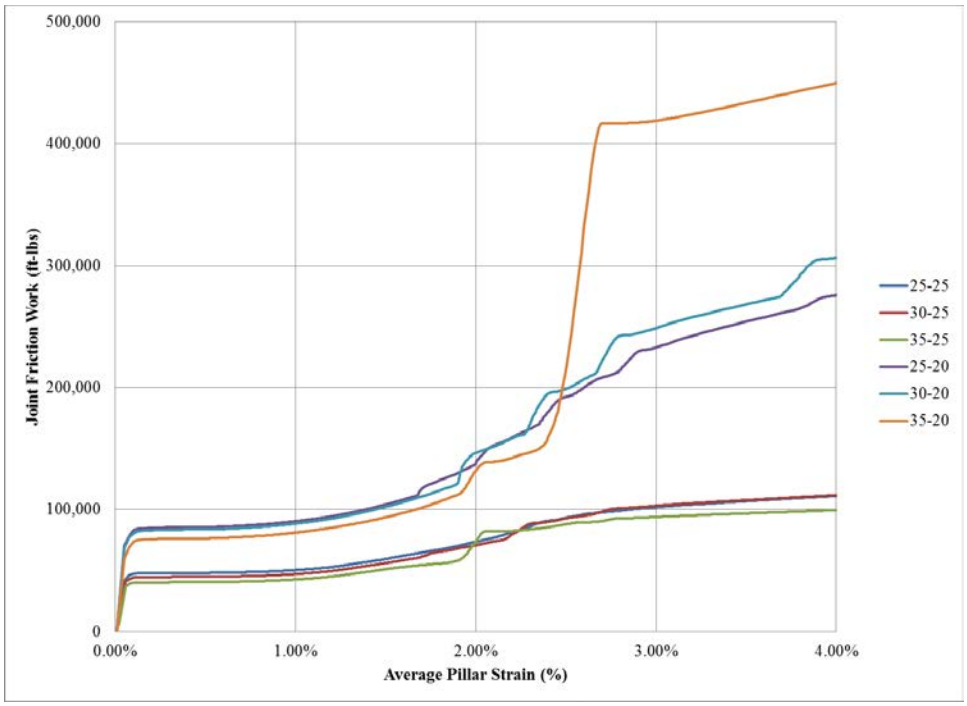

Figure 5-23 Joint Friction Work vs Average Pillar Strain, W/H=10

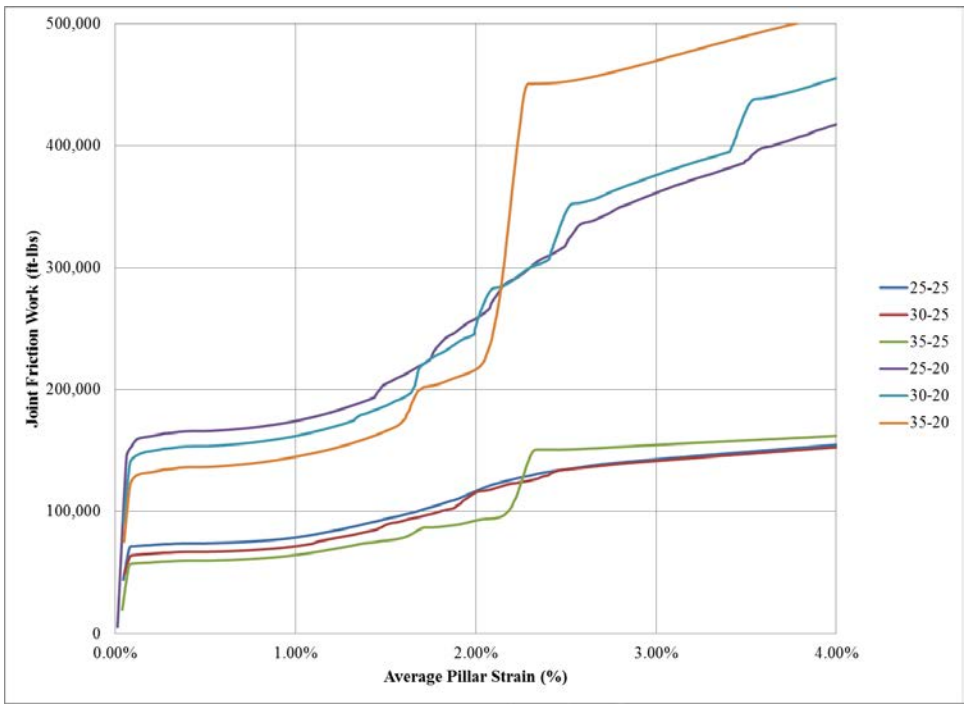

Figure 5-24 Joint Friction Work vs Average Pillar Strain, W/H=12

As with the results of previous findings, the average pillar strain for which each unstable surge in joint friction work transpires also diminishes as the pillar geometry escalates. Likewise, the joint friction work is characteristically grouped by the residual friction level, whereby the higher values of joint friction work occurred at the lower threshold of residual friction angle.

5.3 Shale vs Sandstone Overburden

A wide range of interface properties were numerically explored using an elastic overburden model while examining the aforementioned numerical identifiers of bump potential. However, it is more practical and expedient to research bump potential with a more representative overburden model. As such, the influence of coal pillar interface on bump potential was then investigated modeling massive shale and sandstone in the complete roof and floor sequence to introduce and account for the impact of plastic deformation in the roof and floor strata.

Table 5-4 Coulomb Slip Joint Model Parameters for Shale Overburden

Parameter	Description	Value	Units
jkn	Joint Normal Stiffness	3,600,000	psi/ft
jks	Joint Shear Stiffness	1,800,000	psi/ft
∅	Joint Initial Friction Angle	20-30	degrees
C	Joint Initial Cohesion	50	psi
σ_t	Joint Initial Tensile Strength	15	psi
$\emptyset_r$	Joint Residual Friction Angle	20	degrees
C_r	Joint Residual Cohesion	5	psi
$\sigma_{t,r}$	Joint Residual Tensile Strength	0	psi

Table 5-5 Coulomb Slip Joint Model Parameters for Sandstone Overburden

Parameter	Description	Value	Units
jkn	Joint Normal Stiffness	3,600,000	psi/ft
jks	Joint Shear Stiffness	1,800,000	psi/ft
ø	Joint Initial Friction Angle	25-35	degrees
C	Joint Initial Cohesion	150	psi
σ_t	Joint Initial Tensile Strength	45	psi
$ø_r$	Joint Residual Friction Angle	25	degrees
C_r	Joint Residual Cohesion	15	psi
$\sigma_{t,r}$	Joint Residual Tensile Strength	0	psi

It is commonly expected that sandstone contacts result in higher strength than shale contacts; therefore it is not practically necessary to evaluate each overburden model with respect to the same comprehensive range of interface frictional model as previously implemented. As a result the interface frictional model was examined through deviations in the initial friction angle only while the residual friction angle was maintained as a constant value. Table 5-4 and Table 5-5 identify the complete coulomb slip joint model parameters for both the shale and sandstone overburden model, respectively. The material properties for each of the shale (Table 5-6) and sandstone (Table 5-7) overburden models are summarized and based off commonly referenced publications regarding coal pillar design (Zipf Jr, 2007; Peng, 2008; Esterhuizen et al., 2010a). Each overburden model is assumed to behave according to the ubiquitous joint model, which is a numerical plasticity model which accounts for a specific plane of weakness in a Mohr-Coulomb material (Itasca, 2009). Here the plane of weakness is assumed to be the parallel bedding planes representative of the typical sedimentary features present for both shale and sandstone in coal lithology. Table 5-8 documents the identification system presented in the following results for bump potential based on the overburden properties and interface initial/residual friction angle.

Table 5-6 Shale overburden material properties

Parameter	Description	Value	Units
E	Elastic Modulus	1,500,000	psi
ν	Poisson's Ratio	0.25	
ρ	Density	160	pcf
$\emptyset$	Friction Angle	30	degrees
C	Cohesion	1,250	psi
i	Dilation Angle	15	degrees
σ_t	Tensile Strength	300	psi
$\emptyset_j$	Joint Friction	20	degrees
C_j	Joint Cohesion	250	psi
i_j	Joint Dilation Angle	10	degrees
$\sigma_{t,j}$	Joint Tensile Strength	200	psi

Table 5-7 Sandstone overburden material properties

Parameter	Description	Value	Units
E	Elastic Modulus	4,500,000	psi
ν	Poisson's Ratio	0.25	
ρ	Density	160	pcf
$\emptyset$	Friction Angle	35	degrees
C	Cohesion	1,750	psi
i	Dilation Angle	12.5	degrees
σ_t	Tensile Strength	600	psi
$\emptyset_j$	Joint Friction	25	degrees
C_j	Joint Cohesion	700	psi
i_j	Joint Dilation Angle	10	degrees
$\sigma_{t,j}$	Joint Tensile Strength	400	psi

Table 5-8 Interface study with selected overburden and interface friction models

Model ID	Overburden Properties	Interface Peak-Residual Friction
SH-1	Shale	20-20
SH-2	Shale	25-20
SH-3	Shale	30-20
SS-1	Sandstone	25-25
SS-2	Sandstone	30-25
SS-3	Sandstone	35-25

5.3.1 Pillar Stress-Strain

It is clear that the sandstone overburden model produces an elevated stress-strain relationship compared to the shale overburden for the W/H=8 pillar (Figure 5-25), the W/H=10 pillar (Figure 5-26), and the W/H=12 pillar (Figure 5-27) alike. For the shale overburden, there are only infinitesimal differences in the all three friction models throughout all values of average pillar strain and for all squat pillar dimensions modeled, demonstrating an independence from pillar interface properties with respect to the weaker overburden. Furthermore, the shale overburden model weakens the ordinary post-failure behavior of all pillar geometries, as the W/H=8 pillar exhibits mild strain-softening behavior with the W/H=10 pillar representing the transition to strain-hardening behavior. The sandstone overburden model largely hardens the expected post-failure behavior as all pillar geometries modeled are demonstrating strain-hardening behavior. The highest initial friction angle, which also results in the largest discrepancy between initial and residual shear strength, also shows evidence of unstable failure across all squat pillar designs considered as a sudden drop in stress occurs and should be reflected in a loss of confinement and peak in shear strain rate and kinetic energy release. The strain threshold at which this interface slip occurs tends to decrease as the pillar geometry increases, a conclusion also found in the elastic analysis.

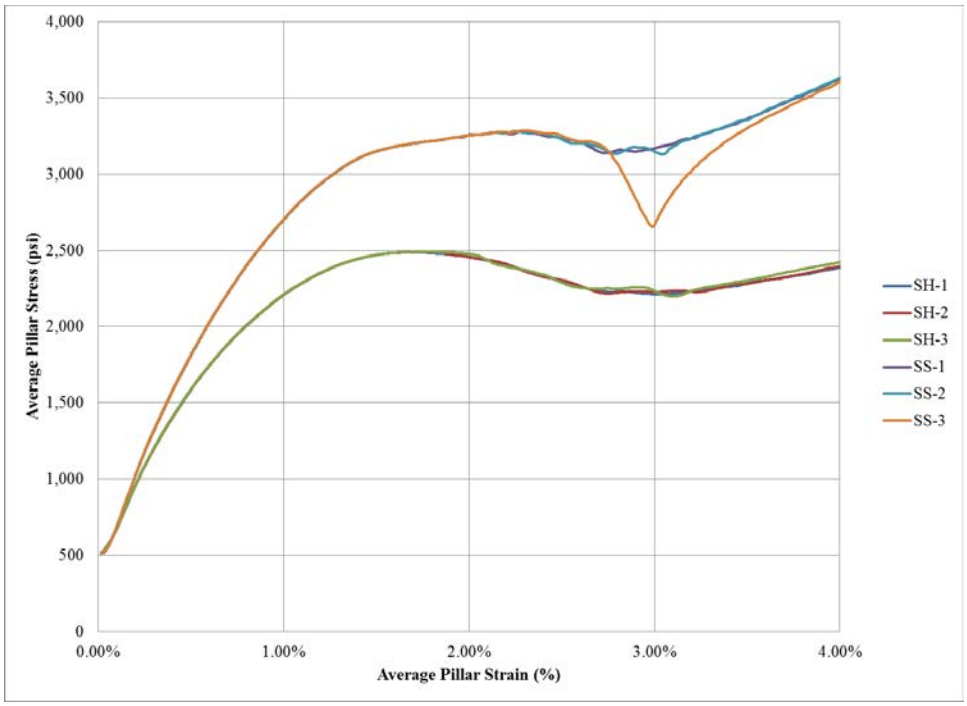

Figure 5-25 Average Pillar Stress versus Average Pillar Strain, W/H=8

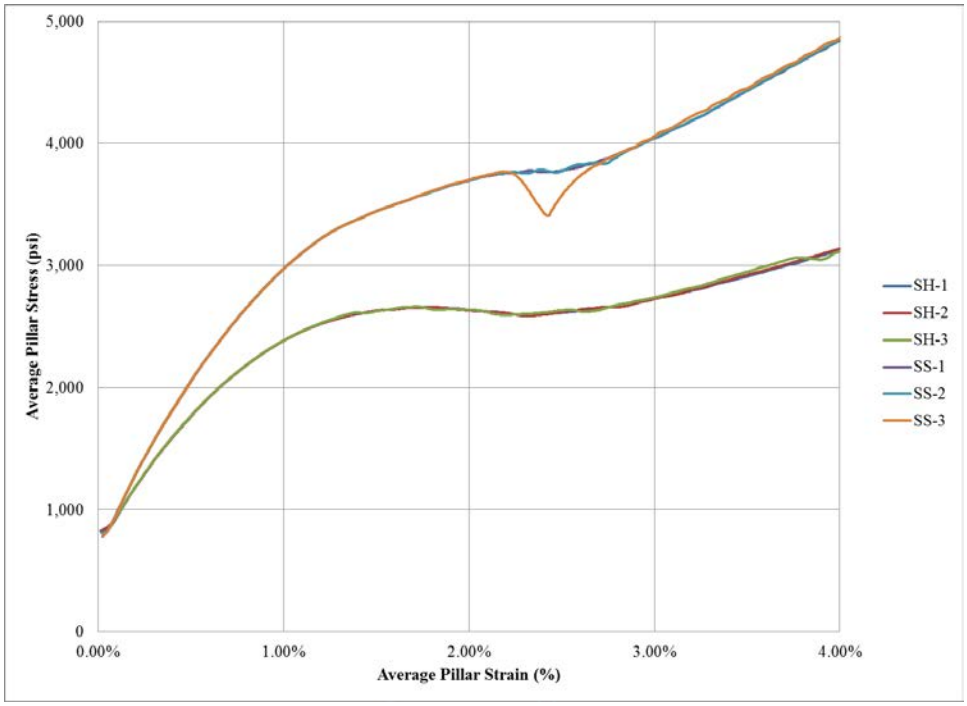

Figure 5-26 Average Pillar Stress versus Average Pillar Strain, W/H=10

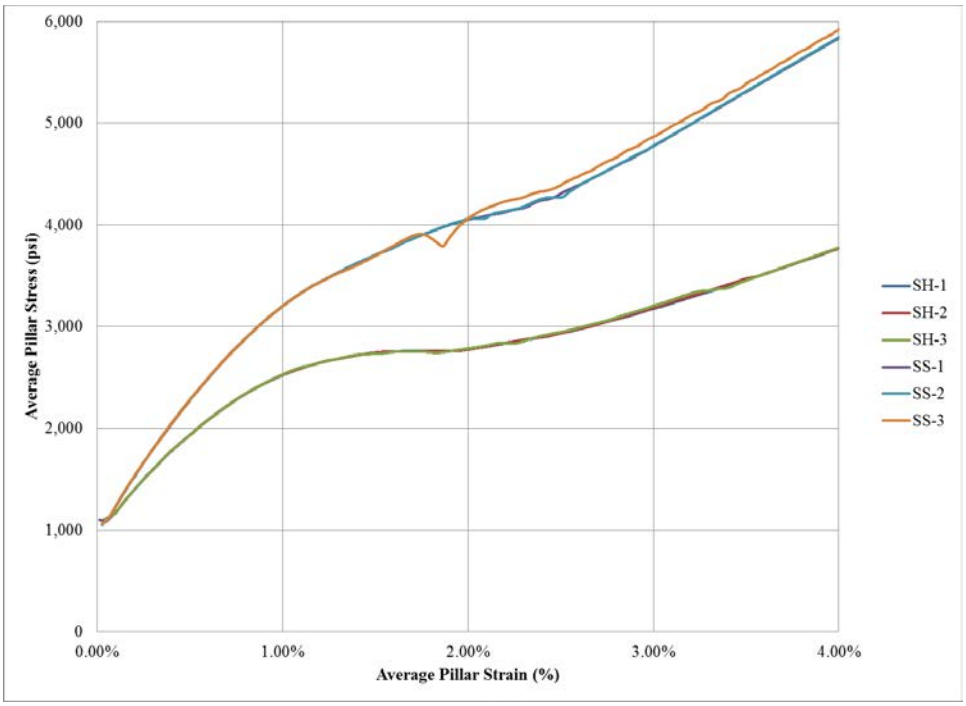

Figure 5-27 Average Pillar Stress versus Average Pillar Strain, W/H=12

Contrary to the findings of the elastic overburden investigation, there is much less volatility and dependence on the coal pillar interface friction model. Undoubtedly this is a function of the plasticity model used for the near-seam strata, which dissipates a higher percentage of the overburden load in the form of plastic work of the roof/floor strata and joint frictional work consumed as shear along the strata bedding planes

5.3.2 Pillar Confinement

The degree of confinement for each the W/H=8 pillar (Figure 5-28), the W/H=10 pillar (Figure 5-29), and the W/H=12 pillar (Figure 5-30) are representative of the findings discovered in the stress-strain relationships. The shale overburden model results in lower confinement across the spectrum of average pillar strain and geometry which consequently resulted in lower pillar strength. This weaker overburden model demonstrates a complete independence with respect to the interface frictional model. The sandstone overburden model results in higher confinement and begins to show a minor dependence on the interface frictional model, particularly at the highest level of initial friction and largest differential in initial/residual friction angle. The sudden loss of pillar strength revealed in the pillar stress-strain relationship for this friction model also

demonstrated a loss of confinement as expected, and this drop in minor principal stress and interface slip occurred at declining levels of average pillar strain as the pillar geometry was increased. Both overburden models demonstrated milder volatility when compared to the elastic overburden model.

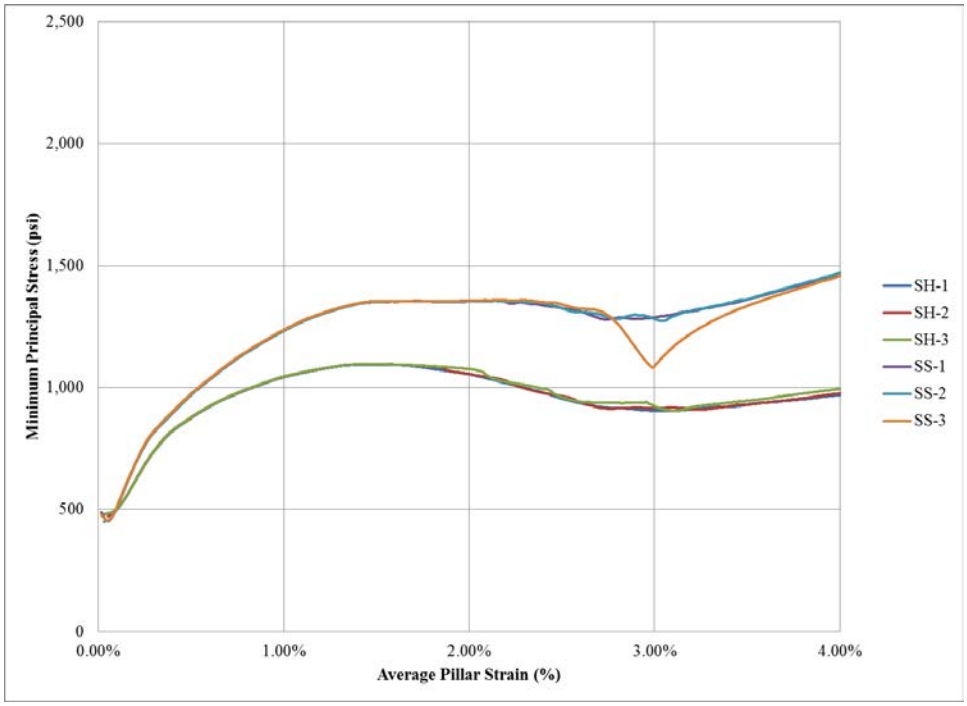

Figure 5-28 Average Confinement versus Average Pillar Strain, W/H=8

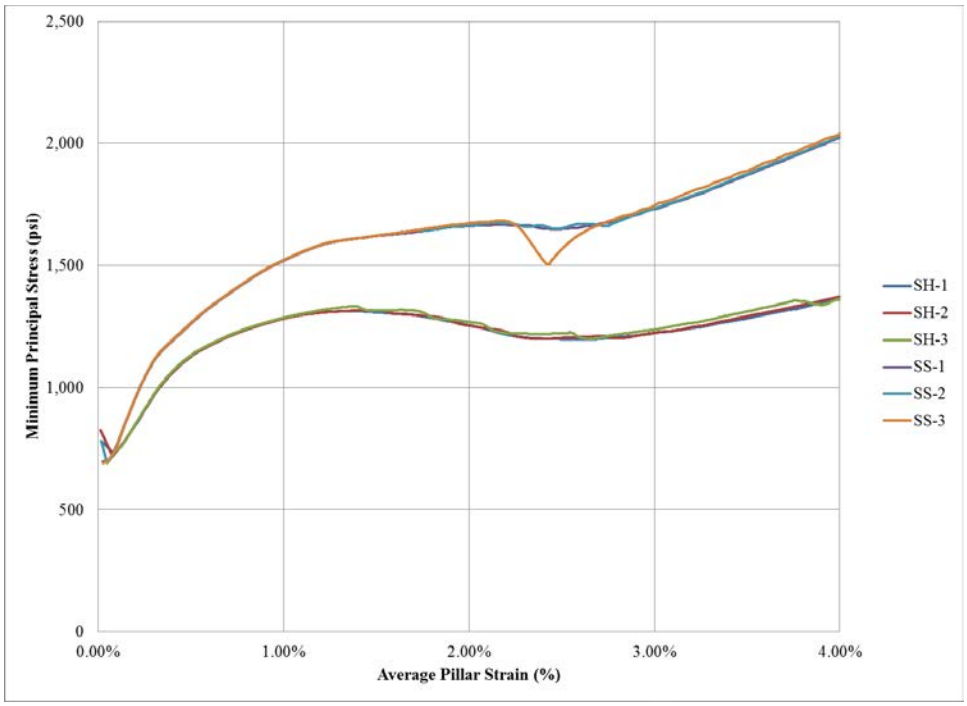

Figure 5-29 Average Confinement versus Average Pillar Strain, W/H=10

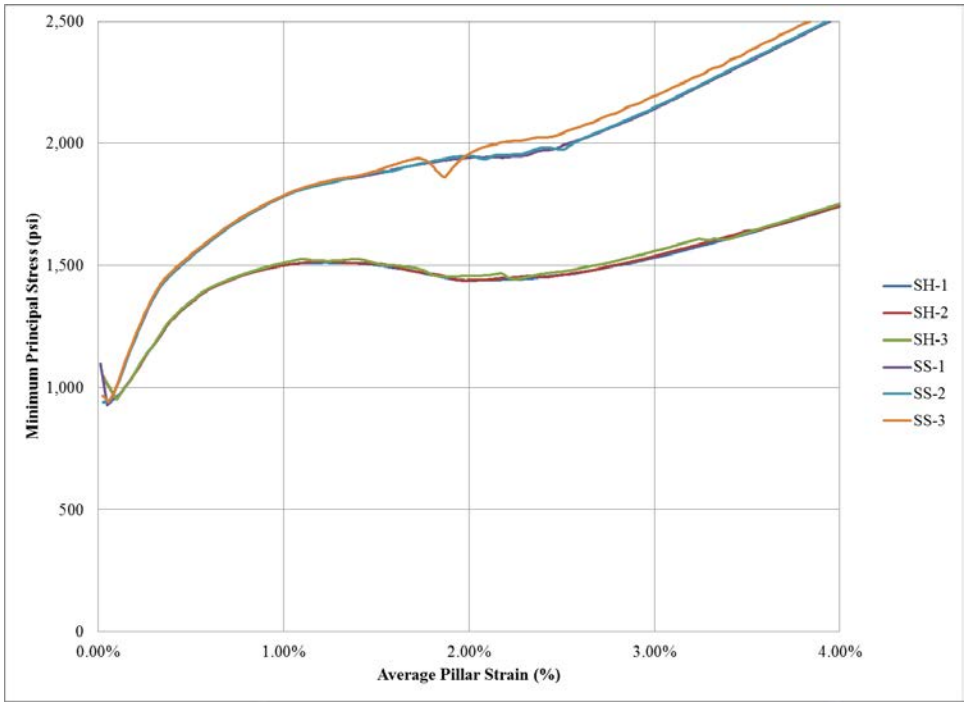

Figure 5-30 Average Confinement versus Average Pillar Strain, W/H=12

5.3.3 Peak Shear Strain Rate

Peak shear strain rate demonstrated less volatility across the spectrum of pillar geometries and frictional models for both the shale and sandstone overburden models than was observed with the elastic overburden model. Table 5-9 documents the peak shear strain rate observed for each of the interface friction models. The peak shear strain rate exhibited significant increases for the initial interface friction angle, residual friction angle, and consequently the differential in initial/residual friction angle increased, suggesting higher probability of unstable failure. The highest differential models showed nearly an order of magnitude larger peak shear strain rate compared to the zero differential models and was perceived to be marginally greater for the sandstone overburden compared to the shale overburden model, which should show up as higher total energy release. The average strain for each observed peak in shear strain rate continually decreased as the pillar geometry increased, an evidence also observed in the peak shear strain rate graphs illustrated for the W/H=8 pillar (Figure 5-31), the W/H=10 pillar (Figure 5-32), and the W/H=12 pillar (Figure 5-33).

Table 5-9 Maximum Peak Shear Strain Rate for each Joint Friction Model

W/H	Model	Joint Friction	Peak SSR (s^-1)	Strain (%)	Avg. Strain (%)
8	SH-1	20-20	0.20	2.33%	2.79%
	SH-2	25-20	1.34	3.09%	
	SH-3	30-20	2.24	2.95%	
	SS-1	25-25	0.33	2.85%	2.87%
	SS-2	30-25	1.60	2.91%	
	SS-3	35-25	2.46	2.86%	
10	SH-1	20-20	0.23	1.88%	2.37%
	SH-2	25-20	1.43	2.70%	
	SH-3	30-20	2.35	2.54%	
	SS-1	25-25	0.32	2.52%	2.48%
	SS-2	30-25	1.73	2.60%	
	SS-3	35-25	2.85	2.32%	
12	SH-1	20-20	0.22	1.61%	2.04%
	SH-2	25-20	1.50	2.31%	
	SH-3	30-20	2.37	2.19%	
	SS-1	25-25	0.35	2.06%	2.10%
	SS-2	30-25	1.70	2.39%	
	SS-3	35-25	2.43	1.85%	

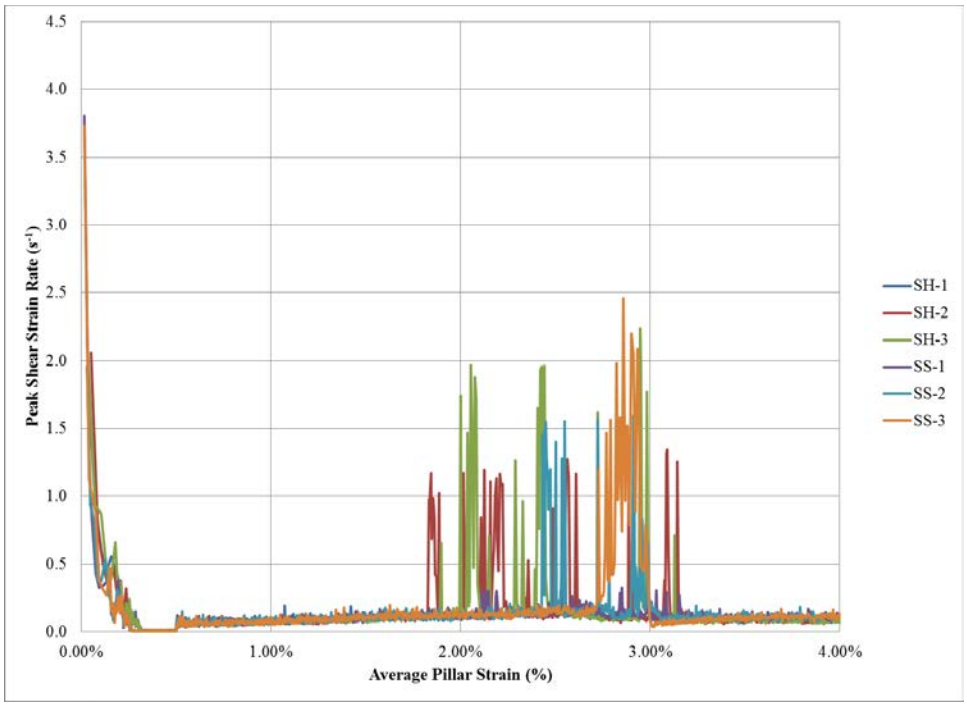

Figure 5-31 Peak Shear Strain Rate vs Average Pillar Strain, W/H=8

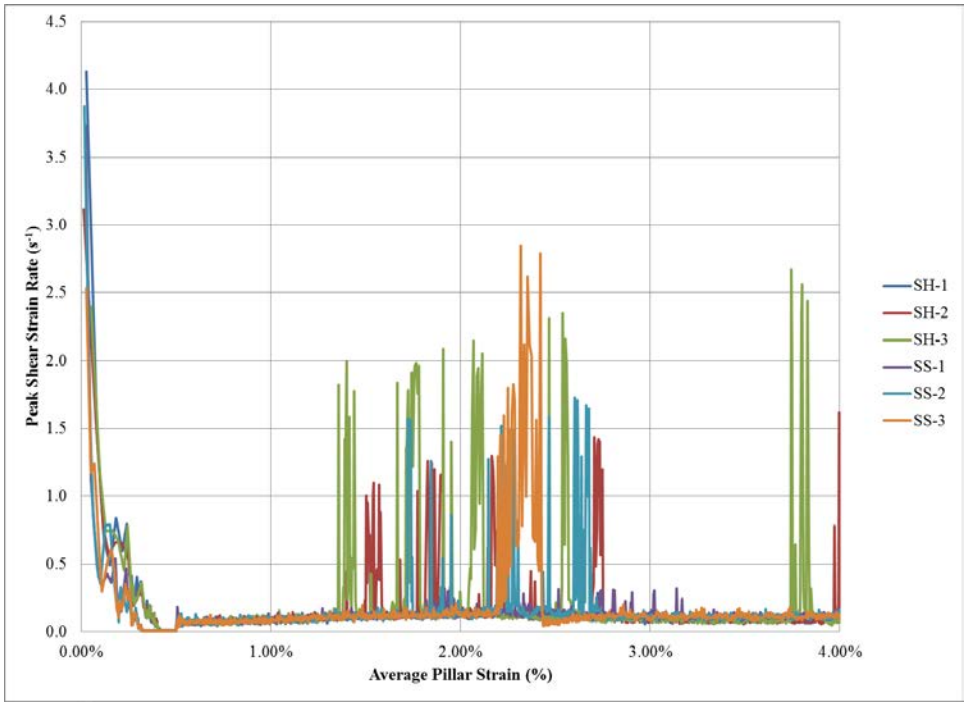

Figure 5-32 Peak Shear Strain Rate vs Average Pillar Strain, W/H=10

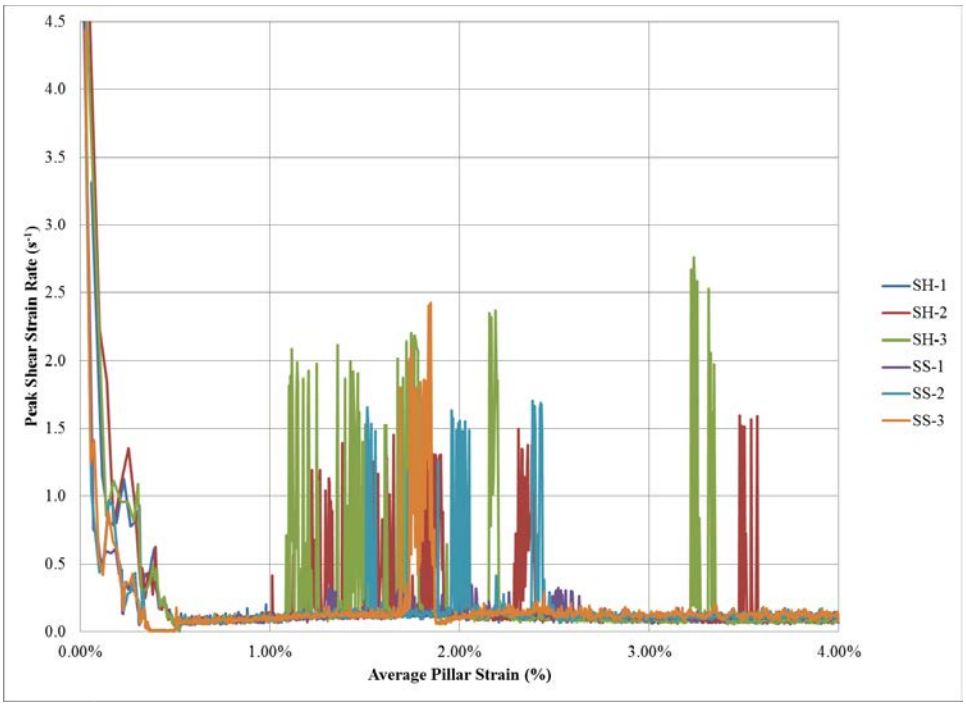

Figure 5-33 Peak Shear Strain Rate vs Average Pillar Strain, W/H=12

This observation is consistent with the results of previous findings of pillar stress-strain and average pillar confinement. When examining the absolute value of peak shear strain rate for the comparative frictional model used for the elastic overburden, the sandstone overburden model was consistently greater (with the exception of the W/H=12 pillar at the largest initial friction angle) while the shale overburden model was universally lower. This suggests a proportional relationship between the stiffness of the overburden model and the probability of unstable failure, a finding consistent with empirical case studies of historical coal bump events. Contrary to the conclusions drawn for the elastic overburden model, both the magnitude and duration of the maximum in peak shear strain rate, which is likely a more dependable indicator of bump potential, were greatest for the W/H=10 pillar, which is comparable to the volatility of the pattern of spikes in shear strain rate. This could implicate the idea that for a given interface frictional model, there could exist a pillar geometry which is more conducive to the probability of a burst potential, which could help explain the intermittent nature of coal bump occurrences.

5.3.4 Total Energy Release

The total energy released appears to be dependent on both the pillar geometry and the residual friction angle. While there appears to be some dependence on the near-seam lithology, particularly at higher levels of strain, most of the observed differences are attributed to the residual interface friction angle. It is unquestionable that as the pillar size increases, the total energy released for a given value of pillar strain also increases. The total energy release versus the average pillar strain for each overburden lithology and interface friction model examined is illustrated for the W/H=8 pillar, W/H=10 pillar, and W/H=12 pillar as Figure 5-34, Figure 5-35, and Figure 5-36, respectively. The shale overburden model exhibits a primarily linear basis across all pillar geometries and interface friction models tested but the sandstone lithology begins to illustrate non-linearity at higher levels of strain values, particularly for the larger W/H ratio pillars. The absolute value of total energy release is very comparable to the values demonstrated for the elastic overburden.

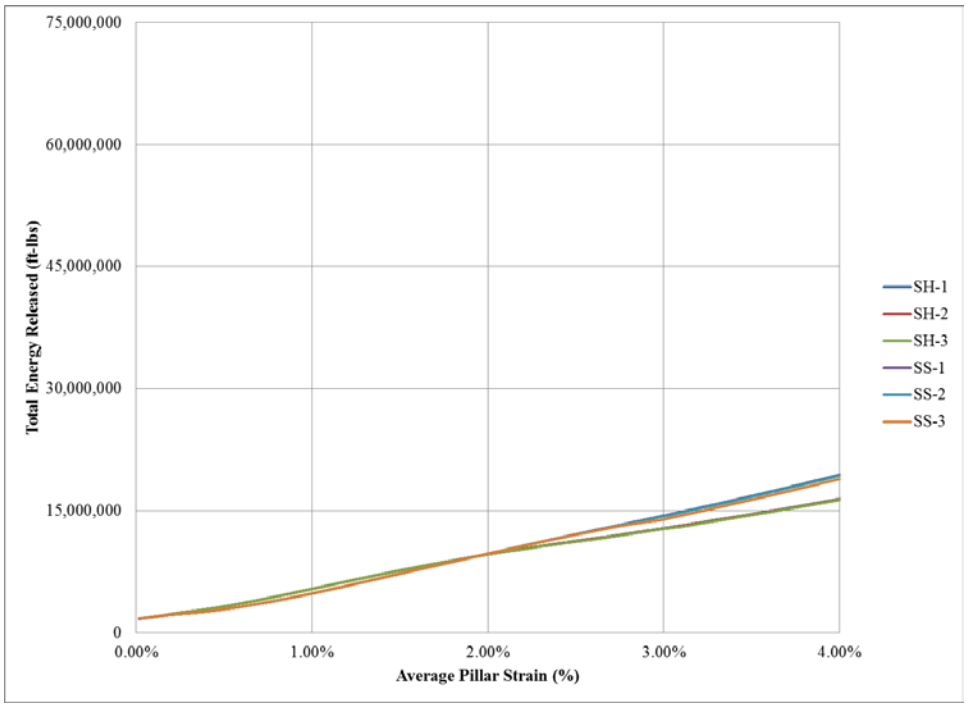

Figure 5-34 Total Energy Released vs Average Pillar Strain, W/H=8

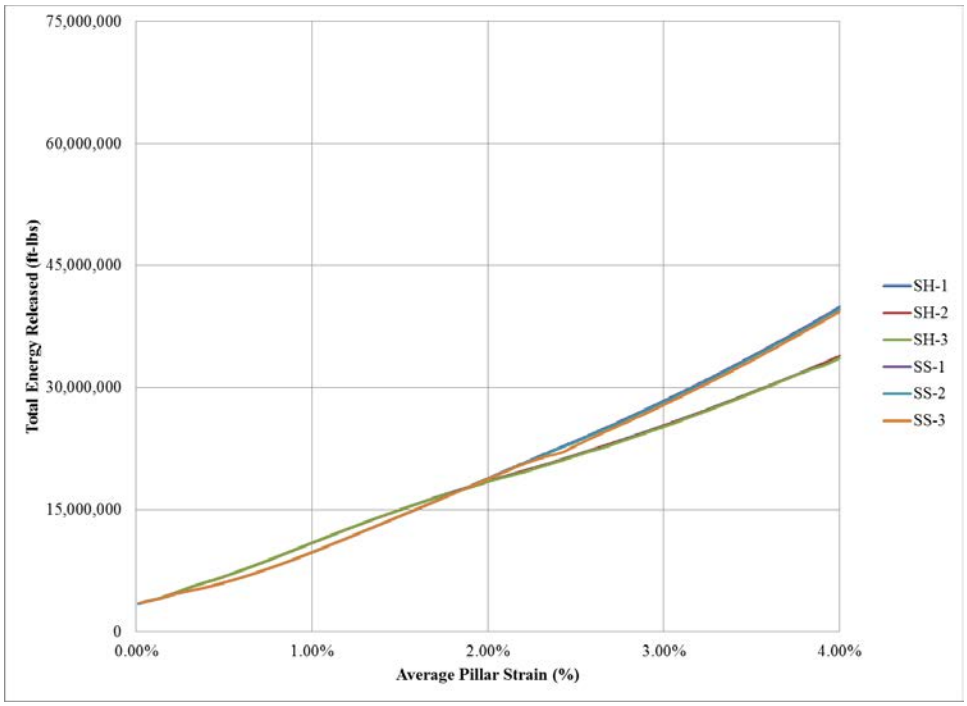

Figure 5-35 Total Energy Released vs Average Pillar Strain, W/H=10

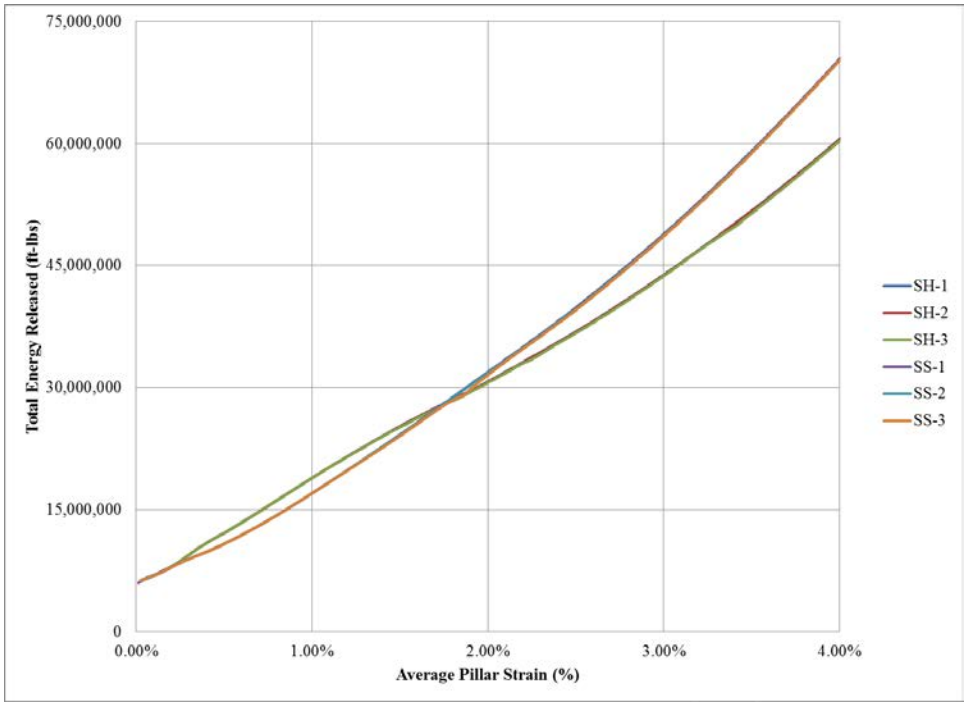

Figure 5-36 Total Energy Released vs Average Pillar Strain, W/H=12

5.3.5 Kinetic Energy

Table 5-10 shows the maximum kinetic energy release for each interface friction model and pillar geometry which was numerically investigated. Consistent with the peak shear strain results, the kinetic energy release increased as the initial friction angle, the residual friction angle, and the differential in initial/residual friction angle increased. However, significant peaks in the kinetic energy release were only noted for the sandstone overburden model with the interface friction model set at the highest initial friction angle, which is consequently the greatest differential in initial and residual friction. The lower friction models assuming sandstone lithology had mixed results relative to the elastic overburden. The presence of shale lithology consistently resulted in lower maximum kinetic energy releases across all interface friction models and pillar geometries when paralleled to the initial elastic overburden model. This indicates that kinetic energy release, which has a direct physical parallel with coal burst potential, is fundamentally as reliant on the near-seam lithology as it is the interface frictional properties.

Table 5-10 Maximum Kinetic Energy Release for each Joint Friction Model

W/H	Model	Joint Friction	Kinetic Energy (ft-lbs)	Strain (%)	Avg. Strain (%)
8	SH-1	20-20	266.53	2.48%	2.39%
	SH-2	25-20	323.49	2.59%	
	SH-3	30-20	425.41	2.09%	
	SS-1	25-25	249.68	2.64%	2.85%
	SS-2	30-25	251.14	3.01%	
	SS-3	35-25	1376.51	2.90%	
10	SH-1	20-20	308.62	2.15%	2.16%
	SH-2	25-20	377.78	2.22%	
	SH-3	30-20	529.14	2.10%	
	SS-1	25-25	312.45	2.37%	2.38%
	SS-2	30-25	329.34	2.43%	
	SS-3	35-25	2293.62	2.35%	
12	SH-1	20-20	331.60	1.76%	1.95%
	SH-2	25-20	357.07	1.89%	
	SH-3	30-20	581.68	2.20%	
	SS-1	25-25	342.02	2.05%	1.98%
	SS-2	30-25	427.03	2.05%	
	SS-3	35-25	1317.53	1.82%	

The elastic overburden model demonstrated similar trends as the sandstone lithology, but exhibited much larger values of maximum kinetic energy release. This finding is most likely attributed to the energy which is dissipated during the plastic deformation of the shale and sandstone lithology, which was numerically incorporated through the implementation of plasticity based constitutive model. It is also important to note that the largest kinetic energy release occurred for the W/H=10 pillar, a consequence which mirrors the numerical outcomes and implications of the peak shear strain rate results. This yet again suggests that optimum pillar geometry may exist for a given geologic setting which could result in inherently higher likelihood for unstable pillar failure in the form of a coal burst. The illustrative results of kinetic energy release versus the average pillar strain are shown for each the W/H=8 pillar (Figure 5-37) the W/H=10 pillar (Figure 5-38), and the W/H=12 pillar (Figure 5-39). Similar to the conclusions drawn from the other numerical bump potential indicators, the average pillar strain for which the kinetic energy release represents a maximum decreases as the pillar size is increased.

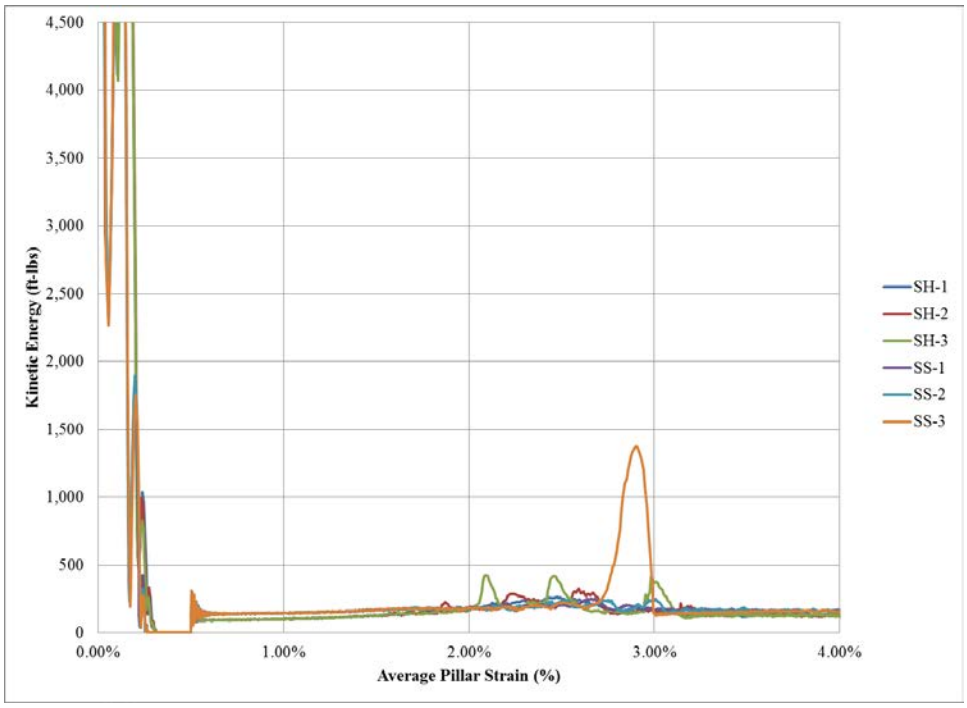

Figure 5-37 Kinetic Energy vs Average Pillar Strain, W/H=8

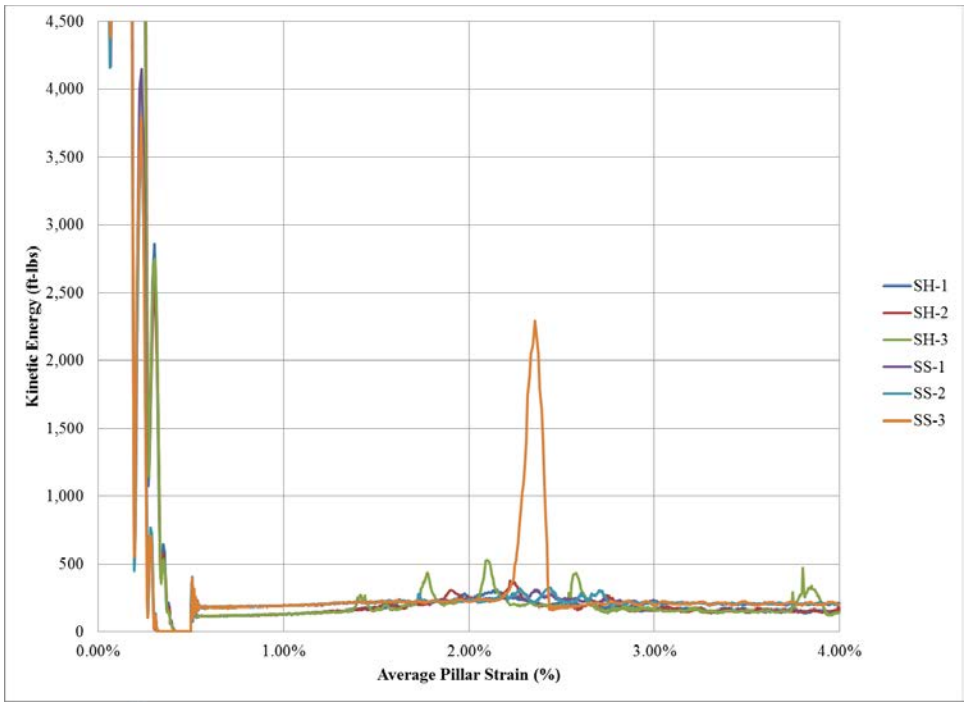

Figure 5-38 Kinetic Energy vs Average Pillar Strain, W/H=10

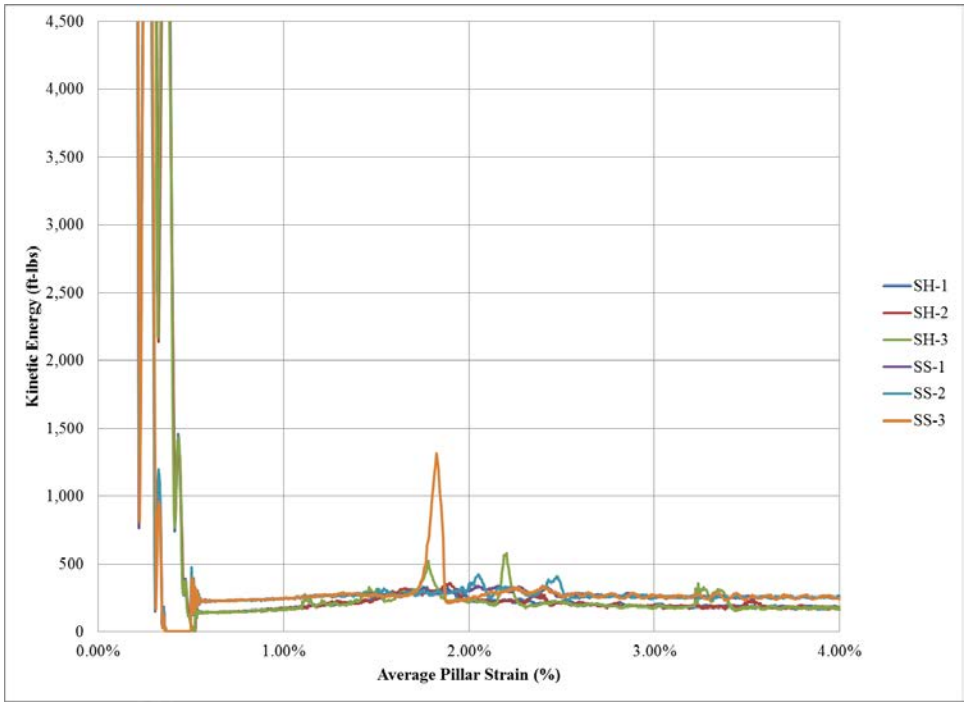

Figure 5-39 Kinetic Energy vs Average Pillar Strain, W/H=12

5.3.6 Joint Friction Work

Sudden increases in joint friction work are representative of unstable frictional heating of the pillar interface which has been physically observed in many coal bump case studies. While the elastic overburden model resulted in numerous examples of unstable interface slip, only the sandstone overburden model at the highest initial friction angle had a similar result. Figure 5-40, Figure 5-41, and Figure 5-42 illustrate the joint friction work versus the average pillar strain for each of the W/H=8 pillar, W/H=10 pillar, and the W/H=12 pillar modeled. While the elastic overburden model implicated the importance of the difference in both the initial and residual friction angle to joint friction work, the near-seam lithology appears to be a more important indicator for the potential of unstable increases in joint frictional heating characteristic of interface stick-slip. Similar to the results of the other bump potential indicators, the largest increase in joint friction work occurred for the W/H=10 pillar, though again the occurrence of this unstable increase occurred at decreasing values of average pillar strain as the pillar size was increased. The absolute value of joint friction work was consistently higher for the shale lithology than the sandstone lithology.

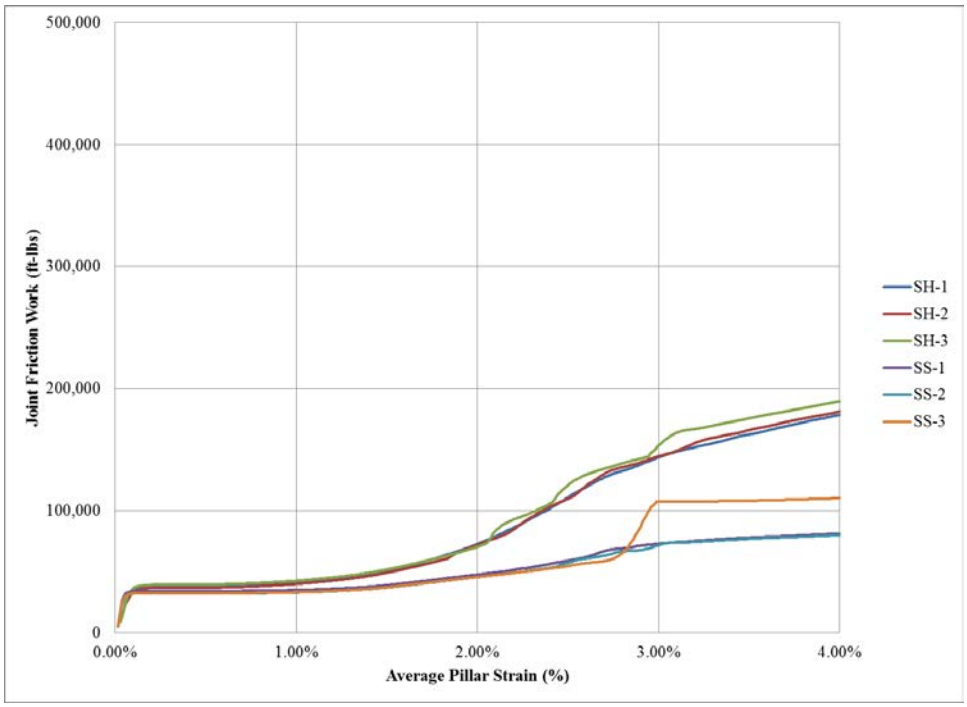

Figure 5-40 Joint Friction Work vs Average Pillar Strain, W/H=8

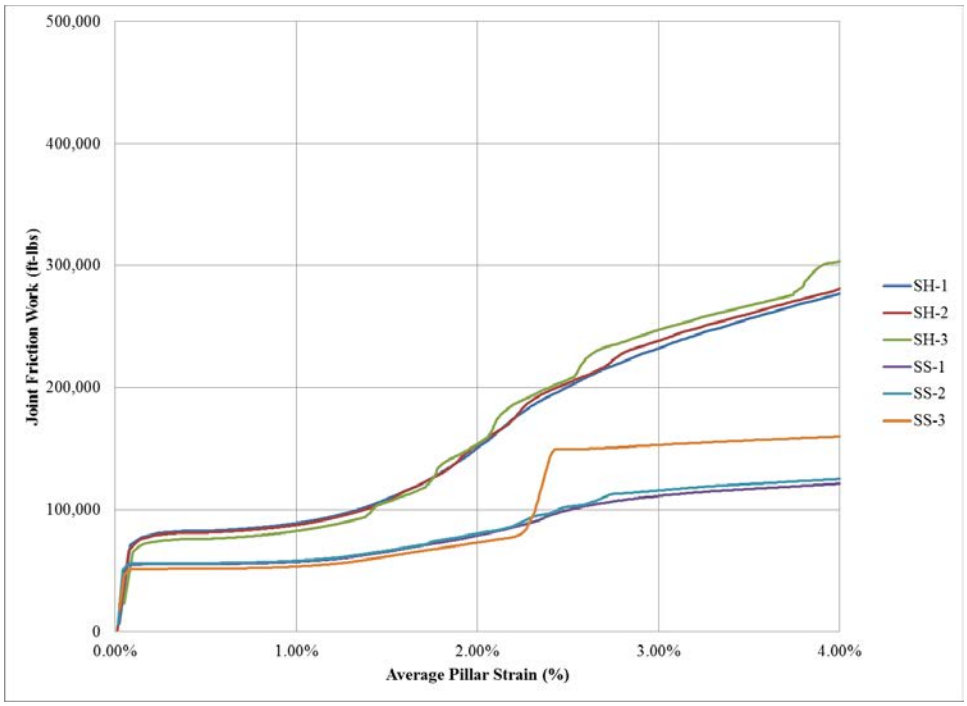

Figure 5-41 Joint Friction Work vs Average Pillar Strain, W/H=10

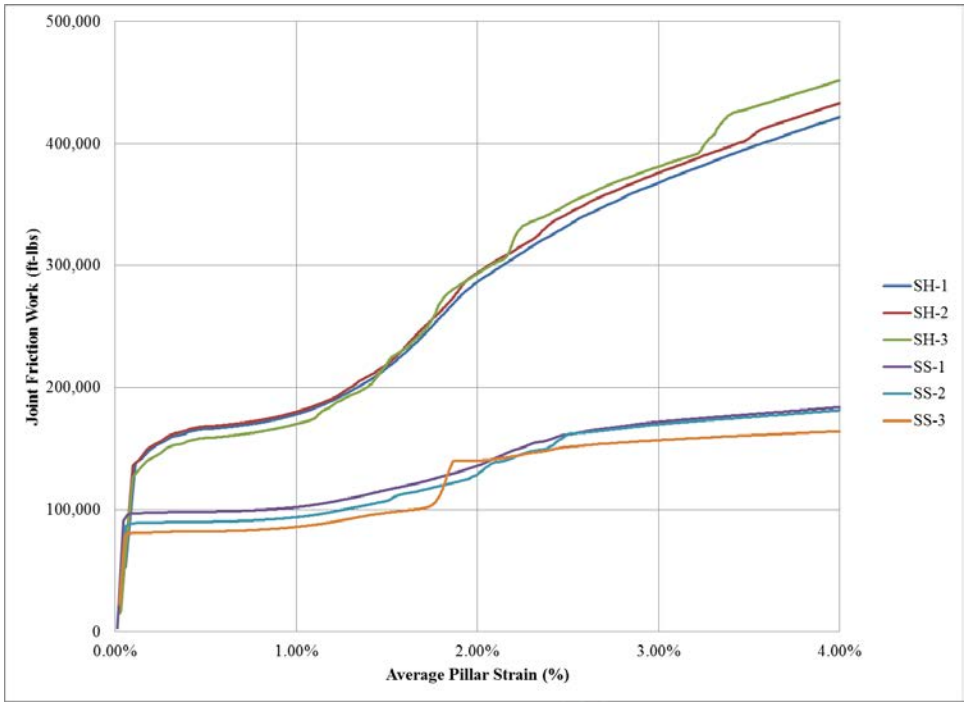

Figure 5-42 Joint Friction Work vs Average Pillar Strain, W/H=12

5.4 Summary of Findings

The influence of coal pillar interface on coal pillar bump potential is certainly immense in many different facets. Initially, quarter pillar models assuming an elastic overburden model for the roof and floor strata was constructed to evaluate the impact of interface frictional properties on squat coal pillar bump potential. With an elastic overburden, the interface properties had a profound impact on variances in each of the coal bump potential indicators. Pillar strength and confinement were naturally dependent on both the initial and residual friction angle, with the former being directly attributable to peak strength and latter being very important to the resultant post-failure behavior. However, the differential between the initial and residual interface friction angle appeared to be a reliable predictor of unstable interface stick-slip, which is demonstrated as a sudden drop in pillar strength and loss of confinement.

This finding was confirmed when examining the peak coal pillar shear strain rate and kinetic energy release, all of which achieved maximum values when the interface frictional model represented the largest differential in initial and residual friction angle. Shear strain rate has been directly correlated with unstable and dynamic propagation of shear fracturing in a quasi-static manner while kinetic energy release is conceptually associated with dynamic releases of stored strain energy which occur during coal bursts. The peak joint friction work, which is an important indicator of unstable frictional heating at the coal pillar interface, also demonstrated the most sudden and intense increases for the same interface frictional model. Furthermore, it is important to note that the unstable occurrences which were predicted for each of the numerical bump potential indicators occurred at decreasing levels of average pillar strain as the pillar size increased. The total energy released transitioned from a primarily linear basis to a higher order function at increasing levels of pillar size, with a dependency on residual friction strength at higher values of pillar strain.

While the elastic overburden model yielded several important implications regarding the importance of interface frictional properties to coal pillar bump potential, it was more important to model and evaluate the impact within the context of more realistic and appropriate overburden properties. Therefore, both a shale and sandstone lithological

model set was established and evaluated with a reduced set of interface frictional properties.

The presence of the weaker shale lithology led to a near independence of squat pillar behavior from interface frictional characteristics and a softening of post-failure behavior. It was obvious that the more rigid and stronger sandstone lithology led to elevated stress-strain behavior and hardening of post-failure behavior, which was accompanied by elevated levels of pillar confinement. The pillar stress-strain relationship only demonstrated unstable behavior for the sandstone lithology at the largest differential frictional model. The pillar stress-strain curve had a rapid drop in strength for all squat pillar geometries, a result which also showed up as a sudden loss of confinement.

Sandstone lithology also led to slightly higher values of peak shear strain rate across all frictional models; however all results implicated a dependence on both the initial and residual frictional strength. The most unstable interface frictional models were consistently recognized as the highest differential interface friction set. It was also obvious that the peak shear strain rate demonstrated a simultaneous dependence on the near-seam lithology, as the shale overburden model resulted in the lowest peak shear strain rates, followed by the elastic overburden and then the sandstone lithology. After comparing to the elastic overburden model, it was clear that total energy release was nearly independent of the near-seam lithology and only exhibited a minor reliance on the interface residual strength at higher values of pillar strain.

The kinetic energy release for both shale and sandstone lithology demonstrated similar trends as the peak shear strain rate including a dependency on both the interface initial and residual friction angle; however, only the sandstone lithology exhibited the ability to produce an unstable peak release of kinetic energy while the weaker shale model consistently resulted in low kinetic energy release. This indicates that kinetic energy release is also fundamentally dependent on near-seam lithology as much as the interface friction characteristics. The results of joint friction work provided near identical conclusions. In summary, the following important implications to coal pillar bump potential were identified:

- Coal pillar interface frictional properties have an important influence on coal pillar bump potential.
- While both the initial and residual interface friction angle are significant, the most important indicator of unstable coal pillar failure was consistently the difference in the initial and residual friction angle. This result implies that high values of this difference are necessary for unstable interface stick-slip behavior, which would result in a sudden loss of pillar strength as a product of loss of confinement, followed by a rapid propagation of shear strain and accompanied peak in kinetic energy release.
- Figure 5-43 and Figure 5-44 illustrate the shear strain increment for the W/H=10 pillar with sandstone lithology for the SS-3 frictional model set. These figures represent the shear strain at 2 percent strain and 2.5 percent strain, respectively. The propagation of shear failure along the pillar interface and through the initially intact elastic core is evident, representing the rapid transition from a stable or functional level of strain to a state whereby a significant portion of the outer pillar demonstrates failure.

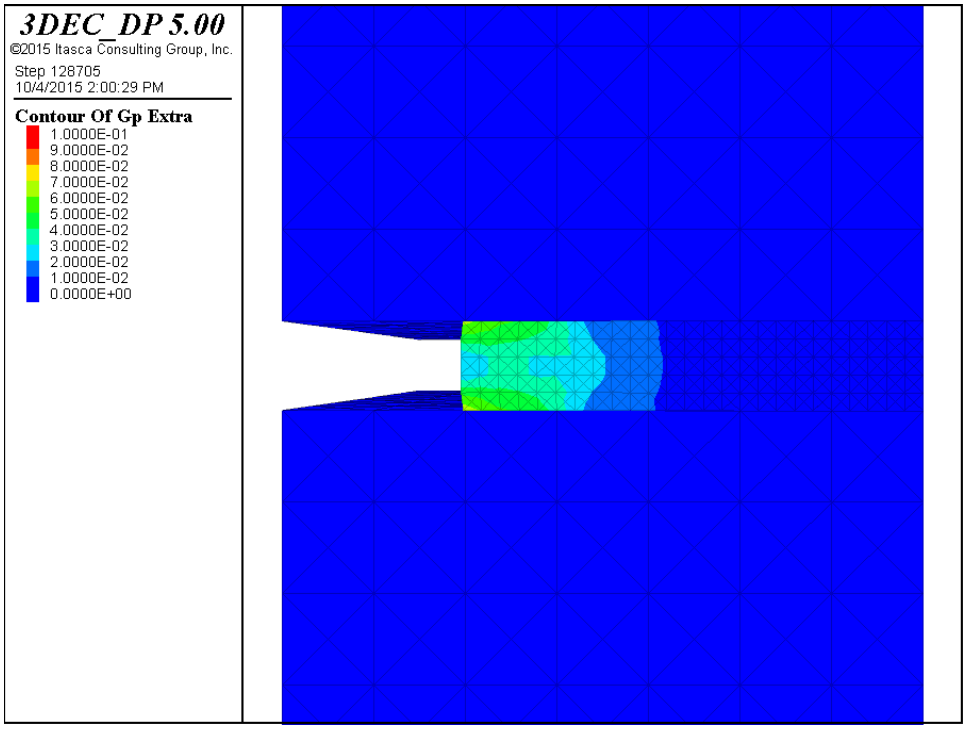

Figure 5-43 Shear strain increment of W/H=10 SS-3 model at 2% Strain

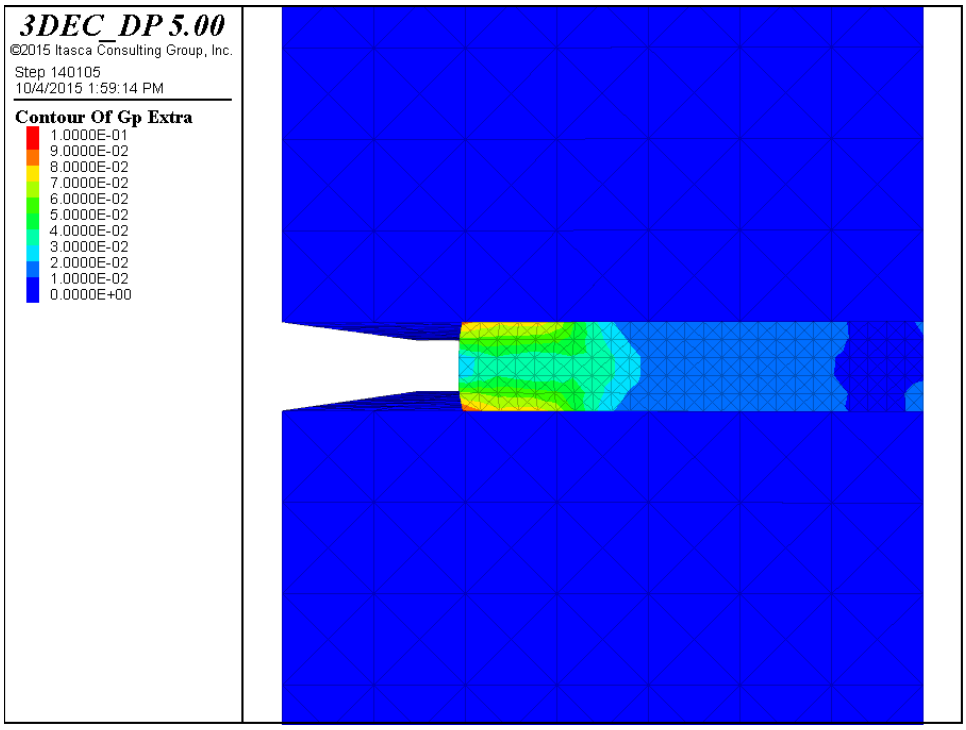

Figure 5-44 Shear strain increment of W/H=10 SS-3 model at 2.5% Strain

- The average pillar strain at which unstable failure occurred continually decreased as the pillar size increased, independent of the near-seam lithology. However, the most obvious unstable failure, represented by maximum values of confinement loss, peak shear strain rate, kinetic energy release, and joint friction work, always occurred for the W/H=10 pillar. This result suggests that for a given interface frictional model, there could potentially exist a pillar geometry which is more conducive to higher probabilities of a coal bump, and may help explain the intermittent and rare nature of these types of failures. Contacts with massive and/or coarse grained lithology (e.g. sandstone) would in many cases exhibit the type of physical characteristics, such as high angle granular features, which would result in mathematically similar frictional properties.
- When implementing a plasticity based model in lieu of the elastic overburden model, unstable failure represented by a loss of confinement, peak shear strain rate, and abrupt increases in joint friction work only occurred with sandstone lithology present. This suggests a relationship between unstable pillar failure and

the stiffness of the surrounding strata, a conclusion which mirrors the findings of many empirical case studies of historical coal bursts.

- The distinct element method employed appears adequate to capture unstable pillar failure. For example, Figure 5-45 and Figure 5-46 show the plan view of shear strain rate for the same W/H=10 pillar with the SS-3 friction model at mid-pillar. At a level of 2 percent average pillar strain, the buildup of high shear strain rate towards the middle of the pillar and surrounding the intact elastic core is captured, while after failure at an average pillar strain value of 4 percent the elastic core is diminished, confinement is lost, and the release of stored strain energy can no longer support high levels of shear strain.

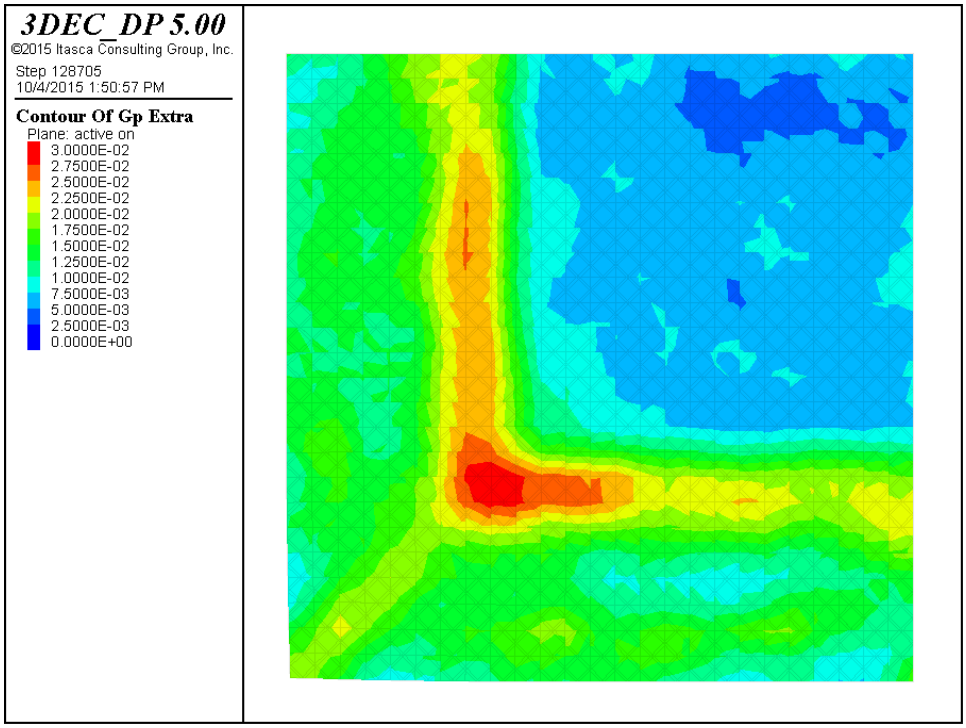

Figure 5-45 Shear strain rate of W/H=10 SS-3 model at 2% Strain

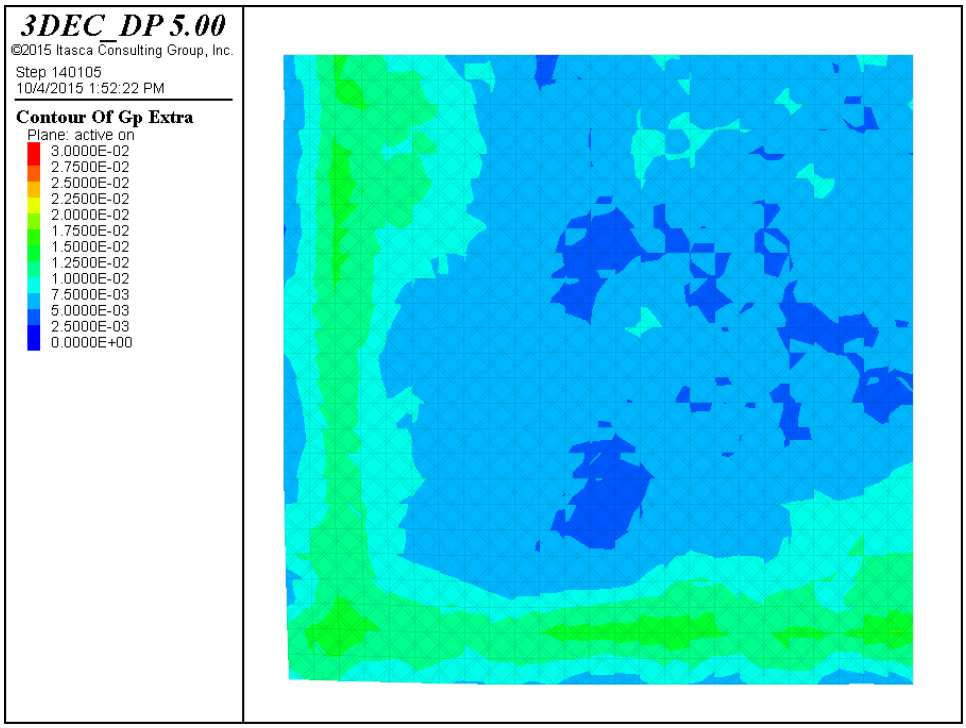

Figure 5-46 Shear strain rate of W/H=10 SS-3 model at 2.5% Strain

- The elastic overburden model demonstrated many of the same trends as the sandstone overburden models, but typically exhibited larger values of kinetic energy release and accelerated increases in joint friction work, which captured the frictional heating of the pillar interface. This finding is attributed to the fact that energy is dissipated in the form of plastic work with the use of the ubiquitous joint plasticity model for both the shale and sandstone lithology. This model allows for slip and failure along discontinuities in the roof/floor strata, whereas the only discontinuity for the elastic overburden is the pillar interface itself.
- Differences in the shale and sandstone lithology are not only based on the distinctions between the interface frictional model used but also include the relative stiffness of the strata and strength of the ubiquitous joints which were ascribed to represent bedding planes in the roof/floor strata. The conclusion that unstable failure is more probable with the rigid sandstone model points towards the concept that failure and slip along prominent discontinuities in the near-seam strata can actually ease and control the failure of the coal pillar itself due of energy dissipation. Not only does this result show up in virtually all the bump

potential numerical identifiers considered, but a snapshot of the zone state for the shale (Figure 5-47) versus sandstone (Figure 5-48) lithology for the W/H=10 pillar at 4 percent average pillar strain demonstrates the obvious failure of the bedding planes in the roof/floor. This finding suggests that it would be prudent to then evaluate the influence of massive lithology which is absent of these discontinuities and the overall impact of various lithological environments.

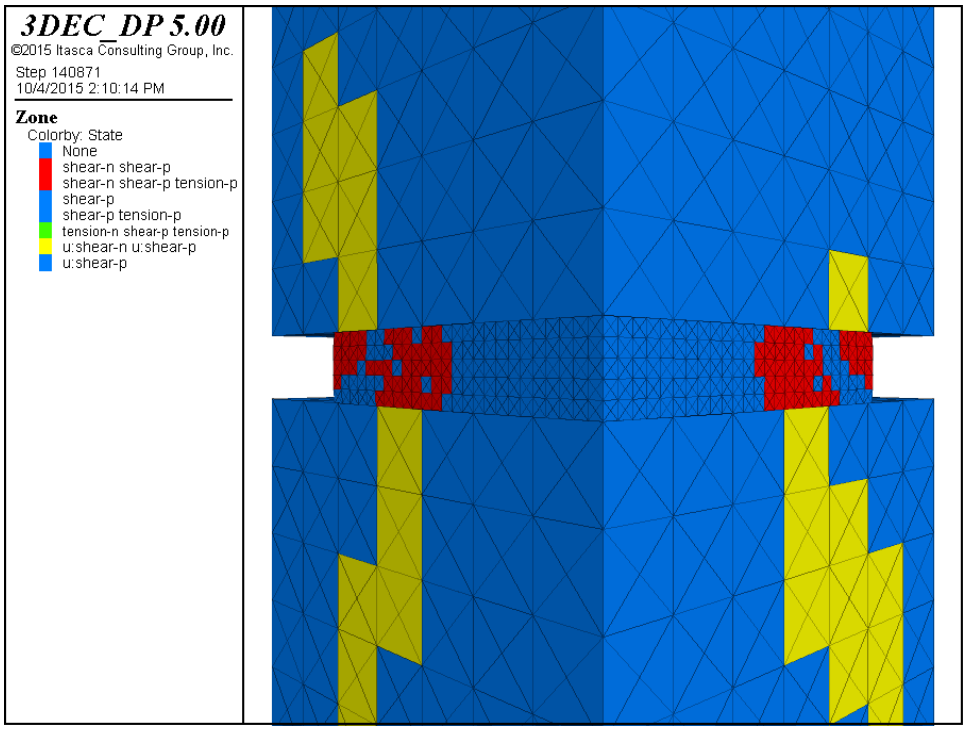

Figure 5-47 Zone state of W/H=10 SH-3 model at 4% Strain

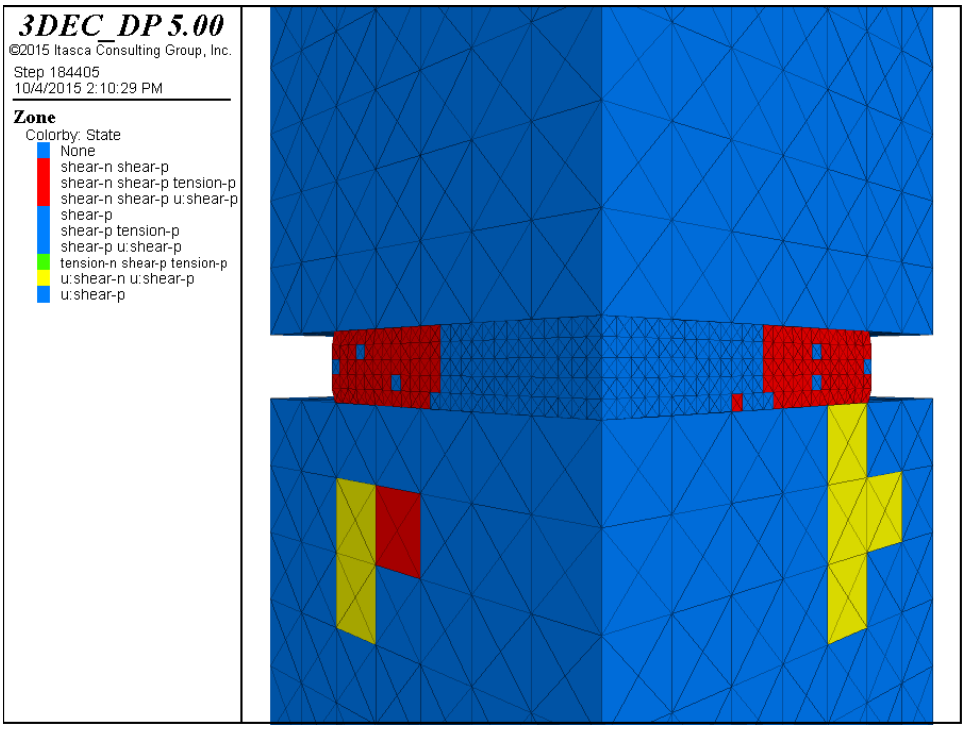

Figure 5-48 Zone state of W/H=10 SS-3 model at 4% Strain

6 Impact of Coal Lithology

The previous chapter identified the significance of coal pillar interface frictional properties on burst potential as recognized through the six (6) numerical bump indicators. However, it is also judicious to examine the impact of the coal seam lithological environment on the propensity for squat coal pillars to bump absent significant variations of interface friction, a concept also recognized in the last chapter. The practice of rock mechanics acknowledges the complexities associated with variability of rock mass properties. The depositional environment of coal measure rocks typically places coals in series primarily with varying grades of shales and sandstones, which present mining engineers with complications as a result of the depositional influences of rock thickness, extent, strength, and discontinuities (Peng, 2008). The lithological environment is undoubtedly the single most important parameter invoked in the study of coal mine ground control, though its importance to the practice of mining engineering is sometimes not fully explored. Peng (2008) contributed this fact to the difficulty in obtaining precise rock mass properties which would be necessary to complete a full engineering mathematical representation.

The contribution of near-seam lithological environment is especially important to the study of coal pillar bump potential. The advent of pre-mining burst risk assessments have often advocated the importance of such geologic factors as massive lithology like sandstones in close proximity to the coal seam in either the roof or floor and even sandstone channels which can act to concentrate stresses (Office of Mine Safety and Health Research, 2010). Many other empirical studies have also documented the importance of lithological factors such as massive strata to coal bump potential (Iannacchionne and Zelanko, 1995a; 1995b; Mark, 2010).

6.1 Sandstone Thickness/Proximity

What is immediately obvious in many of the empirical investigations of coal bump occurrences is the recognition and importance of strong and rigid sandstones in close proximity to the coal seam. Iannachionne and Zelanko (1995a) noted that while many geologic factors have influenced the occurrence of coal pillar bursts, a common factor in both U.S. and foreign events is the proximity to strong, thick, rigid strata such as

sandstone or siltstone. In fact, the study concluded that 86 out of the 95 bump occurrences which contained mine roof descriptions in the USBM Coal Bump Database referenced the presence of sandstone which was often termed as strong, thick, or even massive. Hoelle (2008) investigated nearly twenty (20) coal bumps occurring in the bump-prone coalfield of Harlan County Kentucky occurring over an eight (8) year time period. Upon completing in-situ and laboratory strength testing of floor, coal, and roof samples, monitoring ground response, and back analyzing pillar strength, the presence of thick overburden, sandstone channels, and strong roof and floor was contemplated as one of the main contributing factors to the coal bursts.

While examining dynamic failure of coal pillars in deep overburden, Whyatt (2008) also concluded that strong sandstone strata were often encountered during coal bursts. In the western United States, Agapito and Goodrich (2000) have characterized bump prone geology as including the presence of thick, competent overburden strata which creates high abutment stresses and very competent and strong immediate roof and floor (sandstone and/or siltstone) which act to confine the coal pillar and resist frictional failure. These same features, including deep cover, sandstone channels, and competent roof and floor, were also referenced by Gu (2013). Kias (2013) attributed elevated bump potential due to the presence of sandstone for three reasons: the resulting resistance to fracturing, an assurance that failure occurs in the coal pillar itself and not the roof or floor, and the ability of coal pillar interface to reach a critical stick-slip condition and suddenly lose confinement and strength. This latter concept presented by Kias (2013) was validated in the previous chapter as unstable failure, which was identified with numerical indicators such as loss in confinement, maximums in shear strain rate, peaks in kinetic energy release, and abrupt increases in joint friction work, largely occurred with stronger sandstone lithology and not the weaker shale model. This result further supported a correlation between unstable failure of squat coal pillars and strong, rigid surrounding strata.

Harris and Perry (2015) combined a qualitative analysis of geologic factors and boundary element modeling to reinvestigate the same bump occurrences considered by Hoelle (2008). While high stress as a result of longwall mining and deep overburden were

present, both the thickness and proximity of near-seam sandstone in both the roof and floor were noted as particularly important contributing factors to the occurrence of numerous coal bumps within a single reserve boundary. This finding was used to construct enhanced bump red-zone guidelines to improve understanding and identification of the factors which influenced coal bump potential for mine management.

A sensitivity study which evaluates the importance of strong, massive strata such as sandstone to coal bump potential was undertaken. Both the sandstone thickness and proximity were varied systematically in both the roof and floor, resulting in a total of sixteen (16) distinct element models (Table 6-1). While it desirable to completely and independently isolate these two variables (thickness and proximity), it is not a practical reality. Consequently, the interface frictional properties followed one of only two forms. When shale was present in the roof or floor, the coal pillar interface followed the Coulomb slip joint model parameters for shale overburden previously identified in Table 5-4. However if sandstone contacted the coal pillar, then the representative roof or floor interface was substituted with the Coulomb slip joint model parameters previously embodied for sandstone in Table 5-5. All overburden material was again represented using the ubiquitous joint constitutive model for either shale (Table 5-6) or sandstone (Table 5-7) as formerly implemented.

Table 6-1 Lithology study with selected roof/floor overburden material models

Model ID	Main Roof	Immediate Roof	Immediate Floor	Main Floor
	Sandstone (ft)	Shale (ft)	Shale (ft)	Sandstone (ft)
0B-0T	0	50	50	0
0B-25T	25	25	50	0
0B-40T	40	10	50	0
0B-50T	50	0	50	0
25B-0T	0	50	25	25
25B-25T	25	25	25	25
25B-40T	40	10	25	25
25B-50T	50	0	25	25
40B-0T	0	50	10	40
40B-25T	25	25	10	40
40B-40T	40	10	10	40
40B-50T	50	0	10	40
50B-0T	0	50	0	50
50B-25T	25	25	0	50
50B-40T	40	10	0	50
50B-50T	50	0	0	50

6.1.1 Pillar Stress-Strain

The pillar stress-strain curve results confirm a dependency on near-seam lithology across the spectrum of squat pillar sizes investigated. The results across each of the sixteen models are fairly delineated into two groupings based on the proximity and thickness of the sandstone to the coal seam. Where sandstone was the thickest and in closest proximity to the pillar, the available pillar strength was higher for a given level of average pillar strain. It also had a profound impact on post-failure behavior, as the inclusion of greater sandstone composition/proximity actually led to a transition to purely strain-hardening behavior. The highest strength was achieved when both the main and immediate roof and floor were comprised only of massive sandstone for each of the W/H=8 pillar (Figure 6-1), the W/H=10 pillar (Figure 6-2), and the W/H=12 pillar models (Figure 6-3), respectively. It is critical to note that significant instability in the form of a sudden loss of stress was only recognized when both the main/immediate roof and floor was at least eighty percent sandstone and within ten feet of the pillar while the model comprised entirely of sandstone roof/floor lithology achieved unstable failure at a smaller strain threshold.

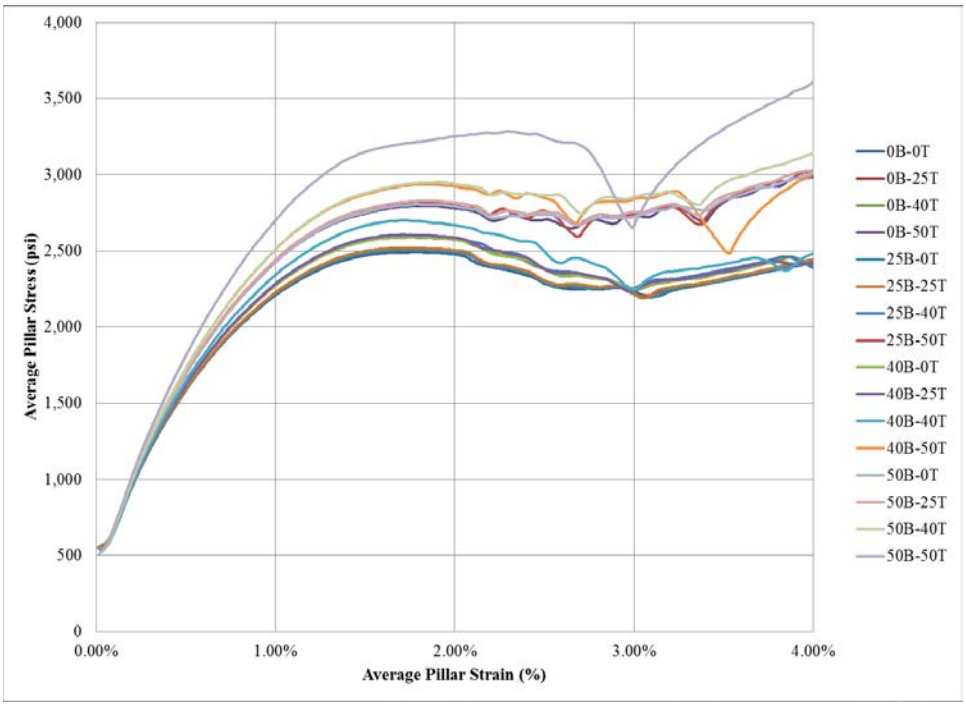

Figure 6-1 Average Pillar Stress versus Average Pillar Strain, W/H=8

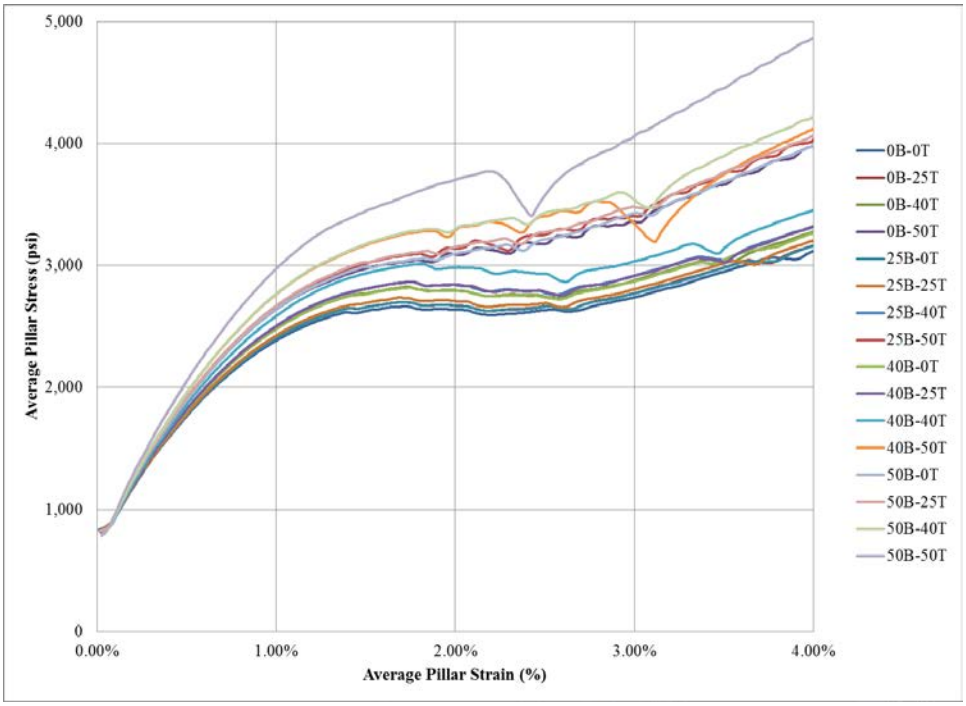

Figure 6-2 Average Pillar Stress versus Average Pillar Strain, W/H=10

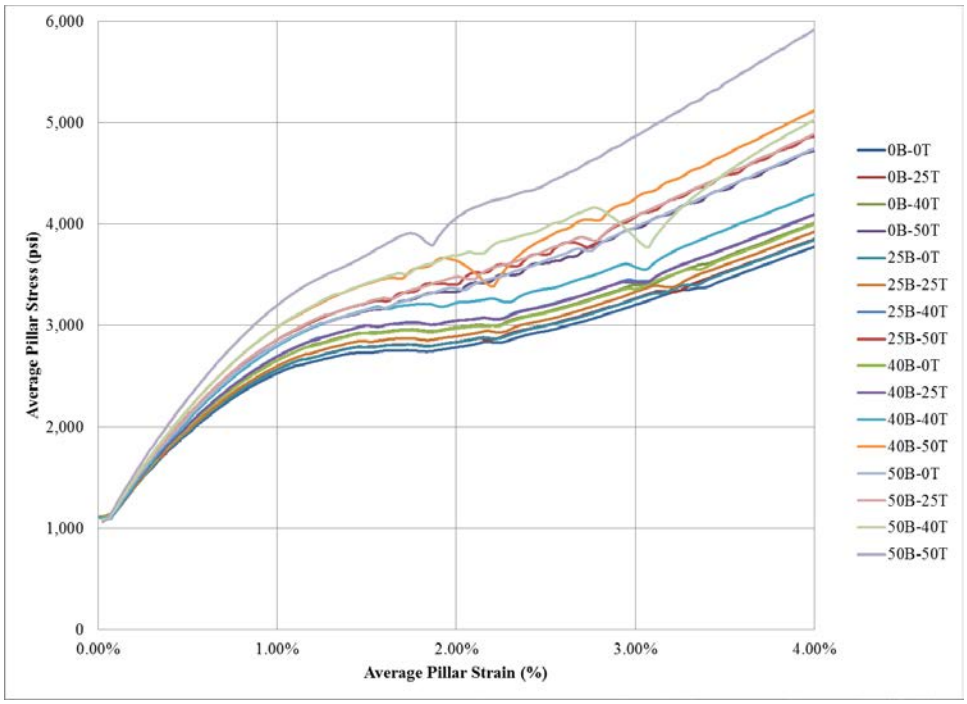

Figure 6-3 Average Pillar Stress versus Average Pillar Strain, W/H=12

While it is obvious that elevated stresses are apparent for greater sandstone thickness and closer proximity, the inclination for unstable failure to occur at lower values of pillar strain may be marginally more aligned with the composition of the roof rather than the floor. In a practical sense, the recognition of floor strata certainly isn't nearly as valuable as roof composition for obvious reasons; however, the results of numerous empirical studies repeatedly reference this concept. Nonetheless, the floor appears to be just as importance as the roof when considering the spectrum of squat pillar sizes examined. The values of average pillar strain for which these unstable failures were recognized generally decreased as the pillar geometry was increased, a finding consistent with the previous chapter regarding the influence of coal pillar interface on bump potential. While the effect of elevated interface friction and the resultant elevated propensity for interface stick-slip behavior was recognized for the sandstone joint model previously employed, it is clear that the near-seam lithology plays an important role on pillar stress response and that the probability of unstable failure certainly increases as both the main and immediate roof become comprised of stronger, rigid lithology in closer proximity to the coal seam.

6.1.2 Pillar Confinement

The results of the pillar stress-strain curves indicated a significant relationship between the probability of an unstable coal pillar failure to occur and the presence of strong, rigid strata such as sandstone in relatively close vicinity to the coal seam. Unstable loss of confinement was recognized for each the W/H=8 pillar (Figure 6-4), the W/H=10 pillar (Figure 6-5), and the W/H=12 pillar (Figure 6-6) for specific lithological environments. The evaluation of these average minimum principal stress curves confirm the ability for near-seam lithology to influence not only coal pillar response, but the manner in which failure occurs. The higher sandstone composition models led to elevated levels of pillar confinement and particularly impacted the post-failure pillar behavior, a conclusion which influenced the elevated pillar stress levels previously recognized. A sudden loss of confining stress is most closely aligned to greater composition of sandstone in the main and immediate roof and floor, a result which mirrors the results of the pillar stress-strain investigation. This loss of confinement appears to occur at decreasing values of pillar strain as the pillar size increases.

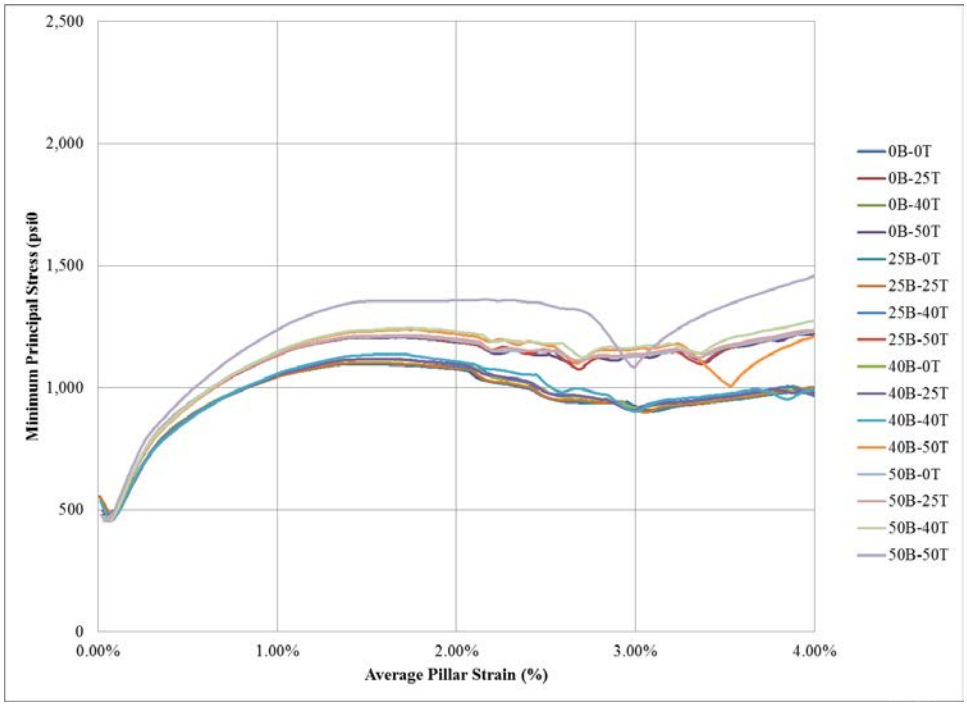

Figure 6-4 Average Confinement versus Average Pillar Strain, W/H=8

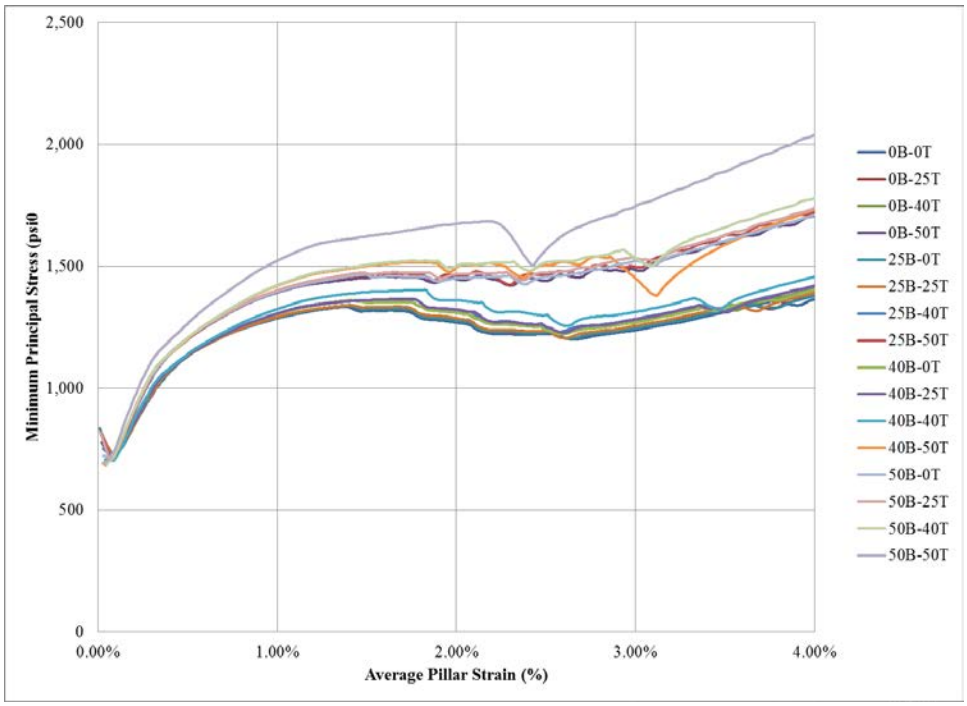

Figure 6-5 Average Confinement versus Average Pillar Strain, W/H=10

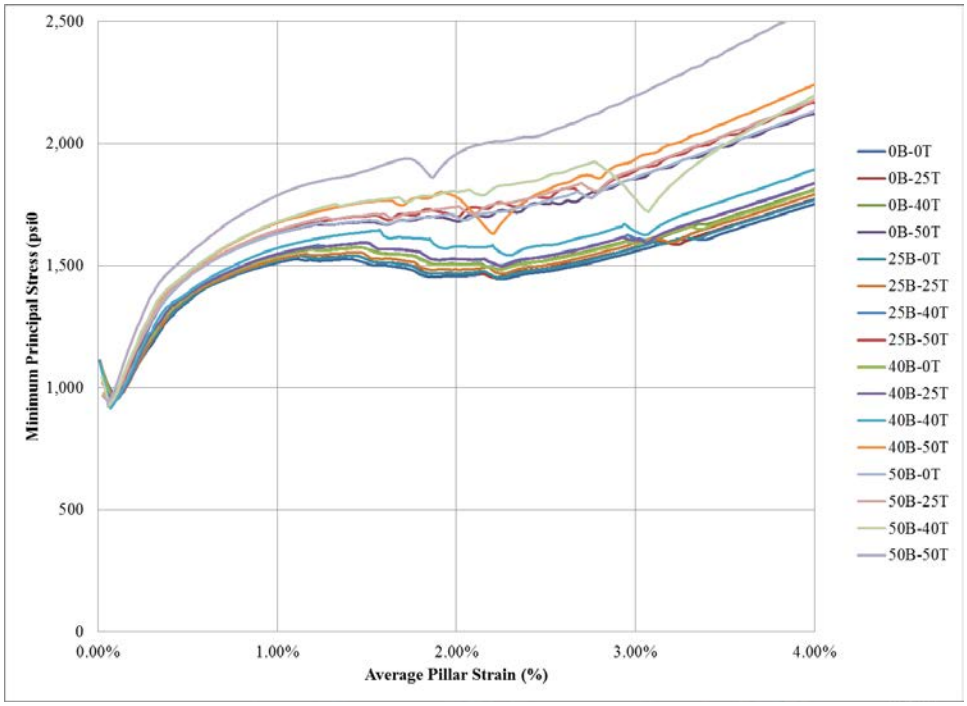

Figure 6-6 Average Confinement versus Average Pillar Strain, W/H=12

6.1.3 Peak Shear Strain Rate

The peak shear strain rate is an important indicator of an accelerated propagation of shear failure within the coal pillar which can lead to dynamic release of strain energy. Table 6-2 shows the maximum peak shear strain rate occurring within the coal pillar and the accompanying value of average pillar strain for each of lithologic models simulated. While the influence of the roof and floor composition is acknowledged, this influence is not nearly as significant as expected or that which was realized with the coal pillar interface friction study. Nonetheless, the highest values did consistently occur when greater compositions of sandstone in the roof and floor in closest proximity to the pillar were considered, though the average pillar strain which resulted was not as predictable as expected. Consistent with the previous findings, the average strain at which peak shear strain rate was sustained did dramatically decrease as the pillar geometry increased. Overall higher peak shear strain rates were realized at larger squat pillar dimensions, a fact most notably tied to the elevated levels of total energy available for release. The peak shear strain rate curves for the W/H=8 pillar, the W/H=10 pillar, and the W/H=12 pillar are illustrated on Figure 6-7, Figure 6-8, and Figure 6-9, respectively.

Table 6-2 Maximum Peak Shear Strain Rate for each Geologic Model

W/H	Model	Peak SSR (s^-1)	Strain (%)	Avg. Strain (%)
8	0B-0T	1.96	2.05%	2.62%
	0B-25T	2.06	2.08%	
	25B-0T	2.16	2.43%	
	40B-0T	2.27	2.42%	
	0B-40T	2.29	2.91%	
	25B-25T	2.32	2.44%	
	40B-25T	2.38	2.41%	
	25B-40T	2.40	2.49%	
	50B-50T	2.46	2.86%	
	0B-50T	2.63	3.26%	
	50B-0T	2.76	2.57%	
	50B-25T	2.79	2.57%	
	25B-50T	2.82	2.55%	
	40B-40T	3.01	2.85%	
	50B-40T	3.03	2.59%	
	40B-50T	3.69	3.46%	
10	25B-0T	2.10	2.08%	2.21%
	0B-0T	2.15	2.07%	
	40B-0T	2.34	1.86%	
	25B-25T	2.40	2.08%	
	0B-25T	2.46	2.52%	
	0B-40T	2.46	2.07%	
	25B-50T	2.50	2.21%	
	25B-40T	2.52	1.80%	
	40B-25T	2.61	2.10%	
	0B-50T	2.72	2.20%	
	50B-0T	2.76	2.29%	
	50B-50T	2.85	2.32%	
	50B-25T	2.85	2.28%	
	40B-40T	2.98	2.49%	
	50B-40T	3.07	2.92%	
	40B-50T	3.43	3.09%	
12	0B-0T	2.37	2.19%	2.13%
	50B-50T	2.43	1.85%	
	25B-0T	2.45	1.78%	
	40B-0T	2.57	1.76%	
	25B-25T	2.59	1.65%	
	0B-40T	2.61	1.66%	
	0B-25T	2.65	1.78%	
	0B-50T	2.75	1.96%	
	25B-40T	2.75	1.79%	
	40B-25T	2.87	1.79%	
	50B-0T	2.90	1.97%	
	40B-40T	2.93	3.36%	
	25B-50T	3.15	2.64%	
	50B-25T	3.37	2.69%	
	40B-50T	3.71	2.14%	
	50B-40T	4.32	3.05%	

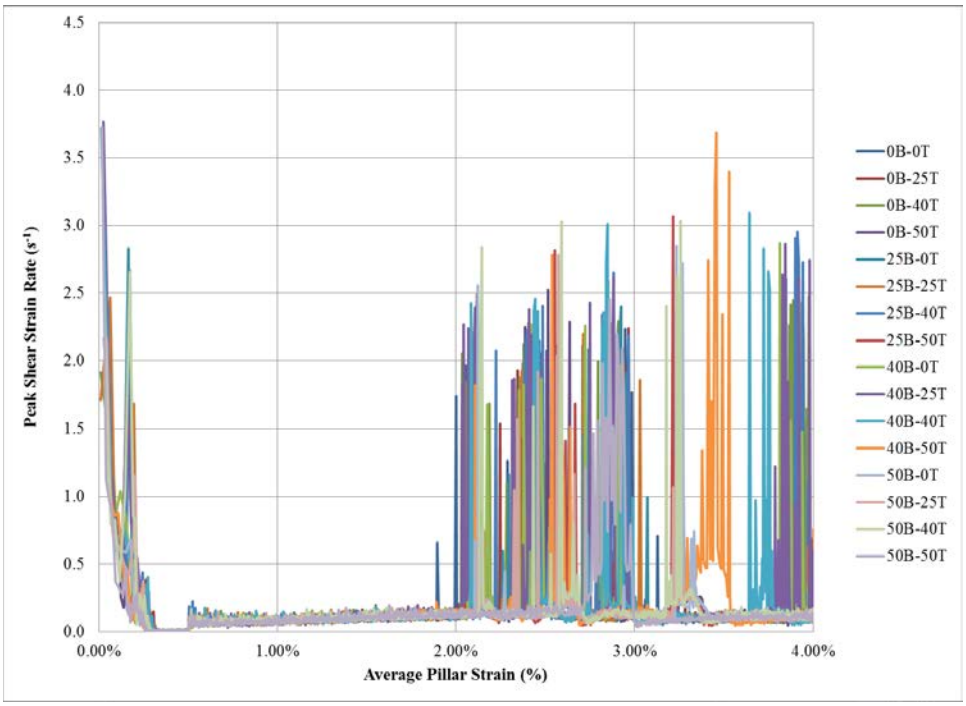

Figure 6-7 Peak Shear Strain Rate vs Average Pillar Strain, W/H=8

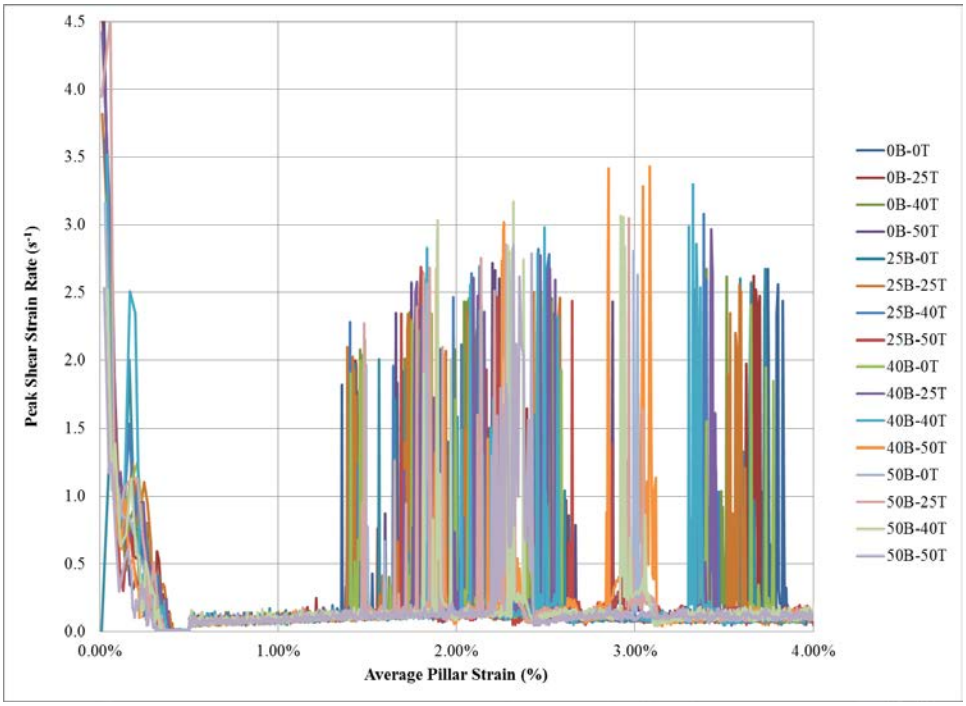

Figure 6-8 Peak Shear Strain Rate vs Average Pillar Strain, W/H=10

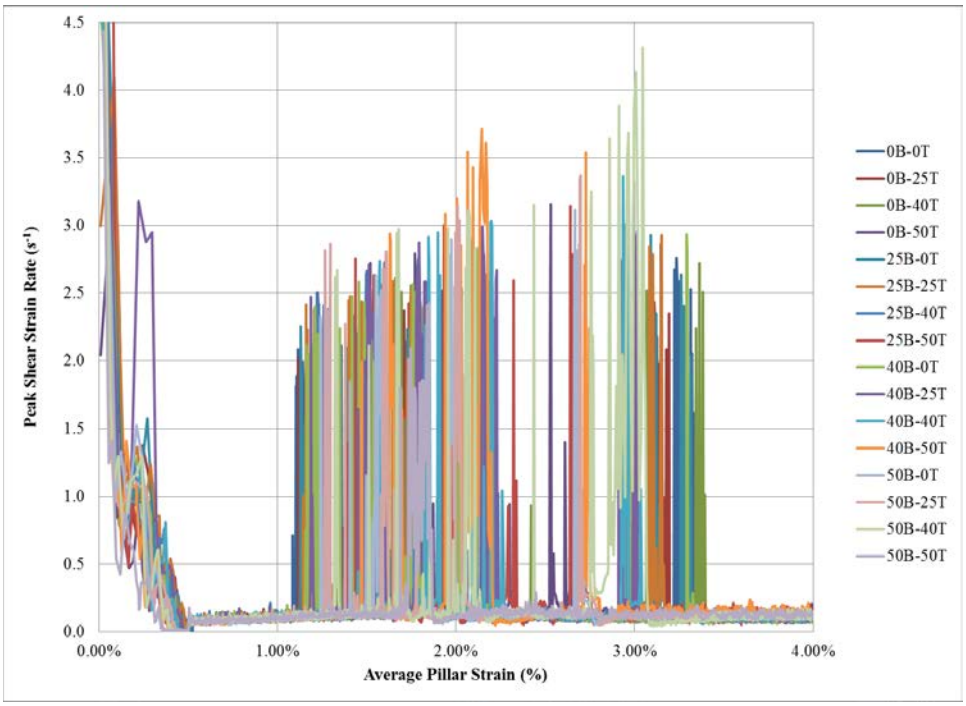

Figure 6-9 Peak Shear Strain Rate vs Average Pillar Strain, W/H=12

6.1.4 Total Energy Release

Previously, it was determined that total energy release, which is a main indication of the available excess energy which could sustain unstable pillar failure, was closely aligned with both the pillar geometry and interface residual friction strength, though at high values of pillar strain lithology did play an increasingly important role. It is again clear that as the pillar size increases, the total energy release curves are clearly transforming in behavior from primarily linear behavior for the W/H=8 pillar (Figure 6-10) and W/H=10 pillar (Figure 6-11) to non-linear behavior for the W/H=12 pillar (Figure 6-12). It is also clear that the composition of both the roof and floor near the coal seam has a profound impact on the total energy release. For minimal composition and proximity of strong strata such as sandstone, the behavior is very consistent across all values of average pillar strain. However, as the sandstone becomes increasingly thick and closer to the seam, the relationship between lithology and the total energy release becomes more volatile. While some of this volatility is explained by the potential failure mechanism of squat coal pillars as unstable shear slip along the interface, it is clear that the mere occurrence of stronger lithology leads to higher quantities of available excess energy.

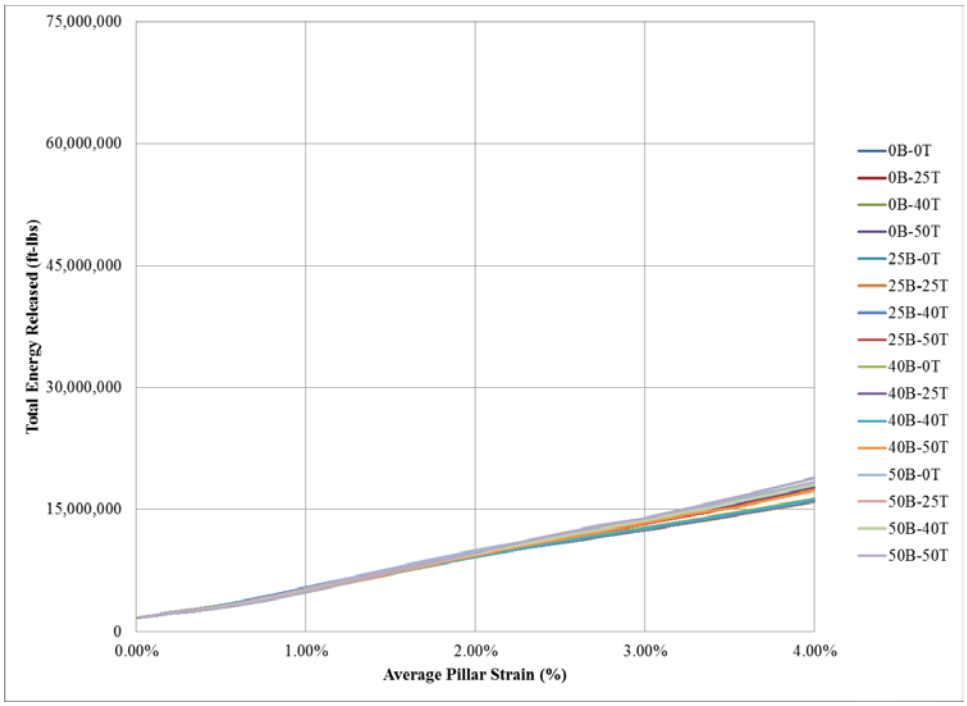

Figure 6-10 Total Energy Released vs Average Pillar Strain, W/H=8

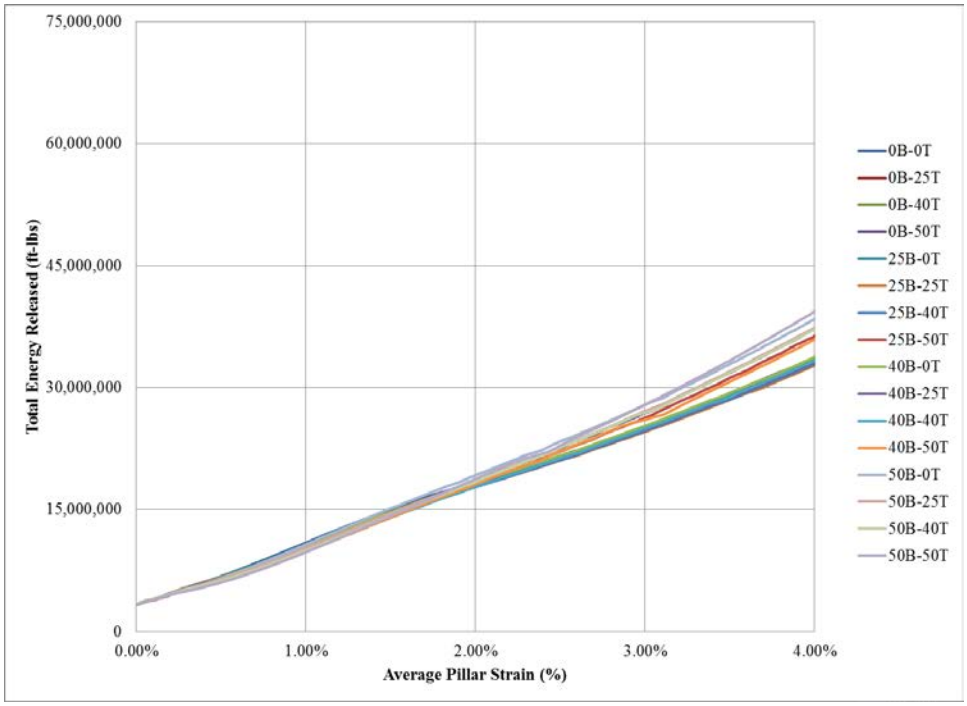

Figure 6-11 Total Energy Released vs Average Pillar Strain, W/H=10

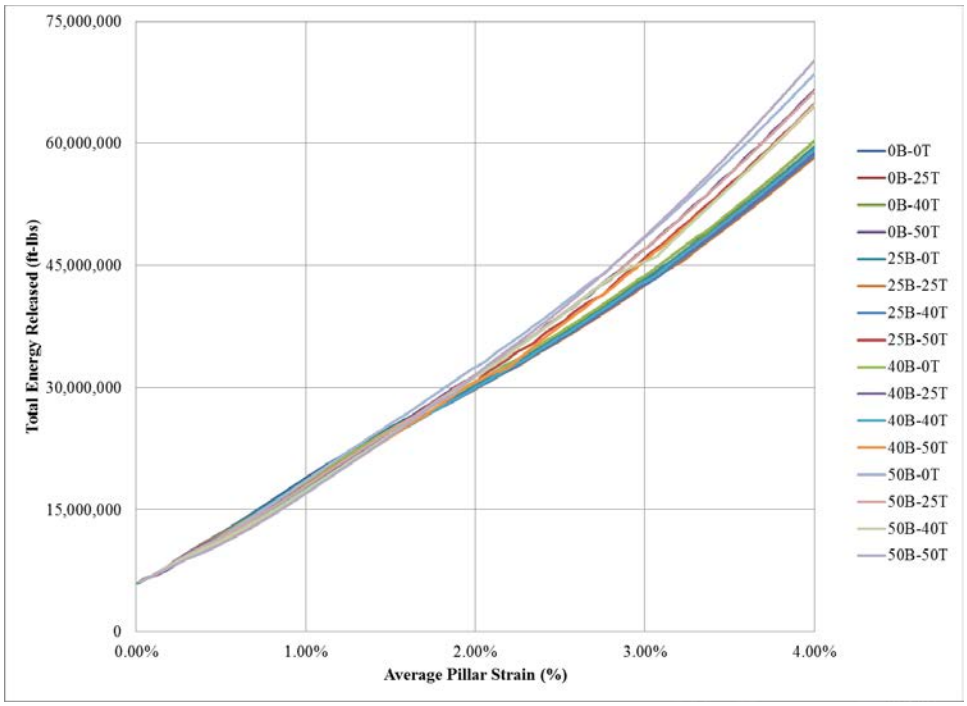

Figure 6-12 Total Energy Released vs Average Pillar Strain, W/H=12

6.1.5 Kinetic Energy

Substantial kinetic energy release, which is a direct physical correlation to dynamic failure and release, was noted for all squat pillar models simulated as shown in Table 6-3. Increasing the pillar geometry appeared to subsequently increase the likelihood of an unstable release of kinetic energy, which was nearly an order of magnitude greater than the lower values numerically observed. Like most of the other results already reported, the average pillar strain at which kinetic energy release reached a maximum value in the model declined as the pillar geometry increased. Furthermore, it is also noted that similar to the peak shear strain rate results previously discussed the volatility in the values of strain for a particular lithologic environment did not implicate a detectable correlation between the lithology and the functional pillar strain, though the general trends indicate that the presence of thicker, more rigid strata like sandstone in closer proximity to the seam does indeed result in higher peaks of kinetic energy release. This outcome suggests that while general trends or factors may be observed, the concept of functional failure is truly dependent on the loading environment and numerous geologic factors, a result

which directly points to the erratic and intermittent nature of coal burst events which have actually transpired in the coal mining industry.

Table 6-3 Maximum Kinetic Energy Release for each Geologic Model

W/H	Model	Kinetic Energy (ft-lbs)	Strain (%)	Avg. Strain (%)
8	50B-0T	310	2.57%	2.65%
	50B-25T	336	2.62%	
	40B-0T	366	2.49%	
	40B-25T	407	2.45%	
	25B-40T	413	2.42%	
	25B-25T	415	2.45%	
	25B-0T	420	2.46%	
	50B-40T	422	2.63%	
	0B-0T	425	2.09%	
	0B-40T	473	2.91%	
	0B-25T	482	2.10%	
	40B-40T	508	2.93%	
	0B-50T	511	3.32%	
	25B-50T	559	2.61%	
	40B-50T	821	3.43%	
	50B-50T	1,377	2.90%	
10	40B-0T	353	1.82%	2.30%
	50B-25T	408	2.32%	
	50B-0T	451	2.33%	
	25B-50T	480	2.24%	
	0B-50T	490	2.24%	
	25B-40T	508	1.81%	
	40B-25T	509	2.14%	
	25B-0T	513	2.09%	
	0B-40T	515	2.08%	
	0B-25T	520	2.57%	
	0B-0T	529	2.10%	
	25B-25T	556	2.10%	
	40B-40T	577	2.56%	
	50B-40T	627	3.02%	
	40B-50T	1,401	3.04%	
	50B-50T	2,294	2.35%	
12	40B-0T	465	1.78%	2.07%
	25B-0T	515	1.78%	
	50B-0T	532	2.00%	
	0B-50T	532	1.96%	
	0B-25T	563	1.80%	
	40B-25T	565	1.83%	
	0B-0T	582	2.20%	
	0B-40T	595	1.79%	
	25B-40T	598	1.84%	
	50B-25T	606	2.73%	
	25B-25T	648	1.78%	
	40B-40T	771	3.00%	
	25B-50T	789	2.71%	
	50B-50T	1,318	1.82%	
	40B-50T	2,387	2.14%	
	50B-40T	3,624	3.00%	

Contrary to the results of the previous chapter, the peak magnitude of kinetic energy release was directly proportional to the pillar geometry for each squat pillar size numerically examined. The peak kinetic energy release versus average pillar strain for each of the squat coal pillar models investigated are illustrated on Figure 6-13 (W/H=8), Figure 6-14 (W/H=10), and Figure 6-15 (W/H=12), respectively. The inference that both the probability and magnitude of peak kinetic energy release are elevated with the presence of stronger lithology closer to the coal pillar is more than likely a consequence of the elevated strength of both the roof and floor strata which can better resist failure and the onset of plastic deformation. It is also important to recognize that even if either one of the roof or floor lithology was primarily or even completely represented with the stronger sandstone overburden model, the presence of the weaker shale overburden model in opposite floor or roof strata consistently negated overall pillar strength and resulted in lower peak kinetic energy release values across all pillar geometries considered.

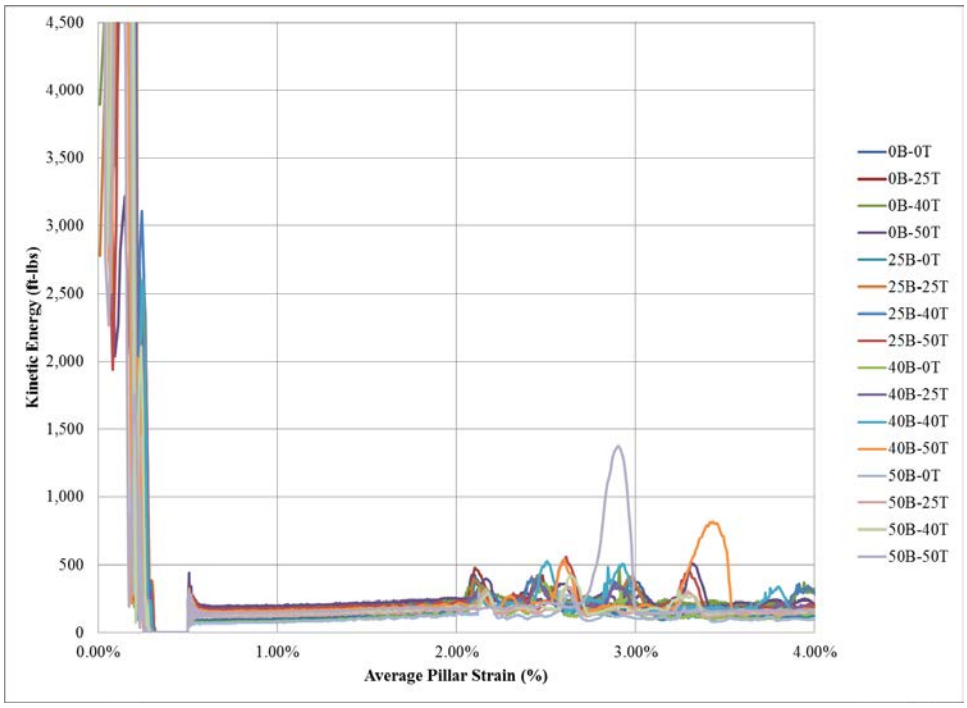

Figure 6-13 Kinetic Energy vs Average Pillar Strain, W/H=8

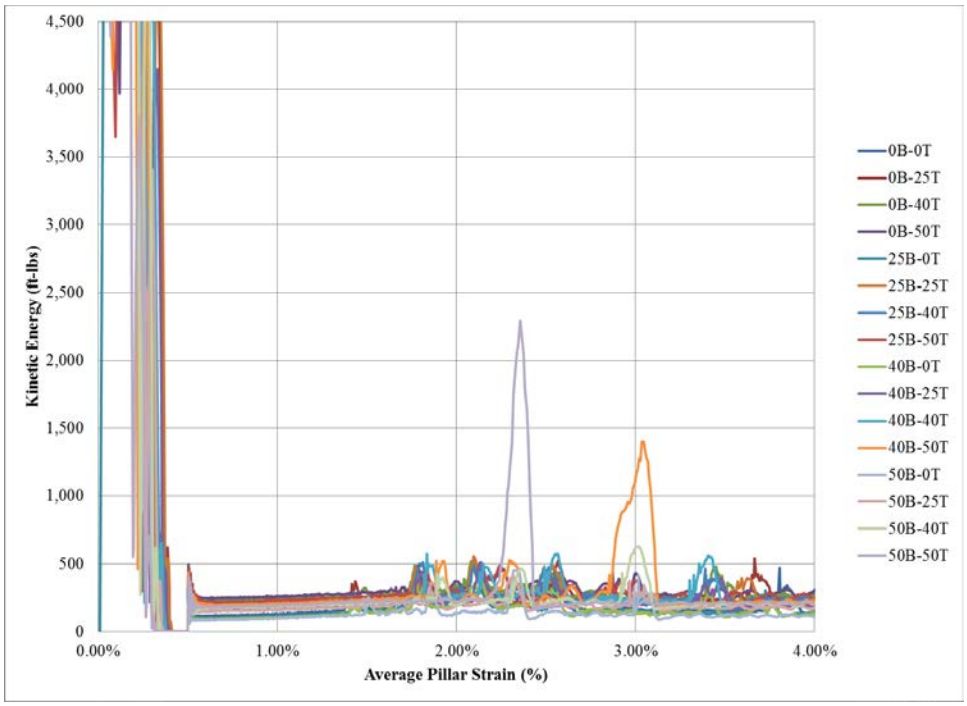

Figure 6-14 Kinetic Energy vs Average Pillar Strain, W/H=10

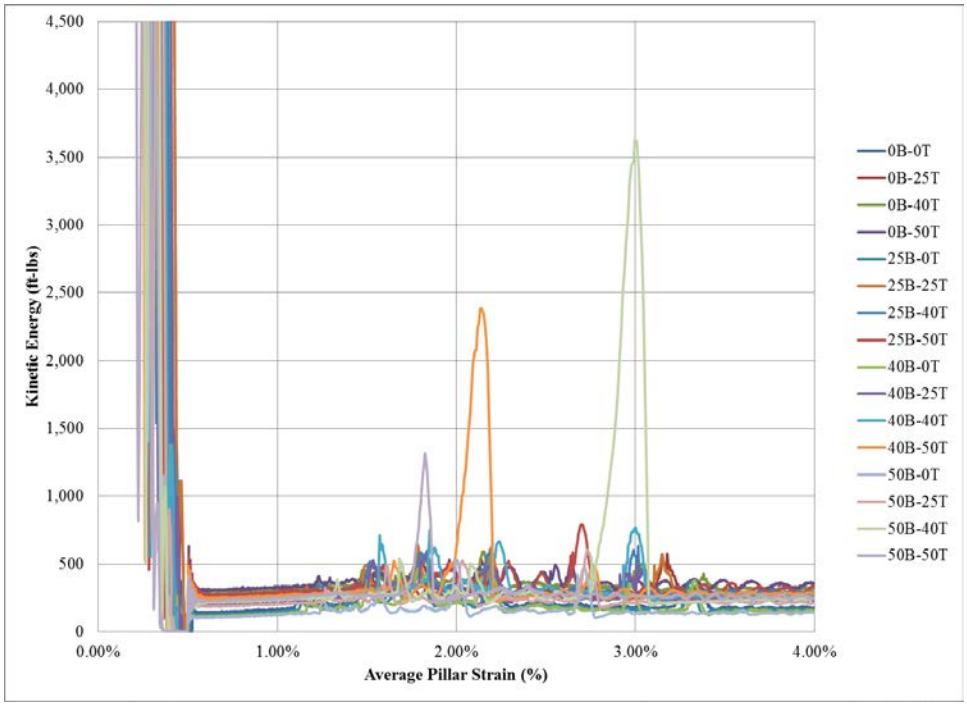

Figure 6-15 Kinetic Energy vs Average Pillar Strain, W/H=12

6.1.6 Joint Friction Work

Accelerated surges in joint friction work were primarily observed in the high sandstone/closer proximity models, a factor which reflects unstable frictional heating of the coal pillar interface. While a correlation between the joint friction work and the interface frictional model were previously discussed, the results illustrated on Figure 6-16 (W/H=8), Figure 6-17 (W/H=10), and Figure 6-18 (W/H=12) also demonstrate a noteworthy relationship between joint friction work and the coal seam lithological environment. It is clear from these relationships that not only did the magnitude of joint friction work increase as both the pillar geometry and sandstone content increased, but the potential for unstable increases in joint friction work representative of deconfinement during interface stick-slip behavior were substantially greater. In fact, the propensity and quantitative measure of this unstable interface stick-slip to occur was increasingly more dependent on the thickness and proximity of strong roof and floor strata relative to the coal seam as the pillar geometry increased. As previously noted, the average pillar strain at which these unstable increases in joint friction work occurred decreased as pillar size increased.

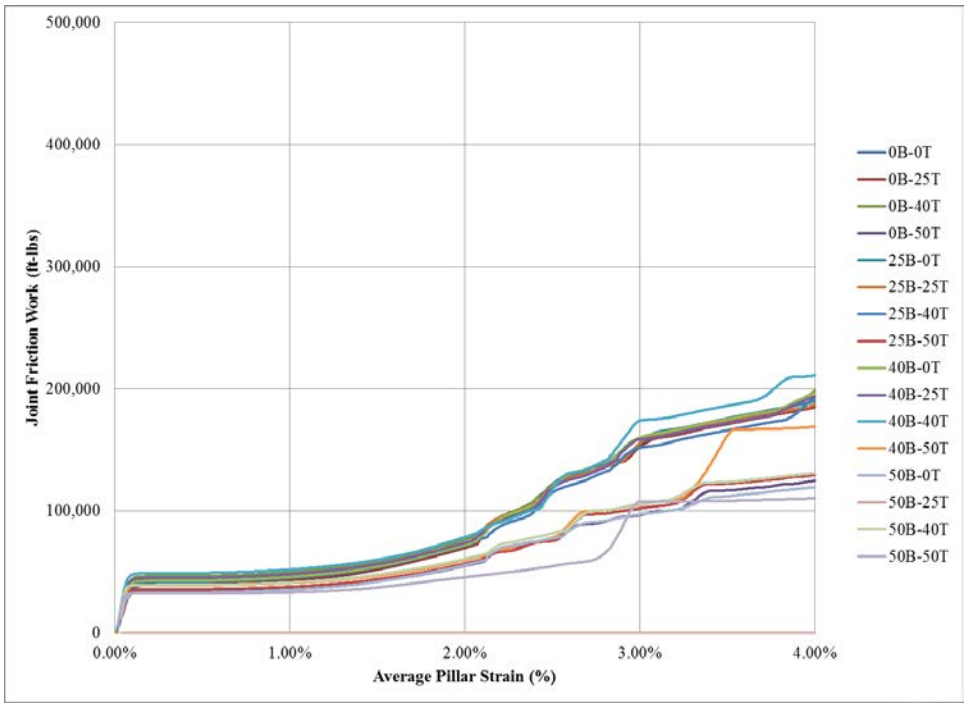

Figure 6-16 Joint Friction Work vs Average Pillar Strain, W/H=8

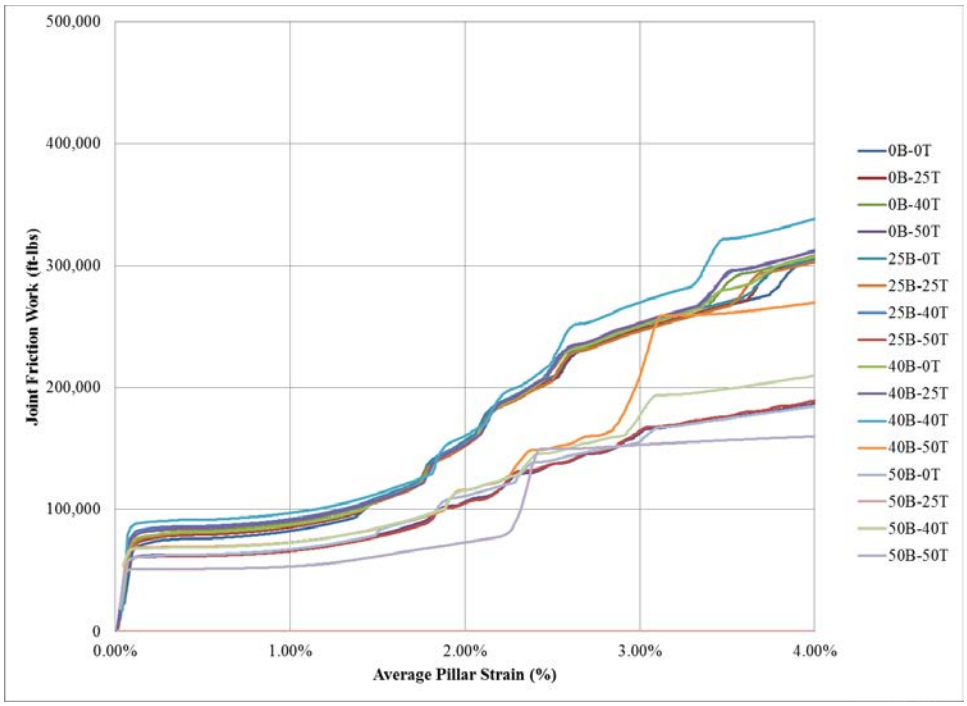

Figure 6-17 Joint Friction Work vs Average Pillar Strain, W/H=10

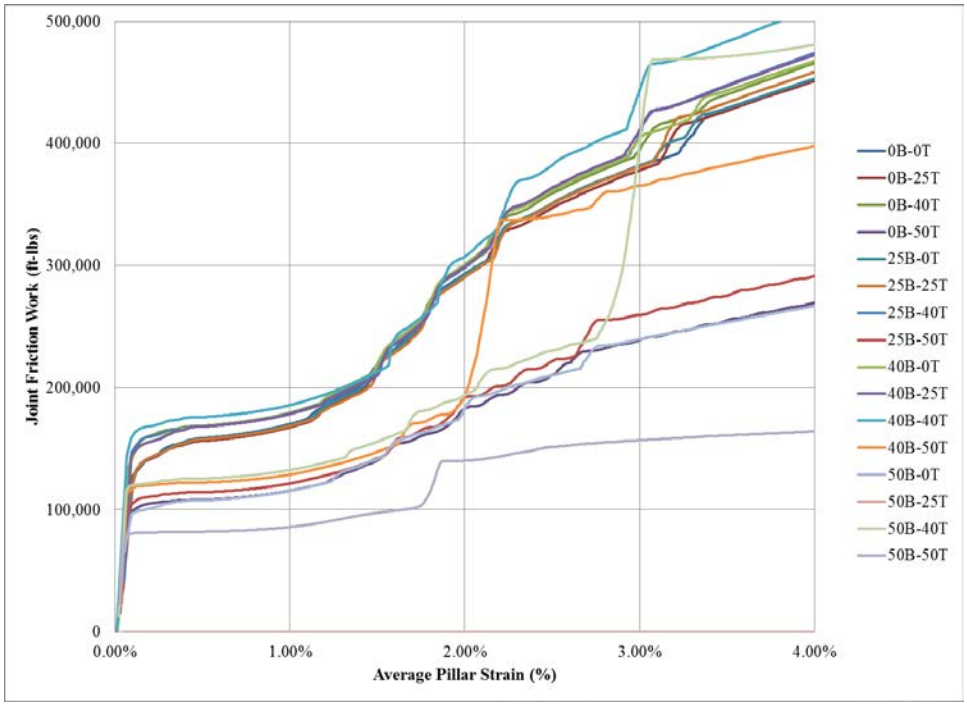

Figure 6-18 Joint Friction Work vs Average Pillar Strain, W/H=12

6.2 Summary of Findings

The impact of near-seam lithology, which includes the composition, strength, extent, and makeup of both the roof and floor, is an extremely important factor to consider when examining coal pillar bump potential. The same squat coal quarter pillar models, were subjected to a sensitivity analysis which varied the thickness and proximity of thick, massive sandstone relative to the coal pillar in both the roof and floor for a total of sixteen models. It is unavoidably impossible to completely isolate lithology as an independent variable from coal pillar interface frictional properties in a practical sense, which was already shown in the previous chapter to have a significant impact on coal bump potential. Nonetheless, the interface frictional model set was reduced to two representative sets: one for the shale overburden model and the second for the sandstone overburden model.

Both average pillar stress-strain and the average pillar confinement were observed to be dependent on the lithological environment of the roof and floor. The presence of thick sandstone which occurred in closer proximity to the roof and/or floor elevated both strength and stress and resulted in hardening of the pillar post-failure behavior. However, its presence also led to the occurrence of an unstable drop in strength for all squat pillars examined, a fact attributed to deconfinement which was mirrored by drops in the minimum principal stress relationships. This conclusion was confirmed when looking at the peak coal pillar shear strain rate and kinetic energy release, all of which demonstrated maximum values when the roof and floor were increasingly composed of sandstone near the coal pillar. Shear strain rate has previously been discussed as an important indicator of the unstable propagation of shear fracturing within a coal pillar, which can result in the dynamic release of stored strain energy. Kinetic energy release is conceptually the physical manifestation of this dynamic failure.

Though the peak shear strain rate achieved within the coal pillar is certainly an important indicator of dynamic pillar failure due to an accelerated propagation of shear failure, the impact of near-seam lithology wasn't as significant as expected or as found during the interface frictional study. And while higher values of peak shear strain rate were typically recognized for more squat pillars with greater composition of sandstone in

closer proximity to the coal seam, the discrete pillar strain values for which these maximums transpired were very inconsistent.

The volatility in the values of the pillar strain at peak shear strain rate does not directly point towards a discernible relationship between lithology and functional pillar strength, though the average strain did consistently decrease as the pillar size increased. This finding is supported by the practical reality that coal bumps are complex features dependent on many loading and geologic considerations, a fact evidenced by the intermittent and unpredictable nature of coal bursts. This same volatility was evidenced by the documented maximum kinetic energy release. It was also clear that the composition of the roof and floor had an impact on the total excess energy available for release, particularly at higher values of average pillar strain. Greater sandstone thickness and closer proximity to the coal seam inherently resulted in higher values of excess energy, a result most likely attributable to increased stress levels.

It was determined in the previous chapter that kinetic energy release is fundamentally dependent on near-seam lithology as much as the interface friction characteristics. In fact, unstable maximums were observed for all squat pillars modeled, and it was concluded that increasing the pillar size actually appeared to result in a subsequent increase in the likelihood of unstable release of kinetic energy. And while there was not a discernible correlation between a particular lithologic environment and the functional pillar strength, general trends were obtained with the most notable one being the presence of strong, rigid strata such as sandstone which is in close proximity to the coal seam is much more likely to produce an unstable release of kinetic energy within a coal pillar. When the lithology of the roof and floor primarily consisted of shale, peaks in both kinetic energy release and shear strain rate were mild and occurred in smaller waves, representative of the smaller stages of yield occurring within the pillar instead of a singular energetic release. This finding points to the fact that functional failure of a squat coal pillar is truly dependent on both the stress environment and a multitude of geologic parameters.

Joint friction work is representative of the unstable frictional heating of the coal pillar interface and is a key indicator of stick-slip behavior which can trigger deconfinement

and a coal burst. Accelerated increases in joint friction work were typically observed only to occur in the presence of thick sandstone near the coal pillar. It was concluded that not only did the magnitude of the joint friction work increase as the pillar size increased, but that as the sandstone content increased the probability for unstable increases in joint friction work were obviously greater. Furthermore, the inclination and sheer magnitude of this unstable interface stick-slip to happen became increasingly more dependent on the roof and floor lithology as the pillar geometry was increased.

In summary, the following results are considered to have significant bearing on coal pillar bump potential:

- The composition of the roof and floor has a profound impact on coal pillar bump potential, notwithstanding the fact that coal pillar interface frictional properties are inherently a function of this lithological environment.
- The propensity for unstable pillar failure to occur was singularly linked to the presence of thick, rigid strata (represented numerically as sandstone) in close proximity to the coal seam. When the roof and/or floor primarily consisted of the weaker shale model, evidence of unstable pillar failure diminished. It is believed that not only does the presence of stronger strata near or on the coal pillar increase the likelihood of an unstable interface frictional set, but elevated levels of strength and excess energy are achieved and the likelihood of stick-slip or accelerated propagation of shear failure within the coal pillar is increased.
- While the presence of stronger roof appears to be slightly more related to unstable pillar failure at lower values of average pillar strain, the floor appears to be nearly as important when considering the entire spectrum of squat pillar geometries considered and levels of strain numerically achieved. The narrowing transfer of stress from the roof, through the pillar, and the subsequent stress expansion to the floor creates an environment which can induce tensile forces in the immediate floor strata. The presence of strong floor can actively resist these tensile stresses and play an important role in confinement and pillar behavior.
- Figure 6-19 and Figure 6-20 illustrate the volumetric strain rate for the W/H=10 pillar with complete sandstone lithology for the 50B-50T lithology model set.

These figures represent the volumetric strain rate at average pillar strain values of 2 percent and 2.5 percent, respectively. The initially clear delineation of the intact elastic core followed by the loss of confinement, strength, and resultant release of strain energy upon failure are immediately obvious.

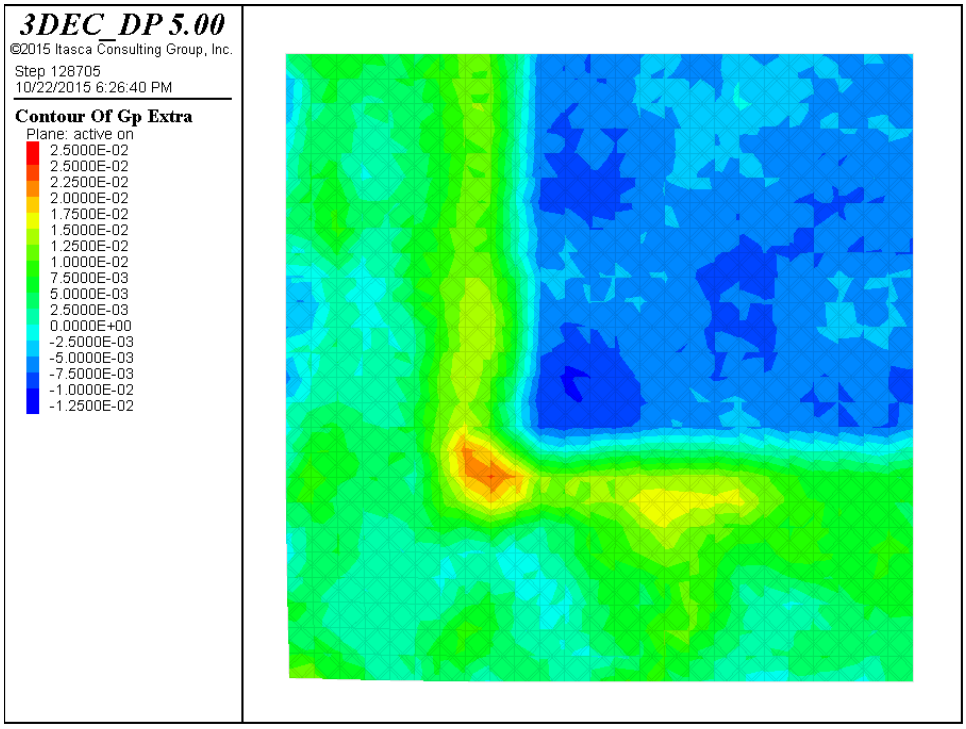

Figure 6-19 Volumetric strain rate of W/H=10 50B-50T model at 2% Strain

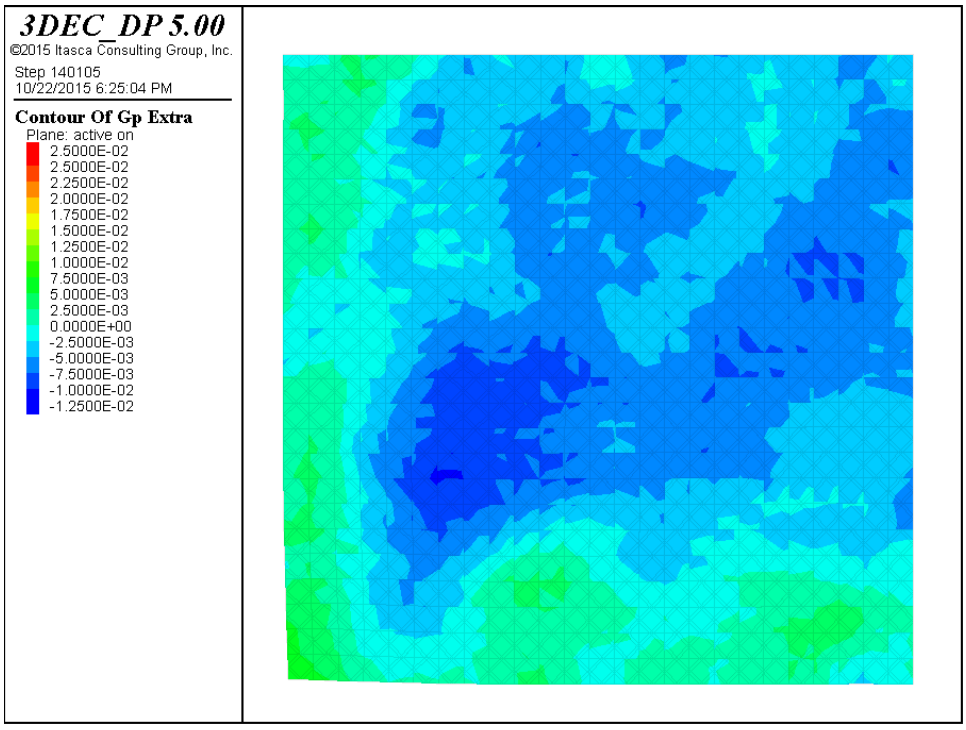

Figure 6-20 Volumetric strain rate of W/H=10 50B-50T model at 2.5% Strain

- Figure 6-21 illustrates the volumetric strain rate for the W/H=10 pillar with complete shale lithology for the 0B-0T lithology model set. Even though functional pillar failure is realized the smaller elastic core remains intact though the outer pillar elements have yielded and are functionally shedding stress inwards towards the core. This result is highly representative of stable yielding failure.

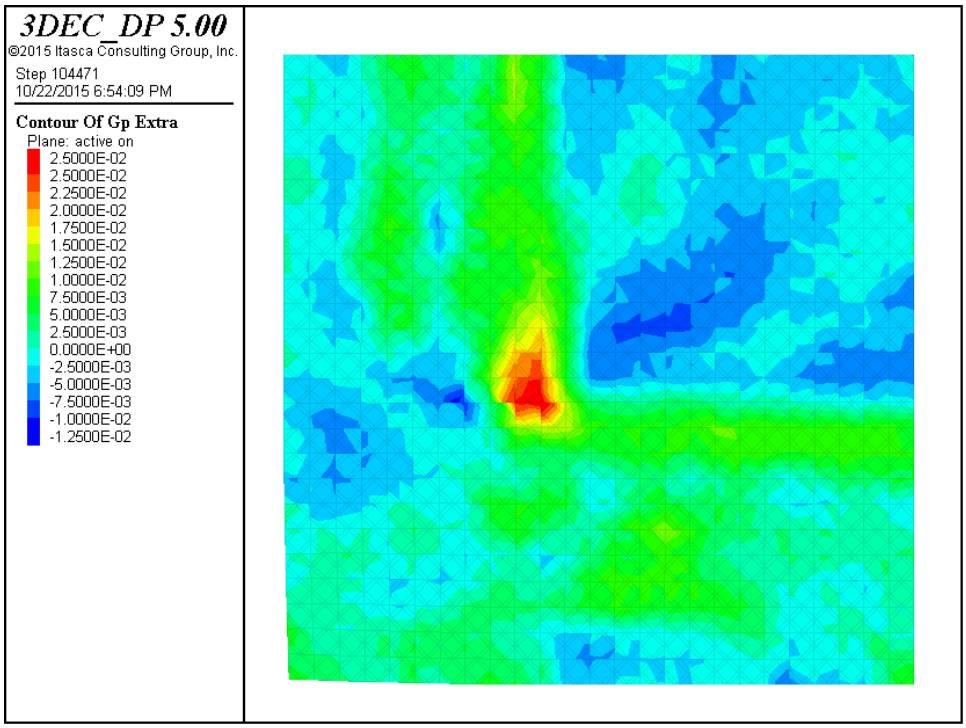

Figure 6-21 Volumetric strain rate of W/H=10 0B-0T model at 2.5% Strain

- The average pillar strain at which unstable failure was realized decreased as the pillar size increased. This stands consistently with the results of Chapter 5. However, contrary to the findings in the previous chapter regarding pillar interface influence, the magnitude of unstable failure appeared to be proportional with the pillar geometry. This finding was confirmed with the evidences suggested by the peak shear strain rate, total energy release, kinetic energy, and joint friction work, all of which demonstrated maximum instability for the W/H=12 pillar model.
- The distinct element method again appears to do a respectable job of capturing unstable coal pillar failure such as which occurs during a coal burst. For example, Figure 6-22 and Figure 6-23 illustrate the displacement magnitude for the W/H=10 pillar with the 50B-50T lithology model set. The displacement magnitude is immediately recognized to shift to a greater magnitude deeper into the pillar from the roof to the floor during the transition from stability to instability. The release of stored strain energy towards the pillar core also results

in an evolution of displacement in the roof from the entry/crosscut towards the pillar center during this transition.

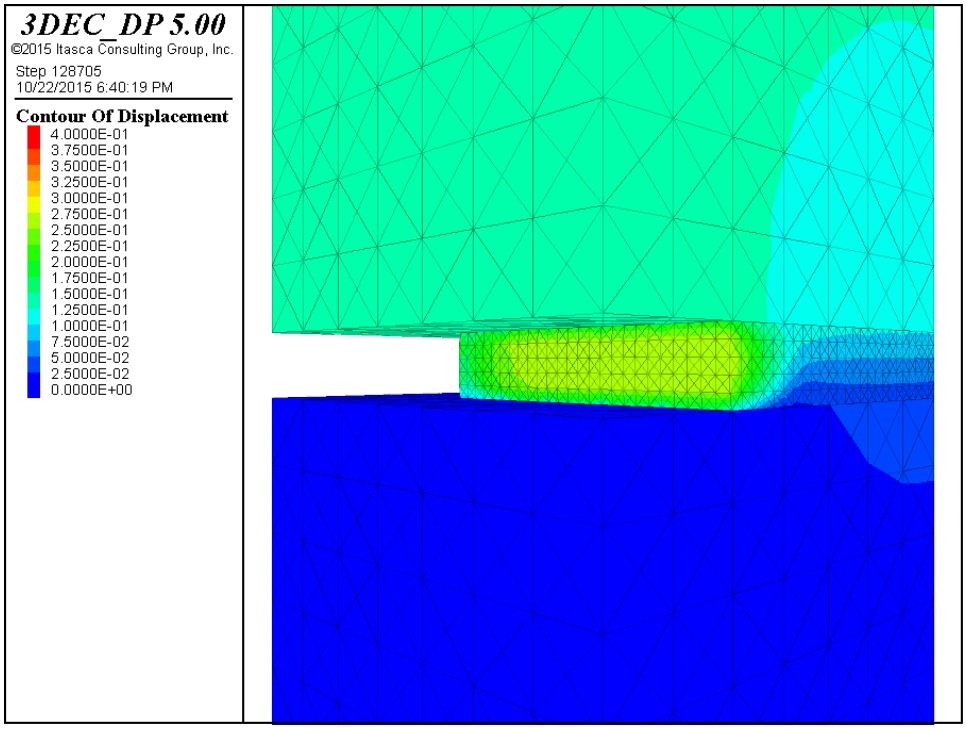

Figure 6-22 Displacement Magnitude of W/H=10 50B-50T model at 2% Strain

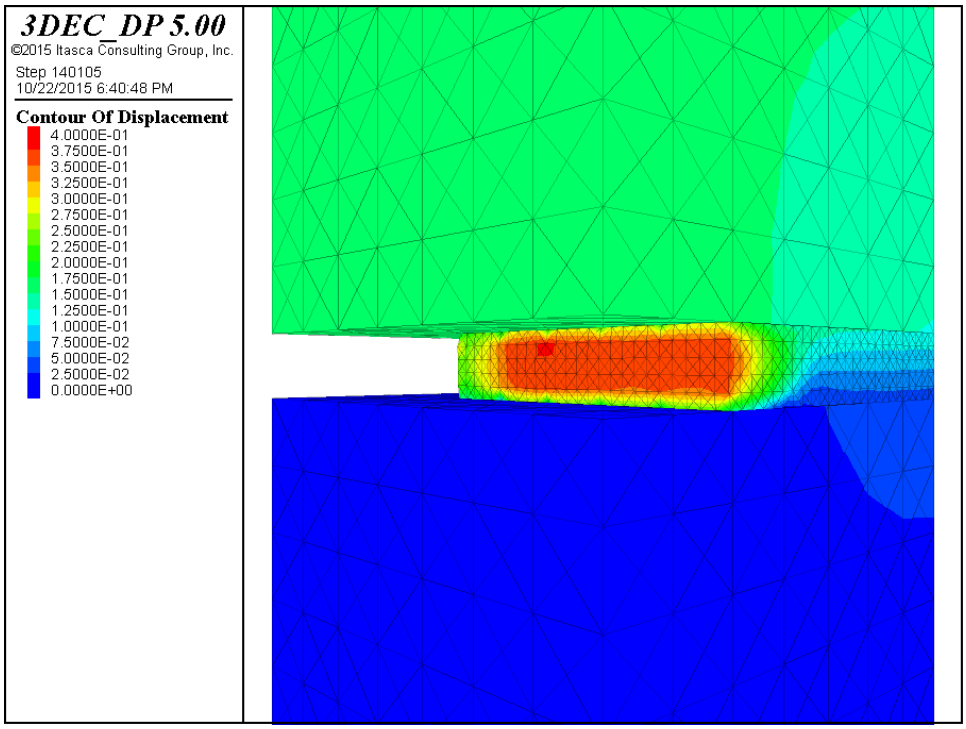

Figure 6-23 Displacement Magnitude of W/H=10 50B-50T model at 2.5% Strain

- While delineation between the interface frictional model between shale and sandstone pillar contact was made for necessarily practical reasons, the main goal of this chapter was to identify the relationship that coal seam lithology had on bump potential. As such, the relative stiffness of the surrounding strata, the resultant distribution of stress, and the strength of the ubiquitous joints which were assigned to represent sedimentary bedding planes in the roof/floor strata are undoubtedly the chief driver of these results. The finding that bump potential inherently increases with the presence of thicker, stronger strata in closer proximity to the coal seam directs us towards the concept energy balance remains a principal key to the understanding of coal bursts.

7 Global Factors and the Ground Response Curve

In previous chapters, the use of discrete element modeling demonstrated the ability to predict an elevated potential for unstable failure by examining six commonly employed numerical bump indicators. These chapters examined only the localized geologic and geometry parameters which influences the stress response of a single coal pillars in an effort to better understand the behavior and bump potential of squat coal pillars. However, it is important to consider not simply the local influences which determine site-specific pillar behavior, but equally the influence of global geologic and geometric considerations which impact this site-specific response.

The response of the surrounding rock mass to changes in stress as a result of the mining process ultimately determines the equilibrium load on a system of pillars (Figure 7-1), therefore the interaction between the ground response and the support system is essential towards understanding of pillar strength and behavior (Esterhuizen et al., 2010b). The authors also examined the influence of the ground response curve on coal pillar behavior, particularly focusing on the effect of depth and panel span using different strength overburden models. The study recognized the importance of the slope of the Ground Response Curve but failure was limited to the coal seam only, with the impact of weak roof and/or floor, side abutment loading, and barrier pillar stability being recommended for further study.

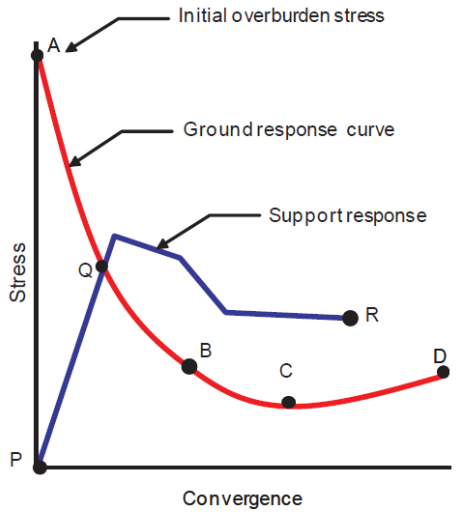

Figure 7-1 Conceptual GRC and support curve (Esterhuizen et al., 2010b)

The Ground Response Curve captures the response of the ground as the in-situ support is being removed, but can be used in conjunction with the support system response to determine the equilibrium point of loading and deformation. Zipf Jr. (1998) cited the ability and practicality of using the local mine stiffness stability criterion towards the prevention of a catastrophic and unstable ground failure. Previously, the concept of the local mine stiffness criterion has examined the slope of the loading system (ground response) at the beginning of failure, which was then compared with the slope, or post-peak stiffness, of the support system (e.g. pillars). A failure is unstable if the post-peak stiffness is larger in absolute behavior than the local mine stiffness, according to the stiffness criterion referenced by Gu (2013). An example of this concept is illustrated on Figure 7-2 where the excess energy is defined as the area delineated between the post-peak support response and the soft ground response curve. Although the study noted that "the role of loading stiffness was disregarded within these studies, although it is a vital aspect to understanding the occurrence of bumps. In order to better understand and predict the conditions which lead to unstable failure, additional research should be made on the combination of brittle rock and the potentially unstable loading conditions"(Garvey, 2013)

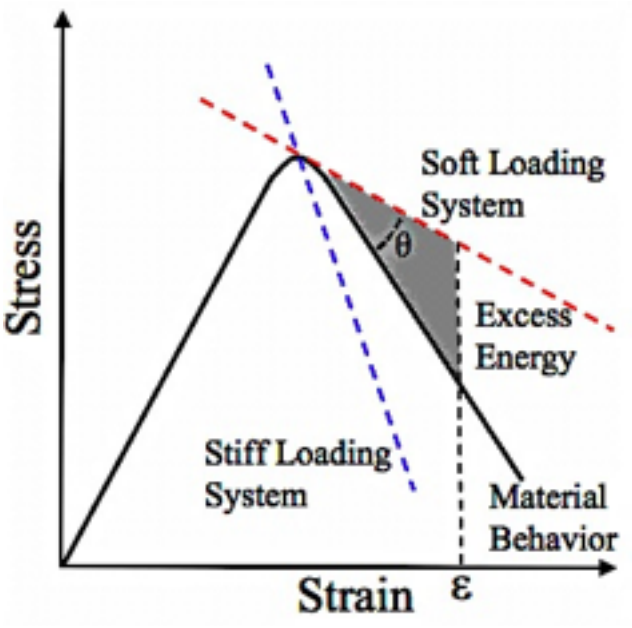

Figure 7-2 Local stiffness for stable versus unstable failure (Gu, 2013)

Major factors which effect the local mine stiffness include the rock elastic modulus, mine geometry, including panel width and barrier pillar width, extraction percentage, and the mining system (Zipf Jr., 1998). The author also understood the limitations of analytical methods to determine the local ground response and advocated for numerical approaches to provide enhanced insight for practical mine design. Consequently, a more thorough investigation of the Ground Response Curve was undertaken. Cover, panel width, mining method, side abutment loading, and barrier pillar width will all be examined within the context of deep cover room and pillar mining to better understand not only the ground response which occurs in the types of geologic environments for which coal bumps have often occurred, but to also set as a precursor for a case study to illustrate the union of localized stress response and the global stress environment towards the enhancement of bump prediction.

The finite difference software FLAC^{3D} has been employed to achieve these goals with a three-dimensional overburden model generally using cubic elements with a width of fifty feet. The model geometry totaled two-thousand feet in width and length to avoid edge influence on the coal panel(s). Gravity loading was utilized for the overburden stress while horizontal stress was assumed to behave as a function of depth as previously discussed in Chapter 4. Similarly, the properties of coal (Table 4-4) were mirrored from the calibrated properties used for single pillar discrete element modeling and the overburden was divided into two classifications: weak and strong. The ubiquitous joint constitutive model was again employed using the same properties defined for shale in Table 5-6 and sandstone in Table 5-7.

The weak overburden classification represented 80 percent shale and 20 percent sandstone, while conversely the strong classification used 20 percent shale and 80 percent sandstone. The overburden was modeled to represent alternating sequences of shale and sandstone at varying thickness. An example of the generalized finite difference model generated is shown in Figure 7-3. For each model, the overburden geometry and properties were created and the panel(s) was then defined within the coal seam. At the onset of initial equilibrium, the panel was excavated and replaced with an equivalent

vertical stress. This vertical stress was incrementally reduced in ten steps with the ground response measured at each step. Both development and retreat mining were examined. Consequently, the calibration of the gob material model follows in the subsequent subchapter.

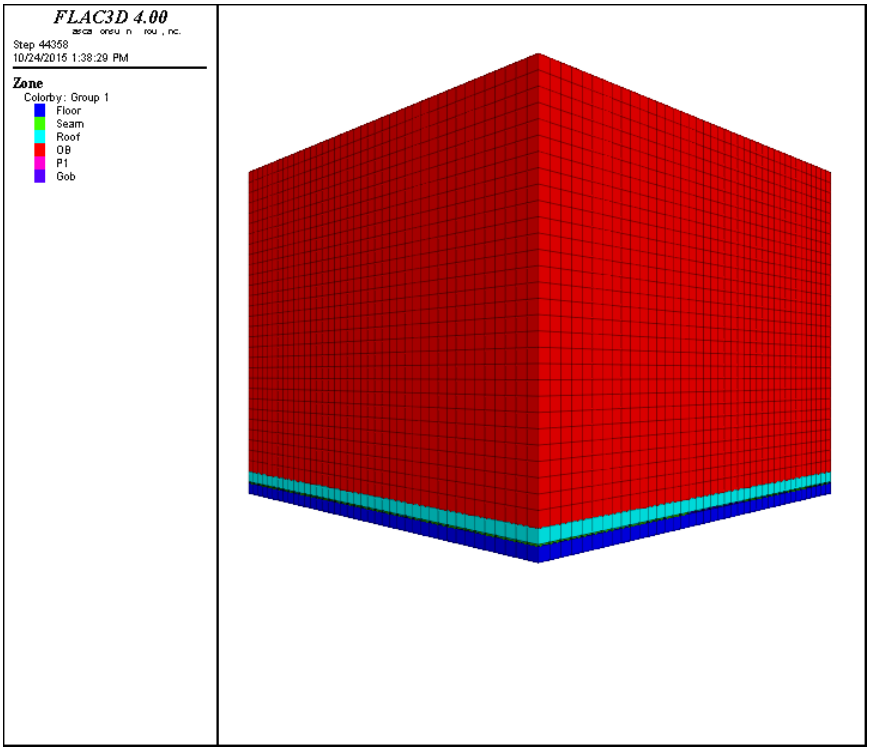

Figure 7-3 Finite difference model for Ground Response Curve at 1500' Cover

7.1 Gob Model

The behavior of gob is an extremely important aspect of evaluating the stress environment for both room and pillar and longwall mining, though it is often characterized as the most misunderstood of material models. Pappas and Mark (1993) investigated the behavior of longwall gob material through lab investigation of simulated gob, seeking to determine gob material stiffness properties. The result was non-linear stress-strain relationship following an exponential hardening curve, behavior which was dependent on both the stress level and rock characteristics. Esterhuizen et al. (2010a) followed these results and employed a hyperbolic equation to represent the gob stress-strain behavior as shown in Equation 7.1. This relationship states that the given stress

level for a simulated gob is a function of the accumulated strain and two constant parameters, both of which are a function of the rock properties, void ratio, gradation, etc.

Table 7-1 highlights the final gob properties which were selected to represent both weak and strong overburden. The double-yield constitutive model was employed within FLAC^{3D} to simulate the gob response for a simulated triaxial test, which also necessitated the input of cap pressure versus strain (Table 7-2). The calibrated gob response for both weak and strong overburden both had very good agreement with the target values as shown on Figure 7-4 as calculated using Equation 7.1.

$$\sigma = \frac{a\varepsilon}{b - \varepsilon} \qquad 7.1$$

Table 7-1 Selected gob properties following Esterhuizen et al. (2010a)

ρ	Density	80	Pcf
∅	Friction Angle	20	degrees
ν	Poisson's Ratio	0.05	
E	Elastic Modulus (Weak)	150,000	psi
a	a Parameter (Weak)	1,110	psi
b	b Parameter (Weak)	0.442	
E	Elastic Modulus (Strong)	450,000	psi
a	a Parameter (Strong)	1,890	psi
b	b Parameter (Strong)	0.427	

Table 7-2 Calibrated values of cap pressure versus strain for weak and strong overburden

Strain (%)	Cap Pressure (psi)	
	Weak Gob	Strong Gob
0	0	0
5	125	225
10	275	475
15	475	875
20	875	1,600
25	1,475	2,725
30	4,000	10,000
35	40,000	60,000
40	400,000	600,000

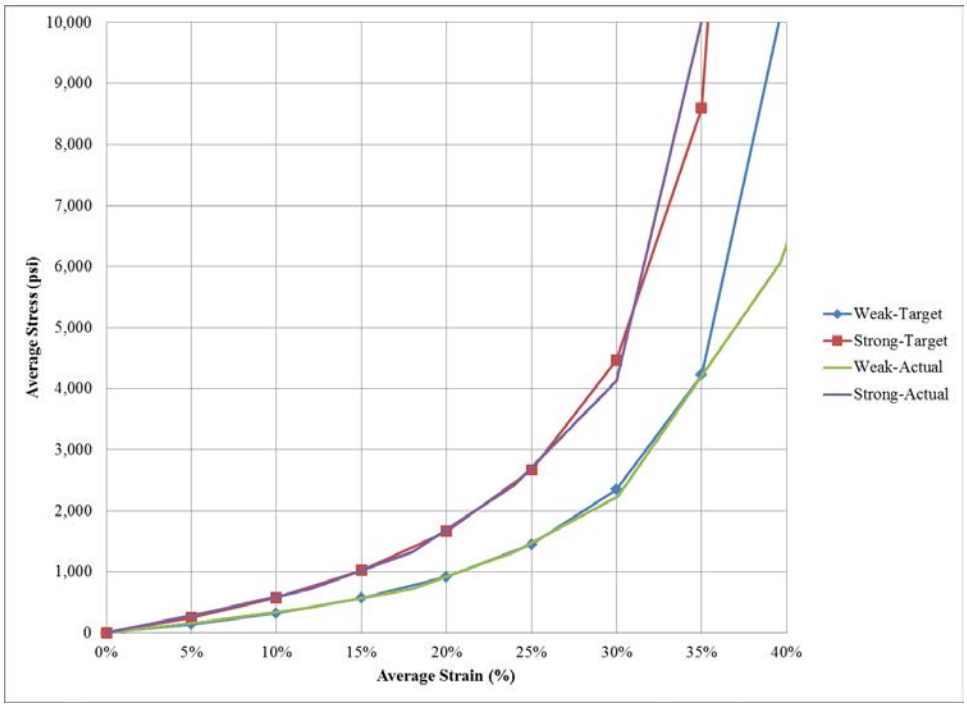

Figure 7-4 Results of gob calibration for both weak and strong overburden model

7.2 Overburden Depth vs Panel Width

First, a single coal panel was examined by looking at the influence of overburden depth and panel width on the Ground Response Curve. The depth of cover was selected to range from 1,000 feet to 2,000 feet, values regularly encountered in the bump prone regions of the Western United States and Central Appalachia, while the panel width was varied from 300 feet to 500 feet, again representative of commonly employed mining configurations for room and pillar mining. Figure 7-5 and Figure 7-6 illustrate the Ground Response Curve for development in both weak and strong overburden, respectively. It is obvious that depth of cover is very important, as it establishes the in-situ stress. However, the panel width and overburden characterization are also very important, as they control the slope and deviation of the ground response as the initial support pressure is reduced. It is apparent that panel width is an important factor in the ground response, particularly at increasing values of strain. However, the overburden material properties are ostensibly more important, and appear to control the overall slope of the Ground Response Curve. Strong overburden results in a steeper ground response, which is desirable from the standpoint of equilibrium with the local support system.

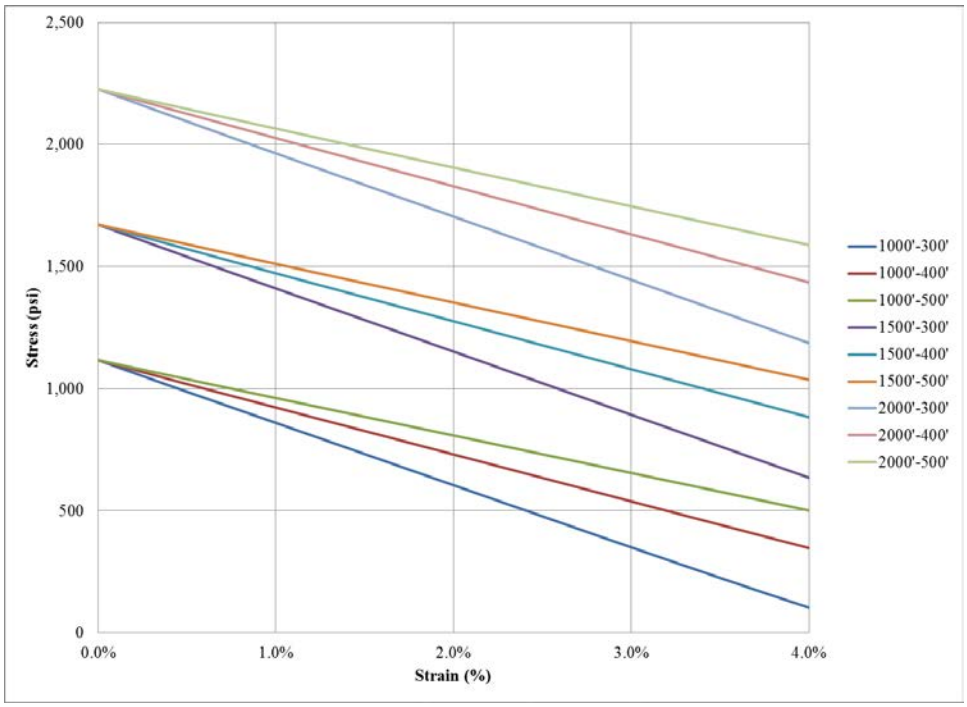

Figure 7-5 Single panel GRC results for development with weak overburden

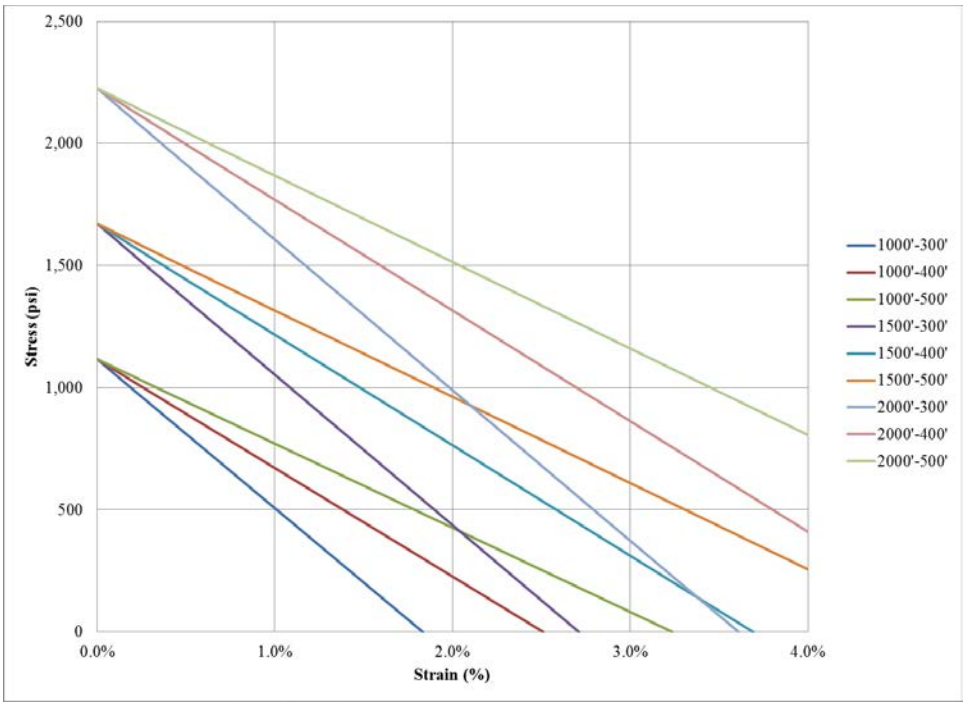

Figure 7-6 Single panel GRC results for development with strong overburden

The significance of both the overburden and panel width has also been previously identified as an importance influence on the ground response. Esterhuizen et al. (2010b) reported that the slope of the ground response curve determines the ultimate deformation of coal pillars, and if the response is stiff deformation will be reduced. The authors also noted the importance of panel span on the ground response, a finding consistent with Mark (2010) who incorporated a pressure arch factor into the ARMPS empirical software used for the analysis of pillar stability in room and pillar coal mines. The effect of overburden depth and panel width were also examined for retreat mining in both weak (Figure 7-7) and strong (Figure 7-8) overburden. The effect of retreat mining is apparent, as stress on the active mining zone is elevated due to the presence of a front gob. Generally, the slope of the ground response is even higher for retreat mining. Again, the stiffness of the overburden is obviously instrumental to the slope of the Ground Response Curve, while the panel width is of secondary importance. However, it would be prudent to consider the interdependence of the two factors. The panel width appears to be a more important factor with the presence of strong overburden, a fact which is most attributable to the arching which occurs under deep cover and narrow panel design.

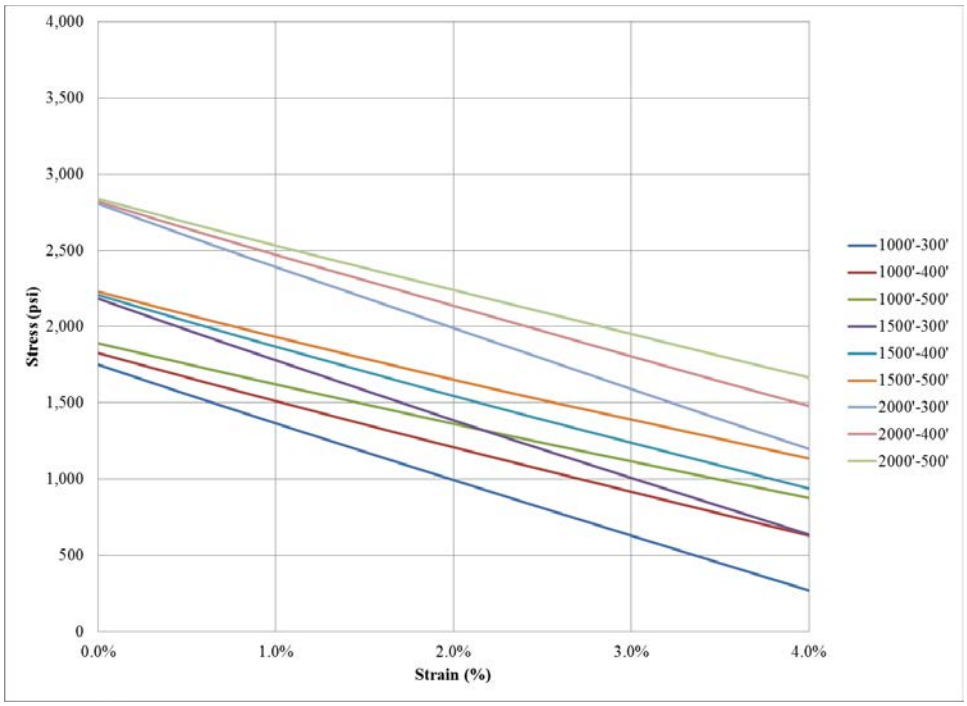

Figure 7-7 Single panel GRC results for retreat with weak overburden

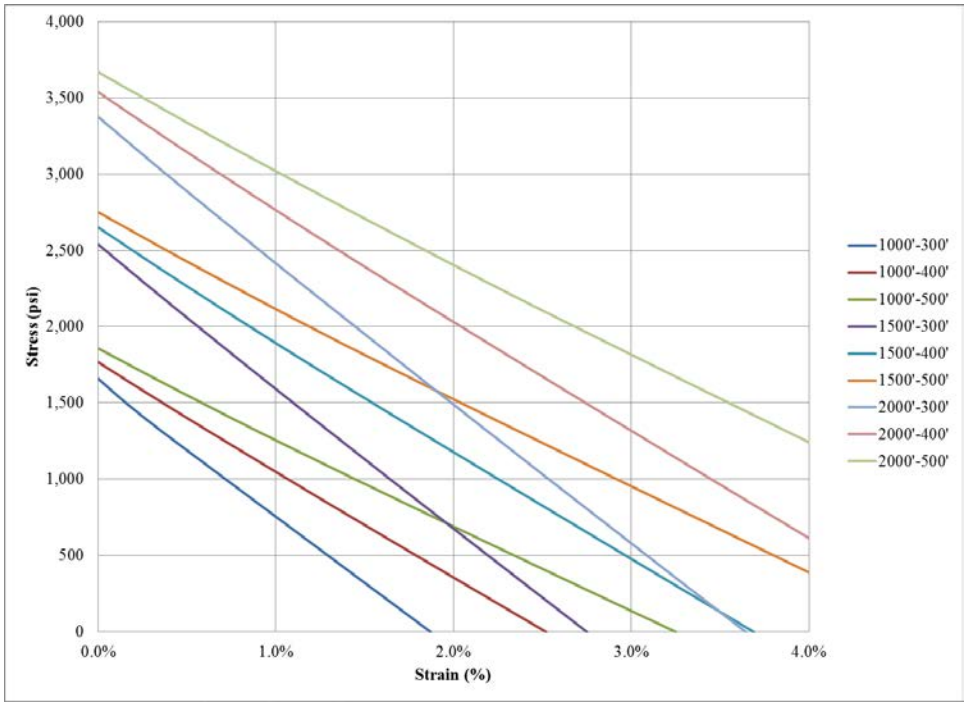

Figure 7-8 Single panel GRC results for retreat with strong overburden

7.3 Side Gob and Barrier Pillars

Next, the influence of side abutment loading from the presence of a retreated side panel was considered, with a barrier pillar width ranging from 100 feet to 200 feet. The panel width was maintained at a constant value of 400 feet. First, development of the active panel was considered for both weak (Figure 7-9) and strong (Figure 7-10) overburden. The initial stress level is now a function of both the depth of cover and loading condition, which becomes slightly elevated with the presence of a side gob, particularly as the cover increases. Similar results are obtained which demonstrate the importance of the overburden depth and stiffness. However, the barrier pillar width between the side gob and the active development panel is not nearly as important, where deviations between input width and the ground response is only slightly observed with the presence of strong overburden. As a result, the barrier pillar width, as long as a reasonable value is implemented in mine design, is considered of secondary importance for development. It is also observed that generally the slope of the Ground Response Curve is mildly shallower when compared to the single panel study, a result which would place the equilibrium deformation of the support response at a slightly higher value of strain.

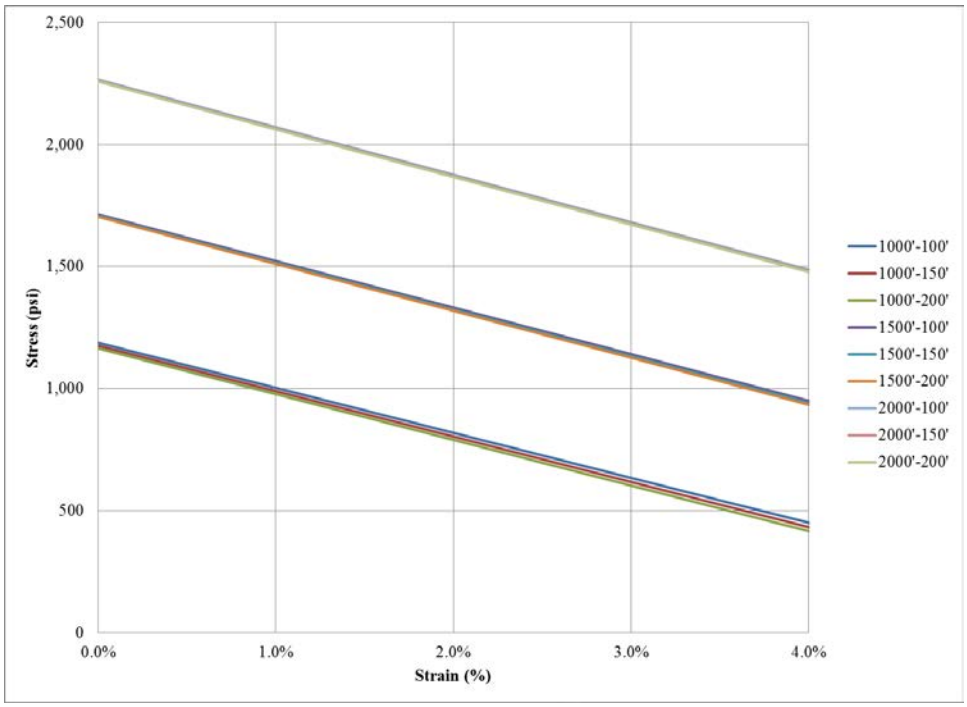

Figure 7-9 Side panel GRC results for development with weak overburden

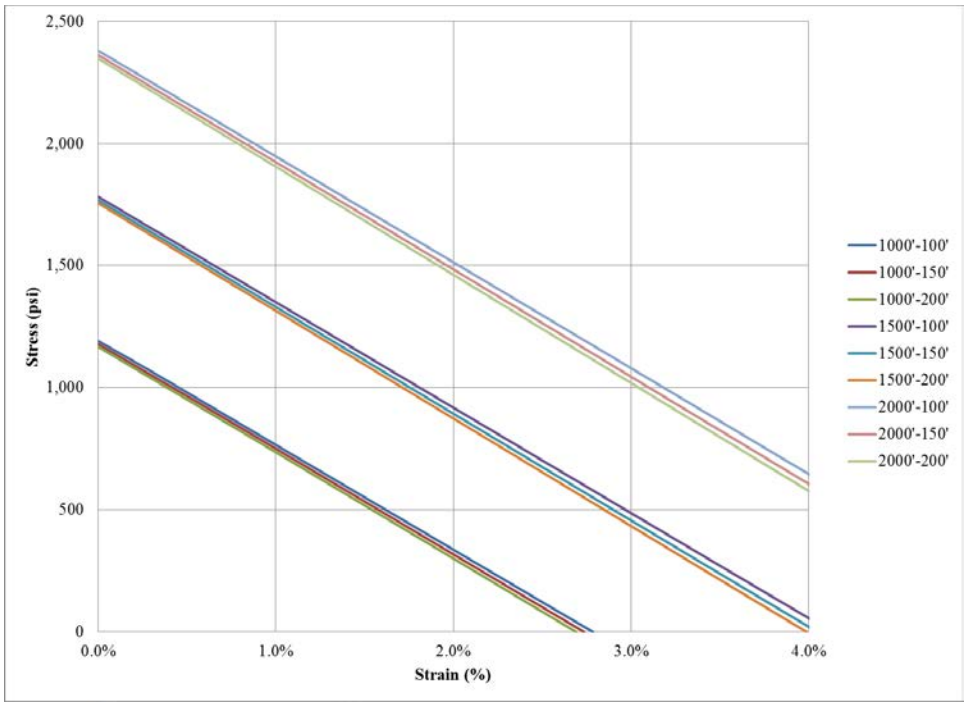

Figure 7-10 Side panel GRC results for development with strong overburden

The results of side abutment loading with retreat mining of the active panel are also presented for both weak (Figure 7-11) and strong (Figure 7-12) overburden. It is recognized that the importance of the barrier pillar is slightly more important to the resulting ground response when retreat mining is conducted, a finding which makes practical sense. Again, the influence of barrier pillar width is more apparent when the overburden is considered strong, though it remains of secondary importance. One particularly interesting finding is the elevation of the initial stress level when retreat mining is conducted in the presence of weak overburden, which is attributed to the higher stresses which cannot easily be transferred to the surrounding strata as a result of arching. It is also important to recognize the greater stresses which are obtained when retreat mining is undertaken in the presence of an existing side gob, even with adequate barrier pillar design. This result implies that the arching of stresses (Figure 7-13), particularly in deeper overburden and strong strata, may be negated by the bridging of side abutment loading to the active panel, regardless of barrier pillar stability. This finding is a contrast to the mechanics of empirical software such as ARMPS, which places a much more significant importance on barrier pillar design.

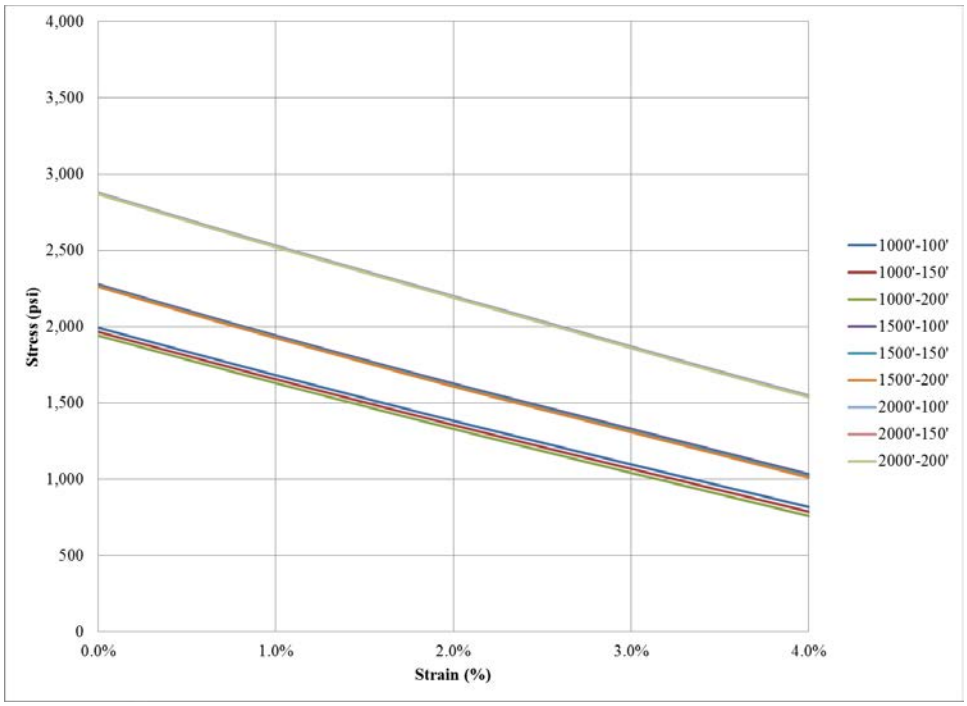

Figure 7-11 Side panel GRC results for retreat with weak overburden

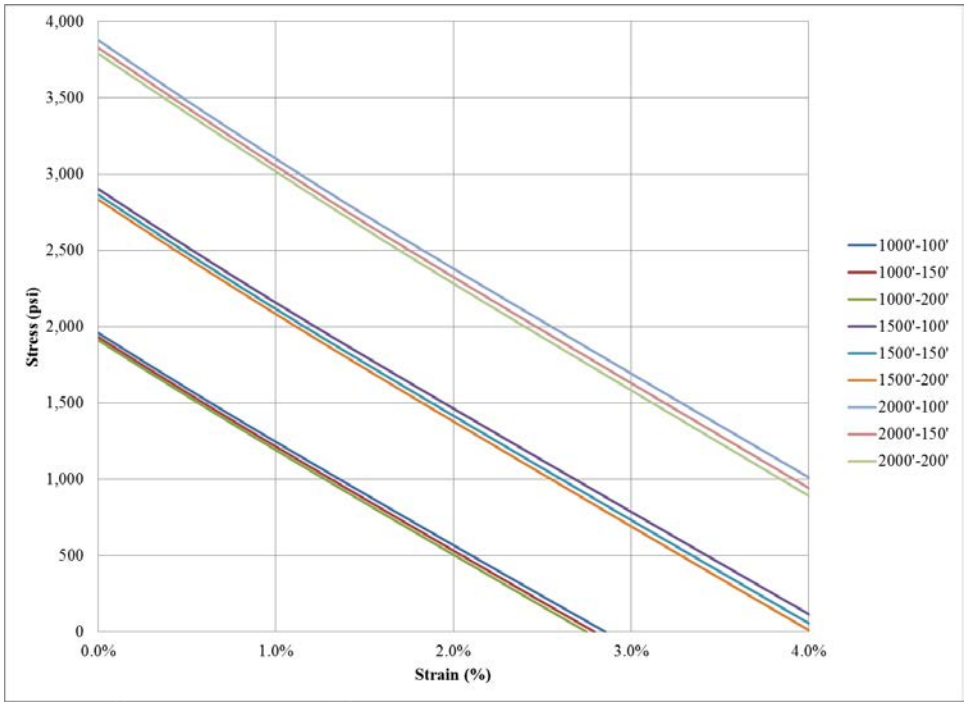

Figure 7-12 Side panel GRC results for retreat with strong overburden

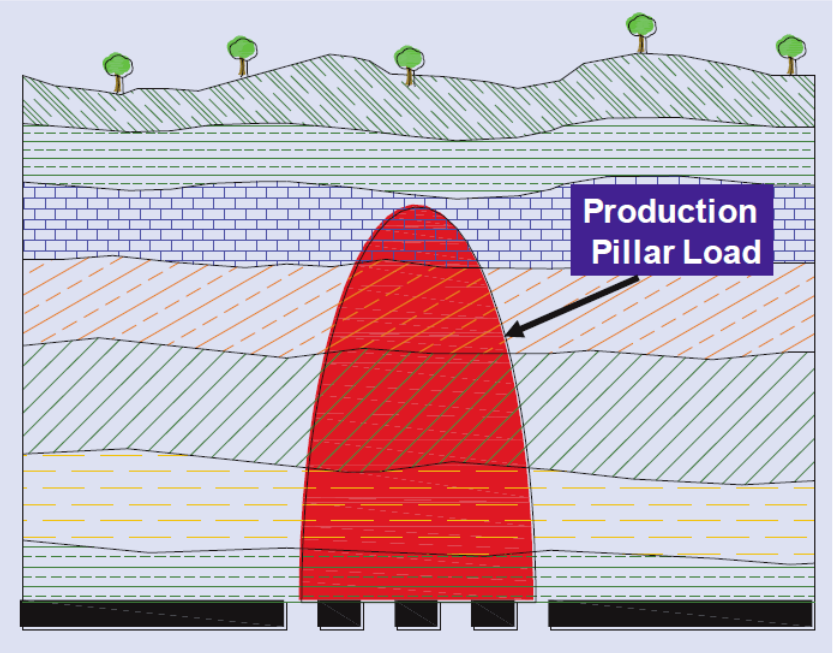

Figure 7-13 Example of pressure arch model (Mark, 2010)

7.4 Case Study

The union of the localized stress response, which is the coal pillar stress-strain relationship and the global stress influence, identified as the Ground Response Curve, ultimately determines the equilibrium of loading and deformation and is the strength of such a detailed analysis with regards to determining coal bump potential. A case study was conducted for the W/H=10 pillar in the presence of massive sandstone lithology and the SS-3 interface friction model (high differential in initial and residual interface friction). This pillar model was previously concluded to have a high bump potential due to sudden loss of strength and confinement as a result of interface stick-slip, and demonstrated the maximum peak in shear strain rate, a surge in kinetic energy release, and a generally unstable increase in joint friction work. The level of average pillar strain at which this unstable failure occurs, which is considered the maximum functional strength of the pillar model, is approximately 2.3 percent. This model was compared to the ground response of eight different mining configurations, including both development and retreat, and single panel and side abutment loading (Table 7-3). To mirror the lithology of the near-seam environment, the overburden was also assumed to be strong and the depth of cover was varied from 1,500 feet to 2,000 feet. For simplicity, the panel

width was assumed to remain constant at 400 feet (which would be the equivalent of a room and pillar system developing 6 to 7 entries) and when present, the barrier pillar width was maintained at a constant value of 150 feet.

Table 7-3 Case study input parameters

Model	Overburden	Method	Cover (ft)	Panel Width (ft)	BP Width (ft)
1	Strong	Dev	1,500	400	-
2	Strong	Ret	1,500	400	-
3	Strong	Dev	2,000	400	-
4	Strong	Ret	2,000	400	-
5	Strong	Dev	1,500	400	150
6	Strong	Ret	1,500	400	150
7	Strong	Dev	2,000	400	150
8	Strong	Ret	2,000	400	150

It is important to consider that the Ground Response Curve is an in-situ representation and the pillar stress-strain response mirrors the excavated state of the coal pillar geometry. Consequently, one or the other must be corrected. As a result, the Ground Response Curve for each proposed mining configuration was corrected to represent the "extracted loading state" as represented by the pillar stress-strain relationship. This was accomplished with Equation 7.2, whereby the given state of stress was corrected to an equivalent "extracted" value simply by the pillar extraction ratio following the work of Esterhuizen et al. (2010b).

$$\sigma_e = \frac{\sigma}{1 - e} \qquad 7.2$$

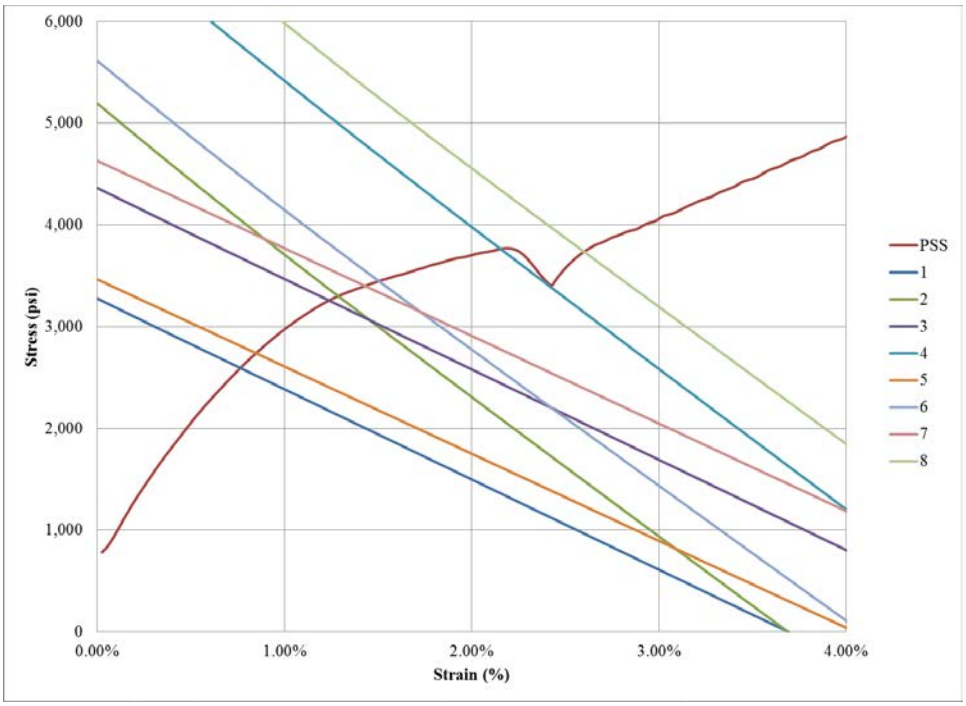

Figure 7-14 Resultant union of W/H=10 pillar response for various loading environments

Figure 7-14 illustrates the combination of the pillar stress-strain relationship and the Ground Response Curve for each of the evaluated mining configurations. Table 7-4 compares the approximate ARMPS SF with the NIOSH recommended SF and the resulting numerical interpretation. The threshold of previously identified strain is easily exceeded in one case and essentially met in another. A third loading environment is met at the onset of plastic deformation while the other five case studies are considered satisfactory. When compared to the ARMPS SF and NIOSH recommended value, these results show excellent agreement. For the W/H=10 pillar examined with massive sandstone in the roof/floor and the SS-3 interface frictional model, the deepest overburden considered with strong overburden properties results in moderate to high bump potential for retreat mining, even without the presence of a side gob. Pillar yielding is noted for the lower tier of overburden when retreat mining adjacent to a previously retreated side panel, while all other results are considered adequate. This type of analysis demonstrates strength of numerically considering the local geologic factors which influence support system response in conjunction with the expected loading environment as a result of the mining configuration and the global geologic properties.

Table 7-4 ARMPS SF compared to NIOSH recommendations and numerical results

Model	ARMPS SF	NIOSH Recommended SF	Numerical Interpretation
1	1.85	1.30	Satisfactory
2	1.31	1.30	Satisfactory
3	1.59	1.30	Satisfactory
4	1.17	1.30	Moderate Bump Potential
5	1.72	1.30	Satisfactory
6	1.24	1.30	Pillar Yielding
7	1.44	1.30	Satisfactory
8	1.08	1.30	High Bump Potential

7.5 Summary of Findings

The Ground Response Curve has been demonstrated to provide meaningful information about the ground response for a particular stress environment and mining configuration. This relationship has traditionally been used to examine local mine stiffness for comparison with the support system response towards the determination of stable versus unstable failure. However, this criterion has obviously been employed towards smaller pillars which typically demonstrate strain-softening behavior. The squat coal pillar designs which are commonly used today typically behave in a strain-hardening manner, particularly in the presence of strong strata which is typically present in the bump prone regions of the Western U.S. and Central Appalachia. It then becomes more pragmatic to consider the equilibrium of the ground response with the local support system to determine the extent and functionality of deformation. Finite difference modeling of numerous plausible stress and mining environments was conducted, particularly focusing on determining the importance of the following parameters to the global stress response:

- Depth of Cover
- Overburden Stiffness
- Mining Method
    - Development/Retreat

    - Side Gob(s)
- Panel Width
- Barrier Pillar Width

It is obvious that the overburden depth is essentially the most important parameter to the ground response. However, the response of the ground to the decreasing stiffness of the coal seam as the mining process occurs is primarily governed by the other factors which are most prominently examined by considering the slope of the Ground Response Curve. Figure 7-15 and Figure 7-16 illustrate the vertical stress present for a single panel loading configuration with two very different panel widths. The larger panel width certainly results in higher overall stresses on the panel as the ability for the strata to bridge loading was decreased. The relationship between depth of cover and panel span has previously been mentioned as an important factor influencing the slope and behavior of the ground response. While mining method and configuration has an obvious implication to the initial stress, the overburden stiffness has a profound impact on the slope of the ground response. With the presence of a stronger, rigid overburden, the ground response becomes steeper due to the increased ability for pressure arching to occur. Figure 7-17 and Figure 7-18 demonstrate this very fact as the vertical stress is increasingly shed to the surrounding strata and barrier pillar in the presence of a strong overburden model. The influence of barrier pillar stability was considered to have secondary importance.

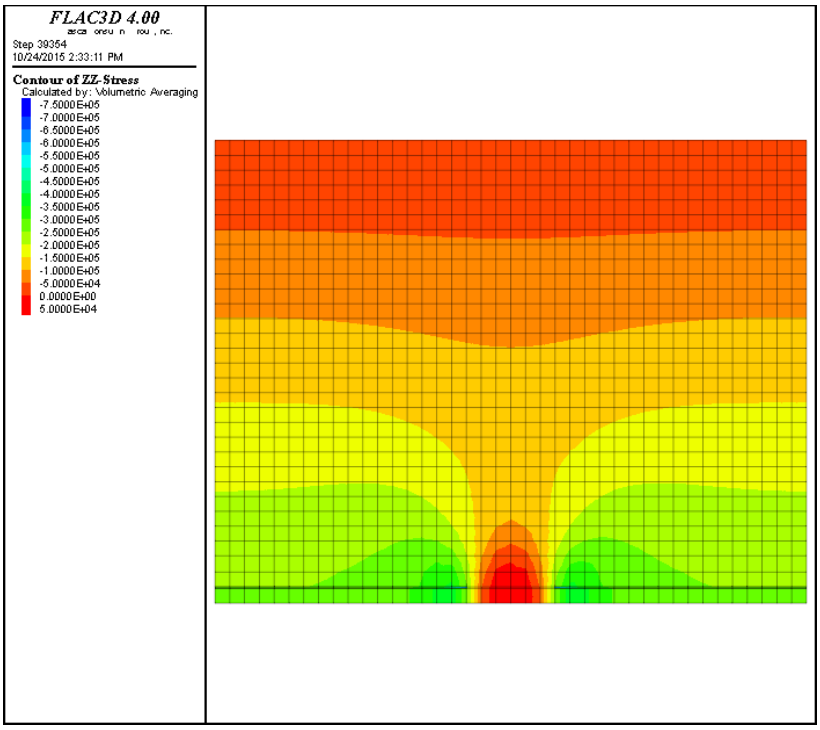

Figure 7-15 Retreated single panel vertical stress at 300' panel width and 1500' cover

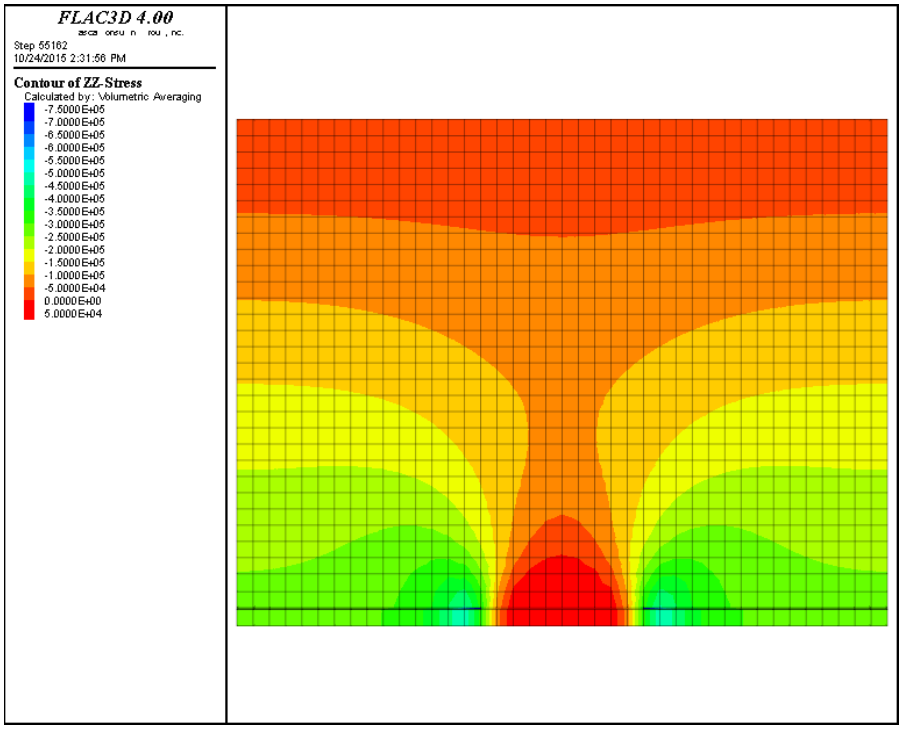

Figure 7-16 Retreated single panel vertical stress at 500' panel width and 1500' cover

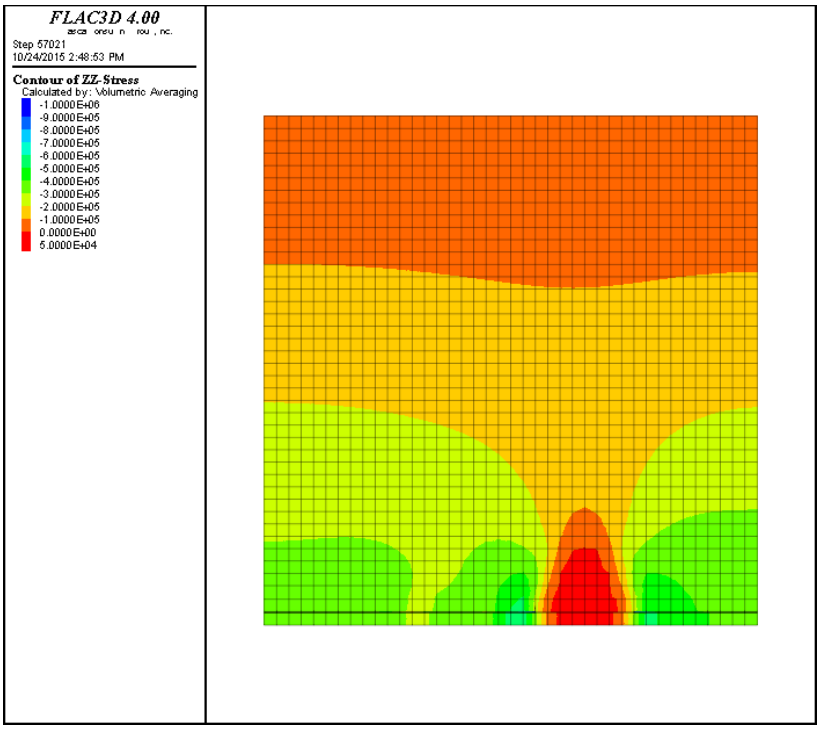

Figure 7-17 Weak side panel vertical stress with 150' barrier pillar and 2000' cover

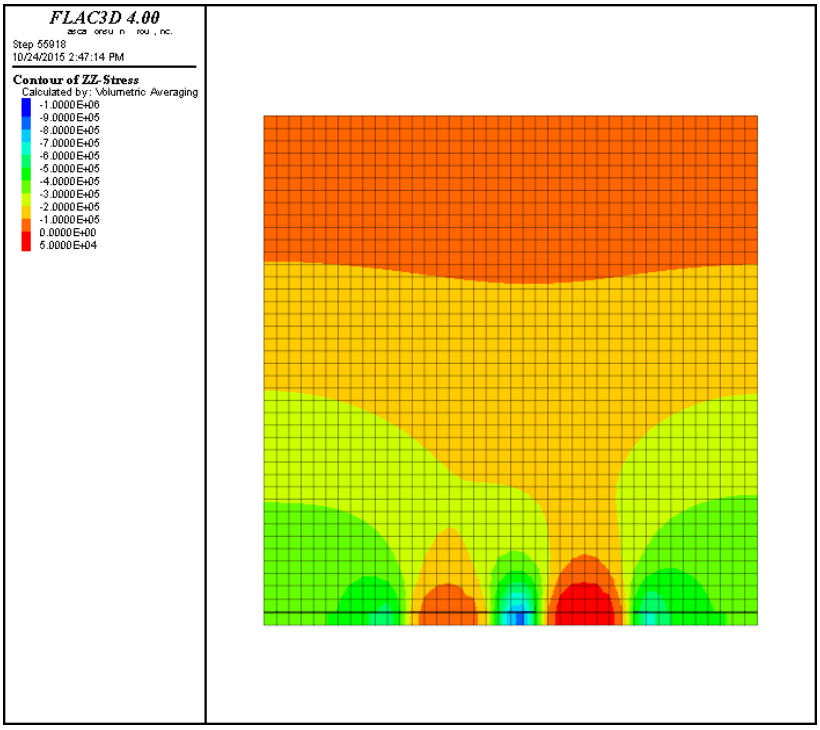

Figure 7-18 Strong side panel vertical stress with 150' barrier pillar and 2000' cover

8 Summary and Future Work

While squat coal pillars are often employed in modern mine design, particularly in the regions where high bump potential is often recognized, the behavior of said pillars have not historically been well-researched. It has traditionally been accepted that squat coal pillars demonstrate principally strain-hardening behavior, thereby making it difficult for mining engineers to clearly identify pillar strength and/or a satisfactory level of strain. The strength of smaller coal pillars has been widely researched and is most closely dependent on pillar geometry, however the strength and behavior of squat coal pillars has been shown to depend on a multiple of geologic and factors at both the local and global scale. A comprehensive numerical study, which included discrete element modeling of local geologic parameters, was combined with finite difference modeling of global factors in an effort to determine and correlate the impact that varying geologic and geometric properties has on squat coal pillar behavior and bump potential. The research objectives of this numerical investigation were previously stated as follows:

- Enhance understanding of pillar loading and behavior for deep cover coal mining, focusing on the mechanics of squat coal pillars and the effects of localized geologic influences with respect to bump potential
- Increase knowledge of the global stress environment for deep cover coal mining with focus on the impact that varying mining, geologic, and geometric considerations have on local stiffness and the resulting ground response
- Focus on the union of knowledge concerning localized factors impacting squat coal pillar behavior and the influence of global contributing factors in order to improve the determination of criteria for high bump potential or “red zones”

It was therefore necessary to incorporate the knowledge learned from practical indicators which were employed within the numerical modeling methods in order to identify and understand unstable failure of coal pillars. All of the numerical indicators which were used have been previously demonstrated to be both employable and reliable when used to determine unstable pillar failure for explicit quasi-static numerical analyses. Consequently, these indicators are based on the theory that failure begins at a singular point and a resultant velocity and acceleration occur, followed by the propagation of an

unstable state of equilibrium. As a result, these numerical identifiers are predicated on the most basic mathematical and engineering physics commonly employed in analytical engineering analysis, including such concepts as the conservation of mass, momentum, and energy. Since coal bursts have historically been aligned with one of two classifications (unstable shear sliding or strain failure), the following six numerical identifiers were successfully employed to investigate squat coal pillar behavior and coal bump potential:

- Pillar Stress-Strain
- Pillar Confinement
- Peak Shear Strain Rate
- Total Energy Release
- Kinetic Energy
- Joint Friction Work

Chapter 5 and Chapter 6 focused on the use of discrete element modeling of single, quarter pillar models to examine the influence that localized geologic influences has on squat coal pillars and burst potential. And while only the pillar interface in roof and floor was explicitly identified as a discontinuity in the model domain, the three-dimensional discrete element software 3DEC was selected because of the existing energy calculations which are quantified during calculations. The results of these two chapters are summarized as follows:

8.1 Influence of Coal Pillar Interface

- The frictional properties of coal pillar interface, which includes the geological pillar contact at the roof and floor, is an extremely important influence on squat coal pillar behavior and bump potential. While the results of most studies indicated the significance of the interface initial and residual friction values, the most important predictor of unstable coal pillar failure was the differential between the initial and residual friction angle. Consequently, relatively high values of this differential were necessary for unstable interface stick-slip failure, which can result in the sudden loss of pillar strength due to a loss of confining

stress. This type of failure would obviously be followed by an abrupt propagation of shear strain and an associated peak in kinetic energy release.

- The level of average pillar strain for which unstable failure was identified decreased as the pillar geometry was increased, independent of the roof and floor lithological properties. However, the magnitude of this instability, which would be noted by the loss of confinement and maximums in peak shear strain rate, kinetic energy release, and joint friction work, did not demonstrate a reliable relationship with the pillar geometry. This conclusion suggests that for a specific set of interface frictional properties, there could potentially exist a pillar geometry which is more conducive to coal bumps, and may help explain the intermittent and rarity of such events.
- When considering a more realistic, plasticity based constitutive model in lieu of assuming an elastic only overburden model, unstable failure due to interface failure only occurred when the stronger, more rigid sandstone lithology was modeled. This provides evidence that a controlled failure and/or slip along prominent discontinuities (e.g. bedding planes) in the immediate roof/floor may actually promote a more stable failure in the form of yielding due to higher energy dissipation in the roof and/or floor strata.
- Both a massive shale and sandstone overburden model were considered with various interface frictional models, however it was clear that the differences in the behavior and resulting analysis of bump potential for both types of lithology were not only based on interface friction but the actual strength and stiffness of the strata. This result pointed towards the need to investigate the relationship between coal bump potential and the stiffness of the surrounding roof/floor strata, which was undertaken in Chapter 6. However it was noted that while the elastic overburden model typically resulted in the same general trends as the massive sandstone model, the values of kinetic energy release and the magnitude of increase in joint friction work were typically higher. This finding was credited to the fact that energy is dissipated in the form of plastic work for both matrix and discontinuities when using the ubiquitous joint model plasticity constitutive model.

8.2 Impact of Coal Lithology

- As predicted, the composition of the roof and floor strata had a significant influence on coal pillar bump potential. While the coal pillar interface frictional properties cannot be completely isolated from a practical standpoint, it was determined that the strength and stiffness of the lithological environment is extremely important. While a clear variance was established between the interface frictional properties between shale and sandstone pillar contact, the principal goal of investigating the importance of near-seam strata on coal bump potential was recognized. Consequently, the relative stiffness of the surrounding strata, the resulting changes in stress distribution throughout the pillar, and the changes to deformation resulting from the differences in strength of ubiquitous joints were unquestionably the primary factors influencing these findings.
- The probability for unstable pillar failure to occur was especially ascribed to the presence of thick, rigid strata in close proximity to the coal seam. Conversely, when the roof and/or floor was principally consistent with the properties of a weaker, less consistent strata such as shale, the numerical evidence of high bump potential was significantly diminished. It was concluded that the presence of strong, massive strata in contact or near the coal seam significantly increases coal bump potential. This is attributed to greater strength due to greater confining stress and elevated levels of excess energy which are achieved as well as an increased propensity for interface stick-slip to occur with accompanying dynamic shear failure propagation. The delineation between the intact and stronger elastic core and the yielding zone surrounding the pillar, which was initially observed, was clearly observed when unstable pillar failure was noted. However, when stable pillar yielding was noted, which occurred in the presence of thinner sandstone thickness at greater distance from the coal seam, the smaller elastic core remained intact though the outer pillar elements had functionally yielded.
- It was undetermined which, the roof or floor, was more important to coal bump potential classification. While the presence of strong or rigid roof seemed to be more closely aligned with pillar failure at the lower ranges of pillar strain, the

properties of the floor appeared to be of equal importance when considering the entirety of pillar designs modeled.

- Similar to the results in Chapter 5, the average pillar strain for which unstable failure was recognized decreased as the pillar geometry was increased. However, the magnitude of unstable failure, evidenced by the largest instabilities of peak shear strain rate, total energy release, kinetic energy, and joint friction work, appeared to be directly proportional with the pillar geometry. This result is actually in contrast to the conclusions from the previous chapter of coal pillar interface. Consequently, it may be concluded that the presence of a relatively unstable interface friction set could fundamentally alter the probability of coal bumps and result in unstable failures which occur as smaller pillar sizes.

8.3 Global Factors and the Ground Response Curve

Chapter 7 focused on the use of finite difference using the FLAC^{3D} software to investigate the ground response of numerous stress and mining configurations which are typically encountered in the bump-prone regions of the United States. The Ground Response Curve provided important information regarding the ensuing ground response as a result of the mining process applied to various loading and geometric configurations. The Ground Response Curve had historically been employed in efforts to determine local mine stiffness and stability analysis with a particular pillar support system; however this effort has primarily been implemented for smaller pillar sizes which typically exhibit strain-softening behavior. The concept of the Ground Response Curve has consequently been applied towards understanding of squat coal pillar behavior and the resulting determination of coal bump potential. Since squat coal pillars are becomingly increasingly common in modern coal operations, and particularly in the deeper or complex multiple seam reserve of the Western United States or Central Appalachia, it is more important than ever to understand the implications of ground response in these environments.

The squat coal pillar designs which are commonly used today typically exhibit strain-hardening behavior, making it difficult to apply the traditional local mine stiffness criterion to stability analysis. It has therefore been demonstrated that it is more prudent

to consider the union of local support response and the global stress environment through an understanding of the equilibrium of the ground response and the pillar response to identify the magnitude and practicality of the resulting deformation. Particularly, the study examined the importance of depth of cover, overburden stiffness, mining method, mining configuration, panel width, and barrier pillar width, on the resulting stress response. The results of this chapter are summarized as follows:

- It was concluded that overburden depth was the single most important parameter which influences the Ground Response Curve, simply by establishing the baseline overburden stress which must be handled and/or redistributed by the overburden and support system. However, the importance of the slope of the Ground Response Curve is equally as essential to understanding the entire ground reaction, as the slope of the Ground Response Curve governs the resultant response as the mining process is assumed.
- While greater values of panel width most assuredly result in larger overall panel stresses, the ability of the ground to redistribute load to surrounding areas and form a pressure arch is principally governed by the overburden stiffness. The presence of stronger, more rigid overburden results in a steeper Ground Response Curve due to an increased propensity for pressure arching to occur. The relationship between the depth of cover and panel span has been widely considered to be an extremely importance factor which influences the slope of the Ground Response Curve in existing literature.
- The mining method and configuration, including the practice of retreat mining, also has a profound impact on the ground response. This includes elevated initial stresses which must be accounted for within the active mining zone. However, contrary to initial thinking the influence of the barrier pillar width and stability was considered to be of secondary importance.
- A case study was conducted which combined the union of the local support system with the global ground response, demonstrating the strength of this new approach to quickly consider multiple loading environments towards the prediction of squat pillar stability and bump potential. The results of this case

study were compared with the ARMPS empirical software and the accompanying NIOSH recommended threshold for stability. Excellent agreement was met.

8.4 Bump Red Zone Guidelines

Table 8-1 Proposed bump red zone guidelines for room and pillar coal mining

Type	Factor	Risk Level		
		Low	Moderate	High
Local Influences	Interface Frictional Properties			
	Interval to Sandstone (Roof)			
	Sandstone Thickness (Roof)			
	Interval to Sandstone (Floor)			
	Sandstone Thickness (Floor)			
Ground Response	Depth of Cover			
	Overburden Stiffness			
	Retreat Mining			
	Side Gob(s)			
	Panel Width			
	Barrier Pillar Width			
Analysis	Pillar Stability			
	Multiple Seam Influence			

Bump red zones have been in use within the mining industry for some time, particularly in the regions which have deeper and/or multiple seam reserves which are difficult and often bump-prone. These types of analysis provide simple yet necessary awareness of an elevated bump potential based any number of factors. The Office of Mine Safety and Health Research (2010) advocated for research to improve understanding of coal bump potential which incorporates enhanced understanding of squat coal pillar behavior, pillar loading in deep overburden, pressure arch theory, and the importance of roof/floor properties, all which is aimed at the development of improved bump risk guidelines. Table 8-1 is an example of the proposed revision to bump red zone guidelines for room

and pillar coal mining based on the perceived order of importance, though a similar expression could easily be applied towards longwall coal mining. This proposal combines the outcomes of investigating the local influences, including coal interface properties and roof/floor lithology, with the factors which influence the resulting ground response, including depth of cover, overburden stiffness, mining method, and panel width. The resulting union provides an analysis of pillar stability, the resulting ground condition, and ultimately a snapshot of coal bump potential. Though it wasn't explicitly considered in this study, the consideration of multiple seam influences is an obviously important aspect to bump potential where applicable for a multitude of reasons.

An example of this type of bump risk analysis can be seen in the work of Harris and Perry (2015). The authors examined both local and global influences which contributed to high burst potential for a bump-prone reserve. Particularly, when examining the occurrence of seventeen case studies from the reserve the authors demonstrated the importance of depth of cover, roof and floor sandstone thickness, and the proximity/interval from the coal seam to the sandstone in both the roof and floor, resulting in a proposed bump risk factor assessment as shown in Table 8-2:

Table 8-2 Example of bump risk factors as concluded by Harris and Perry (2015)

Factor	Level		
	Low	Medium	High
Depth of Cover	<1,100 ft	1,100 ft - 1,500 ft	>1,500 ft
Interval to SS (Roof)	> 10 ft	1 ft - 10 ft	<1 ft
SS Thickness (Roof)	<20 ft	20 ft - 80 ft	>80 ft
Interval to Harlan SS (Floor)	> 10 ft	5 ft - 10 ft	<5 ft

While these conclusions are based on the investigation of a specific bump-prone reserve, the methodology mirrors that which is recommended by this research effort and combines the effect of examining both local and global geologic and geometric parameters. While it is certain that this result cannot be universally applied, the method elevates the importance of examining bump potential and may provide a starting point for initial studies. The resulting bump potential map produced by the authors as illustrated on Figure 8-1 was intended as a convenient tool for the operation to successfully identify

areas of high bump potential. It is obvious that the product very successfully identified in retrospect those areas which had elevated bump potential, though it must be noted that coal bumps are events which cannot be predicted.

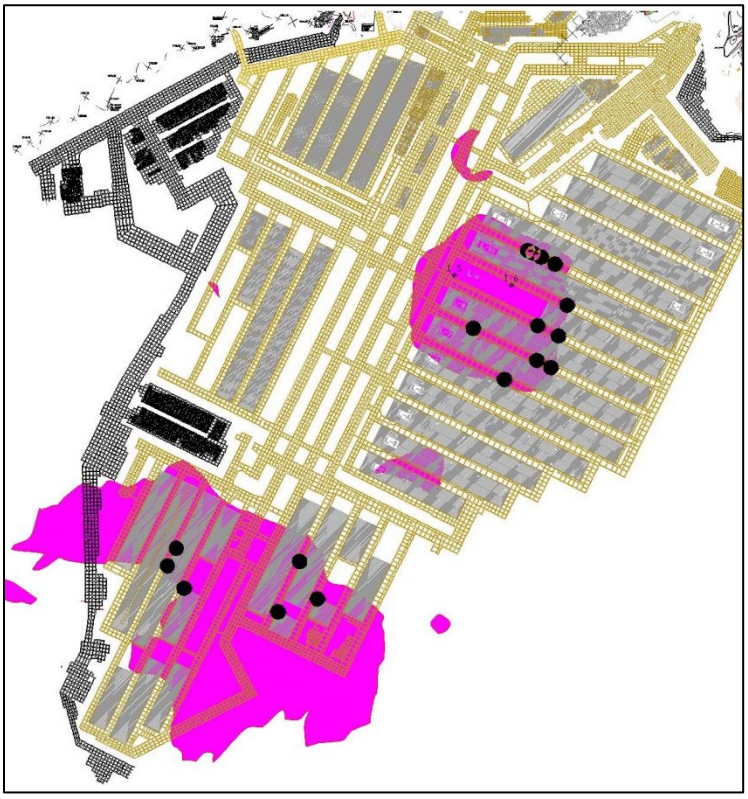

Figure 8-1 Elevated bump potential map with bump locations (Harris and Perry, 2015)

8.5 Future Work

Many improvements towards the understanding of squat coal pillar behavior and coal bump potential could be made by examining the following topics:

- A more comprehensive investigation of the coal pillar interface model with particular focus on the propensity for stick-slip instability to occur and the associated physical parameters which influence this probability
- Research into the determination of a systematic and consistent methodology to deduce and scale the material properties of coal pillar interface and other important discontinuities for use in numerical modeling techniques
- Further examine the behavior of squat coal pillars over a broader range of lithology and geometry

- An analysis regarding the impact of rate dependency on coal pillar interface behavior and the use of alternative joint constitutive models
- The applicability and derivation of a strain rate constitutive relationship for coal and surrounding strata
- Assess the influence and weight of local geologic properties against the global geologic environment when determining the ground response
- Investigation of the impact of multiple seam mining on the resultant ground response, with particular focus on the stress-path dependency and the influence of multiple seam remnant structures on deviations from the traditional pressure arch model

References

1. Agapito, J.F.T., and Goodrich, R.R., 2000, "Five stress factors conducive to bumps in Utah, USA, coal mines," *In Proceedings of the 19th International Conference on Ground Control in Mining*, August, 2000, Morgantown, WV, pp. 93-100.
2. Ai, H.A., and Ahrens, T.J., 2006, "Simulation of Dynamic Response of Granite: A Numerical Approach of Shock-Induced Damage beneath Impact Craters," *In International Journal of Impact Engineering, Volume 33*(1-12), December, 2006, pp. 1-10.
3. Arch Coal, Inc., 2009, *Annual Report*, Retrieved from http://www.sec.gov/Archives/edgar/data/1037676/000095015209001922/c48697e10vk.htm
4. Barczak, T., 2011, "Think Like a Rock," *In Proceedings of the 30th International Conference on Ground Control in Mining*, July 26-28, 2011, Morgantown, WV, 11 pp.
5. Barton, N., 1973, "Review of a new shear strength criterion for rock joints," *In Engineering geology*, Volume 7, 1973, pp. 287-332.
6. Bieniawski, Z.T., 1996, "Section 10 Geomechanics," *In SME Mining Engineering Handbook*, 2nd Edition, Volume 1, December, 1996, Ann Harbor, MI, 182 pp.
7. Dolinar, D., Barczak, T., and Gurley, H., 2009, "Evaluation of Tailgate Ground and Support Interaction in the Illinois Basin for the Development of a Ground Reaction Curve Based Standing Support Design," *In Proceedings of the 28th International Conference on Ground Control in Mining*, July 28-30, 2009, Morgantown, WV, 8 pp.
8. Esterhuizen, G.S., and Mark, C., 2009, "Three-Dimensional Modeling of Large Arrays of Pillars for Coal Mine Design," *In Proceedings of the International Workshop on Numerical Modeling for Underground Mine Excavation Design*, NIOSH, Information Circular, IC 9512, June, 2009, pp. 37-46.
9. Esterhuizen, E., Mark, C., and Murphy, M.M., 2010a, "Numerical Model Calibration for Simulating Coal Pillars, Gob and Overburden Response," *In Proceedings of the 29th International Conference on Ground Control in Mining*, July 27-29, 2010, Morgantown, WV, 12 pp.
10. Esterhuizen, E., Mark, C., and Murphy, M.M., 2010b, "The Ground Response Curve, Pillar Loading and Pillar Failure in Coal Mine," *In Proceedings of the 29th International Conference on Ground Control in Mining*, July 27-29, 2010, Morgantown, WV, 10 pp.
11. Esterhuizen, E., Mark, C., and Murphy, M.M., 2010c, "The Ground Response Curve and Its Impact on Pillar Loading in Coal Mines," *In Proceedings of the 3rd International Workshop on Coal Pillar Mechanics and Design*, July 26, 2010, Morgantown, WV, pp. 123-131.
12. Gaddy, F.L., 1956, "A Study of the Ultimate Strength of Coal as Related to Absolute Size of the Cubical Specimens Tested," *In Virginia Polytechnic Institute Bulletin*, Series No. 112, pp. 1-27.
13. Garvey, R. J., 2013, "A Study of Unstable Rock Failures using Finite Difference and Discrete Element Methods," Ph.D. Thesis, Colorado School of Mines, Golden, CO, 250 pp.

14. Gu, R., 2013, "Distinct Element Model Analyses of Unstable Failures in Underground Coal Mines," Ph.D. Thesis, Colorado School of Mines, Golden, CO, 394 pp.
15. Hakala, M., "Computer Codes in Rock Mechanics," Gridpoint Finland Oy and Juha Antikaimen, 18 pp.
16. Hammah, R.E., and Curran, J.H., 2009, "It is better to be approximately right than precisely wrong: Why simple models work in mining geomechanics," *In 43rd US Rock Mechanics Symposium and 4th U.S.-Canada Rock Mechanics Symposium*, July 28 – July 1, 2009, Asheville, NC, pp. 55-61.
17. Hamza, O., Stace, R., and Reddish, D., 2005, "A study on the effect of strain rate on stiffness and strength in silty mudstone using multistage triaxial testing," *In Post-Mining 2005*, November 16-17, 2005, Nancy, France, 12 pp.
18. Harris, K.W., and Perry, K.A., 2014, "Evaluating bump prone ground with LaModel through a site-specific calibration," *2014 Transactions of the Society for Mining, Metallurgy, & Exploration*, Society for Mining, Metallurgy, & Exploration, Englewood, CO, pp. 441-448.
19. Harris, K.W., and Perry, K.A., 2015, "Combining Qualitative and Numerical Techniques to Improve Bump Potential Recognition," *Accepted for Publication to Mining Engineering*, Society for Mining, Metallurgy, & Exploration, Englewood, CO.
20. Heasley, K., 2009, "An Overview of Calibrating and Using the LaModel Program for Coal Mine Design," *In Proceedings of the International Workshop on Numerical Modeling for Underground Mine Excavation Design*, NIOSH, Information Circular, IC 9512, 2009, pp. 63-74.
21. Heasley, K.A., 2008, "Appendix S: Back Analysis of the Crandall Canyon Mine Using the LaModel Program," *In Report of Investigation, Fatal Underground Coal Burst Accidents, August 6 and 16, 2007, Crandall Canyon Mine, Genwal Resources Inc*, USDOL, Mine Safety and Health Administration, 2008, 46 pp.
22. Heasley, K.A., and Chekan, G.J., 1999, "Practical Boundary-Element Modeling for Mine Planning," *In Proceedings of the Second International Workshop on Coal Pillar Mechanics and Design*, NIOSH Information Circular, IC 9448, June, 1999, Pittsburgh, PA, pp. 73-87.
23. Hoek, E., Carranza-Torres, C., and Corkum, B., 2002, "Hoek-Brown Failure Criterion – 2002 Edition," *In Proceedings of the North American Rock Mechanics Society*, July, 2002, Toronto, Canada, 7 pp.
24. Hoelle, J., 2008, "Coal Bumps in an Eastern Kentucky Coal Mine 1989 to 1997," *In Proceedings of the 27th International Conference on Ground Control in Mining*, July 29-31, 2008, Morgantown, WV, pp. 14-19.
25. Iannachione, A.T., 1990, "The effects of roof and floor interface slip on coal pillar behavior," *In Rock Mechanics: Contributions and Challenges: Proceedings of the 31st U.S. Symposium*, June 18-20, 1990, Colorado School of Mines, Golden, CO, pp. 153-160.
26. Iannacchione, A., and Tadolini, S., 2008, "Coal Mine Burst Prevention Controls," *In Proceedings of the 27th International Conference on Ground Control in Mining*, July 29-31, 2008, Morgantown, WV, pp. 20-28.

27. Iannacchione, A.T., and Zelanko, J.C., 1995a, "Occurrence and Remediation of Coal Mine Bumps: A Historical Review," *In Proceedings: Mechanics and Mitigation of Violent Failure in Coal and Hard-Rock Mines,* USBM, Special Publication, SP 01-95, 1995, pp. 27-68.
28. Iannacchione, A.T., and Zelanko, J.C., 1995b, "Pillar Mechanics of Coal Mine Bursts: A Control Strategy," *In Proceedings of 16th World Mining Congress*, September 12-16, 1994, Sofia, Bulgaria, 9 pp.
29. Indraratna, B., and Haque, A., 2000, *Shear Behaviour of Rock Joints*, A.A. Balkema Publishers, Rotterdam, Netherlands, 164pp.
30. Itasca Consulting Group, Inc., 2009, "Theory and Background," *In FLAC3D Fast Lagrangian Analysis of Continua in 3 Dimensions*, FLAC3D Version 4.0, 2009.
31. Itasca Consulting Group, Inc., 2013a, "Constitutive Models," *In 3DEC 3 Dimensional Distinct Element Code*, 3DEC Version 5.0, 2013.
32. Itasca Consulting Group, Inc., 2013b, "Theory and Background," *In 3DEC 3 Dimensional Distinct Element Code*, 3DEC Version 5.0, 2013.
33. Itasca Consulting Group, Inc., 2013c, "User's Guide," *In 3DEC 3 Dimensional Distinct Element Code*, 3DEC Version 5.0, 2013.
34. Itasca Consulting Group, Inc., 2015, "Energy Calculations," *In UDEC Universal Distinct Element Code*, UDEC Version 6.0, 2015.
35. Jeremic, M.L., 1985, *Strata Mechanics in Coal Mining*, 1st Edition, Laurentian University, Sudbury, Ontario, Canada, 566 pp.
36. Jing, L., and Stephansson, O., 2007, *Fundamentals of Discrete Element Methods for Rock Engineering: Theory and Applications*, 1st Edition, Elsevier, Amsterdam, the Netherlands, 545 pp.
37. Kias, E.M.C., 2013, "Investigation of unstable failure in underground coal mining using the discrete element method," Ph.D. Thesis, Colorado School of Mines, Golden, CO, 250 pp.
38. Kimberley, J., and Ramesh, K.T., 2011, "The Dynamic Strength of an Ordinary Chondrite," *In Meteoritics & Planetary Science, Volume 46*(1), November, 2011, pp. 1653-1699.
39. Lavoie, T., 2011, "An Analytical Geomechanical Upscaling Approach for Modeling Jointed Rock Bass Behavior Using Ubiquitous Joints," *Master's Thesis,* The University of British Columbia, January, 2011, Vancouver, British Columbia, Canada, pp. 186.
40. Levy, M.E., and Visca, P.J., 2009, "Statistical Characterization of Rock Structure using LiDAR," *In 43rd US Rock Mechanics Symposium and 4th U.S.-Canada Rock Mechanics Symposium*, July 28 – July 1, 2009, Asheville, NC, 7 pp.
41. Li, X.B., Lok, T.S., and Zhao, J., 2005, "Dynamic Characteristics of Granite Subjected to Intermediate Loading Rate," *In Rock Mechanics and Rock Engineering, Volume 38*(1), 2005, Austria, pp. 21-39.
42. Liu, Y., 2013, "An Introduction to the Boundary Element Method (BEM) and Its Applications in Engineering," *In Class Notes, University of Cincinnati Mechanical Engineering, CAE Research Lab*, November, 2013, 43 pp.
43. Lu, J., Ray, A., Morsy, K., and Peng, S., 2008, "Effects of Rock/Coal Interface Property on Coal Pillar Strength," *In Proceedings of the 27th International*

Conference on Ground Control in Mining, July 29-31, 2008, Morgantown, WV, pp. 262-267.

44. Maleki, H., 1995, "An Analysis of Violent Failure in U.S. Coal Mines-Case Studies," *In Proceedings: Mechanics and Mitigation of Violent Failure in Coal and Hard-Rock Mines*, USBM, Special Publication, SP 01-95, 1995, pp. 5-25.
45. Mark, C., 1999, "Empirical Methods for Coal Pillar Design," *In Proceedings of the Second International Workshop on Coal Pillar Mechanics and Design*, NIOSH Information Circular, IC 9448, June, 1999, Pittsburgh, PA, pp. 145-154.
46. Mark, C., 2009, "Deep Cover Pillar Recovery in the US," *In Proceedings of the 28th International Conference on Ground Control in Mining*, July 28-30, 2009, Morgantown, WV, 9 pp.
47. Mark, C., 2010, "Pillar Design for Deep Cover Retreat Mining: ARMPS Version 6 (2010)," *In Proceedings of the 3rd International Workshop on Coal Pillar Mechanics and Design*, July 26, 2010, Morgantown, WV, pp. 106-122.
48. Mark, C., and Barton, T.M., 1997, "Pillar Design and Coal Strength," *In Proceedings: New Technology for Ground Control in Retreat Mining*, NIOSH Information Circular, IC 9446, March, 1997, pp. 49-59.
49. Mark, C., Chase, F.E., and Pappas, D.M., 2007, "Analysis of Multiple Seam Stability," *In Proceedings of the 26th International Conference on Ground Control in Mining*, July 31 – August 2, 2007, Morgantown, WV, pp. 5-18.
50. Mark, C., and Gadde, M., 2008, "Global Trends in Coal Mine Horizontal Stress Measurement," *In Proceedings of the 27th International Conference on Ground Control in Mining*, July 29-31, 2008, Morgantown, WV, pp. 319-331.
51. MSHA, 2007, *Crandall Canyon Fatal Accident Report*, Retrieved from http://www.msha.gov/Fatals/2007/CrandallCanyon/FTL07CrandallCanyon.pdf
52. MSHA, 2010, *Upper Big Branch Mine-South Fatal Accident Report*, Retrieved from http://www.msha.gov/Fatals/2010/UBB/FTL10c0331noappx.pdf
53. Newman, D., 2007, "Multiple Seam Mining in Appalachia: State-of-the-Art, State-of-Practice, State-of-the-Future," *In 2007 SME Annual Meeting*, February 25-28, 2007, Salt Lake City, UT.
54. Newman, D., 2008, "Coal Mine Bumps: Case Histories of Analysis and Avoidance," *In Proceedings of the 27th International Conference on Ground Control in Mining*, July 29-31, 2008, Morgantown, WV, 6 pp.
55. Obert, L., Brady, B.T., and Schmechel, F.W., 1976, "The effect of normal stiffness on the shear resistance of rocks," *In Rock Mechanics & Rock Engineering*, Volume 8, 1976, pp. 57-72.
56. Office of Mine Safety and Health Research, 2010, *Research Report on the Coal Pillar Recovery under Deep Cover*, February, NIOSH, OMSHR Research Report, February, 2010, 79 pp.
57. Office of Mine Safety and Health Research, 2011, *Rib Falls: A Major Ground Control Issue*, Retrieved from http://www.cdc.gov/niosh/mining/features/ribfall.html
58. Office of Mine Safety and Health Research, 2012a, *Coal OperatorFatalities, Underground, 2001-2010*, Retrieved from http://www.cdc.gov/niosh/mining/UserFiles/statistics/CoalOperator/f_b1_u_co.JPG

59. Office of Mine Safety and Health Research, 2012b, *Coal Operator Nonfatal Lost-time Injuries, Underground, by Accident Class, 2006-2010*, Retrieved from http://www.cdc.gov/niosh/mining/UserFiles/statistics/CoalOperator/i_p1_u_co.JPG
60. Office of Mine Safety and Health Research, 2012c, *Mining Fatalities, Underground, by Accident Class, 2006-2010*, Retrieved from http://www.cdc.gov/niosh/mining/UserFiles/statistics/AllMining/f_p1_u_a.JPG
61. Office of Mine Safety and Health Research, 2012d, *Mining Fatalities by Commodity, 1911-2010*, Retrieved from http://www.cdc.gov/niosh/mining/UserFiles/statistics/AllMining/f_b3_a_a.JPG
62. Office of Mine Safety and Health Research, 2012e, *Rock Falls*, Retrieved from http://www.cdc.gov/niosh/mining/topics/rockfalls.html
63. Office of Mine Safety and Health Research, 2014, *Brody Mine Accident Highlights Need for Retreat Mining Safety*, Retrieved from http://www.cdc.gov/niosh/mining/features/RetreatMining.html
64. Pappas, D.M., and Mark, C., 1993, "Behavior of Simulated Longwall Gob Material," *In Report of Investigations*, USBM Report of Investigations, RI 9458, 1993, 45 pp.
65. Pariseau, W.G., 2011, "Geomechanics of Crandall Canyon Barrier Pillar Mining," *In 2011 SME Annual Meeting*, February 27-March 2, 2011, Denver, CO, 4 pp.
66. Pate, K., and Haneberg, W.C., 2011, "Photogrammetric and LiDAR 3-D Rock Slope Discontinuity Mapping and Interpretation Surveys to Improve Baseline Information for Supporting Design and Construction of Capital Improvement Projects at Hydroelectric Facilities," *In 45th US Rock Mechanics/Geomechanics Symposium*, June 26 – June 29, 2011, San Francisco, CA, 8 pp.
67. Peng, S.S., 2008, *Coal Mine Ground Control*, 3rd Edition, West Virginia University, Morgantown, WV, 750 pp.
68. Peng, S.S., Patrick, C.W., and Khair, A.W., 1983, "Direct Shear Strength of Appalachian Coals," *In Geotechnical Testing Journal*, *Volume 6*(3), 1983, pp. 144-150.
69. Perry, K.A., Unrug, K.F., Harris, K.W., and Raffaldi, M.J., 2013, "Influence of Roof/Floor Interface on Coal Pillar Performance," *In Proceedings of the 32nd International Conference on Ground Control in Mining*, July 30-August 1, 2013, Morgantown, WV, pp. 53-59.
70. Pine, R.J., Coggan, J.S., Flynn, Z.N., and Elmo, D., 2006, "The Development of a new Numerical Modelling Approach for Naturally Fractured Rock Masses," *In Rock Mechanics and Rock Engineering*, *Volume 39*(5), March, 2006, Austria, pp. 395-419.
71. Poeck, E.C., Zhang, K., Garvey, R., and Ozbay, U., 2015, "Energy Concepts in the Analysis of Unstable Coal Pillar Failures," *In Proceedings of the 34th International Conference on Ground Control in Mining*, July 30-August 2, 2015, Morgantown, WV, 6 pp.
72. Qian, Q., Qi, C., and Wang, M., 2009, "Dynamic strength of rocks and physical nature of rock strength," *In Journal of Rock Mechanics and Geotechnical Engineering*, *Volume 1*(1), 2009, pp. 1-10.

73. Salamon, M.D.G., 1984, "Energy considerations in rock mechanics: fundamental results," *In the Journal of the South African Institute of Mining and Metallurgy, Volume 84* (8), August, 1984, pp. 233-246.
74. Scholtés, L., Donzé, F.D., and Khanal, M., 2001, "Scale effects on strength of geomaterials, case study: coal, "*In Journal of the Mechanics and Physics of Solids, Volume 59* (5), May, 2011, pp. 1131-1146.
75. Sears, M.M., and Heasley, K.A., 2009, "An Application of Energy Release Rate," *In Proceedings of the 28th International Conference on Ground Control in Mining*, July 28-30, 2009, Morgantown, WV, 7 pp.
76. Singh, D.P., Sastry, V.R., and Srinivas, P.S., 1989, "Effect of Strain Rate on Mechanical Behavior of Rock," *In Rock at Great Depth*, 1989, Balkema, Rotterdam, pp. 109-114.
77. Scovazzo, V., 2008, "Comparison of the Mark-Bieniawski and Wilson Pillar Equations Using Site Specific Data," *In Proceedings of the 27th International Conference on Ground Control in Mining*, July 29-31, 2008, Morgantown, WV, pp. 229-234.
78. Scovazzo, V.A., 2010, "Analytical Design Procedure using the Wilson Equation," *In 2010 SME Annual Meeting*, February 28-March 3, 2010, Phoenix, AZ, 6 pp.
79. Slob, S., Hack, H.R.G.K., Feng, Q., Roshoff, K., and Turner, A.K., 2007, "Fracture mapping using 3D laser scanning techniques," *In Proceedings of the 11th Congress of the International Society for Rock Mechanics*, pp. 299-302.
80. Wang, T., Jiang, Y, Zhan, S., and Wang, C., 2014, "Frictional sliding tests on combined coal-rock samples," *In Journal of Rock Mechanics and Geotechnical Engineering, Volume 6*, April, 2014, pp. 280-286.
81. Whyatt, J., 2008, "Dynamic Failure in Deep Coal: Recent Trends and a Path Forward," *In Proceedings of the 27th International Conference on Ground Control in Mining*, July 29-31, 2008, Morgantown, WV, 10 pp.
82. Whyatt, J.K., and Board, M.P., 1991, "Numerical Exploration of Shear-Fracture-Related Rock Bursts Using a Strain-Softening Constitutive Law," *In Report of Investigations*, USBM Report of Investigations, RI 9350, 1991, 20 pp.
83. Wilson, A.H., and Ashwin, D.P., 1972, "Research into the Determination of Pillar Size," *In The Mining Engineer, Volume 131, Part 9*(141), Institution of Mining Engineers, June, 1972, London, United Kingdom, pp. 409-417.
84. Zhang, Q.B., and Zhao, J., 2013, "A Review of Dynamic Experimental Techniques and Mechanical Behavior of Rock Materials," *In Rock Mechanics and Rock Engineering, Volume 47*, September, 2013, pp. 1411-1478.
85. Zipf Jr., R.K., 1998, "Using a postfailure stability criterion in pillar design," *In DHHS (NIOSH) Publication No. 99-114*, June, 1998, pp. 182-192.
86. Zipf Jr., R.K., 2007, "Numerical modeling procedures for practical coal mine design," *In Proceedings of the International Workshop on Rock Mass Classification in Underground Mining*, pp. 153-162.
87. Zou, D., Miller, H.D.S., and Kaiser, P.K., 1989, "Numerical study of violent rock failure by stick-slip on joints," *In Mining Science and Technology, Volume 9* (3), November, 1989, pp. 241-251.

Vita

Kevin Ward Harris is a native of Harlan, Kentucky. He is a graduate of Harlan High School, Class of 2004. He then enrolled at the University of Kentucky in the fall of 2004, graduating magna cum laude from UK with a Bachelor of Science Degree in Mining Engineer in the spring of 2008.

Kevin began a career in industry in the summer of 2008 at Black Mountain Resources, LLC, in Harlan County, Kentucky. Black Mountain was one of the largest privately owned coal operations in the United States at the time. After workings at the operations for nearly three years, he returned to the University of Kentucky in the spring of 2012 to pursue a Doctorate in Mining Engineering, seeking to focus on rock mechanics, ground control, and underground coal mining. Specifically, his goal was to advance knowledge of coal mine ground control and the prediction and subsequent mitigation of coal bump risks.

Kevin is currently the acting secretary of the Kentucky Mining Institute (KMI) and has actively participated in the International Conference on Ground Control in Mining. He was awarded the Syd S. Peng Ground Control in Mining Scholarship in 2014. Along with numerous coauthors, Kevin has contributed to numerous published conference and peer-reviewed articles.